

João Tiago RAMOS BERNARDO DE SANTA RITA SIMÕES

The mechanics of punching in reinforced concrete slabs and  
footings without shear reinforcement

Thèse N° 8387



École  
Polytechnique  
Fédérale  
de Lausanne

2018



# The mechanics of punching in reinforced concrete slabs and footings without shear reinforcement

THÈSE N° 8387 (2018)

PRÉSENTÉE LE 12 MARS 2018

À LA FACULTÉ DE L'ENVIRONNEMENT NATUREL, ARCHITECTURAL ET CONSTRUIT  
LABORATOIRE DE CONSTRUCTION EN BÉTON  
PROGRAMME DOCTORAL EN GÉNIE CIVIL ET ENVIRONNEMENT

ÉCOLE POLYTECHNIQUE FÉDÉRALE DE LAUSANNE

POUR L'OBTENTION DU GRADE DE DOCTEUR ÈS SCIENCES

PAR

João Tiago RAMOS BERNARDO DE SANTA RITA SIMÕES

acceptée sur proposition du jury:

Prof. J.-F. Molinari, président du jury  
Prof. A. Muttoni, Dr M. Fernández Ruiz, directeurs de thèse  
Prof. M. Hallgren, rapporteur  
Prof. G. Sales Soares de Azevedo Melo, rapporteur  
Dr J. Saraiva Esteves Pacheco de Almeida, rapporteur



ÉCOLE POLYTECHNIQUE  
FÉDÉRALE DE LAUSANNE

Suisse  
2018



# Foreword

During the last decades, and particularly since the pioneer works of Kinnunen and Nylander in Sweden in the 1960's, the scientific community has searched for a general and physically consistent approach to describe failures in flat slabs due to punching at slab-column connections. These efforts have nevertheless not yet allowed to reach a general consensus. Partly, this can be explained by the difficulty in obtaining direct measurements on the development of inner punching cracks (which difficult the understanding of the mechanisms triggering failure) but is also justified by the complexity of the phenomenon. Indeed, a complex state of stresses develops in the vicinity of the connection (associated to both radial and tangential components) and the capacity to transfer such stresses in cracked concrete is governed by a number of phenomena such as the aggregate interlock, the response of concrete under confined conditions or the residual resistance of concrete in tension.

Within this context, a significant research effort has been performed in the Structural Concrete Laboratory at École Polytechnique Fédérale de Lausanne during the last two decades, developing the Critical Shear Crack Theory (CSCT) and applying it to cases related to shear and punching shear failures. A number of experimental and theoretical works have been performed so far, to validate and to consolidate its methodology, hypotheses and failure criteria for a number of cases such as slender slabs under symmetric and non-symmetric conditions and footings. Yet, there was still a theoretical need to make a synthesis of these works and to integrate these findings within a more comprehensive mechanical model describing the shear-carrying actions and mechanisms of failure for the various potential situations.

The work of Dr Simões is addressed at this question. After performing a testing programme on squat slabs (where detailed measurements of the kinematics at failure were recorded), he addresses the analysis of the punching shear capacity on the basis of a refined mechanical model accounting in a general manner for the development of a potential critical shear crack and its associated kinematics. The model, grounded on the basic assumptions of the CSCT, allows generalizing previous developments and to propose rational improvements on its failure criterion. As a result, not only refined analyses can be performed and various cases be investigated on the same basis, but also simple closed-form formulations of the failure load are derived with the aim to be incorporated in future codes of practice. The work has also the potential to investigate on the pertinence and analogies of other theoretical approaches to the phenomenon and can constitute thus an element to advance in finding a consensus on the causes and effects of the phenomenon of punching shear.

Lausanne, March 2018

Prof. Dr. Aurelio Muttoni

Dr. Miguel Fernández Ruiz



# Acknowledgements

The work presented in this document was performed in the last five years at the Structural Concrete Laboratory (IBETON) of the École Polytechnique Fédérale de Lausanne (EPFL) under the supervision of Prof. Aurelio Muttoni and Dr. Miguel Fernández Ruiz. I am deeply grateful for the opportunity they gave me to do a PhD under their supervision. I am also grateful for their continuous support, encouragement and guidance throughout this time, without which this work would not be possible. Their enthusiasm, knowledge and energy to make daily progress will always be a source of inspiration to me. I also want to acknowledge the opportunity they gave me to participate in other projects which were not directly related to the goals of my thesis and which allowed me to widen my knowledge in other topics.

I would like to acknowledge the members of the jury, Prof. Jean-François Molinari from EPFL (president), Prof. Guilherme Melo from Universidade de Brasília, Prof. Mikael Hallgren from the Royal Institute of Technology of Stockholm, and Dr. João Almeida from EPFL, for the time spent reading the manuscript, as well as for the valuable comments and relevant questions. Their remarks helped me improving the quality of this thesis.

This thesis results from a compilation of scientific articles written in co-authorship with the directors of the thesis, as well as with Dr. Jan Bujnak and Dr. Duarte Faria. To all of them I want to express my gratitude for their time, contributions and interesting discussions. All the anonymous reviewers of the scientific articles composing this thesis are also recognised for their valuable comments.

Part of the experimental work presented in this document was carried out in the framework of a private project funded by Peikko Group. I would like to thank Peikko Group for supporting the experimental work associated with specimens PP7 to PP9 and providing the shear reinforcement for specimen PS15. Special thanks to Jürgen, who performed the laboratory work associated with the specimens PP7 to PP9.

This thesis included an experimental campaign carried out in the laboratory of structures of École Polytechnique Fédérale de Lausanne. I would like to thank the generous help provided by all the technicians: Armin, François, Frédérique, Gérald, Gilles, Sylvain, Patrick and Serge. I am particularly grateful to Gérald and Gilles for the endless patient and for the time they have spent to explain me everything I needed to perform the experimental work. I also want to thank Jürgen for the time spent helping me and introducing me to laboratory work. During the time I have spent performing experimental work in the laboratory, I had the help of many students who I want to acknowledge: Guillaume, Lestio, Raffa, Sylvain and Yassine.

The assistance of Dr. Olivier Burdet in the preparation of the experimental programme presented in this document was greatly appreciated. Also, his daily availability to answer my work and non-work related questions during these years has been appreciated. Special thanks to Yvonne for all the help with administrative and organizational tasks, for her willingness to help and as well as for her always friendly attitude.

## Acknowledgements

---

During my PhD I had the chance to meet Prof. Linh Hoang from Technical University of Denmark, who I want to thank for the time and valuable advices. I also want to acknowledge the help of Prof. António Pinho Ramos, Dr. Carlos Ospina, Dominik Kueres, Dr. Juan Sagaseta and Dr. Walkner Rupert for providing me documentation during my PhD.

I would like to thank Francisco and Duarte for the proofreading of this thesis. I would also like to acknowledge Bastian, Hugo, Max, Patrick, Raffa and Dr. Olivier Burdet for the abstract translations.

I had so many stimulating discussions during these five years that helped me completing this work. For that, I want to thank Darko, Duarte, Francesco Cavagnis, Francisco, Fabio, Filip, Jesper, Jürgen, Marie-Rose, Max, Patrick, Philippe and Raffa. I greatly appreciated every discussion. Special thanks go for Duarte with whom I have passed uncountable hours discussing work and non-work-related topics. I want to offer my special thanks also to my officemates during these five years, Jürgen, Richard and Patrick, for all the good moments and interesting discussions. I am sincerely grateful to all the remaining IBETON colleagues who helped me in so many different ways and who I am glad to have met: Dan, Damjan, Francesco Moccia, Frédéric Monney, Ioannis, Jaime, Juan Manuel, Mathieu, Michael, Qianhui. I am also grateful to all my former and current colleagues and friends from IBETON and other laboratories who I had the pleasure to meet and who made my stay at EPFL incredible.

I would like to offer my special thanks to Prof. António Pinho Ramos, Prof. Mário Franca and Prof. Luis Neves, who supported my application to the EPFL Doctoral School. I am particularly grateful to Mário for telling me about EPFL and for all the encouragement and support to apply for a PhD here. I had my first contact with research while working under the supervision of Prof. Armando Antão, Prof. Luis Neves, Prof. Nuno Guerra and Prof. Teresa Santana at the Faculdade de Ciências e Tecnologia (FCT) of Universidade Nova de Lisboa (UNL). My special thanks go also for them for introducing me to the research environment while I was still a student of the Master in Civil Engineering at FCT/UNL.

I want to thank my friends André, David, Gonçalo, Hugo, Jorge, Miguel, Pedro, Ricardo and Rafael. Although the time spent together during my PhD was short, I will always remember some unforgettable moments.

Finally, I want to express all my gratitude to my family. I am grateful to my parents-in-law Corinne and Daniel by looking at me as if I was their son. Special thanks go also for my sisters-in-law, Flo, Elisabete and Mariana, to my nephew, Diogo, and to my grandma-in-law, Florentina, for all the pleasant family moments and support. I am grateful to my grandma Corina for her love and support. I am also grateful to my brothers, André and Pedro, for all the support and encouragement, as well as for all the unforgettable family moments we have spent together during these years. I am profoundly grateful to my parents who always provided me with unconditional support and love. To them I want to express my deepest gratitude for all they have done for me and for being always by my side when I needed the most. Finally, I have absolutely no words for the endless patient, support and love of my dear wife Anaïs. You made my life indescribably easier throughout these years. You have walked by my side in the good moments and much more importantly, in the hardest ones. I feel blessed to have you walking by my side.

Thank you all.

Lausanne, March 2018

João

# Abstract

Punching shear failures of structural concrete members have been the focus of attention of numerous works presented over the last decades. Although various rational approaches have been developed to predict these failures, there is still no unanimity on a theory consistently describing the phenomenon. An influential rational approach relating the punching strength to the deformation capacity of the slab at failure was proposed by Kinnunen and Nylander (1960). The Critical Shear Crack Theory (CSCT), whose first principles were published in 1991 by Muttoni and Schwartz, is among the works that were later developed consistently with the ideas of the approach of Kinnunen and Nylander. The CSCT has been the object of intensive research in the last two decades in view of its validation, improvement and extension. Consisting of four published scientific articles, the present work investigates the consistency of the principles of the theory for application to members without transverse reinforcement and different slenderness (footings and slabs).

An experimental programme on the punching behaviour of footings is presented to better understand the analogies and differences between the behaviour of slender and squat members. The measurements show that, in addition to the rotation of the slab, the shear strains also significantly influence the state of deformations at failure of squat members. A theoretical work is developed by applying the upper bound theorem of limit analysis. It shows the existence of a flexural-shear interaction in compact footings, influencing their strength and defining a smooth transition between pure flexural and punching shear regimes. A comparison between the theoretical and the experimental results shows that strain- and size-effects need to be considered to correctly predict the punching strength of compact footings using limit analysis.

To investigate the transition between limit analysis and the CSCT, as well as how CSCT handles the punching failures of squat members, the theoretical principles of the CSCT are reviewed and discussed. This study shows that, by accounting for both flexural and shear deformations in the kinematics of the critical shear crack, the theory is applicable to both slender and squat members. In addition, a recently proposed power-law failure criterion is justified based on the different potential failure modes of slender and squat members. Furthermore, closed-form solutions for punching shear design of members without transverse reinforcement are analytically derived combining the power-law failure criterion and a simplified load-rotation relationship. These expressions are validated by comparing their results with a wide range of experimental results of slabs and footings.

A mechanical model is eventually developed and presented on the basis of the theoretical principles of the CSCT, allowing for a refined calculation of the failure criterion by integration of the stresses developing along the critical shear crack. This model is applied to the case of slender slabs and validated against experimental results, showing a good agreement. A parametric study based on the refined failure criterion allows a theoretical validation of both analytical failure criteria of the CSCT as well as of its main assumptions. Finally, the preliminary results of the application of the mechanical model to prestressed slabs and footings show that the principles of the CSCT are also valid to study these cases.

**Keywords:** structural concrete; punching shear strength; experimental programme; mechanical model; limit analysis; Critical Shear Crack Theory (CSCT); failure criterion; footings; slabs; closed-form design expressions.



# Résumé

Les ruptures par poinçonnement d'éléments en béton armé ont fait l'objet de nombreuses études ces dernières décennies. Bien que diverses approches rationnelles aient été développées pour les décrire, il n'y a pas encore d'unanimité autour d'une théorie qui décrit ce phénomène de manière complète. Une approche rationnelle qui a eu beaucoup d'influence est celle qui a été proposée par Kinnunen et Nylander (1960) ; elle relie la résistance au poinçonnement à la capacité de déformations de la dalle à la rupture. La Théorie de la Fissure Critique (Critical Shear Crack Theory, CSCT en anglais), dont les premiers principes ont été publiés en 1991 par Muttoni et Schwartz, suit les idées de Kinnunen et Nylander. La CSCT a fait l'objet de recherches intensives ces deux dernières décennies, pour en établir la validité, l'améliorer et l'étendre. Sur la base de quatre articles publiés, le présent travail étudie la consistance des principes de la théorie en vue de son application aux éléments sans armature transversale de divers élancements (fondations et dalles).

Un programme expérimental du comportement au poinçonnement des dalles de fondation est présenté, pour mieux comprendre les analogies et les différences entre le poinçonnement des éléments élancés et trapus. Les mesures montrent qu'en plus de la rotation de la dalle, les déformations d'effort tranchant ont une importance significative sur l'état de déformations à la rupture des éléments trapus. Un développement théorique basé sur le théorème de la borne supérieure de l'analyse limite montre qu'il existe une interaction importante entre la flexion et l'effort tranchant dans les fondations trapues, influencent leur résistance et en définissant une transition graduelle entre les régimes de pure flexion et de poinçonnement. Une comparaison entre la théorie et les résultats expérimentaux montre que les effets de déformation et de taille doivent être tenus en compte afin de prédire correctement la résistance au poinçonnement des fondations trapues en appliquant l'analyse limite.

Pour étudier la transition entre l'analyse limite et la CSCT, ainsi que la manière dont la CSCT traite les ruptures par poinçonnement des éléments trapus, les principes théoriques de la CSCT ont été revisités et discutés. L'étude montre qu'en tenant compte des déformations de flexion et d'effort tranchant dans la cinématique de la fissure critique, la théorie est applicable aux éléments élancés aussi bien que trapus. De plus, une nouvelle formulation du critère de rupture sous la forme d'une loi de puissance trouve sa justification dans les deux modes de rupture possible différents pour les éléments élancés et trapus. Finalement, des solutions en forme close peuvent être dérivées pour le dimensionnement au poinçonnement des éléments sans armature transversale sur la base du critère de rupture sous forme de loi de puissance et d'une relation charge-rotation simplifiée. Ces expressions ont été validées en comparant leurs résultats à une large palette de résultats expérimentaux sur des dalles et des fondations.

Un modèle mécanique est présenté, développé sur la base des principes théoriques de la CSCT et permettant un calcul raffiné du critère de rupture par intégration des contraintes qui se développent le long de la fissure critique. Appliqué au cas des dalles élancées, ce modèle est en bon accord avec les résultats expérimentaux. Une étude paramétrique basée sur le critère de rupture raffiné permet une validation théorique des deux critères de rupture de la CSCT ainsi que de ses hypothèses principales. Finalement, une application préliminaire du modèle mécanique au cas des dalles et fondations pré-contraintes montre que les principes théoriques de la CSCT sont aussi applicables pour étudier ces configurations.

**Mots-clés:** béton armé; résistance au poinçonnement; essais; modèle mécanique; théorie de la plasticité; théorie de la fissure critique (CSCT); critère de rupture; fondations; dalles; expressions pour dimensionnement.

# Zusammenfassung

In den letzten Jahrzehnten haben sich viele Arbeiten mit dem Durchstanzversagen von Stahlbetonbauteilen beschäftigt. Trotz der Entwicklung verschiedenster mechanischer Ansätze um dieses Versagen vorherzusagen, herrscht noch immer keine Einigkeit was die beschreibende Theorie angeht. Ein einflussreicher rationeller Ansatz, der die Durchstanzfestigkeit in einen Zusammenhang mit der Verformungskapazität bringt, wurde von Kinnunen und Nylander (1960) vorgeschlagen. Die Theorie des kritischen Schubrisses (Critical Shear Crack Theory auf Englisch, CSCT), im Jahre 1991 von Muttoni und Schwartz erstmals publiziert, ist unter den Arbeiten, die im Einklang mit den Grundlagen der Theorie von Kinnunen und Nylander entwickelt wurden. Die CSCT war das Objekt intensiver Forschung in den letzten beiden Jahrzehnten, was ihre Validierung, Verbesserung und ihren Ausbau angeht. Die vorliegende aus vier veröffentlichten wissenschaftlichen Artikeln bestehende Arbeit untersucht die Beständigkeit der Prinzipien der Theorie im Falle der Anwendung auf Bauteile ohne Schubbewehrung und unterschiedlicher Schlankheit (Fundament- und Deckenplatten).

Zum besseren Verständnis der Analogien und Unterschiede was das Verhalten von schlanken und gedrunenen Bauteilen angeht, wird eine Versuchsreihe, die das Durchstanzverhalten von Fundamenten untersucht, vorgestellt. Die Messungen zeigen, dass neben den Rotationen, auch die Schubverzerrungen einen signifikanten Einfluss auf den Deformationszustand von gedrunenen Bauteilen bei Versagen haben. Eine theoretische Formulierung wird unter Benutzung des kinematischen oberen Grenzwertsatzes der Plastizitätstheorie hergeleitet. Sie zeigt die Existenz einer Biege-Schub-Interaktion in gedrunenen Fundamenten, welche die Festigkeit beeinflusst und einen fließenden Übergang zwischen reinem Biege- und Durchstanzverhalten definiert. Ein Vergleich zwischen den theoretischen und den experimentellen Resultaten zeigt, dass Verzerrungs- und Größeneffekte berücksichtigt werden müssen, um den Durchstanzwiderstand von gedrunenen Gründungen unter Benutzung des Grenzwertsatzes korrekt vorher zu sagen.

Für die Untersuchung des Übergangs zwischen Grenzwertsatz und CSCT sowie der Behandlung von gedrunenen Bauteilen durch die CSCT, werden deren theoretischen Grundlagen überprüft und diskutiert. Die Studie zeigt, dass die Theorie auf schlanke und gedrunene Bauteile anwendbar ist, wenn sowohl Biege- als auch Schubverformungen in der Kinematik des kritischen Schubrisses berücksichtigt werden. Zusätzlich dazu, wird ein kürzlich vorgeschlagenes Potenzgesetz-Versagenskriterium mit den verschiedenen potentiellen Versagensmechanismen von schlanken und gedrunenen Bauteilen gerechtfertigt und erklärt. Des Weiteren werden geschlossene Lösungen für die Durchstanzbemessung von Bauteilen ohne Schubbewehrung analytisch hergeleitet, indem das Potenzgesetz-Versagenskriterium mit einer vereinfachten Last-Verformungsbeziehung kombiniert wird. Diese Formulierungen werden mit einer weiten Reihe von Versuchsergebnissen an Decken- und Gründungsplatten validiert.

In weiterer Folge wird ein mechanisches Modell auf der Basis der theoretischen Prinzipien der CSCT entwickelt, das eine verfeinerte Berechnung des Versagenskriteriums durch Integration der Spannungen im kritischen Schubriss ermöglicht. Dieses Modell, auf schlanke Platten angewandt und mit Versuchsergebnissen validiert, zeigt eine gute Übereinstimmung. Eine auf dem verfeinerten Versagenskriterium basierende Parameterstudie erlaubt eine theoretische Validierung der beiden analytischen Versagensmechanismen der CSCT und ihrer Hauptannahmen. Schlussendlich demonstrieren die vorläufigen Resultate der Anwendung des mechanischen Modells auf vorgespannte Platten und Grün-

dungen die Gültigkeit der Prinzipien der CSCT auch in diesen Fällen.

**Schlüsselwörter:** Stahlbeton; Durchstanzwiderstand; experimentelle Untersuchungen; mechanisches Modell; Grenzwertanalyse; Critical Shear Crack Theory (CSCT); Versagenskriterium; Gründungen; Flachdecken; Platten; Bemessungsansätze in geschlossener Form.

## Riassunto

Le rotture a punzonamento di strutture in calcestruzzo armato sono state oggetto di studio di numerose ricerche svolte negli ultimi decenni. Malgrado vari approcci razionali siano stati sviluppati per descrivere queste modalità di rottura, non è ancora presente una visione unanime su un modello che descriva il problema in maniera consistente. Un approccio razionale il quale legava la resistenza a punzonamento alla capacità di deformazione di una piastra a rottura fu proposta da Kinnunen e Nylander nel 1960. La Teoria della Fessura Critica (CSCT), i cui principi furono pubblicati nel 1991 da Muttoni e Schwartz, è uno tra i lavori che successivamente sono stati sviluppati in maniera consistente seguendo le ipotesi assunte dall'approccio di Kinnunen e Nylander. Negli ultimi due decenni, la Teoria della Fessura Critica è stata oggetto di una ricerca intensiva al fine di validarne le sue ipotesi iniziali e, allo stesso tempo, allo scopo di proporre migliorie e estensioni. Costituito da quattro articoli scientifici pubblicati su rivista, il presente lavoro studia la coerenza dei principi della teoria per l'applicazione ad elementi strutturali non armati a taglio aventi differenti snellezze (piastre e fondazioni).

Un programma sperimentale sulla resistenza a punzonamento di fondazioni è presentato al fine di comprendere in modo migliore le differenze e le analogie tra il comportamento a rottura di elementi strutturali snelli e tozzi. Le misure sperimentali mostrano che, oltre alla rotazione della piastra, le deformazioni a taglio hanno un'influenza importante nello stato di deformazione a rottura di elementi tozzi. Un lavoro teorico è stato, successivamente, sviluppato adottando il teorema cinematico dell'analisi limite. Tale studio mette in evidenza l'interazione tra taglio e momento presente in fondazioni compatte, definendo una transizione graduale tra i regimi di pura flessione e di taglio-punzonamento. Un confronto tra i risultati teorici e sperimentali mostra come l'effetto di deformazione e del fattore di scala debbano essere tenuti in conto al fine di predire correttamente la resistenza a punzonamento di fondazioni tozze nel caso si adotti un calcolo secondo analisi limite.

Per esaminare la transizione tra analisi limite e CSCT, e, allo stesso tempo, allo scopo di studiare come quest'ultima tratti le rotture a punzonamento di elementi tozzi, i principi teorici della CSCT sono stati revisionati e discussi. Questo studio mostra che, tenendo conto delle deformazioni flessionali e taglienti nella cinematica della fessura critica a taglio, la teoria è applicabile sia per elementi snelli che tozzi. Inoltre, un criterio di rottura secondo una legge di potenza, recentemente pubblicato, è stato giustificato sulla base dei differenti potenziali modi di rottura presenti in elementi snelli e tozzi. In aggiunta, soluzioni a forma chiusa per la verifica a taglio-punzonamento di elementi non armati a taglio sono state derivate analiticamente combinando il criterio di rottura secondo legge di potenza e una relazione carico-rotazione semplificata. Queste espressioni sono state validate confrontando le loro predizioni con una vasta gamma di risultati sperimentali ottenuti su piastre e fondazioni.

Un modello meccanico è stato, infine, sviluppato e presentato sulla base dei principi teorici della CSCT, permettendo un calcolo raffinato del criterio di rottura il quale è stato ottenuto integrando gli sforzi interni lungo la fessura critica a taglio. Questo modello è stato applicato al caso di elementi snelli e validato mediante il confronto con risultati sperimentali, risultandone in accordo. Uno studio parametrico basato sul criterio di rottura raffinato ha permesso una validazione teorica sia del criterio di rottura analitico (CSCT) sia delle sue assunzioni. Infine, i risultati preliminari dell'applicazione del modello meccanico a piastre precomprese e fondazioni mostrano che i principi della CSCT restano validi anche per studiare questi casi.

**Parole-chiave:** calcestrutto armato; resistenza a taglio-punzonamento; programma sperimentale; modello meccanico; analisi limite; Teoria della Fessura Critica (CSCT); criterio di rottura; fondazioni; piastre; equazioni di progetto a forma chiusa.

## Resumo

A rotura de elementos de betão armado por punçoamento tem sido o foco de atenção de um grande número de publicações ao longo das últimas décadas. Apesar de terem sido desenvolvidas várias abordagens racionais para descrever este tipo de rotura, ainda não existe unanimidade em torno de uma teoria mecânica que descreva de forma completa e consistente este fenómeno. A teoria apresentada por Kinnunen e Nylander (1960), que relaciona a resistência ao punçoamento com as deformações da laje na rotura, teve um grande impacto nesta área de investigação. Posteriormente e desenvolvida em coerência com o referido trabalho, surgiu a Teoria da Fissura de Corte Crítica (CSCT no acrónimo Inglês), cujos primeiros princípios foram publicados em 1991 por Muttoni e Schwartz. A CSCT foi alvo de uma investigação intensa ao longo das duas últimas décadas com vista à sua validação, melhoria e extensão. O presente trabalho, composto por quatro artigos publicados em revistas científicas, investiga a aplicabilidade dos princípios da CSCT a elementos estruturais sem armadura de esforço transversal e com esbeltezas diferentes (fundações e lajes esbeltas).

Com o intuito de compreender as analogias e diferenças comportamentais de lajes esbeltas e compactas, apresenta-se um programa experimental sobre o punçoamento em fundações de betão armado. Os resultados experimentais demonstram que, para além das deformações de flexão, também as deformações de corte influenciam de forma significativa o estado de deformações na rotura de elementos compactos. É apresentado um trabalho teórico com base na aplicação do teorema superior da análise limite. Este trabalho demonstra a existência de uma interação corte-flexão que influencia a resistência de fundações compactas e que define uma transição entre os regimes de flexão e punçoamento puros. A comparação dos resultados teóricos e experimentais revela a necessidade de considerar os efeitos de deformação e de escala no cálculo da resistência ao punçoamento de fundações compactas com recurso à análise limite.

Os princípios teóricos da CSCT são revistos e discutidos, não só com o objectivo de estudar a transição entre os resultados da análise limite e da CSCT, mas também para compreender a forma como esta teoria trata as roturas por punçoamentos em elementos compactos. Este estudo demonstra que a teoria é aplicável tanto a elementos esbeltos como compactos, visto que de acordo com os seus princípios tanto as deformações por flexão como também as deformações de corte são consideradas na cinemática da fissura de corte crítica. Uma nova formulação do critério de rotura da CSCT recentemente proposta é teoricamente justificada com base nos diferentes modos de rotura de elementos esbeltos e compactos. A combinação deste critério de rotura com uma lei simplificada da carga-deformação permite derivar de forma analítica expressões de forma fechada para o cálculo da resistência ao punçoamento. As expressões referidas são validadas através de comparação com resultados experimentais.

É desenvolvido e apresentado um modelo mecânico para o cálculo da resistência ao punçoamento com base nos princípios teóricos da CSCT. Este modelo permite o cálculo refinado do critério de rotura através da integração das tensões que se desenvolvem ao longo da fissura de corte crítica. Este modelo é aplicado ao caso de lajes esbeltas e validado por comparação com resultados experimentais onde é obtida uma muito boa concordância. Um estudo paramétrico baseado no cálculo refinado do critério de rotura permite validar teoricamente a utilização dos critérios analíticos da CSCT, bem como das suas principais hipóteses. Finalmente, os resultados preliminares resultantes da aplicação do modelo mecânico ao caso de fundações e lajes pré-esforçadas demonstram que os princípios da CSCT são

igualmente válidos para estudar estes casos.

**Palavras-chave:** betão armado; resistência ao punçoamento; programa experimental; modelo mecânico; teoria da plasticidade; Teoria da Fissura de Corte Crítica (CSCT); critério de rotura; fundações; lajes; expressões de dimensionamento.

# Contents

<b>Foreword</b>	<b>i</b>
<b>Acknowledgements</b>	<b>iii</b>
<b>Abstract</b>	<b>i</b>
<b>Résumé</b>	<b>iii</b>
<b>Zusammenfassung</b>	<b>v</b>
<b>Riassunto</b>	<b>vii</b>
<b>Resumo</b>	<b>ix</b>
<b>1 Introduction</b>	<b>1</b>
1.1 Problem statement . . . . .	1
1.2 Punching of reinforced concrete footings, open questions . . . . .	2
1.3 Context of this thesis within the framework of the Critical Shear Crack Theory . . . . .	4
1.4 Objectives of the thesis . . . . .	6
1.5 Structure of the thesis . . . . .	7
1.6 Scientific contributions of the thesis . . . . .	8
1.7 Limitations of the thesis . . . . .	9
1.8 List of publications . . . . .	9
1.9 References . . . . .	10
<b>2 Paper I: Punching shear tests on compact footings with uniform soil pressure</b>	<b>17</b>
2.1 Abstract . . . . .	18
2.2 Introduction . . . . .	18
2.3 Experimental programme . . . . .	20
2.3.1 Specimens and materials . . . . .	20
2.3.2 Test setup and experimental procedure . . . . .	21
2.3.3 Measurement devices . . . . .	23
2.4 Experimental results . . . . .	24
2.4.1 Main results . . . . .	24
2.4.2 Measured deformations . . . . .	25
2.4.3 Global observed behaviour of RC footings subjected to concentrated loads . . . . .	30
2.5 Analysis of experimental evidence . . . . .	32
2.5.1 Influence of span-to-effective depth ratio and column size . . . . .	32
2.5.2 Influence of shear reinforcement . . . . .	33
2.5.3 Flexural-shear interaction . . . . .	33
2.5.4 Influence of top reinforcement . . . . .	34
2.6 Conclusions . . . . .	35

2.7	References . . . . .	36
2.8	Notation . . . . .	38
<b>3</b>	<b>Paper II: Strength of RC footings without transverse reinforcement according to limit analysis</b>	<b>39</b>
3.1	Abstract . . . . .	40
3.2	Introduction . . . . .	40
3.3	Kinematical theorem of limit analysis applied to isolated reinforced concrete footings . .	42
3.3.1	Rate of external work . . . . .	46
3.3.2	Rate of internal energy dissipated in the concrete along the failure surface . . . .	46
3.3.3	Rate of internal energy dissipated in the concrete due to tangential compression	47
3.3.4	Rate of internal energy dissipated in the reinforcement . . . . .	48
3.3.5	Determination of the failure load . . . . .	48
3.4	Influence of different parameters on the load carrying capacity . . . . .	48
3.4.1	Governing failure mechanisms . . . . .	49
3.4.2	Parametric analysis . . . . .	51
3.5	Simplified formulations - practical application . . . . .	53
3.5.1	Flexural-shear failures . . . . .	53
3.5.2	Punching shear failures . . . . .	54
3.6	Comparison with experimental results . . . . .	56
3.7	Conclusions . . . . .	58
3.8	References . . . . .	60
3.9	Notation . . . . .	63
3.10	Appendix . . . . .	65
3.10.1	Rate of internal energy dissipated in the concrete along the failure surface . . . .	65
3.10.2	Rate of internal energy dissipation in the concrete due to tangential bending . . .	66
3.10.3	Rate of internal energy dissipation in the reinforcement . . . . .	67
<b>4</b>	<b>Paper III: The theoretical principles of the CSCT for punching shear failures and derivation of consistent closed-form design expressions</b>	<b>69</b>
4.1	Abstract . . . . .	71
4.2	Introduction . . . . .	71
4.3	The mechanical model of CSCT for punching shear . . . . .	73
4.3.1	Failure mechanism and associated internal stresses . . . . .	73
4.3.2	Application to slender members . . . . .	75
4.3.3	Application to footings and squat members . . . . .	77
4.4	Considerations on the failure criterion of the CSCT . . . . .	78
4.5	Closed-form solution of the CSCT . . . . .	80
4.5.1	Development of closed-form expressions for elements without transverse reinforcement . . . . .	80
4.5.2	Development of closed-form expressions for slab continuity and compressive membrane action . . . . .	82
4.6	Comparison of closed-form expressions against experimental results . . . . .	83
4.6.1	Detailed results for slender slabs . . . . .	86
4.6.2	Detailed results for footings . . . . .	88
4.7	Conclusions . . . . .	89

4.8	References . . . . .	91
4.9	Notation . . . . .	96
4.10	Appendix . . . . .	98
<b>5</b>	<b>Paper IV: Validation of the Critical Shear Crack Theory for punching of slabs without transverse reinforcement by means of a refined mechanical model</b>	<b>101</b>
5.1	Abstract . . . . .	102
5.2	Introduction . . . . .	102
5.3	Analysis of the punching shear behaviour based on experimental observations available in the scientific literature . . . . .	105
5.3.1	Discussion on the cracking pattern observed in the saw-cuts of tested specimens	105
5.3.2	Discussion on the distribution of tangential cracks with flexural origin . . . . .	108
5.3.3	Discussion on the kinematics of the critical shear crack . . . . .	109
5.4	Mechanical model for punching shear failures . . . . .	110
5.4.1	Basis of the mechanical model . . . . .	110
5.4.2	Geometrical definition of regions of the slab with different behaviour . . . . .	111
5.4.3	Shape of the Critical Shear Crack . . . . .	112
5.4.4	Kinematics and displacement field along the critical shear crack . . . . .	114
5.4.5	Internal stresses along the critical shear crack . . . . .	118
5.4.6	Calculation of the punching shear strength . . . . .	127
5.5	Comparison against experimental results . . . . .	127
5.6	Validation of the failure criterion of the Critical Shear Crack Theory . . . . .	130
5.7	Conclusions . . . . .	134
5.8	References . . . . .	136
5.9	Notation . . . . .	142
5.10	Appendix . . . . .	146
5.10.1	Calculation of the depth of the neutral axis . . . . .	146
5.10.2	Constitutive relationships adopted for concrete . . . . .	147
5.10.3	Load-rotation relationship according to Muttoni (2008) . . . . .	150
5.10.4	Numerical procedure to calculate the punching shear strength . . . . .	154
<b>6</b>	<b>A discussion on the extension of the mechanical model for punching failures of prestressed slabs and footings</b>	<b>157</b>
6.1	Introduction . . . . .	157
6.2	Potential extension of the mechanical model to prestressed slabs . . . . .	158
6.2.1	Introduction . . . . .	158
6.2.2	Load-rotation relationship according to Clément <i>et al.</i> (2014) . . . . .	159
6.2.3	Calculation of the refined failure criterion accounting for in-plane stresses . . . . .	162
6.2.4	Brief comparison with experimental results . . . . .	166
6.3	Potential extension of the mechanical model to footings . . . . .	170
6.3.1	Introduction . . . . .	170
6.3.2	Adaptation of load-rotation relationship of Muttoni (2008) to footings . . . . .	171
6.3.3	Calculation of the refined failure criterion for isolated footings . . . . .	174
6.3.4	Validation and comparison against experimental results . . . . .	180
6.4	Conclusions . . . . .	183
6.5	References . . . . .	184

## CONTENTS

---

6.6	Notation . . . . .	187
<b>7</b>	<b>Conclusions and Outlook</b>	<b>191</b>
7.1	Introduction . . . . .	191
7.2	Conclusions . . . . .	193
7.3	Outlook . . . . .	198
7.4	References . . . . .	200

# Chapter 1

## Introduction

### 1.1 Problem statement

The use of flat slabs dates back to the beginning of the 20<sup>th</sup> century when this structural system was developed and its advantages made it immediately very attractive (Maillart, 1926; Fürst and Marti, 1997; Gasparini, 2002; Muttoni, 2008). Compared to the conventional slabs supported on beams and columns, flat slabs proved to be significantly more flexible and easier to build (Moe, 1961; Muttoni, 2008). On the contrary, the concentration of high bending moments and shear forces in the vicinity of the columns, potentially triggering a punching shear failure (Muttoni and Fernández Ruiz, 2010), was early recognized as one of the main disadvantages (Elstner and Hognestad, 1956; Moe, 1961; Fürst and Marti, 1997; Gasparini, 2002).

Punching shear failures of structural concrete members without transverse reinforcement are characterized by the development of a inclined failure surface without being necessary associated significant deformations prior to failure (see e.g. Guandalini *et al.*, 2009; Figure 1.1 for the case of a slender slab). Since the deformation of the system is controlled by the bending reinforcement, the brittleness of punching shear failures strongly depends on the behaviour of the reinforcement at failure, which may be in the elastic regime, partly or fully yielded (Guandalini *et al.*, 2009; Fernández Ruiz and Muttoni, 2017). In addition, such failures may lead to a progressive structural collapse (Mirzaei, 2010; Faria *et al.*, 2012), as they require a redistribution of internal forces in a structure that may already be in a limit design situation (Fernández Ruiz *et al.*, 2010, 2013).

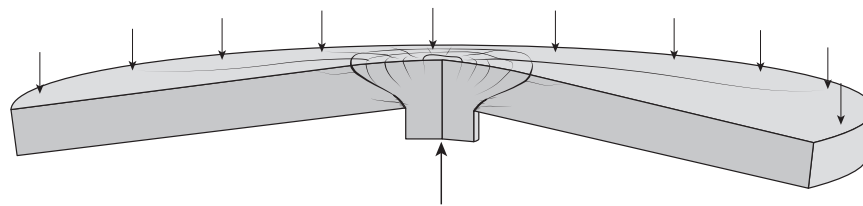
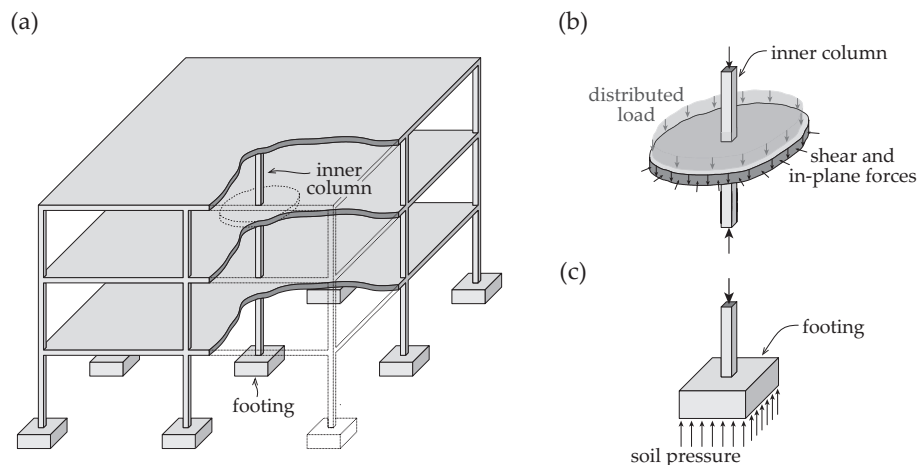


Figure 1.1: Punching shear failure of slender flat slab.

The introduction of mushrooms, column capitals or drop panels was a widely used solution to deal with the issue of punching shear in slabs when they first appeared (Maillart, 1926; Gasparini, 2002; Muttoni, 2008). One of the first experimental works on the punching strength was actually performed on footings and was justified by the increasing construction of tall buildings with reinforced concrete footings subjected to very high shear forces (Talbot, 1913). It was only in the second half of the 20<sup>th</sup> century that slab-column connections without drop panels, mushrooms or capitals became progressively popular (Muttoni, 2008). However, more than one century after the appearance of the first flat slabs, and despite all the efforts made to improve the knowledge on this topic (e.g. Kinnunen and Nylander, 1960; Regan and Braestrup, 1985; Regan, 1986; Shehata and Regan, 1989; Bažant and Cao, 1987; Brooms,

1990; Hallgren, 1996; Yankelevsky and Leibowitz, 1999; *fib*, 2001; Polak, 2005; Park *et al.*, 2011; *fib*, 2017), a general agreement with respect to the phenomena involved in punching shear failures of flat slabs is not yet reached and further experimental and theoretical work is still required.



**Figure 1.2:** (a) Schematic representation of a standard reinforced concrete structure; (b) slab-column connection and (c) isolated footing.

As punching occurs in members subjected to concentrated loads, such failures may not only take place in flat slabs but also in footings, even if both members are geometrically and mechanically very different (Talbot, 1913). Figure 1.2(a) shows schematically a simple structure composed by flat slabs, columns and isolated footings. The sub-systems of an inner slab-column connection and of an isolated footing are represented separately in Figures 1.2(b) and (c), respectively, where it becomes very clear that footings are significantly more compact elements (significantly smaller span-to-effective depth ratio) subjected normally to much higher shear forces (often related to the number of stories).

Even though a considerable number of reinforced concrete footings have been tested in the first half of the 20<sup>th</sup> century (Talbot, 1913; Richart, 1948), punching failures on footings have attracted far less attention than punching failures on slabs in the last decades. Yet, some of the experimental, numerical and theoretical works on the topic suggested that the punching behaviour of footings may be noticeably different from the one of flat slender slabs (e.g. Dieterle and Rostásy, 1987; Hallgren *et al.*, 1998; Hallgren and Bjerke, 2002; Timm, 2003; Broms, 2005; Hegger *et al.*, 2009; Urban *et al.*, 2013b; Siburg and Hegger, 2014; Kueres *et al.*, 2013). Therefore, it is still nowadays not clear if punching shear failures of footings and slabs can be described and theoretically dealt in a consistent manner (Hallgren *et al.*, 1998; Broms, 2005; Kueres *et al.*, 2017b). In order to clarify this topic it is essential to better understand the mechanics of punching shear failures of both slender and squat members.

## 1.2 Punching of reinforced concrete footings, open questions

A number of experimental works focusing on the punching shear behaviour and strength of footings have been performed so far (Talbot, 1913; Richart, 1948; Kordina and Nölting, 1981; Dieterle and Steinle, 1981; Dieterle and Rostásy, 1987; Dieterle, 1987; Hallgren *et al.*, 1998; Li, 2000; Timm, 2003; Hegger *et al.*, 2006, 2007, 2009; Netopilik, 2012; Urban *et al.*, 2013a,b; Siburg and Hegger, 2014; Krakowski *et al.*, 2015; Kueres *et al.*, 2017a; Bonić *et al.*, 2017).

The first tests were carried out in the United States of America already in the first decades of 20<sup>th</sup> century (Talbot, 1913; Richart, 1948). The experimental works that followed were published considerably

later and were performed in Germany (Kordina and Nölting, 1981; Dieterle and Steinle, 1981; Dieterle and Rostásy, 1987; Timm, 2003) and Sweden (Hallgren *et al.*, 1998). Kordina and Nölting (1981) investigated the eccentric punching shear behaviour of footings, Dieterle and Steinle (1981) studied the punching strength of pre-fabricated foundation blocks, whereas Dieterle and Rostásy (1987), Hallgren *et al.* (1998), and Timm (2003) focused specifically on the concentric punching behaviour of footings with and without transverse reinforcement. More recently, the punching shear behaviour of reinforced concrete footings attracted the attention of the Institute of Structural Concrete of RWTH Aachen University, where extensive experimental programmes were carried out (Hegger *et al.*, 2006, 2007, 2009; Ricker, 2009; Siburg and Hegger, 2014; Siburg, 2014; Kueres *et al.*, 2017a). Large experimental campaigns on the punching strength of compact members have also been performed in the last years at University of Lodz in Poland (Urban *et al.*, 2013a,b; Krakowski *et al.*, 2015). Some other isolated experimental programmes were also realized on compact slabs in Canada (Li, 2000; Netopilik, 2012) or footings resting on soil in Serbia (Bonić *et al.*, 2017).

Various interesting experimental findings have been reported in the works above referred. It was shown that the span-to-effective depth ratio plays an important role on the punching shear strength of footings without transverse reinforcement (Hegger *et al.*, 2006, 2009; Urban *et al.*, 2013b; Siburg and Hegger, 2014). The influence of the size of the member on the punching strength has also been reported by Dieterle and Rostásy (1987) and more recently by Siburg and Hegger (2014). Hallgren *et al.* (1998) suggested that the influence of concrete compressive strength on the punching strength is higher in footings than in slabs and similar considerations have been reported by Hegger *et al.* (2009) for very compact footings. The experimental results revealed also that punching failures in squat members can occur for very limited deformations (e.g. Hegger *et al.*, 2009; Urban *et al.*, 2013b; Siburg and Hegger, 2014) and that the inclination of the failure surface is steeper in footings than in slabs (Hegger *et al.*, 2009; Siburg and Hegger, 2014). In spite of these important findings, it is worth to mention that only a part of the experimental programmes previously mentioned included full scale specimens tested under realistic conditions (Hegger *et al.*, 2006, 2009). Consequently, there is still nowadays a need for additional experimental work in order to confirm some of the reported trends and better understand the punching behaviour of compact members.

With respect to the mechanical interpretation of punching shear failures of compact members, some interesting phenomenological descriptions have been presented, as for instance by Hallgren and Bjerke (2002) and Broms (2005). Based on the use of non-linear finite element calculations validated against experimental results, Hallgren and Bjerke (2002) described punching failures of footings without transverse reinforcement as follows: the formation of flexural cracks is followed by the development of inclined shear cracks along which a shear deformation occurs, resulting into high compression stresses in the concrete strut carrying shear; crushing of the concrete strut triggers a redistribution of internal forces which eventually leads to failure. Another mechanical approach has been presented by Broms (2005), who proposed an extension of the mechanical model of Kinnunen and Nylander (1960) to enable its application for compact members as footings by considering a radial stress based criterion including a size effect. However, the calculation of the punching strength of footings has been historically performed based on empirical approaches in an analogous manner to the ones used for flat slabs (Regan and Braestrup, 1985; *fib*, 2001; Hegger *et al.*, 2009). For instance, Kueres *et al.* (2017b) proposed recently an approach to deal with the punching shear failures of flat slabs and footings in a consistent manner. These approaches are justified as a consensus with respect to the analogies and differences between the behaviour of slender and squat members still remains to be achieved. This topic will be addressed in this thesis within the framework of the Critical Shear Crack Theory as described in the following.

### 1.3 Context of the thesis within the framework of the Critical Shear Crack Theory

Various mechanically based models for punching shear failures of reinforced concrete members have been presented in the last decades (e.g. Kinnunen and Nylander, 1960; Braestrup *et al.*, 1976; Hallgren, 1996; Broms, 1990, 2016; Shehata and Regan, 1989; Muttoni and Schwartz, 1991; Yankelevsky and Leibowitz, 1999; Bažant and Cao, 1987; Muttoni and Fernández Ruiz, 2008; *fib*, 2001; Regan and Braestrup, 1985). One of the models that probably most inspired other researchers was the one proposed by Kinnunen and Nylander (1960) (briefly introduced in Chapters 4 and 5). In agreement with the main ideas of Kinnunen and Nylander (1960), Muttoni and Schwartz (1991) developed a theory whose theoretical principles are applicable for both shear and punching shear of reinforced concrete members without transverse reinforcement, the so-called Critical Shear Crack Theory (reviewed in Chapter 4; Muttoni *et al.*, 2017c). According to the principles of this theory applied to punching failures, the inclined concrete strut which carries shear in the vicinity of the column is disturbed by the formation and propagation of a tangential crack with flexural origin (the so-called critical shear crack), refer to Figure 1.3 (Muttoni, 2008; Muttoni and Fernández Ruiz, 2010). In the framework of the CSCT, the punching strength and associated deformation capacity are determined by the intersection of the load-deformation relationship of the slab and the failure criterion, refer to Figure 1.3. The former relationship describes the behaviour of the slab, that is, the crack opening associated with a given level of applied load. The latter relationship defines the maximum shear strength that can be transferred for a given crack opening. It thus results that the punching strength is influenced by the crack opening of the critical shear crack, with lower punching strengths associated to larger crack openings (Muttoni, 2008).

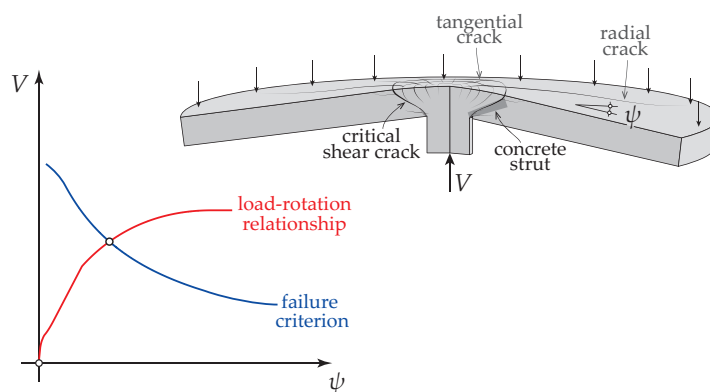


Figure 1.3: Calculation of punching strength according to the Critical Shear Crack Theory (Muttoni, 2008).

Since Aurelio Muttoni was appointed as Professor and head of the Structural Concrete Laboratory at École Polytechnique Fédérale de Lausanne (EPFL) in 2000, punching shear has been one of the main topics of research of this group. The works on this field were mainly focused on the validation and extension of the Critical Shear Crack Theory (CSCT). The first work on this topic was carried out by Guandalini (2005), who performed an extensive experimental programme to investigate the strain- and size-effects (large deformations and large members). The experimental results allowed the validation of the CSCT hyperbolic failure criterion (established in terms of punching strength as a function of the rotation of the slab) already presented in 2003 (Muttoni, 2003) and later published by Muttoni (2008) with an extensive testing validation. Guandalini (2005) also studied the flexural behaviour of axisymmetric slab-column connections by means of a numerical procedure based on the compatibility and equilibrium conditions of a slab sector, allowing the integration of sophisticated moment-curvature relationships.

The PhD thesis of Guandalini (2005) was followed by a series of other thesis focusing on specific subjects related to the punching shear behaviour and strength of slab-column connections and published between 2010 and 2012 (Guidotti, 2010; Mirzaei, 2010; Tassinari, 2011; Lips, 2012; Clément, 2012). Guidotti (2010) investigated the different failure modes of slab-column connections with column loads by combining the theory of plasticity and the CSCT, eventually obtaining an interaction diagram allowing the identification of the several failure regimes (flexural failure, crushing of the slab-column joint or punching shear). Guidotti (2010) based his works on a fully mechanical model to calculate the punching strength of slab-column connections. This model was developed consistently with the principles of the CSCT, thus supporting theoretically the semi-empirical failure criterion previously proposed by Muttoni (2008) and experimentally validated by Guandalini (2005). Mirzaei (2010) investigated the post-punching behaviour, performing an experimental campaign and proposing a specific mechanical model for these cases. Tassinari (2011) extended the application of the CSCT for punching shear failures in cases of asymmetric distribution of shear stresses in the shear-critical region. In addition, Tassinari (2011) dealt also with the cases of slab-column connections with bent-up bars. The case of punching shear of slab-columns connections with transverse reinforcement has been studied by Lips (2012), who performed an experimental campaign where the transverse reinforcement ratio, the shear reinforcement system and the column size were the main investigated variables. The punching shear strength of prestressed slabs has been studied by Clément (2012), who carried out a series of experimental tests where the effects of prestressing (in-plane forces and prestressing moments) were analyzed separately. In addition, Clément (2012) extended the mechanical model of Guidotti (2010) to the case of slabs with in-plane forces.

More recently, Einpaul (2016) performed an experimental campaign of slab-column connections without transverse reinforcement where the slenderness and the column size were varied. Einpaul (2016) investigated also the behaviour of continuous flat slabs, thus allowing for the calculation of the punching strength accounting for the potential effects of slab continuity and membrane action. Within the framework of the CSCT, Einpaul (2016) proposed an improvement of the simplified load-rotation relationship to account for the previously mentioned effects, therefore allowing its simple application in practice. Drakatos (2016) investigated the case of slab-column connections subjected to seismic actions. Still with respect to the punching strength of slab-column connections, Brantschen (2016) investigated also the influence of anchorage and bond of transverse reinforcement in the punching strength of failures occurring within the shear reinforced region.

In addition to the various PhD thesis previously mentioned, various works of collaborators of EPFL and abroad validating and extending the application of the mechanical model of CSCT have been published in the last fifteen years. The failure criterion has been shown to be applicable for punching shear of slabs without transverse reinforcement in a wide range of geometrical and material properties (Guandalini *et al.*, 2009; Mamede *et al.*, 2013; Inácio *et al.*, 2015; Einpaul *et al.*, 2016c; Fernández Ruiz and Muttoni, 2017), non-symmetric punching shear (Sagasetta *et al.*, 2011, 2014), punching shear of continuous slabs (Einpaul *et al.*, 2015, 2016b), punching shear of slabs with column loads (Guidotti *et al.*, 2011), punching shear due to impact loading (Micallef *et al.*, 2014) or seismic action (Drakatos *et al.*, 2016). In addition, the CSCT has been further extended to other cases such as slabs with transverse reinforcement (Fernández Ruiz and Muttoni, 2009; Lips *et al.*, 2012; Einpaul *et al.*, 2016a), fibre reinforced concrete slabs (Maya *et al.*, 2012; Gouveia *et al.*, 2014), slabs with post-installed shear reinforcement (Fernández Ruiz *et al.*, 2010; Inácio *et al.*, 2012) or externally bonded fibre reinforced polymers (Faria *et al.*, 2014) and, still, prestressed slabs (Clément *et al.*, 2013; Clément *et al.*, 2014). Moreover, due to the generality of the CSCT to deal with punching shear failures under different conditions, this the-

ory provides nowadays the theoretical basis of the punching shear provisions included in the SIA 262 (2013) and *fib* Model Code 2010 (Muttoni and Fernández Ruiz, 2010; Muttoni *et al.*, 2013).

Footings and their analogies and differences with flat slabs were some topics within the field of punching shear which have not been deeply addressed before in the framework of the CSCT, even if some studies focusing on the applicability of the *fib* Model Code 2010 to footings have been presented (Siburg *et al.*, 2014; Bonić *et al.*, 2017). This thesis is aimed at developing new knowledge in this field as well as at the manner how CSCT can handle both cases. Finally, a general mechanical model based on the theoretical principles of CSCT, consisting on the improvement of the mechanical models presented by Guidotti (2010) and Clément (2012), is developed for the case of slender slabs, being its extension for the cases of prestressed slabs and reinforced concrete footings also discussed. The thesis results and models are also supported by a specific testing programme whose results allow understanding why the theory is applicable both to squat and slender members.

### 1.4 Objectives of the thesis

Following the context above described, the main objectives of this work are to:

- Contribute with new experimental data on the punching strength of full scale reinforced concrete footings;
- Increase the knowledge on the punching behaviour of reinforced concrete footings by means of detailed experimental measurements;
- Investigate the strength of reinforced concrete footings by means of limit analysis methods;
- Review the principles of the Critical Shear Crack Theory for punching shear failures of slender and squat members without transverse reinforcement;
- Show how the principles of Critical Shear Crack Theory can be applied to deal with the case of squat members;
- Develop closed-form solutions to calculate the punching shear strength and deformation capacity based on the CSCT;
- Validate the closed-form expressions analytically derived for both slender and squat members with databases containing recent experimental programmes;
- Develop a refined mechanical model consistent with the theoretical principles of the CSCT, allowing the theoretical validation of its simplified failure criteria for punching shear failures and associated main hypotheses;
- Investigate the application of the theoretical principles of the CSCT for punching shear failures of prestressed slabs and reinforced concrete footings by applying the developed refined mechanical model.

## 1.5 Structure of the thesis

This document is a compilation of four published scientific journal articles together with an additional chapter. Hence, in addition to the Introduction, this thesis includes six chapters as described below:

- *Chapter 2* presents an article published in the scientific journal *Structural Concrete* (Simões *et al.*, 2016a). This chapter presents an experimental campaign on the punching shear behaviour and strength of compact and isolated reinforced concrete footings. The influence of each of the investigated parameters is described and, based on detailed experimental measurements, the phenomenological behaviour of reinforced concrete footings is discussed.
- *Chapter 3* presents an article published in the scientific journal *Engineering Structures* (Simões *et al.*, 2016c). In this chapter the upper bound theorem of limit analysis is applied to investigate on the strength, governing regimes and corresponding failures modes of reinforced concrete footings without transverse reinforcement. Limit analysis, which consists on the theory commonly used for flexural design, is used to show from the theoretical point of view that a significant flexural-shear interaction occurs in reinforced concrete footings. In addition, a comparison between theoretical and experimental results available in the scientific literature (Dieterle, 1987; Dieterle and Rostásy, 1987; Hallgren *et al.*, 1998) is presented.
- *Chapter 4* presents an article published in the scientific journal *Structural Concrete* (Muttoni *et al.*, 2017c). This chapter presents a review of the Critical Shear Crack Theory for punching shear failures of members without transverse reinforcement. The theoretical principles of the theory are presented and discussed. The transition between limit analysis and the CSCT is discussed. Furthermore, it is explained how the CSCT handles the punching shear failures of both slender and squat reinforced concrete members. In addition, the fourth chapter presents also the analytical derivation and validation against experimental results of closed-form solutions for the punching shear design of members without transverse reinforcement based on the principles of the mechanical model of the CSCT.
- *Chapter 5* presents an article published in the scientific journal *Structural Concrete* (Simões *et al.*, 2018) where a general mechanical description of punching shear failures is presented supported on recent detailed experimental measurements available in the scientific literature. On that basis, a refined mechanical model is formulated for slender slabs consistently with the principles of the Critical Shear Crack Theory. A very good agreement is obtained between the experimental and the theoretical results. The mechanical model is also shown to provide relevant information with respect to the role of the parameters influencing the punching strength of slabs. In addition, the results of the mechanical model not only validate the analytical failure criterion of the CSCT but also corroborate its main hypotheses.
- *Chapter 6* presents a discussion on the potential extension of the mechanical model presented in Chapter 5 for the case of prestressed slabs and reinforced concrete footings. The extension of the mechanical model for prestressed slabs is shown to be simple and mechanically consistent with the experimental observations. With respect to the footings, an adaptation of the load-rotation relationship presented by Muttoni (2008) is proposed and compared with the experimental results of Chapter 2. Eventually, a possible extension of the calculation of the refined failure criterion presented in Chapter 5 for reinforced concrete footings is discussed and validated against experimental results.
- *Chapter 7* summarizes the main conclusions of this thesis and discusses topics for future research.

Although Chapters 2 to 5 are scientific journal articles, the numbering of the figures, tables and equations was modified to respect the layout of the present document. Also the font type and size of the figures of the mentioned chapters were adjusted to consistently agree with the layout of this document. In addition, by being a thesis compiling different journal articles, every chapter includes its own sections of Notation, References and Appendix.

It is worth to mention that although the present document does not include any chapter solely dedicated to the state of the art, every chapter includes its own brief presentation of the works supporting and inspiring the research. Detailed descriptions of other models as well as experimental works dealing with punching shear failures of members without transverse reinforcement is out of the scope of this thesis. State-of-the-art and technical reports compiling such information are available in the scientific literature (e.g Regan and Braestrup, 1985; *fib*, 2001; Polak, 2005; *fib*, 2017) and can be consulted for that purpose.

### 1.6 Scientific contributions of the thesis

The main scientific contributions of the thesis are listed below:

- To contribute with additional experimental data on full scale members tested under realistic conditions and including detailed experimental measurements to improve the knowledge on the phenomenological punching shear behaviour of reinforced concrete footings;
- To investigate the strength of compact reinforced concrete footings without transverse reinforcement using the kinematical theorem of limit analysis, presenting a more general solution than the one originally presented by Braestrup *et al.* (1976);
- To present a review of the CSCT for punching shear failures of members without transverse reinforcement;
- To show that the principles of CSCT can be successfully applied for both slender and squat members, thus validating the application of the CSCT for punching shear failures of squat reinforced concrete members without transverse reinforcement;
- To present the analytical development of closed-form design expressions to calculate both the punching strength and the rotation at failure based on the CSCT;
- To validate the application of closed-form design expressions of CSCT to calculate the punching strength of both slender and squat members by comparing with recent databases of experimental tests;
- To propose a refined mechanical model for slender slabs without transverse reinforcement based on recent experimental findings and supported on the theoretical principles of Critical Shear Theory;
- To validate the simplified failure criterion of CSCT for punching shear failures of members without transverse reinforcement based on the developed refined mechanical model;
- To validate the application of the principles of the CSCT to investigate the punching strength of prestressed slabs and reinforced concrete footings without transverse reinforcement.

## 1.7 Limitations of the thesis

The present document deals with the case of axisymmetric punching shear failures of members without transverse reinforcement subjected to a concentric and monotonic loading. The extrapolation of the experimental results, theoretical considerations or mechanical models discussed in the present document to deal with punching failures occurring in different conditions than those previously stated (e.g. including non-axisymmetric distribution of shear forces; variable loading conditions; members with transverse reinforcement apart from the related observations in *Chapter 2*) is out of the scope of the present document.

## 1.8 List of publications

The publications composing *Chapter 2* to *Chapter 5* are the following:

**Simões J. T., Bujnak J., Fernández Ruiz M., and Muttoni A. (2016a):** „Punching shear on compact footings with uniform soil pressure“. *Structural Concrete*, Vol. 17, No. 4, pp. 603–617.

**Simões J. T., Faria D. V., Fernández Ruiz M., and Muttoni A. (2016c):** „Strength of reinforced concrete footings without transverse reinforcement according to limit analysis“. *Engineering Structures*, Vol. 112, pp. 146–161.

**Muttoni A., Fernández Ruiz M., and Simões J. T. (2017c):** „The theoretical principles of the critical shear crack theory for punching shear failures and derivation of consistent closed-form design expressions“. *Structural Concrete*, pp. 1–17. DOI: 10.1002/suco.201700088.

**Simões J. T., Fernández Ruiz M., and Muttoni A. (2018):** „Validation of the Critical Shear Crack Theory for punching of slabs without transverse reinforcement by means of a refined mechanical model“. *Structural Concrete*, pp. 1–26. DOI: 10.1002/suco.201700280.

Other publications of João Tiago Simões accomplished during the doctorate include:

**Simões J. T., Faria D. M. V., Fernández Ruiz M., and Muttoni A. (2015):** „Limit Analysis for Punching Shear Design of Compact Slabs and Footings“. In: *fib 2015 Symposium, Concrete - Innovation and Design*. Copenhagen, Denmark, p. 13.

**Simões J. T., Fernández Ruiz M., and Muttoni A. (2016b):** „Punching shear strength and behaviour of compact reinforced concrete footings“. In: *11<sup>th</sup> fib International PhD Symposium in Civil Engineering*. Tokyo, Japan, pp. 649–656.

**Muttoni A., Fernández Ruiz M., and Simões J. T. (2017a):** „A discussion on the development of the delamination of concrete cover in the soffit of the slab“. *Structure Magazine - Special Section: Tall buildings*. June, pp. 70–71.

**Muttoni A., Fernández Ruiz M., Simões J. T., Hegger J., Siburg C., and Kueres D. (2017b):** *Background document for section 8.4: Punching*. Tech. rep. EPFL/RTWH - 17-01-R5. November 30<sup>th</sup>, p. 30.

## 1.9 References

- Bažant Z. P.; Cao Z. (1987):** „Size Effect in Punching shear Failure of Slabs“. *ACI Structural Journal*, Vol. 84, No. 1, pp. 44–53.
- Bonić Z.; Davidović N.; Vacev T.; Romić N.; Zlatanović E.; Savic J. (2017):** „Punching Behaviour of Reinforced Concrete Footings at Testing and According to Eurocode 2 and *fib* Model Code 2010“. *International Journal of Concrete Structures and Materials*, Vol. 11, No. 4, pp. 657–676.
- Braestrup M. W.; Nielsen M. P.; Jensen B. C.; Bach F. (1976):** *Axisymmetric Punching of Plain and Reinforced Concrete*. Tech. rep. 75. Structural Research Laboratory, Technical University of Denmark, p. 33.
- Brantschen F. (2016):** „Influence of bond and anchorage conditions of the shear reinforcement on the punching strength of RC slabs“. PhD thesis. Lausanne, Switzerland: EPFL, p. 186.
- Broms C. E. (1990):** „Punching of flat plates - a question of concrete properties in biaxial compression and size effect“. *ACI Structural Journal*, Vol. 87, No. 3, pp. 292–304.
- Broms C. E. (2005):** „Concrete flat slabs and footings: Design method for punching and detailing for ductility“. PhD thesis. Stockholm, Sweden: Department of Structural Engineering, Royal Institute of Technology, p. 114.
- Broms C. E. (2016):** „Tangential strain theory for punching failure of flat slabs“. *ACI Structural Journal*, Vol. 113, No. 1, pp. 95–104.
- Clément T. (2012):** „Influence de la précontrainte sur la résistance au poinçonnement de dalles en béton armé“. PhD thesis. Lausanne, Switzerland: EPFL, p. 224.
- Clément T.; Ramos A. M. P.; Fernández Ruiz M.; Muttoni A. (2013):** „Design for punching of pre-stressed concrete slabs“. *Structural Concrete*, Vol. 14, No. 2, pp. 157–167.
- Clément T.; Ramos A. P.; Fernández Ruiz M.; Muttoni A. (2014):** „Influence of prestressing on the punching strength of post-tensioned slabs“. *Engineering Structures*, Vol. 72, pp. 56–69.
- Dieterle H. (1987):** „Design of reinforced concrete foundations of square columns under centric loading with the help of design diagrams (In German: Zur Bemessung quadratischer Stützenfundamente aus Stahlbeton unter zentrischer Belastung mit Hilfe von Bemessungsdiagrammen)“. *Deutscher Ausschuss für Stahlbeton*, Vol. 387, pp. 94–134.
- Dieterle H.; Rostásy F. (1987):** „Load-carrying behaviour of isolated reinforced concrete foundations of square columns (In German: Tragverhalten quadratischer Einzelfundamente aus Stahlbeton)“. *Deutscher Ausschuss für Stahlbeton*, Vol. 387, pp. 1–91.
- Dieterle H.; Steinle A. (1981):** „Reinforced Concrete Block Foundations (In German: Blockfundamente für Stahlbetonfertigtstützen)“. *Deutscher Ausschuss für Stahlbeton*, Vol. 326, pp. 1–49.
- Drakatos I. S. (2016):** „Seismic behaviour of slab-column connections without transverse reinforcement“. PhD thesis. Lausanne, Switzerland: EPFL, p. 196.
- Drakatos I.-S.; Muttoni A.; Beyer K. (2016):** „Internal slab-column connections under monotonic and cyclic imposed rotations“. *Engineering Structures*, Vol. 123, pp. 501–516.
- Einpaul J. (2016):** „Punching strength of continuous flat slabs“. PhD thesis. Lausanne, Switzerland: EPFL, p. 209.
- Einpaul J.; Fernández Ruiz M.; Muttoni A. (2015):** „Influence of moment redistribution and compressive membrane action on punching strength of flat slabs“. *Engineering Structures*, Vol. 86, pp. 43–57.

- Einpaul J.; Brantschen F.; Fernández Ruiz M.; Muttoni A. (2016a):** „Performance of Punching Shear Reinforcement under Gravity Loading: Influence of Type and Detailing“. *ACI Structural Journal*, Vol. 113, No. 4, pp. 889–900.
- Einpaul J.; Ospina C.; Fernández Ruiz M.; Muttoni A. (2016b):** „Punching shear capacity of continuous slabs“. *ACI Structural Journal*, Vol. 113, No. 4, pp. 861–872.
- Einpaul J.; Bujnak J.; Fernández Ruiz M.; Muttoni A. (2016c):** „Study on influence of column size and slab slenderness on punching strength“. *ACI Structural Journal*, Vol. 113, No. 1, pp. 135–145.
- Elstner R. C.; Hognestad E. (1956):** „Shearing strength of reinforced concrete slabs“. *ACI Journal Proceedings*, Vol. 53, No. 2, pp. 29–58.
- Faria D. M. V.; Lúcio V. J. G.; Ramos A. P. (2012):** „Post-punching behaviour of flat slabs strengthened with a new technique using post-tensioning“. *Engineering Structures*, Vol. 40, pp. 383–397.
- Faria D. M. V.; Einpaul J.; Ramos A. M. P.; Fernández Ruiz M.; Muttoni A. (2014):** „On the efficiency of flat slabs strengthening against punching using externally bonded fibre reinforced polymers“. *Construction and Building Materials*, Vol. 73, pp. 366–377.
- Fernández Ruiz M.; Muttoni A. (2009):** „Applications of the critical shear crack theory to punching of R/C slabs with transverse reinforcement“. *ACI Structural Journal*, Vol. 106, No. 4, pp. 485–494.
- Fernández Ruiz M.; Muttoni A. (2017):** „Size effect in shear and punching shear failures: differences between statically determinate members and redundant structures“. *Structural Concrete*, pp. 1–11. doi: 10.1002/suco.201700059.
- Fernández Ruiz M.; Muttoni A. (2017):** „Size effect on punching shear strength: Differences and analogies with shear in one-way slabs“. In: *Bulletin 81 / ACI SP-315: Punching shear test of structural concrete slabs: Honoring Neil M. Hawkins*. Ed. by Ospina C. E.; Mitchell D.; Muttoni A. Lausanne, Switzerland: International Federation for Structural Concrete, pp. 59–72.
- Fernández Ruiz M.; Muttoni A.; Kunz J. (2010):** „Strengthening of flat slabs against punching shear using post-installed shear reinforcement“. *ACI Structural Journal*, Vol. 107, No. 4, pp. 434–442.
- Fernández Ruiz M.; Mirzaei Y.; Muttoni A. (2013):** „Post-punching behavior of flat slabs“. *ACI Structural Journal*, Vol. 110, No. 5, pp. 801–812.
- fib (2001):** *Bulletin 12: Punching of structural concrete slabs*. Tech. rep. Lausanne, Switzerland: International Federation for Structural Concrete, p. 314.
- fib (2017):** *Bulletin 81 / ACI SP-315: Punching shear of structural concrete slabs: Honoring Neil M. Hawkins*. Tech. rep. Lausanne, Switzerland: International Federation for Structural Concrete, p. 378.
- fib Model Code 2010 (2013):** *Model Code 2010 - Final draft*. Tech. rep. Volumes 1 and 2, Bulletins 65 and 66. International Federation for Structural Concrete.
- Fürst A.; Marti P. (1997):** „Robert Maillart’s design approach for flat slabs“. *Journal of Structural Engineering*, Vol. 123, No. 8, pp. 1102–1110.
- Gasparini D. A. (2002):** „Contributions of C. A. P. Turner to Development of Reinforced Concrete Flat Slabs 1905–1909“. *Journal of Structural Engineering*, Vol. 128, No. 10, pp. 1243–1252.
- Gouveia N. D.; Fernandes N. A. G.; Faria D. F. M.; Ramos A. M. P.; Lúcio V. J. G. (2014):** „SFRC flat slabs punching behaviour – Experimental research“. *Composites: Part B*, Vol. 63, pp. 161–171.

- Guandalini S. (2005):** „Symmetric punching shear of reinforced concrete slabs (In French: Poinçonnement symétrique des dalles en béton armé)“. PhD thesis. Lausanne, Switzerland: EPFL, p. 289.
- Guandalini S.; Burdet O.; Muttoni A. (2009):** „Punching tests of slabs with low reinforcement ratios“. *ACI Structural Journal*, Vol. 106, No. 1, pp. 87–95.
- Guidotti R. (2010):** „Punching shear of slabs with column load (In French: Poinçonnement des planchers-dalles avec colonnes superposées fortement sollicitées)“. PhD thesis. Lausanne, Switzerland: EPFL, p. 189.
- Guidotti R.; Fernández Ruiz M.; Muttoni A. (2011):** „Crushing and Flexural Strength of Slab-Column Joints“. *Engineering Structures*, Vol. 33, No. 3, pp. 855–867.
- Hallgren M. (1996):** „Punching Shear Capacity of Reinforced High Strength Concrete Slabs“. PhD thesis. Stockholm, Sweden: Department of Structural Engineering, Royal Institute of Technology, p. 206.
- Hallgren M.; Bjerke M. (2002):** „Non-linear finite element analyses of punching shear failure of column footings“. *Cement and Concrete Composites*, Vol. 24, No. 6, pp. 491–496.
- Hallgren M.; Kinnunen S.; Nylander B. (1998):** „Punching shear tests on column footings“. *Nordic Concrete Research*, Vol. 21, pp. 1–22.
- Hegger J.; Sherif A.; Ricker M. (2006):** „Experimental Investigations on Punching Behaviour of Reinforced Concrete Footings“. *ACI Structural Journal*, Vol. 103, No. 4, pp. 604–613.
- Hegger J.; Ricker M.; Ulke M.; Ziegler M. (2007):** „Investigations on the punching behaviour of reinforced concrete footings“. *Engineering Structures*, Vol. 29, No. 9, pp. 2233–2241.
- Hegger J.; Ricker M.; Sherif M. (2009):** „Punching Strength of Reinforced Concrete Footings“. *ACI Structural Journal*, Vol. 106, No. 5, pp. 706–716.
- Inácio M.; Ramos A. P.; Lúcio V.; Faria D. V. (2015):** „Punching of high strength concrete flat slabs - Experimental investigation“. *Engineering Structures*, Vol. 103, pp. 275–284.
- Inácio M. M. G.; Ramos A. P.; Faria D. M. V. (2012):** „Strengthening of flat slabs with transverse reinforcement by introduction of steel bolts using different anchorage approaches“. *Engineering Structures*, Vol. 44, pp. 63–77.
- Kinnunen S.; Nylander H. (1960):** *Punching of Concrete Slabs Without Shear Reinforcement*. Tech. rep. 158. Stockholm, Sweden: Transactions of the Royal Institute of Technology, p. 112.
- Kordina K.; Nölting D. (1981):** *Load-carrying behaviour of eccentrically loaded isolated reinforced concrete foundations (In German: Tragverhalten von ausmittig beanspruchten Einzelfundamenten aus Stahlbeton)*. Tech. rep. DFG Research 204/27-30. Braunschweig, Germany: Technical University of Braunschweig, p. 158.
- Krakowski J.; Krawczyk L.; Urban T. (2015):** „Punching of RC Thick Plates - Experimental Test and Analysis“. In: *Proceedings of fib Symposium, Concrete - Innovation and Design*. Copenhagen.
- Kueres D.; Siburg C.; Reissen K.; Hegger J. (2013):** „Experimental and numerical investigations on the punching behavior of thick footings with and without shear reinforcement“. In: *Research and Applications in Structural Engineering, Mechanics and Computation*. Ed. by Zingoni A. London: Taylor & Francis Group, pp. 1543–1548.
- Kueres D.; Ricker M.; Hegger J. (2017a):** „Maximum punching shear capacity of footings with new punching shear reinforcement elements“. In: *Bulletin 81 / ACI SP-315: Punching shear test of structural concrete slabs: Honoring Neil M. Hawkins*. Ed. by Ospina C. E.; Mitchell D.; Muttoni A. Lausanne, Switzerland: International Federation for Structural Concrete, pp. 167–186.

- Kueres D.; Siburg C.; Herbrand M.; Clasen M.; Hegger J. (2017b):** „Uniform Design Method for punching shear in flat slabs and column bases“. *Engineering Structures*, Vol. 136, pp. 149–164.
- Li K. K. L. (2000):** „Influence of size on punching shear strength of concrete slabs“. MA thesis. McGill University, Department of Civil Engineering and Applied Mechanics, p. 78.
- Lips S. (2012):** „Punching of Flat Slabs with Large Amounts of Shear Reinforcement“. PhD thesis. EPFL, p. 217.
- Lips S.; Fernández Ruiz M.; Muttoni A. (2012):** „Experimental Investigation on Punching Strength and Deformation Capacity of Shear-Reinforced Slabs“. *ACI Structural Journal*, Vol. 109, No. 6, pp. 896–900.
- Maillart R. (1926):** „Zur Entwicklung der unterzuglosen Decke in der Schweiz und in Amerika“. *Schweizerische Bauzeitung*, Vol. 87, No. 21, pp. 263–267.
- Mamede N. F. S.; Ramos A. P.; Faria D. M. V. (2013):** „Experimental and parametric 3D nonlinear finite element analysis on punching of flat slabs with orthogonal reinforcement“. *Engineering Structures*, Vol. 48, pp. 442–457.
- Maya L. F.; Fernández Ruiz M.; Muttoni A.; Foster S. (2012):** „Punching shear strength of steel fibre reinforced concrete slabs“. *Engineering Structures*, Vol. 40, pp. 83–94.
- Micallef K.; Sagaseta J.; Fernández Ruiz M.; Muttoni A. (2014):** „Assessing punching shear failure in reinforced concrete flat slabs subjected to localised impact loading“. *International Journal of Impact Engineering*, Vol. 71, pp. 17–33.
- Mirzaei Y. (2010):** „Post-punching behavior of reinforced concrete slabs“. PhD thesis. Lausanne, Switzerland: EPFL, p. 230.
- Moe J. (1961):** *Shearing strength of reinforced concrete slabs and footings under concentrated loads*. Vol. D47. Skokie, Illinois: Portland Cement Association, Research and Development Laboratories.
- Muttoni A. (2003):** „Shear and punching strength of slabs without shear reinforcement (In German: Schubfestigkeit und Durchstanzen von Platten ohne Querkraftbewehrung)“. *Beton- und Stahlbetonbau*, Vol. 98, No. 2, pp. 74–84.
- Muttoni A. (2008):** „Punching shear strength of reinforced concrete slabs without transverse reinforcement“. *ACI structural Journal*, Vol. 105, No. 4, pp. 440–450.
- Muttoni A.; Fernández Ruiz M. (2008):** „Shear strength of members without transverse reinforcement as function of critical shear crack width“. *ACI Structural Journal*, Vol. 105, No. 2, pp. 163–172.
- Muttoni A.; Fernández Ruiz M. (2010):** „MC2010: the critical shear crack theory as a mechanical model for punching shear design and its application to code provisions“. In: *Bulletin 57: Shear and punching shear in RC and FRC elements*. Lausanne, Switzerland: International Federation for Structural Concrete, pp. 31–60.
- Muttoni A.; Fernández Ruiz M. (2010):** „Shear in slabs and beams: should they be treated in the same way?“ In: *Bulletin 57: Shear and punching shear in RC and FRC elements*. Lausanne, Switzerland: International Federation for Structural Concrete, pp. 105–128.
- Muttoni A.; Schwartz J. (1991):** „Behavior of beams and punching in slabs without shear reinforcement“. In: *IABSE Colloquium*. Vol. 62. International Association for Bridge and Structural Engineering. Stuttgart, Germany, pp. 703–708.

- Muttoni A.; Fernández Ruiz M.; Bentz E.; Foster S.; Sigrist V. (2013):** „Background to *fib* Model Code 2010 shear provisions - Part II: punching shear“. *Structural Concrete*, Vol. 14, No. 3, pp. 204–214.
- Muttoni A.; Fernández Ruiz M.; Simões J. T. (2017a):** „A discussion on the development of the delamination of concrete cover in the soffit of the slab“. *Structure Magazine - Special Section: Tall buildings*. June, pp. 70–71.
- Muttoni A.; Fernández Ruiz M.; Simões J. T.; Hegger J.; Siburg C.; Kueres D. (2017b):** *Background document for section 8.4: Punching*. Tech. rep. EPFL/RTWH - 17-01-R5. November 30<sup>th</sup>, p. 30.
- Muttoni A.; Fernández Ruiz M.; Simões J. T. (2017c):** „The theoretical principles of the critical shear crack theory for punching shear failures and derivation of consistent closed-form design expressions“. *Structural Concrete*, pp. 1–17. doi: 10.1002/suco.201700088.
- Netopilik R. J. (2012):** „Punching Shear Behaviour of Thick Reinforced Concrete Slabs“. MA thesis. University of Toronto, p. 243.
- Park H. G.; Choi K. K.; Chung L. (2011):** „Strain-based strength model for direct punching shear of interior slab-column connections“. *Engineering Structures*, Vol. 33, No. 3, pp. 1062–1073.
- Polak M. (2005):** *SP-232: Punching Shear in Reinforced Concrete Slabs*. Tech. rep. Farmington Hills, MI, USA: American Concrete Institute, p. 302.
- Regan P.; Braestrup M. W. (1985):** *Punching shear in reinforced concrete*. Tech. rep. 168. Comité Euro-International du Béton (CEB), p. 232.
- Regan P. E. (1986):** „Symmetric Punching of Reinforced Concrete Slabs“. *Magazine of Concrete Research*, Vol. 38, No. 136, pp. 115–128.
- Richart F. E. (1948):** „Reinforced Concrete Walls and Column Footings, part 1 and 2“. *ACI Journal*, Vol. 45, pp. 97–127 & 237–260.
- Ricker M. (2009):** „Reliability of punching design of isolated foundations (In German: Zur Zuverlässigkeit der Bemessung gegen Durchstanzen bei Einzelfundamenten)“. PhD thesis. RWTH, Aachen, p. 304.
- Sagaseta J.; Muttoni A.; Fernández Ruiz M.; Tassinari L. (2011):** „Non-axis-symmetrical punching shear around internal columns of RC slabs without transverse reinforcement“. *Magazine of Concrete Research*, Vol. 63, No. 6, pp. 441–457.
- Sagaseta J.; Tassinari L.; Fernández Ruiz M.; Muttoni A. (2014):** „Punching of flat slabs supported on rectangular columns“. *Engineering Structures*, Vol. 77, pp. 17–33.
- Shehata I. A.E. M.; Regan P. E. (1989):** „Punching in R. C. Slabs“. *Journal of Structural Engineering*, Vol. 115, No. 7, pp. 1726–1740.
- SIA 262 (2013):** *Code 262 for Concrete Structures*. Zürich, Switzerland: Swiss Society of Engineers and Architects.
- Siburg C. (2014):** „Consistent punching design in flat slabs and foundations (In German: Zur einheitlichen Bemessung gegen Durchstanzen in Flachdecken und Fundamenten)“. PhD thesis. RWTH, Aachen, p. 197.
- Siburg C.; Hegger J. (2014):** „Experimental Investigations on Punching Behaviour of Reinforced Concrete Footings with structural dimensions“. *Structural Concrete*, Vol. 15, No. 3, pp. 331–339.

- Siburg C.; Ricker M.; Hegger J. (2014):** „Punching shear design of footings: critical review of different code provisions“. *Structural Concrete*, Vol. 15, No. 4, pp. 497–508.
- Simões J. T.; Faria D. M. V.; Fernández Ruiz M.; Muttoni A. (2015):** „Limit Analysis for Punching Shear Design of Compact Slabs and Footings“. In: *fib 2015 Symposium, Concrete - Innovation and Design*. Copenhagen, Denmark, p. 13.
- Simões J. T.; Bujnak J.; Fernández Ruiz M.; Muttoni A. (2016a):** „Punching shear on compact footings with uniform soil pressure“. *Structural Concrete*, Vol. 17, No. 4, pp. 603–617.
- Simões J. T.; Fernández Ruiz M.; Muttoni A. (2016b):** „Punching shear strength and behaviour of compact reinforced concrete footings“. In: *11<sup>th</sup> fib International PhD Symposium in Civil Engineering*. Tokyo, Japan, pp. 649–656.
- Simões J. T.; Faria D. V.; Fernández Ruiz M.; Muttoni A. (2016c):** „Strength of reinforced concrete footings without transverse reinforcement according to limit analysis“. *Engineering Structures*, Vol. 112, pp. 146–161.
- Simões J. T.; Fernández Ruiz M.; Muttoni A. (2018):** „Validation of the Critical Shear Crack Theory for punching of slabs without transverse reinforcement by means of a refined mechanical model“. *Structural Concrete*, pp. 1–26. doi: 10.1002/suco.201700280.
- Talbot A. N. (1913):** „Reinforced Concrete Wall Footings and Column Footings“. *Engineering Experiment Station - University of Illinois*, Vol. 67, pp. 114.
- Tassinari L. (2011):** „Poinçonnement symétrique des dalles en béton armé avec armature de poinçonnement“. PhD thesis. Lausanne, Switzerland: EPFL, p. 197.
- Timm M. (2003):** „Punching of foundation slabs under axisymmetric loading (In German: Durchstanzen von Bodenplatten unter rotationssymmetrischer Belastung)“. PhD thesis. Braunschweig, Germany: Technische Universität Carolo-Wilhelmina zu Braunschweig, p. 159.
- Urban T.; Goldyn M.; Krakowski J.; Krawczyk L. (2013a):** „Experimental investigation on punching behaviour of thick reinforced concrete slabs“. *Archives of Civil Engineering*, Vol. 59, No. 2, pp. 157–174.
- Urban T.; Krakowski J.; Goldyn M.; Krawczyk L. (2013b):** *Punching of RC thick plates*. Tech. rep. 19. Poland: Department of Concrete Structures, Technical University of Lodz.
- Yankelevsky D. Z.; Leibowitz O. (1999):** „Punching shear in concrete slabs“. *International Journal of Mechanical Sciences*, Vol. 41, No. 1, pp. 1–15.



# Chapter 2

## *Paper I*

### **Punching shear tests on compact footings with uniform soil pressure**

This chapter is the postprint version of the article titled *Punching shear tests on compact footings with uniform soil pressure* published in Volume 4 (pages 603-617) of the journal *Structural Concrete* in 2016 (DOI: 10.1002/suco.201500175). The authors of this publication are João Tiago Simões (PhD Candidate), Jan Bujnak (Research and Development Manager in Peikko), Miguel Fernández Ruiz (Senior lecturer at EPFL and thesis director) and Aurelio Muttoni (Professor at EPFL and thesis director). The complete reference is the following:

**Simões J. T., Bujnak J., Fernández Ruiz M., and Muttoni A. (2016a):** „Punching shear on compact footings with uniform soil pressure“. *Structural Concrete*, Vol. 17, No. 4, pp. 603–617.

The 8 specimens composing the experimental programme presented in this article were tested in two phases. In the first one, specimens PP7 to PP9 were tested in IBETON as part of a private project financed by Peikko. The contribution of Dr. Jürgen Einpaul in the experimental work performed in the first phase is deeply acknowledged. The second phase, including 5 specimens (PS11 to PS15), was performed in the framework of this thesis.

The main contributions of João Tiago Simões to the creation of this article were the following:

- Preparation of specimens PS11 to PS15;
- Preparation of the setup for testing specimens PS11 to PS15;
- Preparation of the measuring systems used to record the behaviour of specimens PS11 to PS15;
- Analysis of the experimental results of specimens PS11 to PS15;
- Contribution to increase the understanding of the kinematics of compact reinforced concrete footings under uniform soil pressure;
- Production of the figures included in the article;
- Preparation of the manuscript of the article.

## 2.1 Abstract

Punching shear is usually the governing failure criterion when selecting the depth of reinforced concrete footings. Despite the fact that large experimental programmes aimed at the punching strength of slender flat slabs have been performed in the past, only a few experimental campaigns on full-scale compact reinforced concrete footings can be found in the literature. This paper presents the results of an experimental programme including eight reinforced concrete footings with a nominal thickness of 550 mm. These experiments investigated the influence of column size, member slenderness and the presence of compression and shear reinforcement. The tests were performed using an innovative test setup to ensure a uniform soil pressure. The experimental results show that slenderness influences the punching shear strength as well as the effectiveness of the shear reinforcement. The experiments also show that an important interaction occurs between bending and shear for high levels of shear force near the column (the typical case of compact footings or members with large amounts of shear reinforcement). Different continuous measurements recorded during the experimental tests allow a complete description of the kinematics and strains at failure. On that basis, experimental evidence is obtained showing that crushing of the concrete struts near the column is the phenomenon that triggers the punching failure of compact footings.

**Keywords:** experimental investigation, footings, punching shear strength, shear reinforcement, column size, shear slenderness, punching behaviour.

## 2.2 Introduction

Several experimental investigations regarding the punching shear behaviour of reinforced concrete footings have been performed in the past (Talbot, 1913; Richart, 1948; Kordina and Nölting, 1981; Dieterle and Rostásy, 1987; Dieterle, 1987; Hallgren *et al.*, 1998; Timm, 2003; Hegger *et al.*, 2006; Ricker, 2006; Hegger *et al.*, 2007, 2009; Ricker, 2009; Netopilik, 2012; Urban *et al.*, 2013a,b; Siburg and Hegger, 2014; Siburg, 2014; Krakowski *et al.*, 2015). They can be classified on the basis of the test setup, where four types can be distinguished. The first test setup refers to the cases where the footings were supported on a bed of springs and were loaded through a column stub (Talbot, 1913; Richart, 1948) (see Figure 2.1(a)). This arrangement may reproduce actual conditions for perfectly elastic soils, but the analysis of the results due to the non-uniform distribution of the reaction pressure (which depends on the deformations of the footings and varies during the test) is not straightforward. A second configuration often used consists of footings resting on line or concentrated supports, with the load being applied by a column stub or steel plate, see Figure 2.1(b) (Hallgren *et al.*, 1998; Timm, 2003; Netopilik, 2012; Urban *et al.*, 2013a,b; Krakowski *et al.*, 2015). A similar configuration, which is considered to be part of the same group, is the application of a finite number of concentrated loads at a certain distance from the column, which is fixed to a reaction frame. This configuration therefore presents two slightly different options: i) equal displacements and ii) equal force at the line of supports or concentrated loads. Although useful information for analysing the influence of different geometrical and mechanical properties can be obtained from this type of experimental test, both the inclination of the compression struts and the punching failure surface are geometrically defined by the test setup (the latter developing between the edge of the column and the inner radius of the supports). Therefore, in most of the tests on footings subjected to concentrated loads, the failure surface might not have developed in a completely free manner, instead being defined geometrically by the load arrangement.

As shown schematically in Figure 2.1(c), another test setup configuration currently used consists of applying an effective uniform loading replicated through the use of several load points (Kordina and Nölting, 1981; Dieterle and Rostásy, 1987; Dieterle, 1987; Hegger *et al.*, 2006; Ricker, 2006; Hegger *et al.*, 2007, 2009; Ricker, 2009; Siburg and Hegger, 2014; Siburg, 2014). These load points are supposed to represent the resultant of a uniform pressure in each sub-area. It should nevertheless be noted that if the distance between load points becomes large, these tests might also lead to a geometrical definition of the failure surface. In fact, this is an important issue when testing full-scale specimens with this configuration, since a finite number of load points has to be applied over a large surface. Recently, a more realistic configuration has been used (Hegger *et al.*, 2006; Ricker, 2006; Hegger *et al.*, 2007, 2009; Ricker, 2009), consisting of footings supported on sand and loaded through the column (see Figure 2.1(d)). The failure surface can develop freely in this configuration, but - similarly to the situation in the test configuration with footings supported on a bed of springs - soil pressure concentrations can occur. In addition, soil behaviour may be difficult to characterize and pressure measurements are needed in order to know the exact distribution of the soil reaction. Nevertheless, these tests represent a valuable experimental contribution, allowing the investigation of the soil-structure interaction.

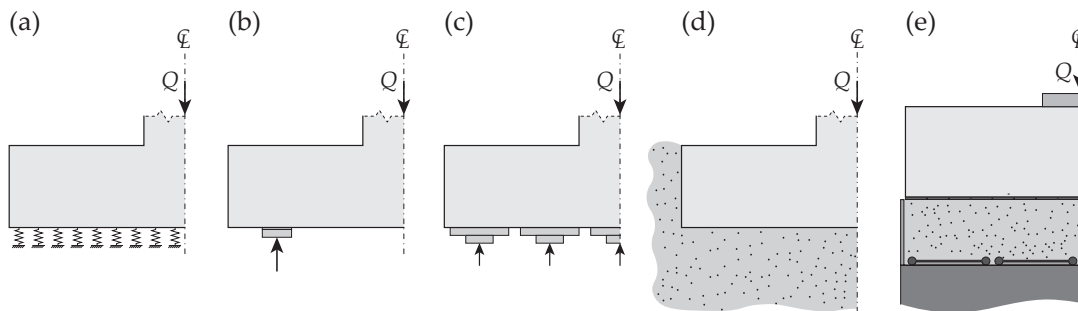


**Figure 2.1:** Typical test setup configurations used in experimental investigations of the punching shear strength of footings.

For the reasons discussed previously, few experimental full-scale tests under complete uniform soil pressure are available and more data is still needed. An experimental investigation of eight full-scale reinforced concrete footings with an innovative test setup is presented in this paper (Figure 2.1(e)). This setup enables the application of a uniform soil pressure to the bottom surface of the specimens. For that purpose, a group of flat jacks connected in series (equal pressure) was placed in the bottom of a rigid box, which was then filled with a layer of sand  $\sim 300$  mm deep, thus ensuring a uniform distribution of the load and, consequently, the application of a uniform soil pressure. A sheet of polytetrafluoroethylene (PTFE) and small aluminium plates were also placed between the footings and the layer of sand to reduce the friction between soil and footing. Some parameters were kept constant - nominal bottom flexural reinforcement ratio (0.75 %), nominal concrete compressive strength (30 MPa) and nominal thickness (550 mm) - and others varied. The parameters whose influence was investigated were: column size, footing side length (allowing variations in shear slenderness), the presence of shear reinforcement and the presence of horizontal reinforcement in the theoretical compression zone. With respect to the shear slenderness, in this paper it will be defined as the ratio between the clear shear span and the effective depth, where the effective clear shear span is defined as the distance between the edge of the footing and the edge of the column measured in the principal directions of the reinforcement (placed orthogonally).

Every test was tracked with several continuous measurements to allow an understanding of the kinematics and strains in the specimen. Four different behaviour regimes could be clearly distinguished and they are described in this paper.

## 2.3 Experimental programme

### 2.3.1 Specimens and materials

The footings were square with a side length of 2.12 m (PS11, PS12, PP7, PP8) or 1.59 m (PS13, PS14, PS15, PP9). The columns used were also square with a side length of 0.30 m (PS11, PS13, PS14, PS15, PP7, PP9) or 0.45 m (PS12, PP8). The bottom flexural reinforcement was arranged orthogonally and its nominal reinforcement ratio was kept constant for all eight specimens (ratio of 0.75 %, 22 mm diameter bars at a constant spacing of 100 mm, see Figure 2.2). Horizontal reinforcement in the top face (theoretical compression surface) was also used, but only for some specimens (footings PS14 and PS15 had no top reinforcement). When provided, the compression reinforcement was kept constant (with a ratio of 0.39 %, consisting of 16 mm diameter bars at a constant spacing of 100 mm). Both bottom and top reinforcement was bent near the edges (Figure 2.2). The nominal cover was 20 mm.

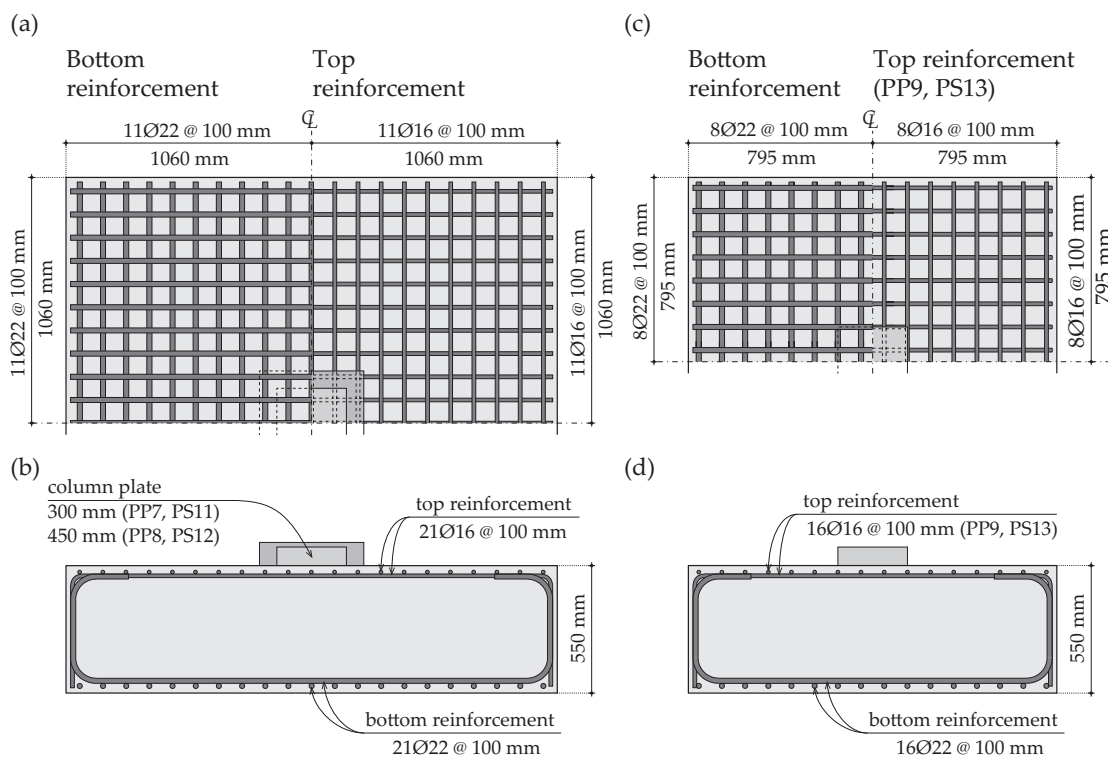


**Figure 2.2:** Plan and section view of layout of flexural reinforcement: (a) and (b) PS11, PS12, PP7, PP8; (c) and (d) PS13, PS14, PS15 and PP9.

Footings PP7, PP8, PP9 and PS15 had shear reinforcement consisting of 25 mm diameter double-headed shear studs in a radial arrangement. The layout of the shear reinforcement for each footing is presented in Figure 2.3: PP7 had three perimeters with 16 studs, PP8 three perimeters with 20 studs and PP9 and PS15 two perimeters with 16 studs. In order to ensure the correct positions of the studs, steel strips ( $800 \times 30 \times 4$  mm for PP7 and PP8, and  $550 \times 30 \times 4$  mm for PP9 and PS15) were welded to the heads of the studs and the position of the flexural reinforcement was adjusted slightly where necessary.

The concrete used in all footings was of normal strength (nominal concrete compressive strength of 30 MPa) with a maximum aggregate size of 16 mm. Concrete cylinders (320 mm high, 160 mm diameter) were cast, tested and used to verify the concrete strength. Ordinary reinforcing steel with a characteristic yield strength of 500 MPa was used in all the footings for both flexural and shear reinforcement.

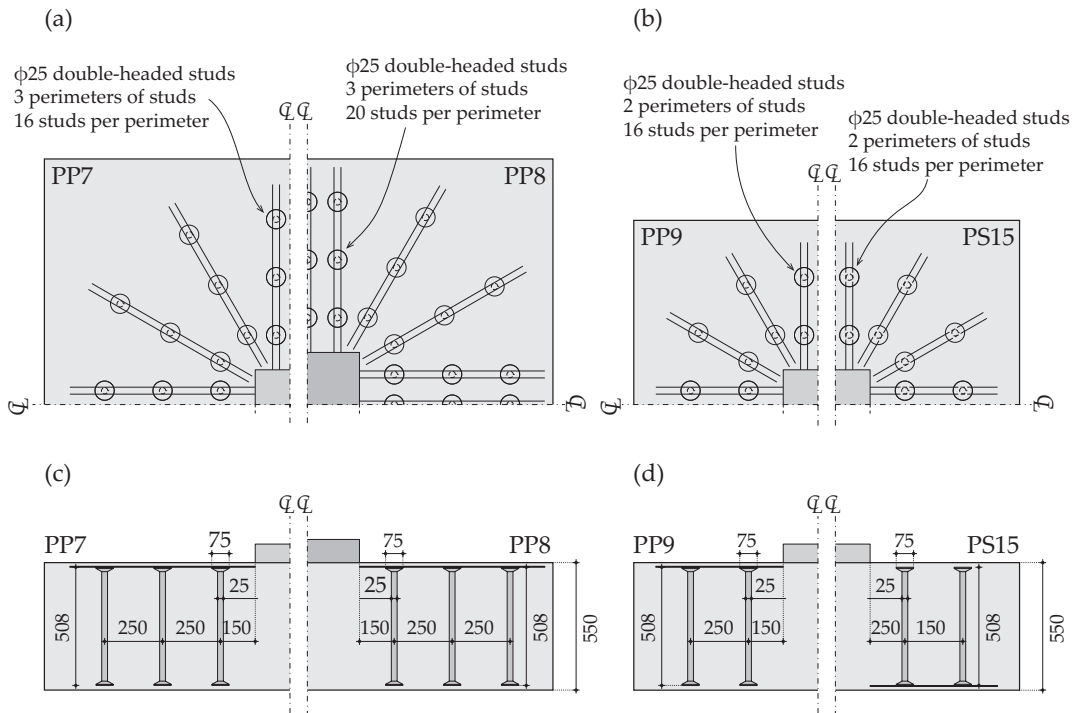


Figure 2.3: Layout of shear reinforcement: (a) plan of PP7 and PP8, (b) plan of PP9 and PS15, (c) section through PP7 and PP8, and (d) section through PP9 and PS15.

Its corresponding mechanical properties were measured on three different samples of each different diameter. The cylinder concrete compressive strength on the day of the punching tests and the yield strength of the reinforcement for each specimen can be found in Table 2.1.

Table 2.1: Main properties of experimental investigation ( $B$  refers to the side length of the square footing;  $c$  is the side length of the square column;  $d$  is the effective depth;  $a$  is the shear span defined as  $(B - c)/2$ ;  $\rho$  is the flexural reinforcement ratio;  $f_y$  is the yielding strength of flexural reinforcement;  $f_c$  is the concrete compressive strength measured in cylinders;  $n_s$  is the number studs per perimeter;  $n_p$  is the number of perimeters of studs;  $\phi_w$  is the diameter of the studs;  $f_{yw}$  is the yielding strength of the studs).

Specimen	$B$ [mm]	$c$ [mm]	$d$ [mm]	$a/d$ [-]	$c/d$ [-]	$\rho$ [%]	$f_y$ [MPa]	$f_c$ [MPa]	$n_s$	$n_p$	$\phi_w$ [mm]	$f_{yw}$ [MPa]
PS11	2.12	0.3	0.509	1.79	0.59	0.74	517	29.5	—	—	—	—
PS12	2.12	0.45	0.512	1.63	0.88	0.735	517	31.1	—	—	—	—
PS13	1.59	0.3	0.506	1.27	0.59	0.756	517	32.1	—	—	—	—
PS14	1.59	0.3	0.51	1.26	0.59	0.75	537	31.9	—	—	—	—
PP7	2.12	0.3	0.497	1.83	0.6	0.758	580	33.7	16	3	25	567
PP8	2.12	0.45	0.51	1.64	0.88	0.738	580	34.5	20	3	25	567
PP9	1.59	0.3	0.516	1.25	0.58	0.741	580	34.8	16	2	25	567
PS15	1.59	0.3	0.511	1.26	0.59	0.749	537	32.2	16	2	25	578

### 2.3.2 Test setup and experimental procedure

The test setup is shown in Figure 2.4. It consisted of a loading system under the footing and a reaction frame above it (also used as a loading system in some cases). The loading system under the footing consisted of a box containing a group of flat jacks hydraulically connected with a copper tube (16 jacks for the larger specimens, nine for the smaller ones). The flat jacks were square with a side length of 500 mm and a nominal height of 55 mm. An electric pump was used to introduce water into the group

of flat jacks to inflate them. The application of a uniform pressure to the bottom surface of the footing was ensured through the introduction of a layer of sand between it and the flat jacks (compensating for the gaps between their effective areas). The sand was confined laterally by the faces of a box made from four steel channel sections. A sheet of PTFE was placed between the sand and the lateral surfaces of the box, thus avoiding that the uplift of the sand would be constrained by friction. A gap of approx. 20 mm was additionally left between the lateral surfaces of the footing and the lateral surfaces of the box to allow expansion of the bottom surface of the footing. In order to reduce friction between the sand and the specimen, a sheet of PTFE and aluminium plates ( $130 \times 130 \times 5$  mm) were placed between them.

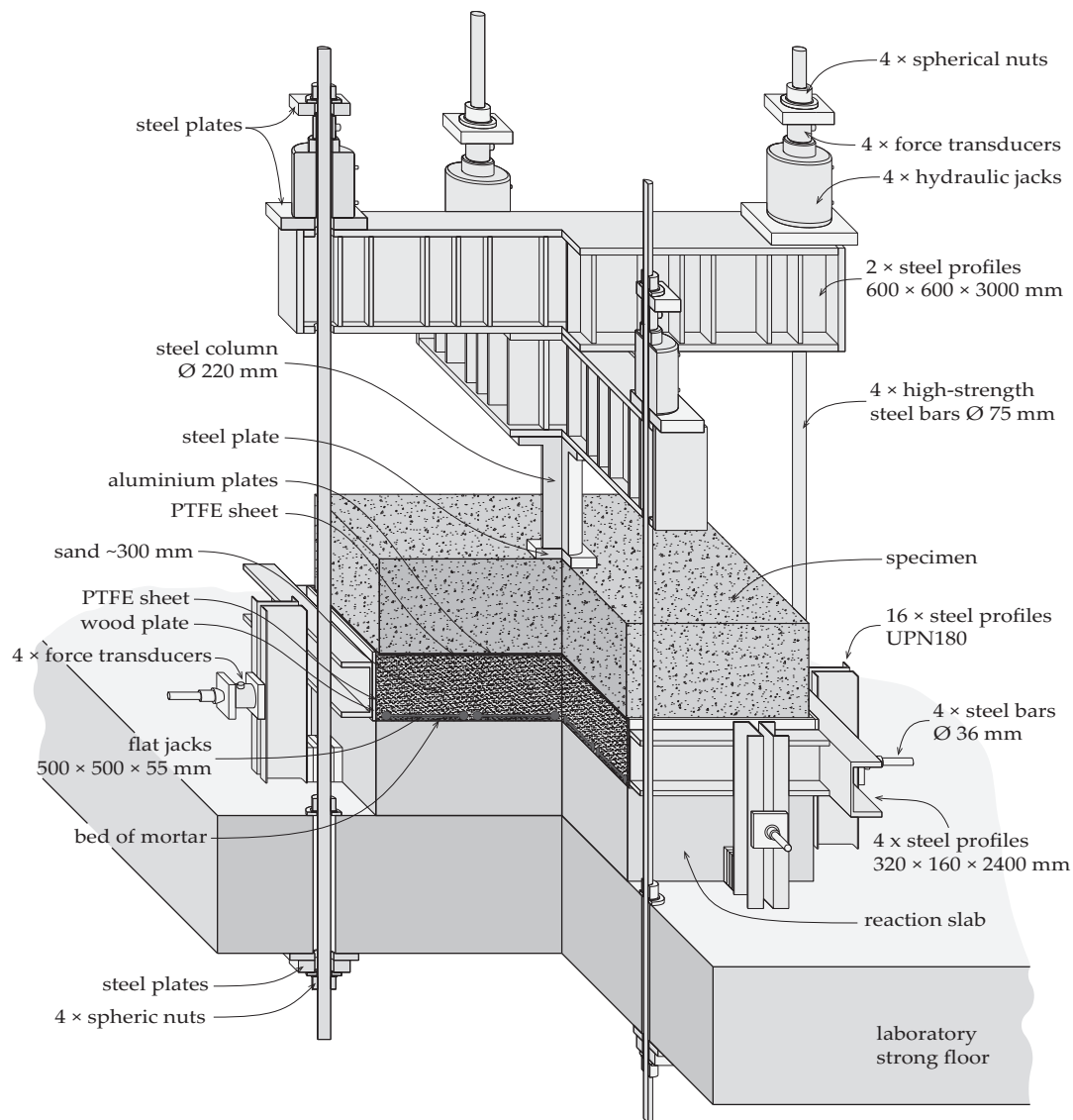


Figure 2.4: Schematic representation of test setup.

The reaction frame above the footing consisted of two perpendicular steel beams connected to a high-strength steel column. The two steel beams were fixed to the strong floor of the laboratory with four high-strength  $\text{Ø } 75$  mm threaded bars. The column was simulated by a square steel plate placed between the footing and the high-strength steel column. A thin layer of plaster was placed between the steel column plate and the specimens in order to avoid any local stress concentrations.

For specimens PP7 and PP8, the entire load was applied through the loading system under the footing. For the remaining tests, four hydraulic jacks were placed on top of the reaction frame. These jacks were used to apply part of the load at the beginning of the test, thus reducing the necessary deformation of the flat jacks.

With respect to the experimental procedure, a loading rate of 50 kN/min was applied. Load steps were used during the loading of specimens PP7 to PP9 and PS11 to PS13 to perform measurements whose results are beyond the scope of this paper.

### 2.3.3 Measurement devices

A general overview of the main measurement devices is shown in Figure 2.5. The applied force was measured with four load cells placed on top of the reaction frame, four strain gauges placed on the steel column with the oil pressure measured in the hydraulic jacks (placed on the top of the reaction frame) and with the water pressure measured in the flat jacks under the sand bed. Negligible differences were observed between the different devices.

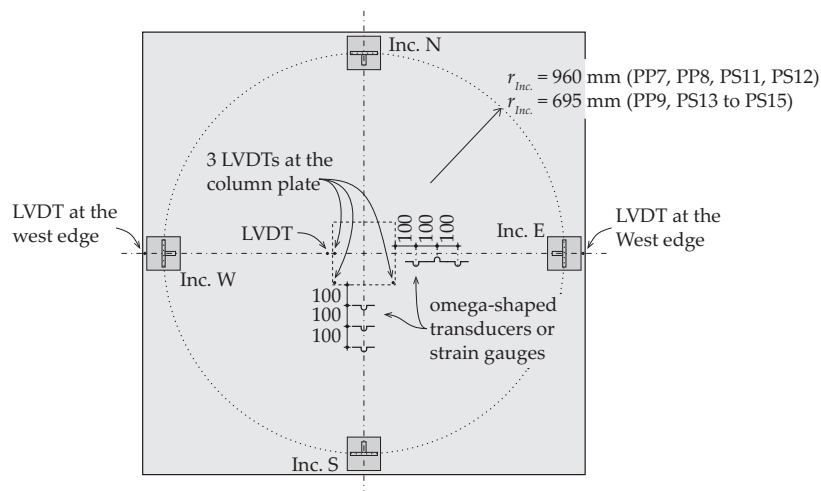


Figure 2.5: Schematic representation of the main measurement devices and their locations.

The footing rotation was measured on the top surface of the footing with four inclinometers aligned with the axis and placed 100 mm from the edge of the footing. The strains at the concrete top surface were measured in radial and tangential directions with the help of three omega-shaped gauges (PP7 to PP9, PS11 to PS13) or strain gauges (PP14 and PS15) with a base length of 100 mm. Vertical displacements were also measured at different locations on the top surface with linear variable differential transformers (LVDT), notably at the edges of the footing aligned with the axis. Three LVDTs were also placed on the steel column plate, enabling the calculation of the vertical displacement at its centre.

The changes in the thickness of the footing were also measured in specimens PS11 to PS15 at different distances from the column edge. The strains in the bottom flexural reinforcement of specimen PS12 were measured at different locations using strain gauges with a base length of 6 mm. Deformations of double-headed shear studs were measured using the same strain gauges. The expansion of the top and south lateral surfaces of specimens PS14 and PS15 was measured with LVDTs, as will be described later.

## 2.4 Experimental results

### 2.4.1 Main results

The main results of the experimental campaign are presented in Table 2.2. After testing, cracking was observed on the bottom surface, regularly spaced and coincident with the location of the reinforcing bars in both directions (see, for instance, Figure 2.6). To investigate the tangential cracking and punching cone, the specimens were sawn along (at least) the weak axis (axis with smaller effective depth of reinforcement).

**Table 2.2:** Results of experimental investigation ( $Q_{R,with}/Q_{R,without}$  refers to the ratio of strengths of the corresponding specimens with and without shear reinforcement).

Specimen	$Q_R$ [MN]	$Q_{flex}$ [MN]	$\frac{Q_R}{Q_{flex}}$	$\frac{Q_R}{d^2 \cdot \sqrt{f_c}}$ [ $\sqrt{\text{MPa}}$ ]	$\frac{Q_{R,with}}{Q_{R,without}}$
PS11	4.769	10.059	0.474	3.389	–
PS12	6.839	12.065	0.567	4.678	–
PS13	6.285	11.422	0.55	4.333	–
PS14	5.896	11.421	0.516	4.013	–
PP7	7.651	11.014	0.695	5.336	1.57
PP8	10.868 <sup>1</sup>	13.469	0.807 <sup>1</sup>	7.114 <sup>1</sup>	1.52 <sup>1</sup>
PP9	9.02	13.054	0.691	5.743	1.33
PS15	8.26	11.363	0.727	5.575	1.39

<sup>1</sup> Experimental test stopped due to large deformations

The cracking patterns observed are presented in Figure 2.7 (where the punching cone can be clearly seen). The specimens with shear reinforcement (PP7, PP9 and PS15) failed in punching inside the shear-reinforced zone by crushing of the concrete struts near the loading plate. The test on specimen PP8 with shear reinforcement was stopped after large plastic deformations. Nevertheless, shear cracks can be very clearly seen, indicating that a punching failure was probably about to occur.

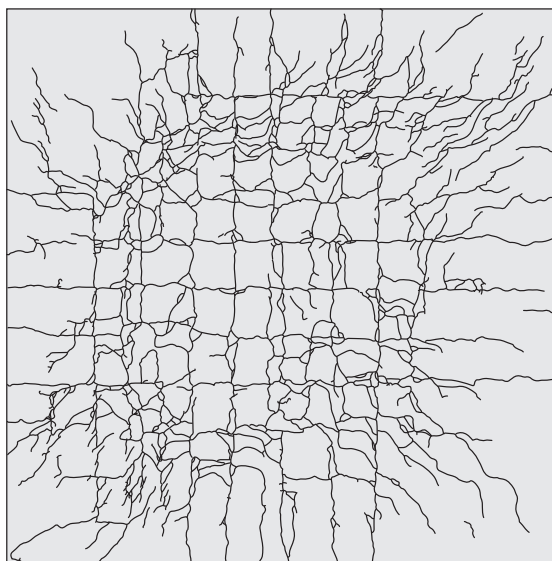


**Figure 2.6:** Schematic representation of cracking pattern on bottom surface of specimen PS14 after testing.

On the basis of the saw-cuts (Figure 2.7), failure can be associated with the crushing observed along the failure surface, notably, close to the column (where various parallel cracks appear). The specimens with shear reinforcement exhibited a more ductile failure than those without shear reinforcement. With the exception of specimen PP8, every footing with transverse reinforcement presented a clear crushing failure characterized by the development of a failure surface between the edge of the column and the first perimeter of studs.

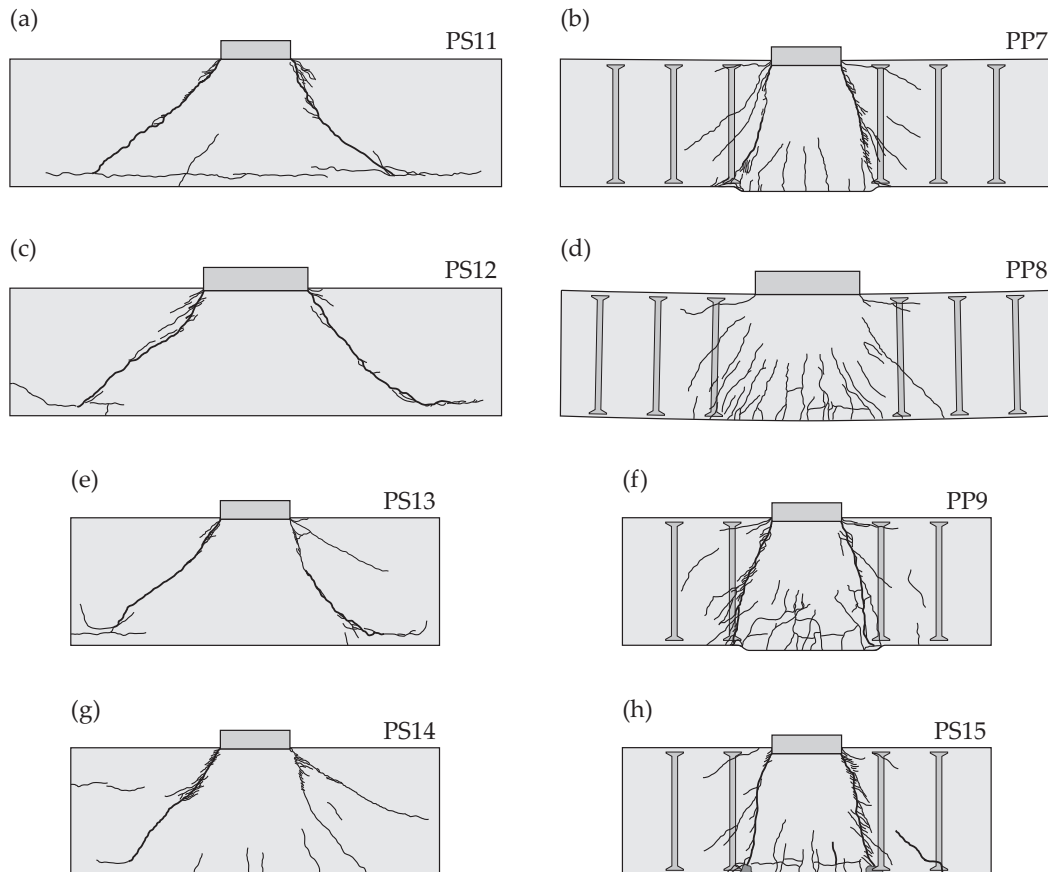


Figure 2.7: Schematic representations of the saw-cuts: (a) PS11; (b) PP7; (c) PS12; (d) PP8; (e) PS13; (f) PP9; (g) PS14; (h) PS15.

It is also important to note from Figure 2.7 that the inclination of the failure surface of footings without shear reinforcement appears to be dependent on the shear slenderness, with steeper surfaces observed for more compact slabs. This is in agreement with previous experimental campaigns presented in the literature (Hegger *et al.*, 2009; Ricker, 2009; Siburg and Hegger, 2014; Siburg, 2014).

## 2.4.2 Measured deformations

### 2.4.2.1 Rotation and deflections

The load-rotation curves of the test specimens are presented in Figure 2.8, where the specimens without shear reinforcement are compared with the corresponding shear-reinforced specimens. From that figure it can be observed that the presence of shear reinforcement enhances the strength and the deformation capacity. Both footings with and without shear reinforcement experienced a decrease in the tangent flexural stiffness. For specimens without transverse reinforcement, this was observed close to the failure load, whereas for specimens with shear reinforcement, this decrease was observed at lower load levels (see Figure 2.8).

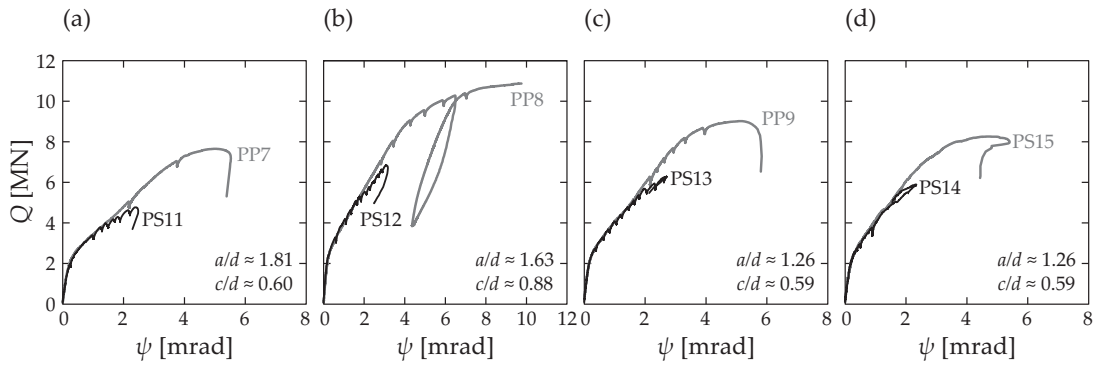
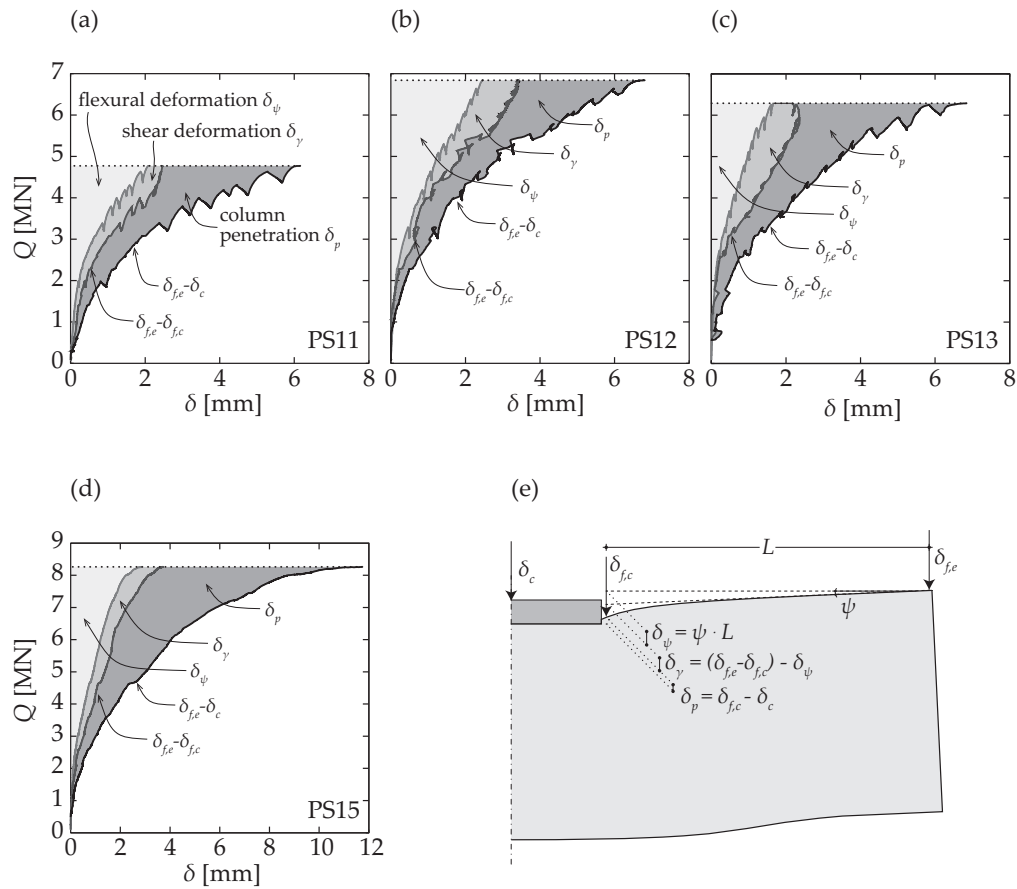


Figure 2.8: Load-rotation curves of the corresponding specimens without and with shear reinforcement: (a) PS11 and PP7; (b) PS12 and PP8; (c) PS13 and PP9; (d) PS14 and PS15.

Figures 2.9(a) - 2.9(d) show the load-displacement curves obtained using different measurement devices for three specimens without shear reinforcement (PS11 to PS13) and for one specimen with shear reinforcement (PS15). The displacements presented in this figure were calculated based on the rotations measured with four inclinometers and on the displacement measured with LVDTs at the column plate or edge (Figure 2.9(e)). Three different components can be distinguished, corresponding to flexural deformations  $\delta_\psi$ , shear deformations  $\delta_\gamma$  and, finally, column penetration  $\delta_p$ , as shown in Figure 2.9(e). It is important to note that the information shown in Figure 2.9 is calculated based on the measured deformations at the top surface of the specimens. It is also important to note that part of the deformation, considered here as column penetration, may also be considered as a shear deformation (here it will be separated for clarity). In this respect, it can be seen that the punching failures of the footings without shear reinforcement presented an enhanced total deformation capacity (sum of flexural, shear and column penetration) with respect to slender flat slabs (Guandalini *et al.*, 2009) (where the flexural deformation component is dominant).

The three specimens without shear reinforcement shown in Figures 2.8(a) - 2.8(c) differ in the span-to-effective depth ratio and the column size. For all specimens, the sum of the shear deformation and column penetration can be of the same, or even higher, magnitude than the flexural deformations. It is also possible to verify that the column penetration, which can be seen as a very local deformation, can reach non-negligible values, particularly for the most compact footings, as a result of high levels of shear force. It is interesting to note that for the smallest column size, the shear deformation stabilized or even decreased near failure. This result is explained by the fact that a part of the shear deformation is accounted for as a column penetration.

Based on the measurements recorded, the deformed shape of the footing during loading can be drawn as shown in Figure 2.9(e), where the three components (flexural and shear deformations plus column penetration) are taken into account qualitatively. Figure 2.9(d) refers to footing PS15, which corresponds to a shear-reinforced footing without horizontal top reinforcement. In the case of shear-reinforced specimens, the three deformation components can again be clearly distinguished. Although an increase in flexural deformations is observed close to failure in the case of the shear-reinforced specimen (a plateau seems to be reached in the load-rotation curves, see Figure 2.8(d)), a more significant increase in the column penetration is again observed.



**Figure 2.9:** Load-displacement curves showing, separately, the flexural deformation (estimated based on the rotation of the footing), shear deformation and column penetration of: (a) PS11, (b) PS12, (c) PS13, (d) PS15; (e) Scheme of recorded measurements: outer rotation  $\psi$  by inclinometers, vertical displacement at edge of footing  $\delta_{f,e}$  with an LVDT, vertical displacement of footing 25 mm from column edge  $\delta_{f,c}$  and vertical displacement at centre of column plate  $\delta_c$ .

#### 2.4.2.2 Strains in bottom flexural reinforcement

The strains in the bottom flexural reinforcement of specimen PS12 were tracked along the weak axis in both the radial and tangential directions. The location of the 32 strain gauges is shown in Figure 2.10(a) (where strain gauge J23 is not considered here in after due to measurement problems during the test). Although the specimen is square and not circular, strain gauges J17 to J32 can be considered as indicators of tangential strains.

The results are presented in Figures 2.10(b) and 2.10(c) for radial and tangential directions respectively. Each value represented in these two figures results from the average value of two strain gauges placed at a distance of 50 mm, e.g.  $\epsilon_{s,r}$  at  $r = 25$  mm is the average of J1 ( $r = 0$  mm) and J2 ( $r = 50$  mm), where  $r$  is the radial distance from the centre of the specimen. It is interesting to note that a peak on the strains profile develops at the edge of the column in the radial direction (although the average value at this position is below the yielding strain, the strain gauge placed at  $r = 250$  mm reached the yielding strain locally). It should also be noted that the tangential strains measured near the edge of the footing are larger than those measured in the radial direction.

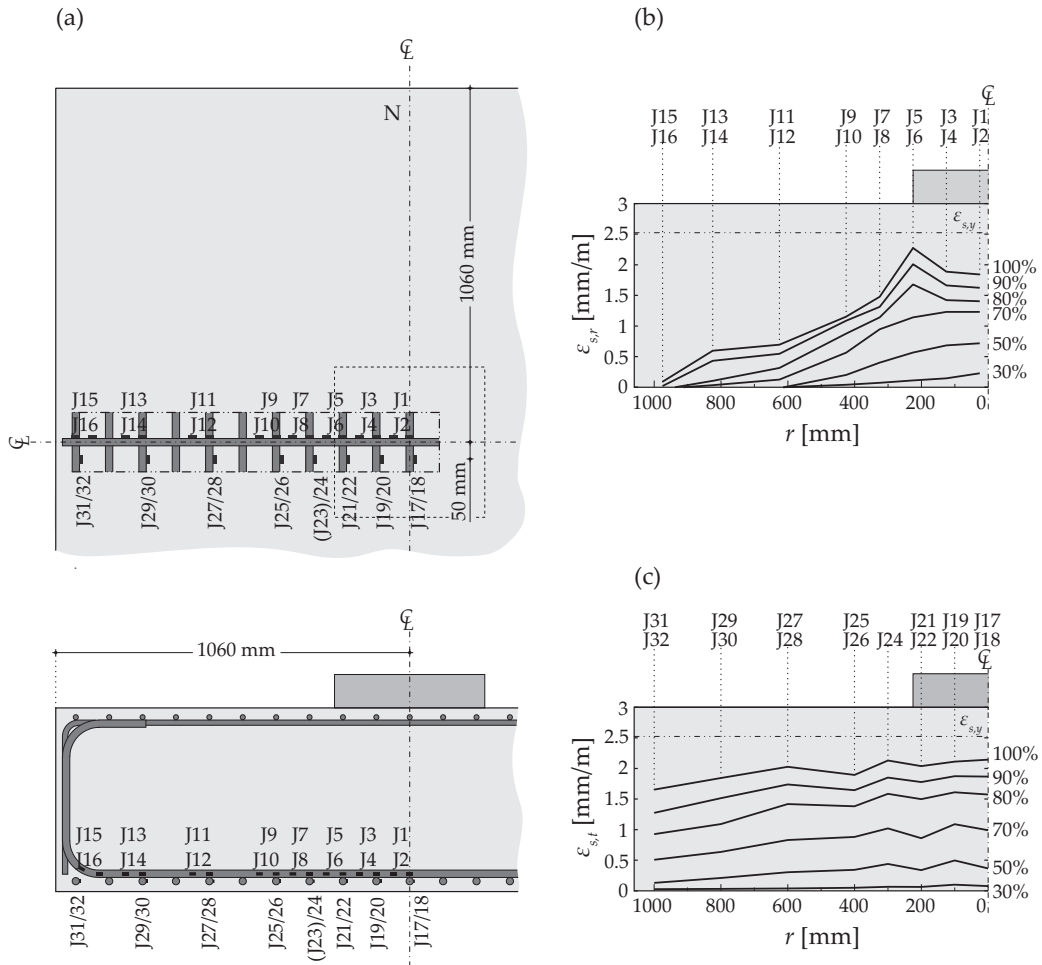
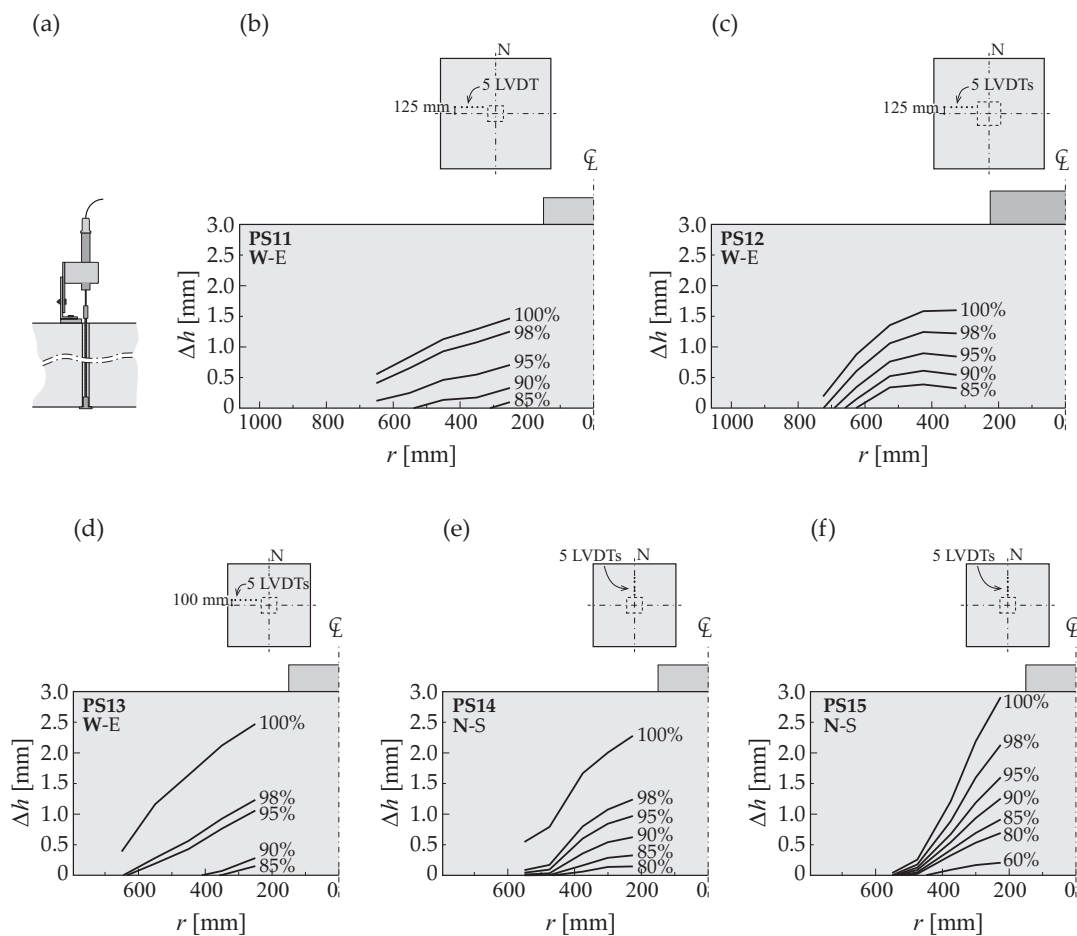


Figure 2.10: Strains in the bottom flexural reinforcement of specimen PS12: (a) location of the 32 strain gauges used (16 in radial and 16 in tangential direction along the axis in the weak direction), (b) radial strains J1-J16, and (c) tangential strains J17-J32 (J23 not considered) (percentages indicate load level compared with maximum load).

### 2.4.2.3 Changes in the thickness of the footings

The changes in the thickness of the specimens were measured at different points in specimens without shear reinforcement and also in the shear-reinforced footing PS15 (measurement details are shown in Figure 2.11(a)). The results are presented in Figure 2.11, where it remains clear that the variation in the thickness at maximum load tends to be more pronounced for the most compact footings (see Figures 2.11(b) - 2.11(e)). It should be noted that the changes in thickness measured correspond to the vertical component of shear cracks developing inside the footing.

It is possible to verify that the changes in the thickness of the footings start to be significant at values of  $\sim 80\%$  of the maximum load for the specimens without shear reinforcement. It is also interesting to note that changes in thickness tend to be more pronounced near the column. With respect to the shear-reinforced specimen (Figure 2.11(f)), it was shown that the changes in the thickness variation start at  $\sim 60\%$  of the maximum load, which corresponds to the load at which the changes in the thickness of the reference specimen - without shear reinforcement - can also be observed.



**Figure 2.11:** Changes in thickness for different load levels and locations of measuring points: (a) detail of measurement device; (b) PS11, (c) PS12, (d) PS13, (e) PS14, (f) PS15 (percentages indicate load level compared with maximum load).

#### 2.4.2.4 Strains at the concrete top surface

The strains at the concrete top surface were measured near the column plate. The radial and tangential strains measured for specimen PS11 (most slender specimen) are shown in Figures 2.12(a) and 2.12(b) respectively. With respect to radial strains, an elongation was measured, with higher values obtained for smaller distances from the column plate. This elongation increases with increasing levels of load up to  $\sim 80\%$  of the total load, after which it starts decreasing. At failure, values of radial strain at the concrete top surface near the column are very small. This behaviour, which was measured consistently during this experimental campaign, has already been observed in footings in previous experimental investigations (e.g. Dieterle and Rostásy, 1987; Dieterle, 1987; Hegger *et al.*, 2006; Ricker, 2006; Hegger *et al.*, 2007, 2009; Ricker, 2009; Siburg and Hegger, 2014; Siburg, 2014). This behaviour is very different from that normally observed in flat slender slabs (e.g. Kinnunen and Nylander, 1960; Guandalini *et al.*, 2009; Lips, 2012; Lips *et al.*, 2012), where a shortening (related to compression) was measured in the soffit of the slab up to a certain value, after which a decompression was normally observed. With respect to the tangential strains at the concrete top surface, it should be noted that a shortening (related to compression) proportional to the rotation (as a result of flexural deformations) was measured up to a certain value, where a tendency towards stabilization or even a slight decrease in the tangential strains could be measured consistently.

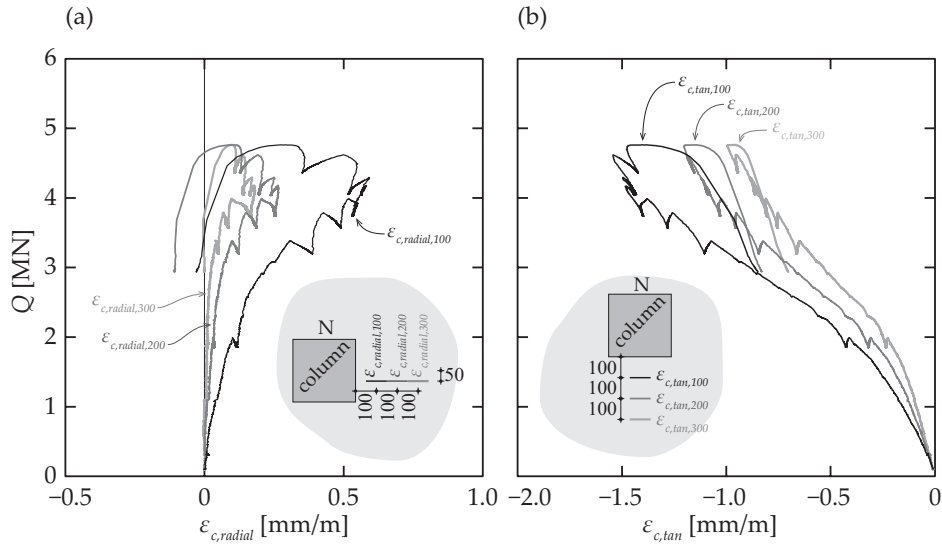


Figure 2.12: Strains at the concrete top surface of test PS11 in (a) radial and (b) tangential directions (positive values indicate elongation).

### 2.4.3 Global observed behaviour of RC footings subjected to concentrated loads

The punching shear strength of the specimens with shear reinforcement is normally governed by one of the three following failure modes: crushing of the concrete struts between the column and the first perimeter of shear reinforcement, a failure within or outside the shear-reinforced area (Fernández Ruiz and Muttoni, 2009). The shear-reinforced specimens in this paper which reached failure exhibited a crushing of the concrete struts near the loading plate, with the development of a failure surface between the column edge and the first shear reinforcement perimeter. Although the potential failure modes of shear-reinforced specimens are well established, the phenomena that trigger the failure of footings without shear reinforcement is still an object of discussion. In that respect, the continuous measurements recorded in the shear-critical region (near the column) in this experimental campaign provide valuable additional information.

The main deformations measured in the shear-critical region are presented in Figure 2.13. Five different measurements are presented: rotation measured near the edges of the footing  $\psi$ , column penetration  $\delta_p$ , changes in the thickness of the specimen measured at a distance of 100 mm from the edge of the steel column plate  $\delta_h$  and the radial  $\epsilon_{c,radial}$  and tangential  $\epsilon_{c,tan}$  strains at the top concrete surface, both measured at a distance of 100 mm from the edge of the steel column plate. The results presented in Figure 2.13 correspond to (a) specimen PS11 and (b) specimen PS13, which are the most slender and the most compact specimens without shear reinforcement respectively. It is important to note that in both diagrams the load is normalized by the maximum load. With respect to the results, four different regimes of behaviour can be distinguished:

1. Up to  $\sim 30\%$   $Q/Q_R$ , an elastic behaviour can be observed. This led to an increase in rotation (uncracked flexural stiffness), an increase in tangential compression (negative tangential strains) proportional to the rotation, an increase in the radial tension (as a result of local shear deformation near the column, see Figure 2.9) and an increase in the support penetration (probably partly due to crushing of the plaster between steel column plate and footing). No changes in the thickness of the specimens were observed.

2. From  $\sim 30$  to  $\sim 80$  %  $Q/Q_R$  for PS11 and  $\sim 30$  to  $\sim 75$  %  $Q/Q_R$  for PS13, flexural cracks start developing (this was confirmed after visual inspection of the bottom surfaces after testing, see, for instance, Figure 2.6) and a decrease in the flexural stiffness can be observed in the load-rotation curve. The tangential compression strains at the concrete top surface increase in proportion to the rotation. The radial tension at the top concrete surface is still increasing as a consequence of a local shear deformation near the column and the penetration of the column accelerates slightly. In the transition between this and the following stage, changes in the thickness of the footing were measured, which may be justified by the appearance of inclined cracks due to the flexural-shear interaction.
3. From  $\sim 80$  to  $\sim 90$  %  $Q/Q_R$  for PS11 and from  $\sim 75$  to  $\sim 85$  % for PS13, the rotation and the column penetration increase, but the corresponding stiffnesses are still approximately equal to the previous regime. The tangential compression at the concrete top surface is still increasing. However, a different behaviour may be observed: the changes in the thickness become important and the radial tension measured at the concrete top surface attains its maximum, remaining approximately constant.
4. Finally, from  $\sim 90$  %  $Q/Q_R$  (PS11) or  $\sim 85$  %  $Q/Q_R$  (PS13) up to maximum load, a slight loss of flexural stiffness (also observed to occur in Figure 2.8) is observed, accompanied by a pronounced loss of shear stiffness. The tangential compression at the concrete top surface near the column remains constant or even decreases (decompression). The radial tension at the concrete top surface decreases almost down to zero and the changes in the thickness of the footing and the column penetration accelerate and become very significant.

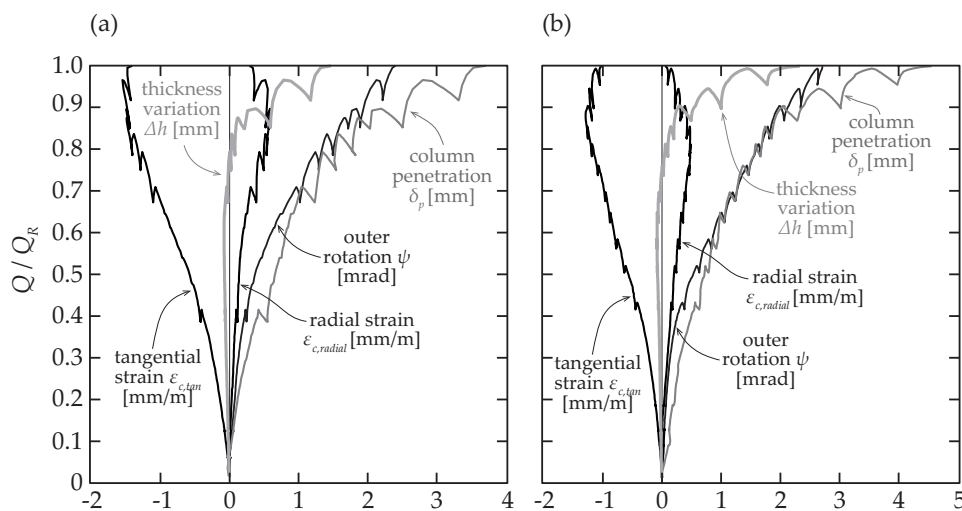


**Figure 2.13:** Representation of different deformations recorded in the shear-critical region for footings: (a) PS11, (b) PS13; rotation measured at the concrete top surface, column penetration, thickness variation measured 100 mm from edge of column plate, radial and tangential strains at the concrete top surface measured 100 mm from edge of column plate with omega-shaped gauges (see Figures 2.5 and 2.11 for more details of the locations of measurement devices).

The four regimes described above were clearly observed for the four footings without shear reinforcement. The limits of each regime depend, however, on the mechanical and geometrical properties. For instance, regime (4) appears to be more significant for more compact footings. This stage might be assumed to correspond to crushing of the concrete struts near the column, which can be confirmed by the signs of crushing observed along the saw-cuts (see Figure 2.7). Crushing of the concrete struts near the column would also explain the tangential decompression observed at the concrete top surface (as a

consequence of the pronounced lateral expansion of the concrete close to failure (Guidotti *et al.*, 2011). At this stage, the column is penetrating into the footing and the sliding surface forming at the top of the concrete struts is confirmed by the measurements of the changes in thickness (see Figure 2.11). It is also interesting to note that the experimental evidence collected in the campaign presented in this paper are in accordance with those presented by Hallgren and Bjerke (2002), who also observed similar regimes when analysing the punching behaviour of footings using nonlinear finite element analyses.

## 2.5 Analysis of experimental evidence

### 2.5.1 Influence of span-to-effective depth ratio and column size

The span-to-depth ratio depends on the footing and column sizes as well as the effective depth. Whereas the nominal value of the latter parameter was kept constant in the experimental investigation presented here, the first two were varied. The maximum loads normalized by the square of the effective depth and the square root of the cylinder concrete compressive strength are presented in Table 2.2 and shown graphically in Figure 2.14 as a function of shear slenderness (equal column size) and column size (for equal side length of footings). The results show that an increase in the shear slenderness reduces the load-carrying capacity for the cases of footings without shear reinforcement (see Figure 2.14(a)) due to:

- an increase in the percentage of load outside the failure surface, where the load has to be carried by inclined struts (increase in shear force), and
- a decrease in the inclination of the failure surface (Figure 2.7), which is associated with a decrease in the average shear strength per unit length, according to theoretical considerations (Braestrup *et al.*, 1976; Simões *et al.*, 2016b).

As shown in Figure 2.14b, increasing the column size leads to an increase in the load-carrying capacity for footings both with and without shear reinforcement. This may be justified not only by the increase in the column perimeter (associated with lower shear stresses acting), but also by the inherent decrease in the shear slenderness (as the side length of the footings was kept constant).

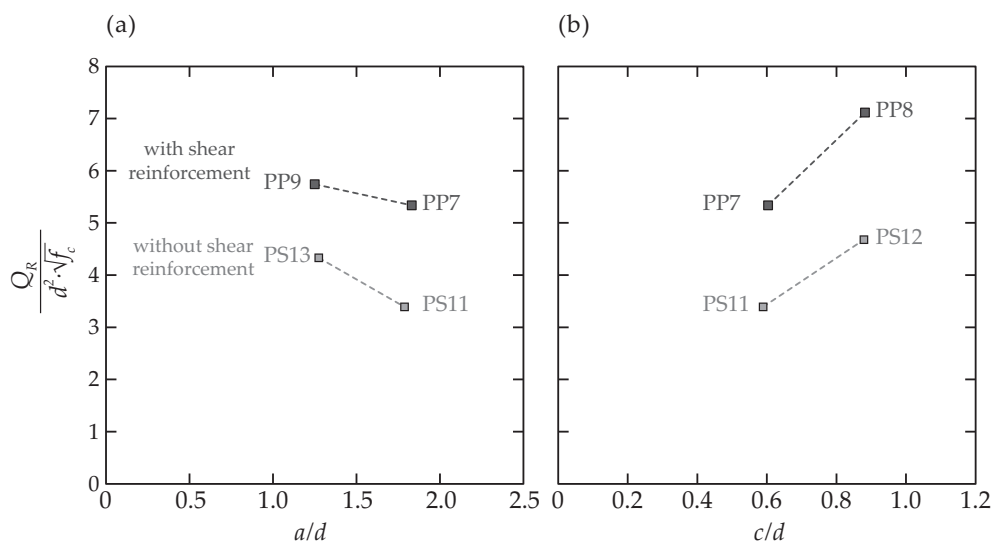


Figure 2.14: Normalized load-carrying capacity as a function of (a) span-to-effective depth ratio and (b) column size-to-effective depth ratio.

## 2.5.2 Influence of shear reinforcement

As was shown previously (see Figures 2.8 and 2.14), the shear reinforcement can enhance the punching strength and deformation capacity compared with specimens without shear reinforcement. Its effectiveness was nevertheless shown to be dependent on the span-to-effective depth ratio, as can be seen in Figure 2.14. This has been shown previously for footings having stirrups as shear reinforcement (Hegger *et al.*, 2009; Ricker, 2009; Siburg and Hegger, 2014; Siburg, 2014) and is here confirmed for the case of double-headed shear studs. The shear reinforcement controls the development of transverse strains, as can be seen by comparing the changes in the thickness of footings PS14 and PS15 (see Figures 2.11(e) and 2.11(f)) with the activation of the shear reinforcement in footing PS15 (see Figure 2.15). The first perimeter of shear studs in specimen PS15 is activated from approx. 80 % of the maximum load of the reference specimen PS14, which corresponds to the level of load after which important changes in the thickness of the specimens were measured (Figure 2.11). The excellent anchorage conditions of the shear reinforcement used in this experimental campaign (double-headed studs with anchorage head size equal to three diameters) enables its full activation upon the onset of transverse strains.

The decrease in the effectiveness of the shear reinforcement with decreasing shear slenderness may be physically explained by the location and inclination of the concrete struts. Considering that the principal transverse strains develop normal to the compressive strains and that the principal compressive strains have approximately the same direction as the concrete struts, a decrease in the angle between the concrete struts and the shear reinforcement leads to a lower efficiency of the latter (Vecchio and Collins, 1988). This is the case for footings with a low span-to-effective depth ratio, which have a steeper compression field and, consequently, lower angles between the concrete struts and the shear reinforcement.

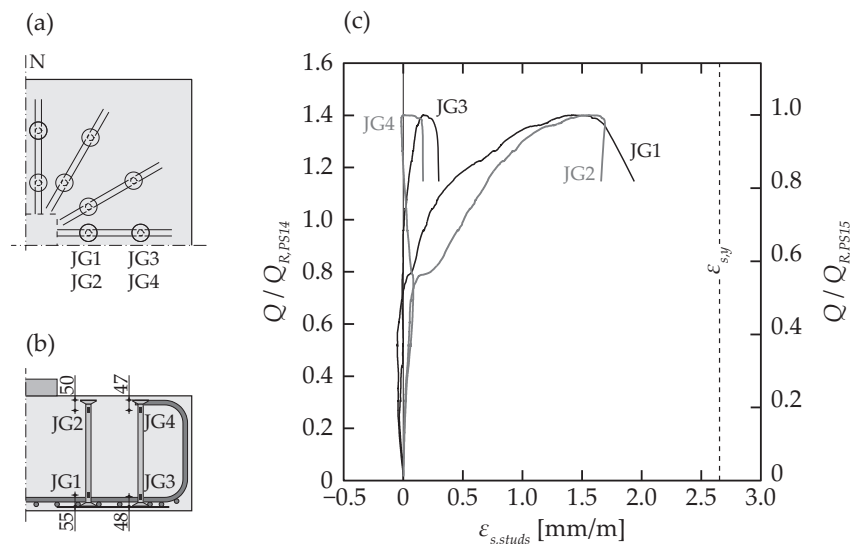


Figure 2.15: Strains in shear reinforcement of specimen PS15: (a) plan, (b) section (showing locations of strain gauges), and (c) corresponding load-deformation curves.

## 2.5.3 Flexural-shear interaction

It is shown in Figure 2.8 that the load-rotation curves of the specimens with shear reinforcement reach a plateau before failure. The strengths at the plateau are significantly lower than those predicted by classical yield line theory (Johansen, 1962; Gesund, 1983) and presented in Table 2.2. This has been

shown to occur for slabs with large amounts of shear reinforcement (Lips, 2012; Lips *et al.*, 2012). This phenomenon can be seen as a flexural-shear interaction, as shown using the kinematic theorem of limit analysis (Simões *et al.*, 2016b). This effect is very important for compact footings (Simões *et al.*, 2016b) since it leads to theoretical values of strength significantly lower than those obtained for a pure flexural failure.

### 2.5.4 Influence of top reinforcement

Specimens PS14 and PS15 differ from specimens PS13 and PP9 respectively because horizontal reinforcement was not used in the theoretical compression surface. The objective was to study the potential influence of this reinforcement on the failure mode and strength of the footings. According to theoretical considerations (Simões *et al.*, 2016b), horizontal reinforcement in the compression zone can act as confinement reinforcement for the inclined strut near the column, thus increasing the load capacity. The ratio of the normalized loads (see Table 2.2) of the specimens with and without horizontal flexural reinforcement confirms that a small increase in the load-carrying capacity can be achieved by including this reinforcement (8 % increase for specimens without shear reinforcement, PS13/PS14, and 3 % for specimens with shear reinforcement, PP9/PS15).

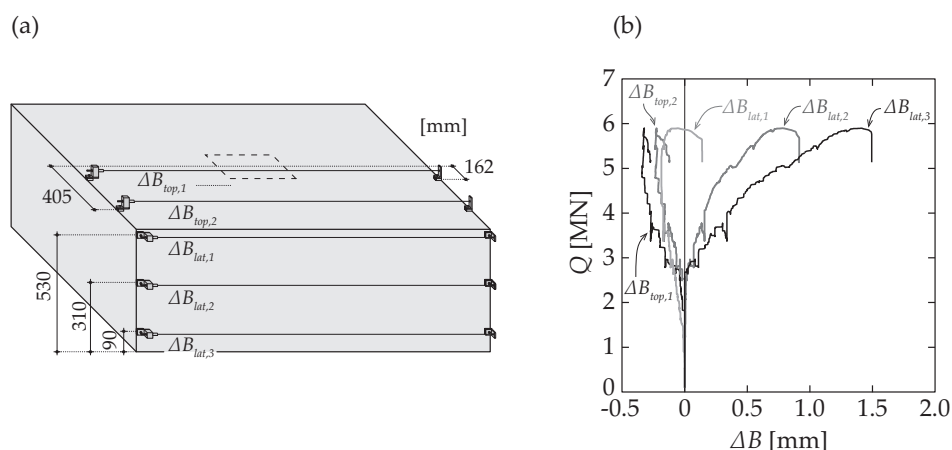


**Figure 2.16:** Changes in width of specimen PS14: (a) representation of measurement devices used, (b) results (positive values indicate elongation).

The expansion of the top and lateral surfaces of specimen PS14 was measured with LVDTs (see Figure 2.16(a)) and the results are shown in Figure 2.16(b). An elongation of the bottom surface (measured at the bottom of the lateral surface) and a shortening of the top surface were measured up to 80 % of the maximum load, probably resulting from the flexural behaviour. After that, although the bottom surface continues to elongate, the shortening of the top surface stabilizes. This may be justified by the expansion of the diagonal concrete strut (Guidotti *et al.*, 2011), which compensates for the continuous contraction expected due to the flexural behaviour. Whereas for specimen PS13 (with top flexural reinforcement) no cracks on the top surface could be observed after failure, radial cracks could be seen on the top surface of specimen PS14 (without top reinforcement). Although the expansion of the top surface of specimen PS13 was not measured, the differences in the load-carrying capacity and the crack pattern on the top surface indicate that the presence of top reinforcement might increase the strength of footings without shear reinforcement (this topic should be clarified by future experimental and analytical research).

## 2.6 Conclusions

An experimental investigation of eight full-scale reinforced concrete footings with and without shear reinforcement is presented in this paper. The bottom flexural reinforcement (0.75 %) and the nominal thickness (550 mm) were kept constant, while the influences of column size, slenderness and the presence of top horizontal reinforcement and shear reinforcement were investigated. Detailed measurements in the shear-critical region were recorded during the experimental tests. The main experimental evidence is summarized in the following:

1. The punching strength of reinforced concrete footings without shear reinforcement is shown to increase with decreasing shear slenderness. Further, the inclination of the critical shear crack appears to be steeper for low span-to-effective depth ratios.
2. The punching strength of reinforced concrete footings can be significantly increased by incorporating double-headed shear studs. The effectiveness of this reinforcement has been shown experimentally to be dependent on the shear slenderness, being less effective for low span-to-effective depth ratios.
3. Although flexural deformations might be important for describing the punching behaviour of footings, significant shear deformations also occur due to the high levels of shear force.
4. A careful analysis of the measurements recorded in the shear critical region indicates that crushing of the concrete diagonal strut close to the column is the phenomenon that triggers failure. Observations of the saw-cuts after testing confirm the presence of crushed concrete in this zone.
5. An important flexural-shear interaction was observed in the case of footings with shear reinforcement, where a plateau appears to be reached in the load-rotation curves.
6. The load corresponding to this flexural-shear plateau is significantly lower than the theoretical flexural capacity calculated based on the yield line method. This reduction may be explained by the high concentrations of shear forces at the edge of the column, which increases the depth of the compression zone and, consequently, decreases the lever arm.
7. The flexural-shear regime described above has to be taken into account in the design and assessment of reinforced concrete footings. A rational-based method to predict the flexural-shear capacity of reinforced concrete footings is needed.

## 2.7 References

- Braestrup M. W.; Nielsen M. P.; Jensen B. C.; Bach F. (1976):** *Axisymmetric Punching of Plain and Reinforced Concrete*. Tech. rep. 75. Structural Research Laboratory, Technical University of Denmark, p. 33.
- Dieterle H. (1987):** „Design of reinforced concrete foundations of square columns under centric loading with the help of design diagrams (In German: Zur Bemessung quadratischer Stützenfundamente aus Stahlbeton unter zentrischer Belastung mit Hilfe von Bemessungsdiagrammen)“. *Deutscher Ausschuss für Stahlbeton*, Vol. 387, pp. 94–134.
- Dieterle H.; Rostásy F. (1987):** „Load-carrying behaviour of isolated reinforced concrete foundations of square columns (In German: Tragverhalten quadratischer Einzelfundamente aus Stahlbeton)“. *Deutscher Ausschuss für Stahlbeton*, Vol. 387, pp. 1–91.
- Fernández Ruiz M.; Muttoni A. (2009):** „Applications of the critical shear crack theory to punching R/C slabs with transverse reinforcement“. *ACI Structural Journal*, Vol. 106, No. 4, pp. 485–494.
- Gesund H. (1983):** „Flexural Limit Analysis of Concentrically Loaded Column Footings“. *ACI Journal Proceedings*, Vol. 80, No. 3, pp. 223–228.
- Guandalini S.; Burdet O.; Muttoni A. (2009):** „Punching tests of slabs with low reinforcement ratios“. *ACI Structural Journal*, Vol. 106, No. 1, pp. 87–95.
- Guidotti R.; Fernández Ruiz M.; Muttoni A. (2011):** „Crushing and Flexural Strength of Slab-Column Joints“. *Engineering Structures*, Vol. 33, No. 3, pp. 855–867.
- Hallgren M.; Bjerke M. (2002):** „Non-linear finite element analyses of punching shear failure of column footings“. *Cement and Concrete Composites*, Vol. 24, No. 6, pp. 491–496.
- Hallgren M.; Kinnunen S.; Nylander B. (1998):** „Punching shear tests on column footings“. *Nordic Concrete Research*, Vol. 21, pp. 1–22.
- Hegger J.; Sherif A.; Ricker M. (2006):** „Experimental Investigations on Punching Behaviour of Reinforced Concrete Footings“. *ACI Structural Journal*, Vol. 103, No. 4, pp. 604–613.
- Hegger J.; Ricker M.; Ulke M.; Ziegler M. (2007):** „Investigations on the punching behaviour of reinforced concrete footings“. *Engineering Structures*, Vol. 29, No. 9, pp. 2233–2241.
- Hegger J.; Ricker M.; Sherif M. (2009):** „Punching Strength of Reinforced Concrete Footings“. *ACI Structural Journal*, Vol. 106, No. 5, pp. 706–716.
- Johansen K. W. (1962):** *Yield-line Theory*. Cement and Concrete Association.
- Kinnunen S.; Nylander H. (1960):** *Punching of Concrete Slabs Without Shear Reinforcement*. Tech. rep. 158. Stockholm, Sweden: Transactions of the Royal Institute of Technology, p. 112.
- Kordina K.; Nölting D. (1981):** *Load-carrying behaviour of eccentrically loaded isolated reinforced concrete foundations (In German: Tragverhalten von ausmittig beanspruchten Einzelfundamenten aus Stahlbeton)*. Tech. rep. DFG Research 204/27-30. Braunschweig, Germany: Technical University of Braunschweig, p. 158.
- Krakowski J.; Krawczyk L.; Urban T. (2015):** „Punching of RC Thick Plates - Experimental Test and Analysis“. In: *Proceedings of fib Symposium, Concrete - Innovation and Design*. Copenhagen.
- Lips S. (2012):** „Punching of Flat Slabs with Large Amounts of Shear Reinforcement“. PhD thesis. EPFL, p. 217.

- Lips S.; Fernández Ruiz M.; Muttoni A. (2012):** „Experimental Investigation on Punching Strength and Deformation Capacity of Shear-Reinforced Slabs“. *ACI Structural Journal*, Vol. 109, No. 6, pp. 896–900.
- Netopilik R. J. (2012):** „Punching Shear Behaviour of Thick Reinforced Concrete Slabs“. MA thesis. University of Toronto, p. 243.
- Richart F. E. (1948):** „Reinforced Concrete Walls and Column Footings, part 1 and 2“. *ACI Journal*, Vol. 45, pp. 97–127 & 237–260.
- Ricker M. (2006):** „Punching in RC footings considering the soil-structure-interaction“. In: *Proceedings of 6<sup>th</sup> International PhD Symposium in Civil Engineering*. Zürich.
- Ricker M. (2009):** „Reliability of punching design of isolated foundations (In German: Zur Zuverlässigkeit der Bemessung gegen Durchstanzen bei Einzelfundamenten)“. PhD thesis. RWTH, Aachen, p. 304.
- Siburg C. (2014):** „Consistent punching design in flat slabs and foundations (In German: Zur einheitlichen Bemessung gegen Durchstanzen in Flachdecken und Fundamenten)“. PhD thesis. RWTH, Aachen, p. 197.
- Siburg C.; Hegger J. (2014):** „Experimental Investigations on Punching Behaviour of Reinforced Concrete Footings with structural dimensions“. *Structural Concrete*, Vol. 15, No. 3, pp. 331–339.
- Simões J. T.; Bujnak J.; Fernández Ruiz M.; Muttoni A. (2016a):** „Punching shear on compact footings with uniform soil pressure“. *Structural Concrete*, Vol. 17, No. 4, pp. 603–617.
- Simões J. T.; Faria D. V.; Fernández Ruiz M.; Muttoni A. (2016b):** „Strength of reinforced concrete footings without transverse reinforcement according to limit analysis“. *Engineering Structures*, Vol. 112, pp. 146–161.
- Talbot A. N. (1913):** „Reinforced Concrete Wall Footings and Column Footings“. *Engineering Experiment Station - University of Illinois*, Vol. 67, pp. 114.
- Timm M. (2003):** „Punching of foundation slabs under axisymmetric loading (In German: Durchstanzen von Bodenplatten unter rotationssymmetrischer Belastung)“. PhD thesis. Braunschweig, Germany: Technische Universität Carolo-Wilhelmina zu Braunschweig, p. 159.
- Urban T.; Goldyn M.; Krakowski J.; Krawczyk L. (2013a):** „Experimental investigation on punching behaviour of thick reinforced concrete slabs“. *Archives of Civil Engineering*, Vol. 59, No. 2, pp. 157–174.
- Urban T.; Krakowski J.; Goldyn M.; Krawczyk L. (2013b):** *Punching of RC thick plates*. Tech. rep. 19. Poland: Department of Concrete Structures, Technical University of Lodz.
- Vecchio F. J.; Collins M. P. (1988):** „The modified compression-field theory for reinforced concrete elements subjected to shear“. *ACI Journal*, Vol. 83, No. 2, pp. 219–231.

## 2.8 Notation

### Latin characters

#### Lower Case

$a$	shear span
$b_0$	control perimeter
$c$	side length of square column
$d$	effective depth of flexural reinforcement
$f_c$	cylinder concrete compressive strength
$f_y$	yield strength of bottom flexural reinforcement
$f_{yw}$	yield strength of shear reinforcement
$n_s$	number of studs per perimeter
$n_p$	number of shear reinforcement perimeters
$r$	radius

#### Upper Case

$B$	width of specimen
$L$	distance between LVDTs at edge of footing near the column
$Q$	load
$Q_R$	maximum load
$Q_{flex}$	flexural capacity

### Greek characters

#### Lower Case

$\delta$	vertical displacement
$\delta_p$	column penetration
$\delta_\psi$	vertical displacement associated with flexural deformation
$\delta_\gamma$	vertical displacement associated with shear deformation
$\delta_{f,e}$	vertical displacement directly measured at concrete top surface 10 mm from edge of specimen
$\delta_{f,c}$	vertical displacement directly measured at concrete top surface 25 mm from column
$\delta_c$	vertical displacement indirectly measured at centre of column plate
$\varepsilon_{c,r}$	radial strain at concrete surface
$\varepsilon_{c,t}$	tangential strain at concrete surface
$\varepsilon_{s,y}$	reinforcement yielding strain
$\varepsilon_{s,r}$	radial strain in flexural reinforcement
$\varepsilon_{s,t}$	tangential strain in flexural reinforcement
$\rho$	flexural reinforcement ratio
$\phi_w$	diameter of transverse reinforcement
$\psi$	outer rotation

#### Upper Case

$\Delta_B$	change in side length of specimen
$\Delta_h$	change in thickness of specimen

### Acronyms

CSCT	Critical Shear Crack Theory
LVDT	Linear Variable Differential Transformer
PTFE	Polytetrafluoroethylene

# Chapter 3

## *Paper II*

### **Strength of reinforced concrete footings without transverse reinforcement according to limit analysis**

This chapter is the postprint version of the article titled *Strength of reinforced concrete footings without transverse reinforcement according to limit analysis* published in Volume 112 (pages 146 – 161) of the journal *Engineering Structures* in 2016 (DOI: 10.1016/j.engstruct.2016.01.010). The authors of this publication are João Tiago Simões (PhD Candidate), Duarte V. Faria (Postdoctoral researcher at EPFL), Miguel Fernández Ruiz (Senior lecturer at EPFL and thesis director), Aurelio Muttoni (Professor at EPFL and thesis director). The complete reference is the following:

**Simões J. T., Faria D. V., Fernández Ruiz M., and Muttoni A. (2016):** „Strength of reinforced concrete footings without transverse reinforcement according to limit analysis“. *Engineering Structures*, Vol. 112, pp. 146–161.

The work presented in this article was performed by João Tiago Simões under the supervision of Duarte V. Faria, Miguel Fernández Ruiz and Aurelio Muttoni.

The main contributions of João Tiago Simões to the creation of this article were the following:

- Performing all the calculations presented in article;
- Analyze the presented results;
- Development the simplified formulae allowing the calculation of the strength of RC footings according to the upper bound theorem of limit analysis in an approximative manner;
- Comparison of the experimental results report by Hallgren *et al.* (1998) and Dieterle and Rostásy (1987) to the theoretical results;
- Production of the figures included in the article;
- Preparation of the manuscript of the article.

### 3.1 Abstract

Isolated footings are reinforced concrete elements whose flexural and punching shear strengths are usually governing for their design. In this work, both failure modes and their interaction are investigated by means of the kinematical theorem of limit analysis. Previous works in this domain have traditionally considered failure mechanisms based on a vertical penetration of a punching cone. In this work, two enhanced failure mechanisms are investigated considering not only a vertical penetration of the punching cone, but also a rotation of the outer part of the footing, allowing to consider the role of both bottom and top reinforcements on the failure load. A rigid-plastic behaviour with a Mohr-Coulomb yield criterion is considered for the concrete and a uniaxial rigid-plastic behaviour is assumed for the reinforcement bars. The analysis shows that a smooth transition between flexural and punching shear failure occurs, corresponding to a flexural-shear regime. With respect to the punching shear failure regime, it is shown that the top reinforcement might play an important role (a fact usually neglected by previous investigations). Simplified formulations, allowing easy calculation of the load carrying capacity of footings, are derived and compared to the solutions according to limit analysis. Both theoretical and approximated solutions are finally compared with experimental results, showing consistent agreement.

### 3.2 Introduction

Concrete footings are commonly used as foundations for buildings and bridges. Although the load carrying capacity of footings subjected to a concentrated loading originated from a column has been the object of different research works (e.g. Talbot, 1913; Richart, 1948; Moe, 1961; Kordina and Nölting, 1981; Dieterle and Rostásy, 1987; Dieterle, 1987; Hallgren *et al.*, 1998; Hallgren and Bjerke, 2002; Timm, 2003; Broms, 2005; Hegger *et al.*, 2006; Ricker, 2006; Hegger *et al.*, 2007; Ricker, 2009; Urban *et al.*, 2013; Siburg and Hegger, 2014; Siburg, 2014), there is still not yet a consensus on a consistent method with physical basis for its design. In this paper, a rational approach is presented on the basis of the kinematical theorem of limit analysis, providing an upper bound solution for the load carrying capacity of these members. The approach may be applied to footings subjected to a distributed soil reaction (as the case of footings with a uniform soil reaction, see Figure 3.1(a)) or to footings with concentrated reactions (as the case of pile caps, see Figure 3.1(b)).

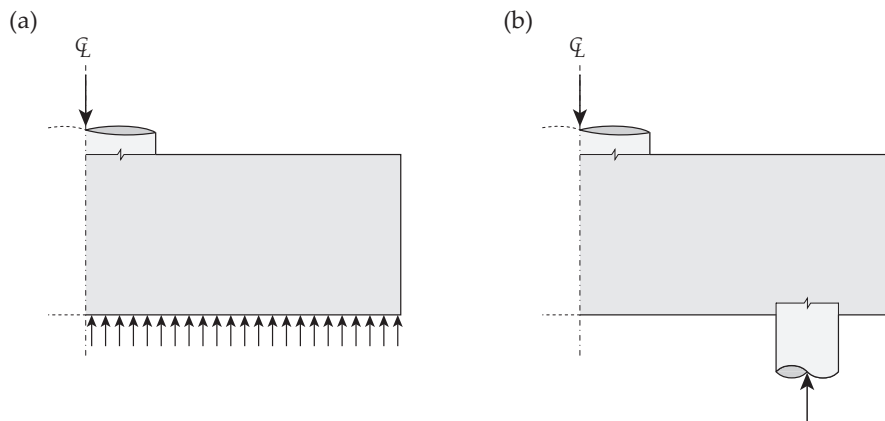
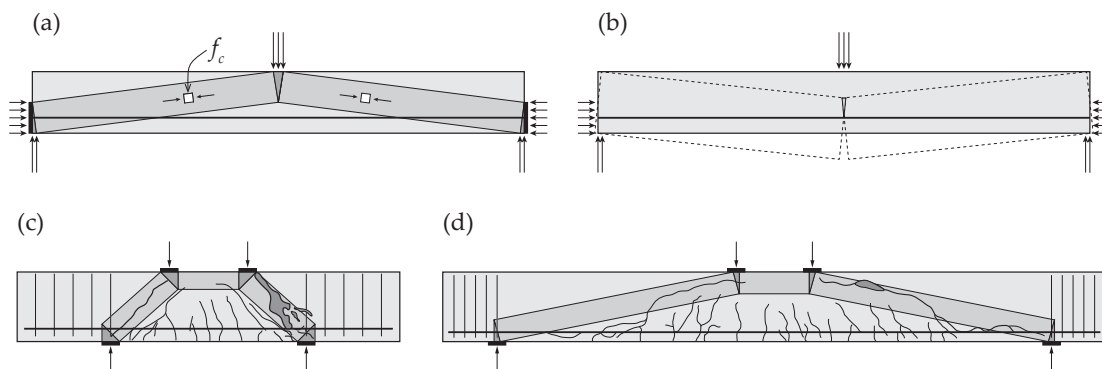


Figure 3.1: Schematically representation of (a) footing with uniform reaction and (b) pile caps with concentrated reactions.

One of the first applications of limit analysis to reinforced concrete members subjected to in-plane shear was proposed by Drucker (1961), who developed both a lower and an upper bound solution for a beam without shear reinforcement (refer to Figure 3.2(a) and (b)). Drucker (1961) also showed that the proposed upper and lower bound solutions provided the same failure load and thus corresponded to the exact solution according to limit analysis. According to Drucker (1961), failure in shear occurs by crushing of the inclined compression strut (with or without yielding of longitudinal reinforcement). This has been observed to be consistent with experimental evidences only for beams with low slenderness (see Figure 3.2(c), for beam B1 of Leonhardt and Walther (1962)). For larger slenderness (Figure 3.2(d), beam B6 of Leonhardt and Walther (1962)), failure occurs instead by an unstable propagation of a critical shear crack developing through the compression strut. In these latter cases, the strength is no longer controlled by the concrete crushing and strain localization occurs. Thus, size effect and other phenomena govern (Muttoni and Schwartz, 1991; Muttoni and Fernández Ruiz, 2008) and the application of limit analysis is in principle unsuitable for these cases. Analogously to the behaviour observed in beams, the strength of slender two-way slabs without shear reinforcement might be governed by the development of a critical shear crack, thus being in the range where limit analysis is not applicable (Muttoni and Fernández Ruiz, 2008). On the contrary, footings and compact slabs failing in punching can be considered to be similar to beams with low shear slenderness failing by crushing of concrete struts, thus corresponding to the range of cases where limit analysis may be applied.



**Figure 3.2:** (a) Stress field and (b) kinematically admissible failure mechanism proposed by Drucker (1961) for simply supported beams without transverse reinforcement subjected to a single load: cracking pattern and location of theoretical strut of (c) beam B1 and (d) beam B6 by Leonhardt and Walther (1962).

Limit analysis has already been applied in several cases focusing on the flexural and shear capacity of plain and reinforced concrete elements as joints, beams and slabs (e.g. Drucker, 1961; Johansen, 1962; Gesund and Dikshit, 1971; Braestrup, 1974; Jensen, 1975; Braestrup *et al.*, 1976; Müller, 1978; Nielsen *et al.*, 1978b,a; Braestrup, 1979; Morley, 1979; Braestrup, 1981; Gesund, 1983, 1985; Jiang and Shen, 1986; Muttoni, 1990; Bortolotti, 1990; Kuang, 1991; Muttoni *et al.*, 1997; Salim and Sebastian, 2002; Chen, 2007; Fernández Ruiz and Muttoni, 2007; Nielsen and Hoang, 2011; Jensen and Hoang, 2012). With respect to punching shear in slabs, Braestrup *et al.* (1976), Nielsen *et al.* (1978a) and Braestrup (1979), presented a first theoretical solution based on the kinematical theorem, considering the concrete as a rigid-plastic material with a modified Coulomb yield criterion. The adopted failure mechanism consisted on a vertical shift of the outer slab portion, see Figure 3.3. Later, Jiang and Shen (1986), Bortolotti (1990), Kuang (1991) and Salim and Sebastian (2002) also applied the upper bound theorem, adopting the same mechanism proposed by Braestrup *et al.* (1976), but with some modifications, namely, in the adopted failure criterion for the concrete.

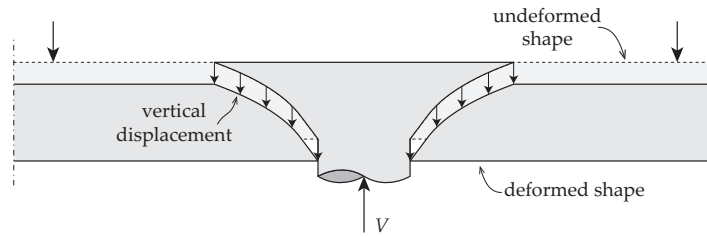


Figure 3.3: Kinematically admissible failure mechanism proposed by Braestrup *et al.* (1976) and Braestrup (1979).

A drawback of the above mentioned works, based on limit analysis to punching shear in slabs, is that the adopted failure mechanism only considers a vertical displacement along the failure surface, therefore neglecting the possibility of rotations leading to the activation of both bottom flexural and top reinforcement (and thus allowing only the analysis of punching regimes and not flexural or combined flexural-shear regimes). Moreover, all the above mentioned works deal mostly with punching shear strength of general slabs, where the application of this theory becomes potentially questionable (influence of size effect and other phenomena (Muttoni and Fernández Ruiz, 2008)).

In the present work, a theoretical solution for the load carrying capacity of axisymmetric isolated footings with low slenderness is presented. Two different failure mechanisms were selected as potentially governing. Both failure mechanisms consider that two footing portions are separated by a failure surface, which is assumed to be rotationally symmetric. The inner portion is considered to be rigid, while the outer portion deforms due to tangential moments according to a conical shape. Contrary to previous works, the mechanisms considered in the present paper lead to the consideration not only of the internal energy dissipated along the failure surface, but also of the internal energy dissipated in the bottom and top reinforcement, as well as in the concrete compression zone due to tangential bending. The governing failure mechanism is obtained in each case by minimization of the failure load accounting for the fact that both failure mechanisms provide an upper bound solution of the actual failure load.

On that basis, simplified solutions are also proposed, consistent with the upper bound solutions developed. Finally, both approximated and optimized solutions are compared with available experimental tests results, showing the consistency and accuracy of the approach.

### 3.3 Kinematical theorem of limit analysis applied to isolated reinforced concrete footings

In limit analysis, materials are assumed to behave in a perfectly plastic manner (Nielsen and Hoang, 2011). The application of the limit analysis is based on limit state theorems, and, in this paper, the kinematical theorem is used, providing an upper bound of the load carrying capacity. Global equilibrium is investigated stating that the rate of internal energy dissipated has to be balanced by the rate of external work for a licit (kinematically admissible) mechanism.

In this work, a rigid-plastic compressive behaviour of concrete with a Mohr-Coulomb yield criterion is assumed, see Figure 3.4 (a) and (b). Also the normality condition (strain rate vector normal to the yield locus) is respected. Due to the brittle behaviour of concrete in tension, tensile strength is neglected (introduced as a tension cut-off in the plasticity surface). In order to take into account the brittleness of concrete in compression as well as the influence of transverse strains on concrete strength, a plastic

compressive strength  $f_{cp}$  is considered, which is given by (Fernández Ruiz and Muttoni, 2007):

$$f_{cp} = f_c \cdot \eta_{fc} \cdot \eta_\varepsilon \quad (3.1)$$

where  $f_c$  refers to the cylinder concrete compressive strength,  $\eta_\varepsilon$  and  $\eta_{fc}$  represent the reduction factors accounting, respectively, for the presence of transverse strains and for the brittleness of high-strength concrete. Although different approaches have already been proposed to calculate the value of the reduction factor accounting for the presence of transverse strains  $\eta_\varepsilon$  (e.g. Vecchio and Collins, 1986; Muttoni, 1990; Muttoni *et al.*, 1997; Vecchio, 2000) and of a global reduction factor  $\eta = \eta_\varepsilon \cdot \eta_{fc}$  (e.g. Nielsen and Hoang, 2011), further investigations remain to be done in this field, specifically in what regards the characterization of the state of strains of footings when subjected to concentrated loads. Thus, constant values of  $\eta_\varepsilon$  will be assumed in this work (and are considered constant for all internal dissipation contributions, refer to Section 3.6). Regarding the reduction factor accounting for the brittleness of the high-strength concrete, it may be obtained as (Muttoni, 1990; Muttoni *et al.*, 1997; Fernández Ruiz and Muttoni, 2007, 2008):

$$\eta_{fc} = \left( \frac{f_{c0}}{f_c} \right)^{1/3} \leq 1 \quad (3.2)$$

with  $f_{c0} = 30$  MPa (Fernández Ruiz and Muttoni, 2007). The consideration of the Mohr-Coulomb yield criterion with a tension cut-off leads to the definition of three potential regimes occurring along the failure surface (refer to Figure 3.4 (b)), whose strain rates as well as principal stresses may be defined as follows:

$$\text{Regime A : } \begin{cases} \frac{\dot{\varepsilon}_3}{\dot{\varepsilon}_1} = -\frac{1-\sin(\varphi)}{1+\sin(\varphi)} \\ \sigma_3 = -f_{cp} + \frac{1+\sin(\varphi)}{1-\sin(\varphi)} \end{cases} \quad (3.3)$$

$$\text{Regime B : } \begin{cases} -\frac{1-\sin(\varphi)}{1+\sin(\varphi)} < \frac{\dot{\varepsilon}_3}{\dot{\varepsilon}_1} < 0 \\ \sigma_1 = 0 \\ \sigma_3 = -f_{cp} \end{cases} \quad (3.4)$$

$$\text{Regime C : } \begin{cases} \frac{\dot{\varepsilon}_3}{\dot{\varepsilon}_1} = 0 \\ \sigma_1 = 0 \\ -f_{cp} < \sigma_3 < 0 \end{cases} \quad (3.5)$$

where  $\dot{\varepsilon}_1$ ,  $\dot{\varepsilon}_3$  and  $\sigma_1$ ,  $\sigma_3$  are respectively the principal strain rates and the principal stresses;  $\varphi$  is the concrete friction angle, herein considered equal to  $\varphi = 37^\circ$  (i.e.  $\tan(0.75)$ , Nielsen and Hoang (2011)). A uniaxial rigid-plastic behaviour in both compression and tension of reinforcement steel bars is also assumed, refer to Figure 3.4(c) (i.e., dowel action is neglected). It has to be noted that positive strain rates and stresses refer to tension.

The geometrical and material properties used to describe the problem are presented in Figure 3.5(a) (see Notation in Section 3.9). For a given footing geometry, two failure mechanisms (shown in Figure 3.5(b) and (c)) are considered. The minimum load carrying capacity that results from the analysis using both mechanisms is the considered upper bound failure load. Both mechanisms consider that two portions of the footing are separated by an axisymmetric narrow plastic zone (see Figure 3.5(a)), where the velocity field results from the relative rotation  $\dot{\psi}$  (Figure 3.5) around an instantaneous centre of rotation.

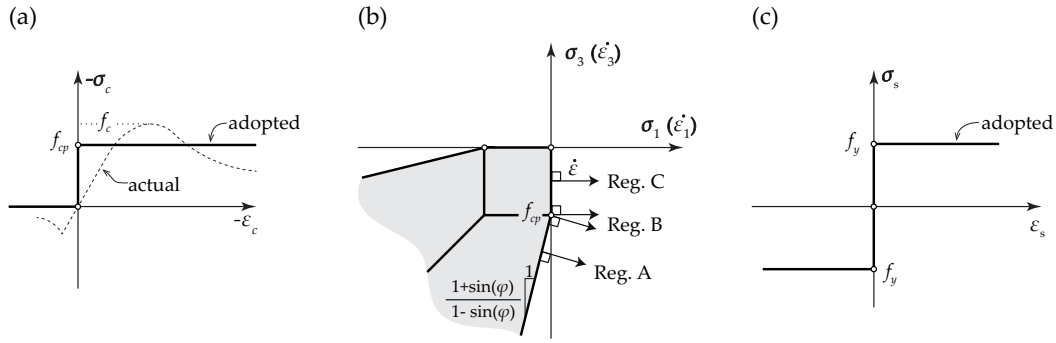


**Figure 3.4:** (a) Rigid-plastic compressive behaviour considered for concrete; (b) Mohr-Coulomb yield criterion with normality condition and (c) uniaxial rigid-plastic behaviour under tension and compression admitted for reinforcement bars.

The kinematics considered for both mechanisms differ in the admissible location for the instantaneous centre of rotation, as well as in the rotation direction. As shown in Figure 3.5(b), in the first mechanism (M1), the location of the instantaneous centre of rotation in the radial axis is considered to be behind the edge of the column ( $r_{ICR} \in ]-\infty, r_c]$ ), while in the vertical direction it is admitted to be above the bottom reinforcement ( $z_{ICR} \in ]0; \infty[$ ). The kinematically admissible mechanism M1 presents a counter-clockwise rotation when the instantaneous centre of rotation is not in the infinite. This mechanism is often assumed to be the one occurring in flexural as well as punching shear failures of flat slabs. For flexural failures, the instantaneous centre of rotation is close to the tip of the failure surface at the column edge, leading to a failure with an important rotation component. For the punching shear failure, the location of the instantaneous centre of rotation in radial direction shifts towards infinite ( $r_{ICR} \rightarrow -\infty$ ). In the latter case, the mechanism consists of a vertical shift of the outer portion of the footing, without activation of both bottom and top reinforcements (as dowelling of the reinforcement is neglected). This case corresponds to the failure mechanism originally proposed by Braestrup *et al.* (1976), where only the internal energy dissipated along the failure surface contributes to the load carrying capacity.

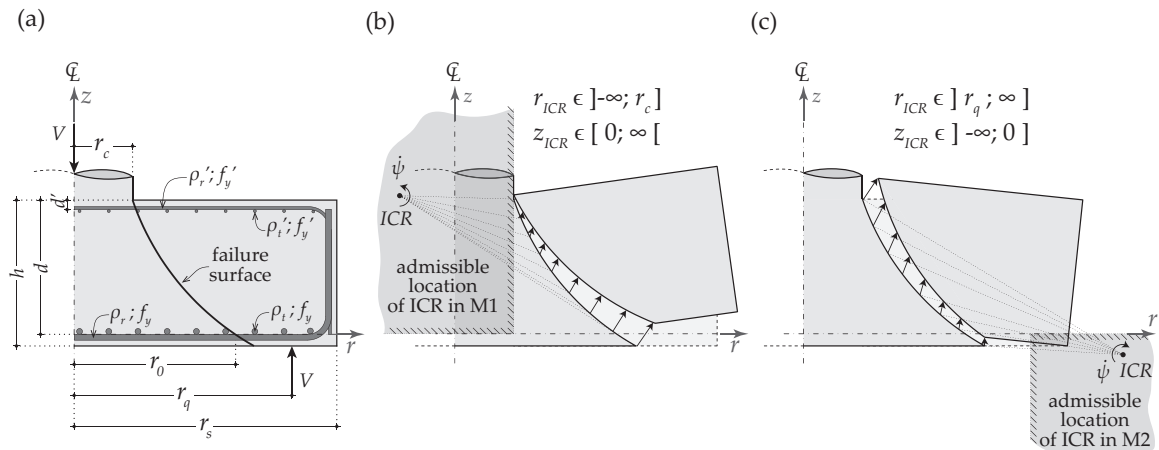


**Figure 3.5:** (a) Geometrical and mechanical properties of a footing; kinematically admissible mechanism (b) M1 and (c) M2 with location of the corresponding instantaneous centre of rotation (ICR).

As shown in Figure 3.5(c), the location of the instantaneous centre of rotation in the kinematics admitted for the second mechanism (M2) is assumed to be below or at the level of the bottom reinforcement ( $z_{ICR} \in ]-\infty; 0]$ ) and outside the radius where the reaction resultant is applied ( $r_{ICR} \in ]r_q; \infty[$ ). The ro-

tation considered (clockwise) is opposite to the one assumed in the first mechanism. The kinematics of this mechanism allows a failure mode without activation of the bottom reinforcement (when the instantaneous centre of rotation is located at the same level), which, as will be later shown, may govern in some cases. As for mechanism M1, also mechanism M2 allows a failure mode which corresponds to a shift of the outer portion of the footing, without dissipation of energy in the bottom and top reinforcements. This situation occurs when the radius of the instantaneous centre of rotation moves towards infinite ( $r_{ICR} \rightarrow \infty$ ), leading again to the solution originally proposed by Braestrup *et al.* (1976).

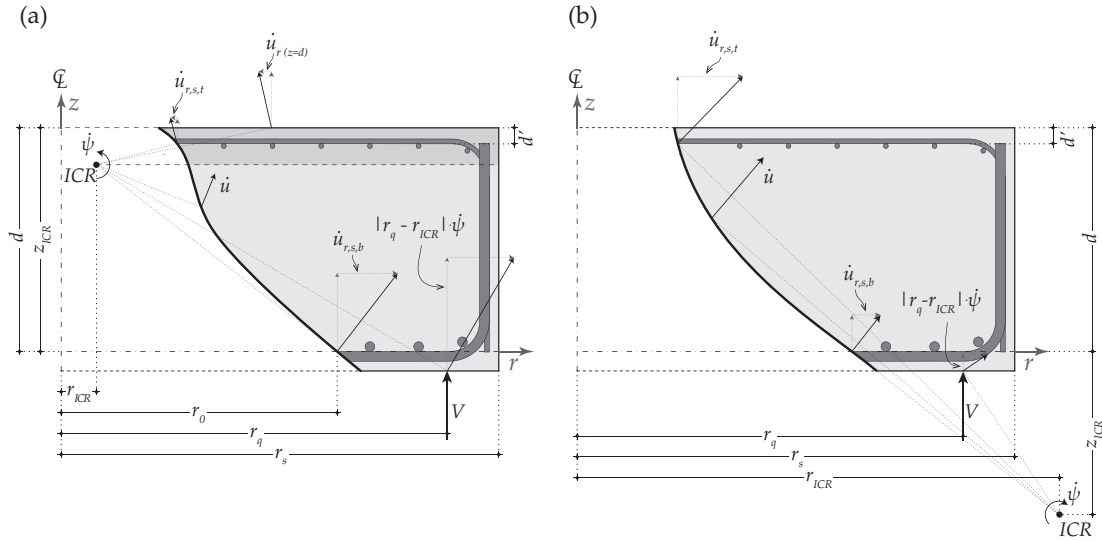


Figure 3.6: Example of mechanisms (a) M1 and (b) M2 and corresponding velocities.

The rate of external work and the components of the rate of internal energy dissipated can be computed for each mechanism based on the velocity field occurring along the failure surface, which is a function of the geometry of this surface and of the location of the instantaneous centre of rotation. An example of a failure mechanism and its velocity field is shown in Figure 3.6 for mechanisms (a) M1 and (b) M2. As shown in Figure 3.6, the velocity  $\dot{u}$  along the failure surface may be expressed as:

$$\dot{u} = \sqrt{(r - r_{ICR})^2 + (z - z_{ICR})^2} \cdot \dot{\psi} \quad (3.6)$$

being its radial component  $\dot{u}_r$  given by:

$$\dot{u}_r = |z - z_{ICR}| \cdot \dot{\psi} \quad (3.7)$$

where  $r$  and  $z$  represent the radial and the height coordinates, respectively. While the reaction resultant applied to the footing provides the only component of the external work, different components of dissipation of internal energy might be activated: (i) shear transfer along the failure surface, (ii) compression in the concrete near top surface in the outer portion due to tangential bending, (iii) bottom and top reinforcements. For a given location of the instantaneous centre of rotation ( $r_{ICR}, z_{ICR}$ ) and for an assumed geometry of the failure surface, each component of the rate of external work and of the rate of internal energy dissipated may be computed as detailed in the following sections.

### 3.3.1 Rate of external work

The rate of external work  $P_e$  is given by:

$$P_e = V \cdot |r_q - r_{ICR}| \cdot \dot{\psi} \quad (3.8)$$

where the shear force  $V$  corresponds to the soil reaction applied to the footing outside the failure surface and  $r_q$  describes the location of the soil reaction resultant (Figure 3.6). In the cases of uniform soil reaction, the total load  $Q$  is obtained considering also the soil reaction inside the failure surface:

$$Q = V \cdot \frac{r_s^2}{r_s^2 - r_0^2} \quad (3.9)$$

where  $r_0$  refers to the radius of the failure surface at the level of the bottom reinforcement. In the present work, it is considered that the failure surface develops between the top surface and the bottom reinforcement (i.e. the cover of the bottom reinforcement is neglected). The radius  $r_q$  may be calculated by means of:

$$r_q = \frac{\int_0^{2\pi} \int_{r_0}^{r_s} r \cdot (r \cdot dr d\theta)}{\int_0^{2\pi} \int_{r_0}^{r_s} r \cdot dr \cdot d\theta} = \frac{2}{3} \cdot \frac{(r_s^3 - r_0^3)}{(r_s^2 - r_0^2)} \quad (3.10)$$

In some tests, or in the case of pile caps, the reaction is concentrated at  $r_q$  and  $Q = V$ . While for uniform soil reaction cases, the failure surface may reach the bottom surface in between the edge of the column and the edge of the footing, in the cases of concentrated reactions, the failure surface may only be located in between the edge of the column and the inner radius of the loading areas (considering that supports are rigid).

### 3.3.2 Rate of internal energy dissipated in the concrete along the failure surface

The energy dissipated along the failure surface is one of the components contributing to the total rate of internal energy dissipated in both mechanisms (Figure 3.7). The calculation of this component was already investigated by several researchers (e.g. Jensen, 1975; Braestrup *et al.*, 1976; Nielsen *et al.*, 1978a; Braestrup, 1979, 1981; Nielsen and Hoang, 2011). This dissipation of energy occurs in a narrow plastic zone with a thickness  $\Delta$ . The dissipation of energy along the failure surface can be analyzed considering an infinitesimal part of it and assuming a velocity field as the one represented in Figure 3.7(b), where a radial view of the plastic zone that develops in the failure surface is shown. As derived in Section 3.10.1 (Appendix), the rate of internal energy dissipated along the failure surface  $P_{i,c,FS}$  may be computed as:

$$P_{i,c,FS} = -\pi \cdot f_{cp} \cdot \dot{\psi} \cdot \int_0^d [\sin(\chi) - 1] \cdot \sqrt{(r - r_{ICR})^2 + (z - z_{ICR})^2} \cdot \frac{r}{\cos(\alpha)} dz \quad (3.11)$$

where  $\alpha$  refers to the angle between the failure surface and the vertical axis;  $\chi$  represents the angle between the failure surface and the velocity. Depending on this latter angle, three different regimes of dissipation of energy, corresponding to the regimes shown in Figure 3.4 (b), may occur. In Regime A, which represents a sliding failure, the angle between the failure surface and the velocity is equal to the concrete friction angle ( $\chi = \varphi$ ), corresponding to the regime where dissipation of energy is maximum. In this case, the geometry of the failure surface generatrix is a logarithmic spiral, since it is known that the angle between the normalized vector tangent to the failure surface generatrix at a certain point, and the normalized vector connecting this point and the instantaneous centre of rotation has to be equal to the complementary angle of the concrete friction angle. It can be noted that if the

instantaneous centre of rotation moves towards infinity, the geometry of the failure surface generatrix in Regime A becomes a straight line. In Regime B, the angle between the failure surface and the velocity is in between the concrete friction angle and  $90^\circ$ . The last regime corresponds to the case where the velocity is normal to the failure surface, which is the reason why it is called as separation failure. In the latter case, neglecting the concrete tensile strength, there is no dissipation of energy. The geometry of the failure surface generatrix in Regime C is known to be a straight line, as the normalized vector tangent to the failure surface at a certain point has to be equal to the normalized vector that connects the same point and the instantaneous centre of rotation.

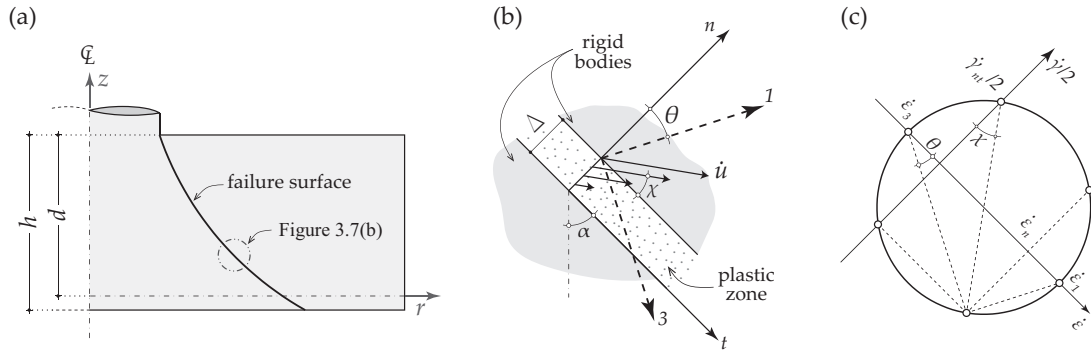


Figure 3.7: (a) General representation of failure surface; (b) radial view of an infinitesimal segment of narrow plastic zone occurring along the failure surface and (c) Mohr's circle.

### 3.3.3 Rate of internal energy dissipated in the concrete due to tangential compression

As can be seen in Figure 3.6(a), for mechanism M1, when the instantaneous centre of rotation is inside the slab in terms of height ( $0 < z_{ICR} < d$ ), and only in this case, tangential compression in the concrete in the outer portion of the footing occurs. This component of dissipation of energy is zero in mechanism M2, since its kinematics does not allow the development of tangential compression in the concrete. The tangential compression near the top surface in a footing sector is represented in Figure 3.8. It is shown in Section 3.10.2 (Appendix) that the rate of internal energy dissipated corresponding to this component is given by:

$$P_{i,c,t} = \pi \cdot (r_s - r_c) \cdot \langle d - z_{ICR} \rangle^2 \cdot f_{cp} \cdot \dot{\psi} \quad (3.12)$$

where  $\langle d - z_{ICR} \rangle$  is equal to zero when the component  $d - z_{ICR}$  is negative, corresponding therefore to the cases where there is no compression in the concrete due to tangential bending of the outer portion of the footing.

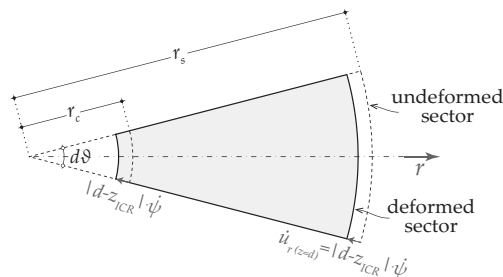


Figure 3.8: Top view of footing sector representing the concrete tangential compression.

### 3.3.4 Rate of internal energy dissipated in the reinforcement

When the failure mechanism considers a velocity field with a non-zero radial component at the level of the reinforcement, dissipation of energy occurs in both radial and tangential directions. For mechanism M1, the bottom reinforcement is considered to be in tension, while the top reinforcement may be in tension or compression, depending upon the location of the instantaneous centre of rotation (above or below the top reinforcement, respectively). In mechanism M2, both reinforcements are in tension. The rate of internal energy dissipated in bottom ( $P_{i,s,b}$ ) and top reinforcements ( $P_{i,s,t}$ ) are derived in Section 3.10.3 (Appendix), being shown to be respectively given by:

$$P_{i,s,b} = 2 \cdot \pi \cdot d \cdot f_{cp} \cdot [r_0 \omega_r + (r_s - r_0) \cdot \omega_t] \cdot |z_{ICR}| \cdot \dot{\psi} \quad (3.13)$$

$$P_{i,s,t} = 2 \cdot \pi \cdot d \cdot f_{cp} \cdot [r_c \cdot \omega_r + (r_s - r_c) \cdot \omega_t] \cdot |z_{ICR}| \cdot (d - d') \cdot \dot{\psi} \quad (3.14)$$

where  $\omega_r$  and  $\omega'_r$  are respectively bottom and top mechanical reinforcement ratios in radial direction;  $\omega_t$  and  $\omega'_t$  are respectively bottom and top mechanical reinforcement ratios in tangential direction; being given in a general manner by  $\omega = \rho \cdot f_y / f_{cp}$ . For simplicity, it is considered here that the radial reinforcement ratio is constant along the radius.

### 3.3.5 Determination of the failure load

The rate of work equation states that the rate of external work has to be equal to the total rate of internal energy dissipated as:  $P_e = P_i$  (according to the convention followed in Chen (2007) and Nielsen and Hoang (2011)). The rate of the external work (given by Eq. (3.8)) and each component of the total rate of internal energy dissipated (Eqs. (3.11)-(3.14)) are non-negative scalars.

The solution to the problem (location of the instantaneous centre of rotation and geometry of the failure surface) results from the minimization of the failure load. As shown in Braestrup *et al.* (1976), the generatrix of the failure surface in the Regime B can be found by calculus of variations, using Lagrange-Euler equations (Courant and Hilbert, 1953). Alternatively, the problem may also be solved numerically, dividing the failure surface in a finite number of segments, and searching for both the location of the instantaneous centre of rotation and the geometry of the failure surface that lead to the lowest load carrying capacity. This corresponds to a constrained non-linear optimization problem, since the location of the instantaneous centre of rotation as well as the angle between the failure surface and the velocity are constrained. In the following, results will be presented solved by means of a numerical optimization of the geometry of the failure surface and the location of the instantaneous centre of rotation.

## 3.4 Influence of different parameters on the load carrying capacity

In this section, the results given by the optimization of the proposed kinematical approach are presented and the influence of the most important parameters is investigated. The results presented in this section consider: (i) uniformly distributed soil reaction applied to bottom surface; (ii) equal reinforcement ratio in both radial and tangential directions for bottom and top reinforcements ( $\rho = \rho_r = \rho_t$ ) and ( $\rho' = \rho'_r = \rho'_t$ ) (iii) effective depth of top reinforcement equal to  $d' = 0.1 \cdot d$ . The remaining parameters are the footing (parameter  $r_s/d$ ) and column sizes (parameter  $r_c/d$ ), as well as the bottom ( $\omega = \rho \cdot f_y / f_{cp}$ ) and the top ( $\omega' = \rho' \cdot f'_y / f_{cp}$ ) mechanical reinforcement ratios. The load carrying capacity is normalized using the concrete plastic compressive strength ( $f_{cp}$ ) and the square of the effective depth ( $d^2$ ).

### 3.4.1 Governing failure mechanisms

Figure 3.9(a) depicts the relationship between the normalized load carrying capacity and the bottom mechanical reinforcement ratio, considering both mechanisms, for a case having as parameters  $r_s/d = 2.0$ ,  $r_c/d = 0.5$  and without top reinforcement ( $\omega' = 0$ ). In the same figure, also the flexural capacity computed based on the yield line pattern shown in Figure 3.10 is presented:

$$Q_{flex} = 2 \cdot \pi \cdot m_R \cdot \frac{r_s}{r_q - r_c} \cdot \frac{r_s^2}{r_s^2 - r_c^2} \quad (3.15)$$

where  $r_s^2 / (r_s^2 - r_c^2)$  is introduced in order to consider the uniform soil reaction under the column and  $r_q$  is given by Eq. (3.10) using  $r_0 = r_c$ . The moment capacity of the section  $m_R$ , which depends upon the location of the neutral axis (above, below or at the level of the top reinforcement), is calculated again assuming a rigid-plastic behaviour for concrete and steel:

$$m_R = \begin{cases} f_{cp} \cdot (\omega + \omega') \cdot d \cdot (d' - \frac{c}{2}) + \omega \cdot f_{cp} \cdot d \cdot (d - d') & , \text{if } \omega + \omega' < d'/d \\ f_{cp} \cdot (\omega - \omega') \cdot d \cdot (d' - \frac{c}{2}) + \omega' \cdot f_{cp} \cdot d \cdot (d - d') & , \text{if } \omega - \omega' > d'/d \\ f_{cp} \cdot d \cdot \left( \frac{d'^2}{2 \cdot d} + \omega \cdot (d - d') \right) & , \text{otherwise} \end{cases} \quad (3.16)$$

Figure 3.9(b)-(g) present several failure mechanisms for the cases highlighted in Figure 3.9(a), representing mechanisms M1 and M2. The principal strain directions along the failure surface (computed using Eq. (3.318)), which represent the principal direction of the compression, are also represented.

A clear flexural failure mode is shown to occur only for fairly low amounts of bottom mechanical reinforcement ratio (refer to Figure 3.9 (a)), where the load carrying capacity given by mechanism M1 is very close to the flexural capacity computed using Eq. (3.15). As shown in Figure 3.9(a), mechanism M1 is governing for low amounts of bottom mechanical reinforcement ratio, defining a transition between flexural and punching shear failures. In fact, mechanism M1 considers in its kinematics the rotation known to occur for a flexural failure (Figure 3.9(b)). On the contrary, mechanism M2 considers a clockwise rotation, therefore leading to a failure mechanism more related to a translational movement (associated to punching failures) during the flexural-shear failure regime (Figure 3.9(c)). While for mechanism M1, the instantaneous centre of rotation is close to the column, thus leading to an important component of rotation, in mechanism M2, the instantaneous centre of rotation is far from it, leading to a dominant translational movement with low rotation associated. Therefore, in mechanism M1 (Figure 3.9(b)), a steep failure surface with biaxial compression (Regime A) close to the top surface, and a separation failure (Regime C) without dissipation of energy, close to the bottom surface, is observed. Hence, in mechanism M1, a considerable amount of the rate of internal energy dissipated occurs in the bottom reinforcement due to the important component of rotation in its failure mode. This is the reason why an increase of the bottom mechanical reinforcement leads to a significant increase in the load carrying capacity, accompanied by a reduction of the rotation component. For higher values of the bottom mechanical reinforcement ratio, the significance of the rotation decreases, reducing the influence of the bottom reinforcement. At this point, the dissipation of energy in the concrete along the failure surface increases, and the biaxially compressed zone extends towards the bottom surface. The evolution of the described process regarding mechanism M1 may be observed with the help of Figure 3.9 (b), (d) and (e), where it is possible to follow the decrease of the rotation component and the growth of the importance of Regime A along the failure surface.

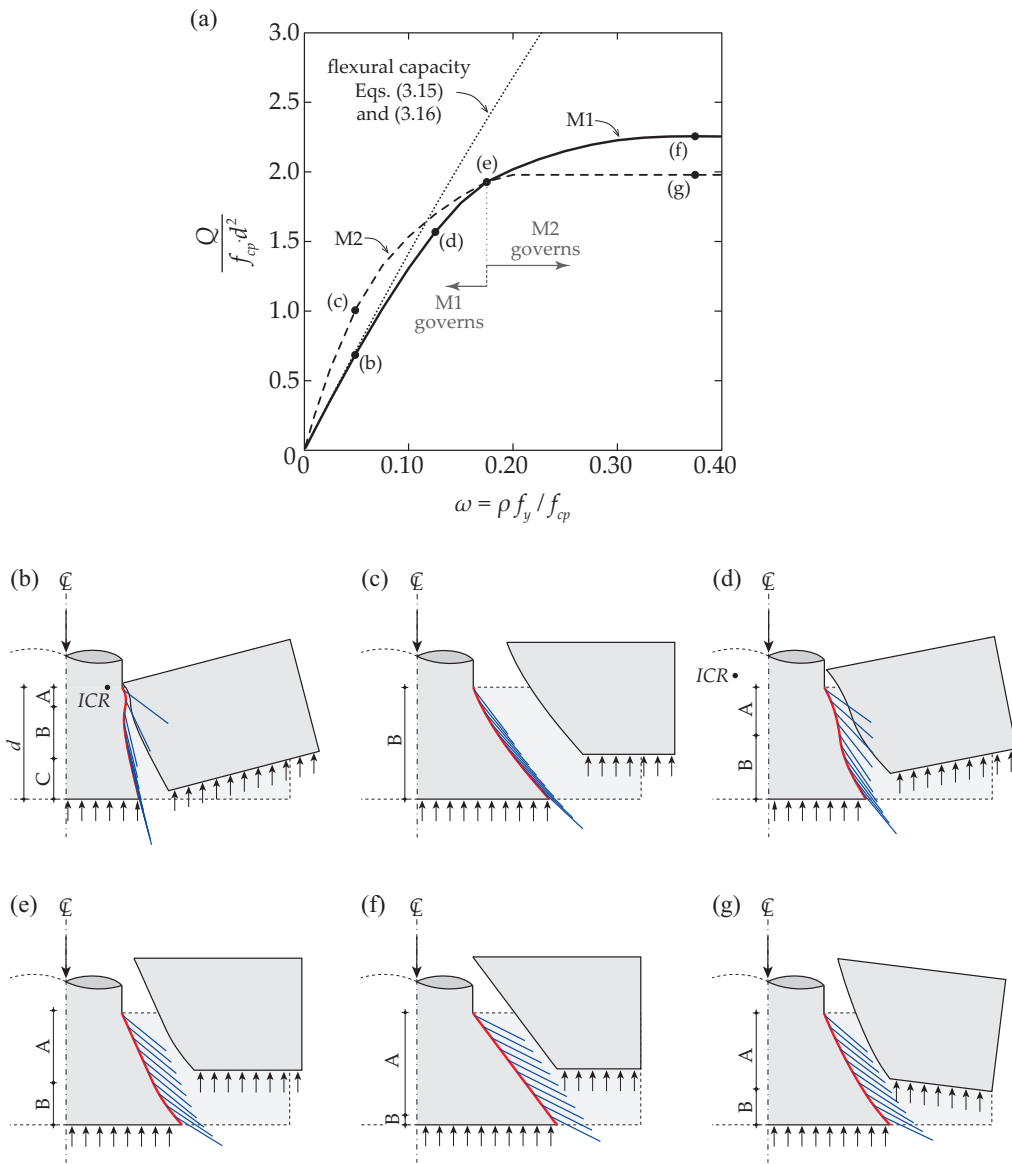


**Figure 3.9:** Analysis of a general case with  $r_s/d = 2.0$ ,  $r_c/d = 0.5$  and  $\omega' = 0$ : (a) normalized load carrying capacity as a function of the bottom mechanical reinforcement ratio; failure mechanisms with principal strain directions along the failure surface (for blue lines representing the principal compressive strains direction): (b) M1 with  $\omega = 0.05$ ; (c) M2 with  $\omega = 0.05$ ; (d) M1 with  $\omega = 0.125$ ; (e) M1 and M2 with  $\omega \approx 0.175$ ; (f) M1 with  $\omega = 0.375$  and (g) M2 with  $\omega = 0.375$ .

The transition between mechanisms M1 and M2 occurs when the rotation component disappears. This corresponds to the case where the instantaneous centre of rotation is in the infinite and the failure mechanism corresponds to a pure translational movement with a horizontal component (Figure 3.9(e)). For increasing values of the bottom mechanical reinforcement ratio, mechanism M1 leads to a reduction of the horizontal component of this translational movement, until the failure mechanism consists only in a vertical shift of the outer portion of the footing (Figure 3.9(f)). This process is characterized by a decrease of the dissipation of energy in the bottom reinforcement, as a consequence of the decrease of the radial component of the velocity. This reduction is accompanied by an increase of the energy dissipated along the failure surface, which results from the increment of the length of Regime A along the failure surface (compare Figure 3.9(e) and (f)). However, as it can be observed in Figure 3.9(a), for fairly large values of the bottom mechanical reinforcement ratio, this solution does not correspond to

the lowest upper bound solution, since another failure mechanism is governing. The failure mechanism governing in this case, represented in Figure 3.9(g), includes an important rotation component contrary to the one normally considered in a flexural failure. In this failure mechanism, the instantaneous centre of rotation is located close to the footing and at the level of the bottom reinforcement, thus not activating it. From the comparison of Figure 3.9(f) and (g), respectively, corresponding to failure mechanisms M1 and M2 for equal bottom mechanical reinforcement ratio, it is possible to observe that the second mechanism leads to a lower contribution of the biaxially compressed zone (Regime A).

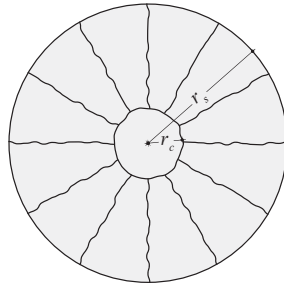
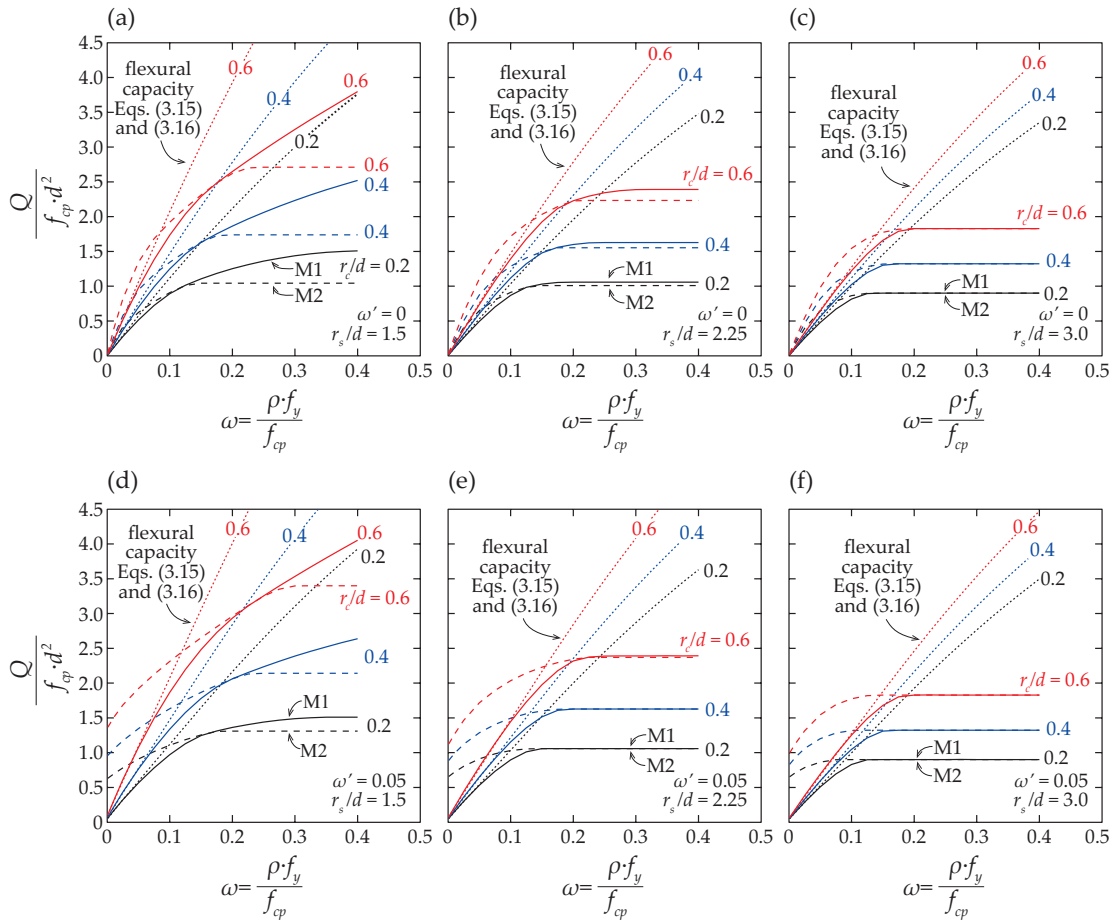


Figure 3.10: Yield line pattern considered in flexural failure of a circular footing with a circular column.

### 3.4.2 Parametric analysis

The results presented in Figure 3.9 are extended in Figure 3.11 for several cases varying the footing size (ratio  $r_s/d = 1.5; 2.25; 3.0$ ), the column size (ratio  $r_c/d = 0.2; 0.4; 0.6$ ), as well as the top mechanical reinforcement ratio ( $\omega' = 0; 0.05$ ). In Figure 3.11 is also shown the normalized flexural capacity, computed according to Eqs. (15) and (16). Although the influence of the ratios  $r_s/d$ ,  $r_c/d$  and  $\omega'$  is important, the evolution of the normalized load carrying capacity with the bottom mechanical reinforcement ratio presented for the general case of Figure 3.9, is also observed in all the cases shown in Figure 3.11. Although the influence of top mechanical reinforcement ratio (when reasonable values of it are adopted) tends to be reduced in the cases where mechanism M1 is governing, it shows a considerably influence in the results where mechanism M2 governs. This influence may be observed comparing Figure 3.11(a)-(c) with Figure 3.11 (d)-(f), respectively, where the consideration of a low amount of top mechanical reinforcement ratio ( $\omega' = 0.05$ ) leads to a significant increase of the load carrying capacity. A large value of top mechanical reinforcement ratio leads to a limit situation corresponding to the instantaneous centre of rotation located at infinite in the radial axis, thus leading to a failure mode characterized by a vertical movement of the outer portion of the footing. In this case, both mechanism M1 and M2 lead to the same failure mechanism and load carrying capacity, which corresponds to the solution originally proposed by Braestrup *et al.* (1976). This phenomenon may be observed, for example, comparing the case of  $r_s/d = 2.25$  and  $r_c/d = 0.4$  presented in Figure 3.11 (b) and (e). An increase of the punching shear strength with the increase of the top mechanical reinforcement ratio is related to a decrease of the rotation component and to the increase of the biaxially compressed zone along the failure surface. This is the kinematical reason why the top reinforcement becomes more efficient for more compact slabs and larger column sizes, since these are the cases where a larger clockwise rotation component in the punching shear regime exists (mechanism M2 governing, compare e.g. Figure 3.11(a) and (c)). It is interesting to note that although this conclusion is obtained through a kinematical approach, it is physically consistent with the fact that the development of confinement stresses, due to the presence of top reinforcement, enables the improvement of the capacity of the diagonal compression strut carrying shear that develops inside the footing (Guidotti *et al.*, 2011).



**Figure 3.11:** Normalized load carrying capacity with bottom mechanical reinforcement ratio for different column sizes to effective depth ratios  $r_c/d$ : (a)  $\omega' = 0$  and  $r_s/d = 1.5$ ; (b)  $\omega' = 0$  and  $r_s/d = 2.25$ ; (c)  $\omega' = 0$  and  $r_s/d = 3.0$ ; (d)  $\omega' = 0.05$  and  $r_s/d = 1.5$ ; (e)  $\omega' = 0.05$  and  $r_s/d = 2.25$ ; (f)  $\omega' = 0.05$  and  $r_s/d = 3.0$ .

With respect to the ratio of the column size (ratio  $r_c/d$ ), it may be observed that for larger column sizes, although the failure surface is slightly steeper, not only the radius of the failure surface at the level of the bottom reinforcement, but also the area of the failure surface is larger, leading to a higher load carrying capacity.

As shown in Figure 3.11, and as previously explained, the punching shear strength increases with increasing column size, with increasing top mechanical reinforcement ratio and with decreasing footing size. As a consequence, the flexural-shear regime becomes more important, covering a larger range of bottom mechanical reinforcement ratios, meaning that this regime is relevant for the analysis of footings.

Although the presented analysis has been carried for uniform soil reaction, it may also be performed for concentrated reactions, leading to the same general conclusions. In these cases, as observed by Braestrup *et al.* (1976), when concrete tensile strength is neglected, as in the present work, the failure surface develops between the column and the inner radius of the support, accounting for the size of the loading areas (necessary to distribute the reaction forces).

### 3.5 Simplified formulations - practical application

The application in the practice of the kinematical approach above presented would be time consuming. For this reason, the development of simplified expressions, allowing a simpler, yet accurate, calculation of the load carrying capacity of footings becomes important. The application of the expressions that will be presented in the following is limited to the cases of footings (i) without shear reinforcement, (ii) considered to be subjected to a uniform soil reaction and (iii) with  $r_c/d \leq 1.2$ ,  $1.0 \leq a/d \leq 3.0$  (where  $a = r_s - r_c$ ) and  $2.0 \leq r_s/r_c \leq 12.0$ . For simplicity reasons, only cases without top reinforcement will be investigated. This consideration is sufficiently approximated for practical purposes as the top reinforcement does not yield to significant differences except for very compact members with large columns (refer to Figure 3.11). In accordance to what is presented in the previous section, two different regimes are considered: flexural-shear regime for low amounts of bottom mechanical reinforcement ratio and punching shear regime for large amounts of the same parameter.

In accordance to what is presented in the previous section, two different regimes are considered: flexural-shear regime for low amounts of bottom mechanical reinforcement ratio and punching shear regime for large amounts of the same parameter.

#### 3.5.1 Flexural-shear failures

It was previously shown that this regime, where an interaction between flexural and shear behaviour is observed, leads to lower load carrying capacity than the one predicted considering a flexural failure with the yield pattern shown in Figure 3.10 (Eqs. (3.15) and (3.16)). In fact, a flexural failure considers a compression zone resulting from a pure flexural behavior, thus being only a function of the bottom and top mechanical reinforcement ratios (Eq. (3.16)). However, this does not occur for compact footings subjected to a concentrated load. In these cases, a concentration of large shear forces near the column is observed, resulting from a compression strut whose radial force component equilibrates most of the force of the whole tension reinforcement. For this reason, the height of the compression zone in the radial direction is significantly larger than in the tangential direction. For cases without shear reinforcement as those treated in this chapter, the latter can even disappear as the instantaneous centre of rotation is located outside the footing.

Due to the inclination of the actual compression strut carrying shear and the location of its resultant, the effective lever arm is reduced with respect to the one corresponding to a flexural analysis (Figure 3.12(b)). The location of the resultant of the compression strut at the edge of the column ( $z_c$  in Figure 3.12(a)) can be calculated on the basis of the results of the optimized theoretical solution using equilibrium conditions, as the load carrying capacity and the reinforcement forces are known. A good estimation of these results is given by the following equation:

$$\frac{z_c}{d} = \frac{\omega}{2} \cdot \left( 1 + 0.4 \cdot \frac{r_s}{r_c} \cdot \frac{d}{r_q - r_c} \right) \quad (3.17)$$

where  $r_q$  is calculated using Eq. (3.10) with  $r_0 = r_c$ . The load carrying capacity  $Q_{fs}$  can thus be calculated according to Eq. (3.15) but using a reduced moment capacity  $m_R$  accounting for the reduced lever arm, defined as:

$$\bar{m}_R = f_{cp} \cdot d^2 \cdot \omega \left( 1 - \frac{z_c}{d} \right) \quad \text{with } z_c/d \text{ from Eq. (3.17)} \quad (3.18)$$

It has to be noted that this equation is valid only for the flexural-shear failure as yielding of bottom reinforcement is assumed. For large amounts of bottom reinforcement, pure shear regime becomes governing.

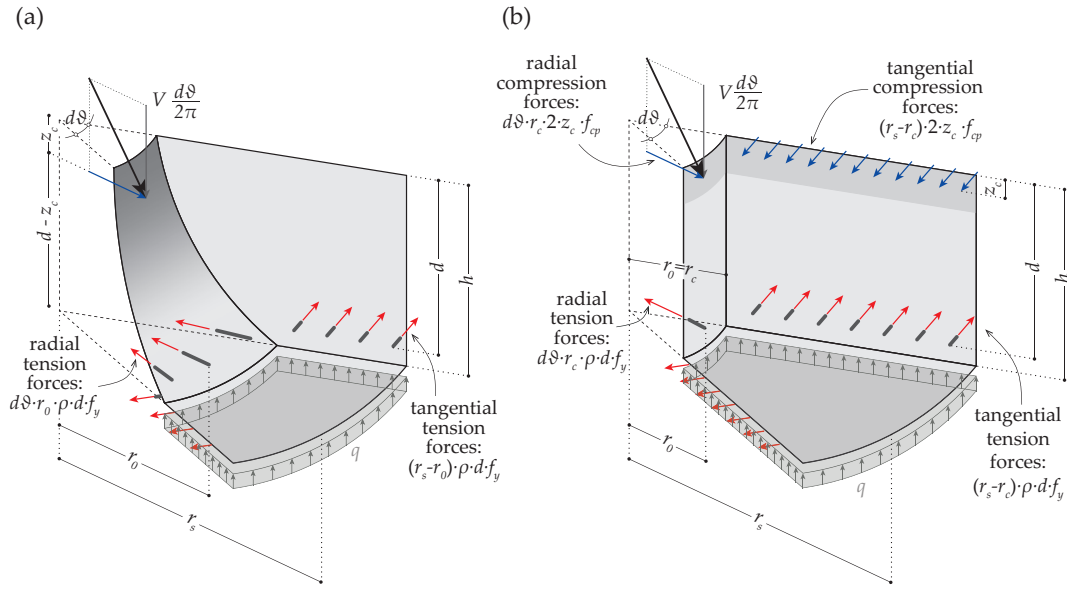


**Figure 3.12:** Schematic representation of a rigid-body of footing uniformly loaded in the flexural-shear regime: (a) actual failure mechanism obtained with the kinematical theorem of limit analysis and (b) failure mechanism considered in the calculation of the flexural-shear capacity through the simplified formulation.

### 3.5.2 Punching shear failures

Considering that sufficient amount of bottom flexural reinforcement is used to avoid a flexural-shear failure, a punching shear failure without plastic activation of the flexural reinforcement governs. In this regime, the load carrying capacity relies only on the internal energy dissipated by the concrete along the failure surface. Thus, a nominal control section where an effective shear stress is to be verified helps investigating this regime (typical approach of design codes). The location of this control section has to be a function of the inclination of the failure surface as well as of the distribution of the internal energy dissipated along the failure surface. A steeper inclination of the failure surface as well as a higher concentration of the energy dissipated near the column requires a control section closer to it. Besides being important to define the location of a nominal control section, the inclination of the failure surface is also important to define the amount of uniform soil reaction that acts inside the failure zone.

Figure 3.13 depicts the secant inclination  $\beta$  of the failure surface as a function of the shear slenderness ratio  $a/d$ , for different values of the column size to effective depth ratio  $r_c/d$ . This inclination is defined as:

$$\cot(\beta) = \frac{r_0 - r_c}{d} \quad (3.19)$$

It is shown in Figure 3.13 that this inclination is mostly a function of the shear slenderness (it decreases with increasing of the shear slenderness). This is in accordance with different experimental evidences (e.g. Hegger *et al.*, 2009; Ricker, 2009; Siburg and Hegger, 2014; Siburg, 2014), which have shown a relationship between the inclination of the shear crack of the punching cone and the shear slenderness, with steeper shear cracks observed for more compact footings. Based on the results of the kinematical approach herein presented, a simple formula for the secant inclination  $\beta$  can be proposed:

$$\beta = \frac{\pi/2}{0.8 + 0.5 \cdot \frac{a}{d}} \text{ [rad]} \quad (3.20)$$

Based on this inclination, the radius of the failure surface  $r_0$  at the level of the bottom reinforcement can be calculated according to Eq. (3.19). On that basis, it is also possible to define the part of the uniform soil reaction acting inside the failure zone (and thus do not influencing the shear strength) and the total load carrying capacity  $Q_p$  corresponding to this regime:

$$Q_p = V_p \cdot \frac{r_s^2}{r_s^2 - r_0^2} \quad (3.21)$$

where  $V_p$  represents the effective shear strength in the case of punching shear regime, thus corresponding to the uniform soil reaction outside the radius of the failure surface at the level of bottom reinforcement. Based on the column radius as well as on the radius of the failure surface at the level of the bottom reinforcement, a control section and its corresponding perimeter  $b_0$  may be defined as:

$$b_0 = 2 \cdot \pi \cdot [r_c + 0.2 \cdot d \cdot \cot(\beta)] \quad (3.22)$$

Parameter 0.2 defines a control section located at  $0.2 \cdot d \cdot \cot(\beta)$  from the column edge. This choice is justified by the curvature of the failure surface with a steeper inclination near the column, precisely where a concentration of energy dissipation tends to occur (see Figure 3.13(c)-(f)).

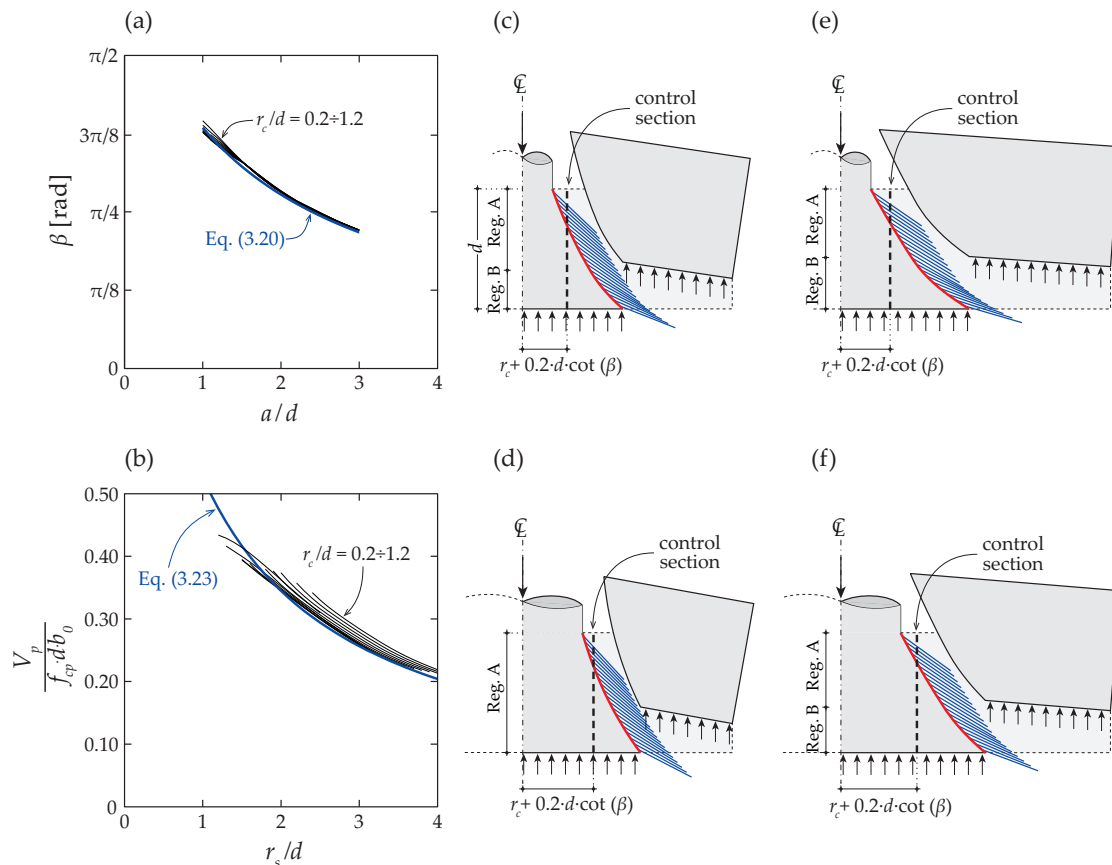


**Figure 3.13:** (a) Theoretical and approximated values of the inclination of the failure surface as a function of the shear slenderness for different column sizes to effective depth ratios; (b) normalized effective punching strength as a function of footings size to effective depth ratio for different column sizes to effective depth ratios; failure mechanisms corresponding to punching shear regime with principal strain directions along the failure surface and control section: (c)  $r_s/d = 1.75$  and  $r_c/d = 0.25$ ; (d)  $r_s/d = 1.75$  and  $r_c/d = 0.50$ ; (e)  $r_s/d = 2.25$  and  $r_c/d = 0.25$ ; (f)  $r_s/d = 2.25$  and  $r_c/d = 0.50$ .

The punching shear carrying capacity, normalized by the plastic concrete compressive strength  $f_{cp}$  and by the control section  $b_0 \cdot d$ , is shown as a function of the footing size in Figure 3.13(b) for different column sizes. The figure shows that the normalized effective punching shear strength is mostly a function of the footing size to effective depth ratio  $r_s/d$ . An increase of this parameter leads to a decrease of the normalized effective punching load, which is in accordance to what is physically expected. A simplified expression can be proposed to calculate the normalized effective punching strength as a function of the footing size to effective depth ratio:

$$V_p = \frac{1}{0.9 + \frac{r_s}{d}} \cdot f_{cp} \cdot b_0 \cdot d \quad (3.23)$$

It can be noted that  $f_{cp}$  is calculated using Eq. (3.1) to account for concrete brittleness and the presence of transverse strains. The results obtained with the proposed expression are also shown in Figure 3.13(b), approximating fairly well the results numerically obtained through the optimization of the kinematical approach above presented.

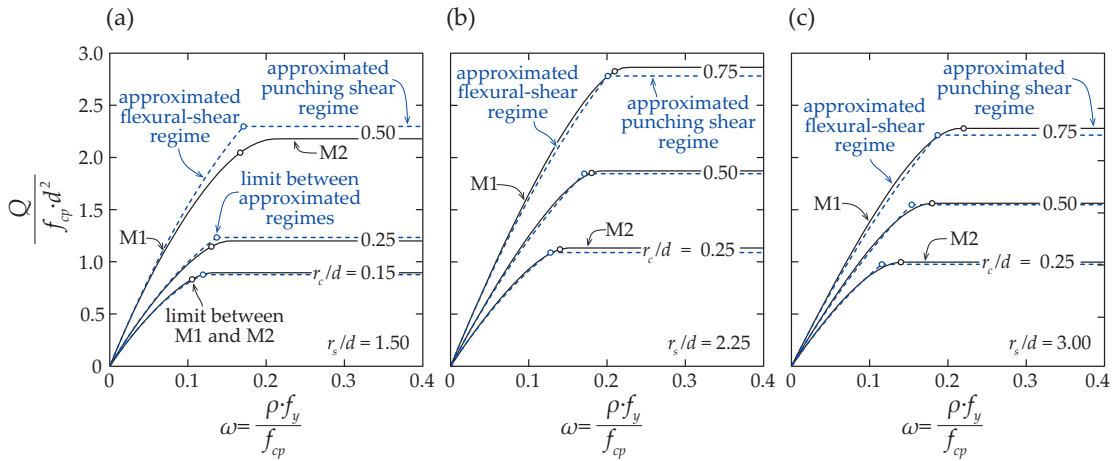


**Figure 3.14:** Load carrying capacity calculated obtained with optimized kinematical solution and simplified expressions as a function of the bottom mechanical reinforcement ratio for different column sizes to effective depth ratios: (a)  $r_s/d = 1.50$ ; (b)  $r_s/d = 2.25$  and (c)  $r_s/d = 3.0$ .

The lowest failure load obtained by the simplified expressions proposed for each regime is the governing load carrying capacity. A general comparison of the normalized load capacity obtained through the optimized solution of the kinematical approach above presented and the proposed simplified expressions is presented in Figure 3.14, for different footing and column sizes (span to effective depth ratio  $a/d$  varying from 1.0 to 2.9). A very good agreement of the optimized kinematical solution by the proposed expressions can be observed.

### 3.6 Comparison with experimental results

Several experimental investigations concerning the punching shear strength of footings have been performed in the past (e.g. Talbot, 1913; Richart, 1948; Kordina and Nölting, 1981; Dieterle and Rostásy, 1987; Hallgren *et al.*, 1998; Timm, 2003; Hegger *et al.*, 2006; Ricker, 2006; Hegger *et al.*, 2007, 2009; Ricker, 2009; Urban *et al.*, 2013; Siburg and Hegger, 2014; Siburg, 2014). The experimental investigations presented by Hallgren *et al.* (1998) and Dieterle and Rostásy (1987) are particularly interesting, since both testing campaigns contained several tests with the same loading conditions and where all the parameters ( $r_s; r_c; r_q; d; \omega'$ ) were kept approximately constant, only varying the bottom mechanical reinforcement ratio  $\omega$ .

**Table 3.1:** Description of experimental tests performed by Hallgren *et al.* (1998) and Dieterle and Rostásy (1987).

Source	Specimen	Footing's shape	$r_s^a$ [m]	Column's shape	$r_c^b$ [m]	$d$ [m]	$f_{c,cube}^c$ [MPa]	$\rho^d$ [%]	$f_y$ [MPa]	$V_{R,test}$ [MN]	
Hallgren <i>et al.</i> (1998) <sup>e</sup>	S1	Square	0.48	Circular	0.125	0.242	49.8	0.40	621	1.363	
	S2					0.243	35.5	0.40		1.015	
	S3					0.250	37.2	0.39		1.008	
	S4					0.232	32.1	0.66		0.992	
	S7					0.246	18.0	0.40		0.622	
	S8	0.245	39.3	0.25	0.915						
	S9	0.244	31.9	0.40	0.904						
	S12	Circular	0.48	Circular	0.125	0.242	34.1	0.42	621	1.049	
	S13					0.244	24.7	0.42		0.803	
Dieterle and Rostásy (1987)	B-1	Square	0.846	Square	0.191	0.296	28.2	0.20	453	1.054	
	B-2					0.294	28.4	0.42		451	1.522
	B-3					0.293	33.8	0.62		415	2.065
	B-4					0.292	28.9	0.83		395	1.902
	B-4/2					0.290	30.4	0.89		458	2.090
	B-4/3					0.294	29.2	0.86		464	2.068
	B-4/4					0.292	29.8	0.83		395	1.889
V2	0.294	33.0	0.40	486	1.800						

<sup>a</sup> In the case of square footings,  $r_s$  is calculated considering an equal area for the bottom surface.

<sup>b</sup> In the case of square columns,  $r_c$  is computed assuming an equal column perimeter.

<sup>c</sup> To compare with the theoretical results, an  $f_c = 0.8 \cdot f_{c,cube}$  is considered.

<sup>d</sup> The reinforcement ratio was considered equal in both radial and tangential directions; its value was assumed to be equal to the average reinforcement ratio determined in orthogonal direction.

<sup>e</sup> For the square footings of Hallgren *et al.* (1998),  $r_q$  is simplified considering to be equal to the one of the experimental tests in circular footings ( $r_q = 337$  mm).

The parameters selected to compare the theoretical solution with the experimental values represent average values of the experimental tests considered in the comparison (the main properties of each experimental test are shown in Table 3.1, where a circular column with an equal perimeter of a rectangular column was considered and, in the case of square footings,  $r_s$  was calculated considering an equal area for the bottom surface). The plastic concrete compressive strength was calculated according to Eq. (3.1) considering a constant value for the reduction factor accounting for the presence of transverse strains  $\eta_\epsilon$ . Actually, this factor is not constant within the group of experimental tests considered, since it is a function of the state of strains in the region of the theoretical failure surface (Vecchio and Collins, 1986; Vecchio, 2000; Fernández Ruiz and Muttoni, 2008), therefore depending on the bottom mechanical reinforcement ratio. Higher values of the latter ratio are associated to lower transverse strains. For this reason, two different values of the reduction factor accounting for the presence of transverse strains are considered in the comparison between the experimental results of Hallgren *et al.* (1998) and the theoretical values of the normalized load carrying capacity, computed based on the optimization of the kinematical solution, shown in Figure 3.15(a)  $\eta_\epsilon = 0.5$  and (b)  $\eta_\epsilon = 0.6$ . These values are in agreement with the reductions factors usually adopted for concrete with shear cracks (Fernández Ruiz and Muttoni, 2008; Nielsen and Hoang, 2011; *fib* Model Code 2010, 2013). The results show a fairly good agreement between theory and experimental results. It is interesting to note that the test results with lower amounts of bottom mechanical reinforcement ratio approximate better the theoretical results for smaller values of the reduction factor  $\eta_\epsilon$ . On the contrary, for the footings with larger amounts of bottom mechanical reinforcement ratio, a better agreement is found (and thus smaller strains at failure) if a higher value is considered for the reduction factor  $\eta_\epsilon$ .

Figure 3.15(b) shows a comparison with the tests performed by Dieterle and Rostásy (1987) (main properties shown in Table 3.1). According to the authors of the experimental campaign, the four tests with  $\rho > 0.8\%$  presented a bond failure at the plane of the bottom flexural reinforcement, leading to a potentially premature punching shear failure. Nevertheless, it is not clear if bond failure was the cause

of a premature punching failure or was just a consequence of punching. For that reason, the referred experimental tests are also considered herein. For this group of tests, a reduction factor accounting for the presence of transverse strains  $\eta_\epsilon$  varying within 0.45 and 0.55 is considered (slightly lower than for the previous series). The different range of values considered for each group of experimental tests may be justified by the different geometrical and material properties, as well as different loading conditions and potential bond failures. As this group of experimental tests was conducted with a uniform loading applied to the bottom surface of the footings, the simplified expressions are also presented in Figure 3.15(b) approximating very well the optimized solution of the kinematical approach of limit analysis.

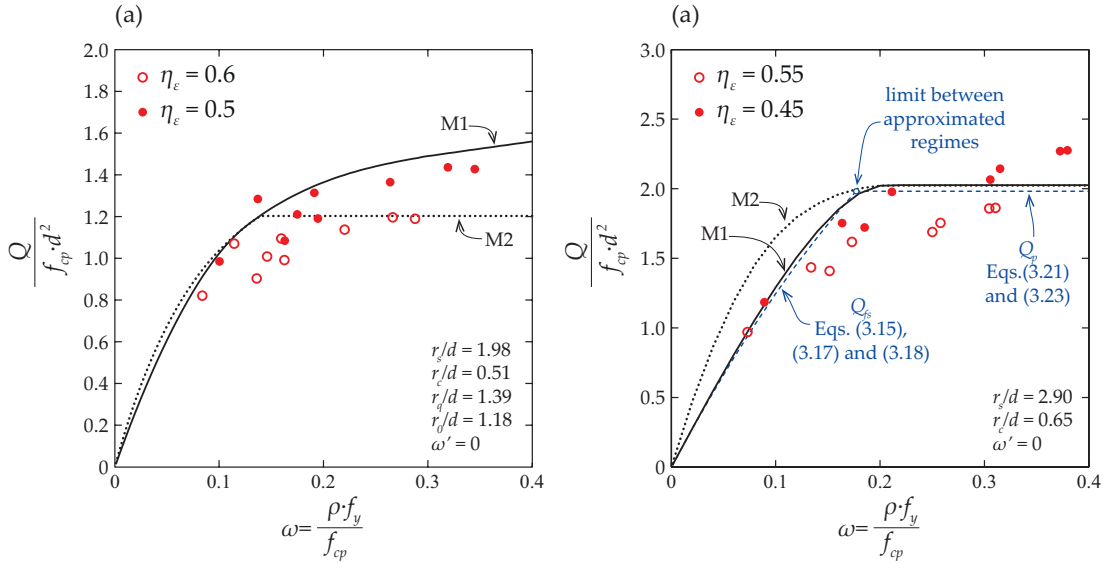


**Figure 3.15:** Comparison between theoretical and experimental values of load carrying capacity from: (a) Hallgren *et al.* (1998), considering  $r_s/d = 1.98$ ,  $r_c/d = 0.51$ ,  $r_q/d = 1.39$ ,  $r_0/d = 1.18$  and  $\omega' = 0$ ; (b) Dieterle and Rostásy (1987) considering  $r_s/d = 2.90$ ,  $r_c/d = 0.65$  and  $\omega' = 0$ .

Although the comparisons between experimental results and theoretical values have shown a fairly good agreement for both groups of experimental tests, it remains clear that the value of the reduction factor  $\eta_\epsilon$  to be applied in order to take into account the state of strains has to be further investigated. In addition, the potential influence of size is also a topic of future works.

### 3.7 Conclusions

The kinematical theorem of limit analysis is used in order to determine the load carrying capacity of isolated footings subjected to concentrated loads. The concrete is considered to have rigid-plastic behaviour with a Mohr-Coulomb yield criterion.

A rigid-plastic behaviour in both compression and tension is also adopted for the reinforcement bars. The influence of each physical parameter in the load carrying capacity based on the proposed approach is assessed. The main conclusions are:

1. Pure flexural failure only occurs for fairly low amounts of bottom mechanical reinforcement, while pure punching shear failure results only for large amounts of flexural reinforcement;
2. For intermediate amounts of flexural reinforcement, a combined flexural-shear mechanism becomes governing, allowing a smooth transition between flexural and punching shear failure modes. It is shown that this regime is particularly important for compact footings and larger columns,

thus showing its importance when predicting the load carrying capacity of footings;

3. In what respects the punching shear regime, it is shown that the consideration of a failure characterized by a translational vertical movement of the outer portion of the footing might overestimate the punching shear strength in the cases of low amounts of top mechanical reinforcement ratios. This difference is more important for compact footings and for larger column sizes. In these cases, the top reinforcement ratio might play an important role;
4. A physical explanation for the previous conclusion on the influence of the top reinforcement, is that this reinforcement enables the development of confining stresses along the failure surface, increasing the capacity of the compression strut that carries shear directly inside the footing;
5. Simplified formulations for practical use are presented for the cases of footings subjected to uniform soil reaction, incorporating simplified expressions that allow the calculation of the load carrying capacity corresponding to each regime. It is shown that the simplified formulations proposed approximate fairly well the optimized kinematical solution;
6. The lower load capacity observed in the flexural-shear regime, when compared to the pure flexural capacity, is explained by the loss of lever arm due to the increase of the compression height at the column edge, where both shear and radial compression are carried by an inclined compression strut. This shows that the Johansen's yield line theory (Johansen, 1962) developed for thin slabs is not really applicable for compact footings;
7. In what respects the punching shear regime, it is shown that the inclination of the failure surface is mostly a function of the shear slenderness and that the control section for assessing the shear strength should be located rather close to the column (closer than values usually adopted for punching design of flat slabs). This is justified by the fact that the failure surface presents, in a wide range of cases, a curved geometry with a steeper inclination close to the column, precisely where an important amount of internal energy is dissipated;
8. The proposed plastic approach is shown to approximate fairly well the experimental results of Hallgren *et al.* (1998) and Dieterle and Rostásy (1987);
9. Further investigation remains to be done regarding the value of the reduction factor that takes into account the state of transverse strains of the footings on the concrete strength and potentially also size effect.

### 3.8 References

- Bortolotti L. (1990):** „Punching shear strength in concrete slabs“. *ACI Structural Journal*, Vol. 87, No. 2, pp. 208–219.
- Braestrup M. W. (1974):** „Plastic analysis of shear in reinforced concrete“. *Magazine of Concrete Research*, Vol. 26, No. 89, pp. 221–228.
- Braestrup M. W. (1979):** „Punching shear in concrete slabs“. In: *Plasticity in reinforced concrete*. International Association for Bridge and Structural Engineering. IABSE colloquium, pp. 115–136.
- Braestrup M. W. (1981):** „Structural concrete as a plastic material“. In: *Advanced mechanics of reinforced concrete*. International Association for Bridge and Structural Engineering. Delft, Holland: IABSE colloquium, pp. 3–16.
- Braestrup M. W.; Nielsen M. P.; Jensen B. C.; Bach F. (1976):** *Axisymmetric Punching of Plain and Reinforced Concrete*. Tech. rep. 75. Structural Research Laboratory, Technical University of Denmark, p. 33.
- Broms C. E. (2005):** „Concrete flat slabs and footings: Design method for punching and detailing for ductility“. PhD thesis. Stockholm, Sweden: Department of Structural Engineering, Royal Institute of Technology, p. 114.
- Chen W. F. (2007):** *Plasticity in reinforced concrete*. J. Ross Publishing.
- Courant R.; Hilbert D. (1953):** *Methods of Mathematical Physics*. Vol. 1. New York, USA: Interscience Publishers.
- Dieterle H. (1987):** „Design of reinforced concrete foundations of square columns under centric loading with the help of design diagrams (In German: Zur Bemessung quadratischer Stützenfundamente aus Stahlbeton unter zentrischer Belastung mit Hilfe von Bemessungsdiagrammen)“. *Deutscher Ausschuss für Stahlbeton*, Vol. 387, pp. 94–134.
- Dieterle H.; Rostásy F. (1987):** „Load-carrying behaviour of isolated reinforced concrete foundations of square columns (In German: Tragverhalten quadratischer Einzelfundamente aus Stahlbeton)“. *Deutscher Ausschuss für Stahlbeton*, Vol. 387, pp. 1–91.
- Drucker D. C. (1961):** *On structural concrete and the theorems of limit analysis*. IABSE reports. Zürich, Switzerland: International Association for Bridge and Structural Engineering.
- Fernández Ruiz M.; Muttoni A. (2007):** „On development of suitable stress fields for structural concrete“. *ACI Structural Journal*, Vol. 104, No. 4, pp. 495–502.
- Fernández Ruiz M.; Muttoni A. (2008):** „Shear strength of thin-webbed post-tensioned beams“. *ACI Structural Journal*, Vol. 105, No. 3, pp. 308–317.
- fib Model Code 2010 (2013):** *Model Code 2010 - Final draft*. Tech. rep. Volumes 1 and 2, Bulletins 65 and 66. International Federation for Structural Concrete.
- Gesund H. (1983):** „Flexural Limit Analysis of Concentrically Loaded Column Footings“. *ACI Journal Proceedings*, Vol. 80, No. 3, pp. 223–228.
- Gesund H. (1985):** „Flexural limit design of column footings“. *Journal of Structural Engineering*, Vol. 111, No. 11, pp. 2273–2287.
- Gesund H.; Dikshit O. P. (1971):** „Yield line analysis of the punching problem at slab/column intersections“. *ACI Special Publication*, Vol. 30, pp. 177–202.

- Guidotti R.; Fernández Ruiz M.; Muttoni A. (2011):** „Crushing and Flexural Strength of Slab-Column Joints“. *Engineering Structures*, Vol. 33, No. 3, pp. 855–867.
- Hallgren M.; Bjerke M. (2002):** „Non-linear finite element analyses of punching shear failure of column footings“. *Cement and Concrete Composites*, Vol. 24, No. 6, pp. 491–496.
- Hallgren M.; Kinnunen S.; Nylander B. (1998):** „Punching shear tests on column footings“. *Nordic Concrete Research*, Vol. 21, pp. 1–22.
- Hegger J.; Sherif A.; Ricker M. (2006):** „Experimental Investigations on Punching Behaviour of Reinforced Concrete Footings“. *ACI Structural Journal*, Vol. 103, No. 4, pp. 604–613.
- Hegger J.; Ricker M.; Ulke M.; Ziegler M. (2007):** „Investigations on the punching behaviour of reinforced concrete footings“. *Engineering Structures*, Vol. 29, No. 9, pp. 2233–2241.
- Hegger J.; Ricker M.; Sherif M. (2009):** „Punching Strength of Reinforced Concrete Footings“. *ACI Structural Journal*, Vol. 106, No. 5, pp. 706–716.
- Jensen B. C. (1975):** „Lines of discontinuity for displacements in the theory of plasticity of plain and reinforced concrete“. *Magazine of Concrete Research*, Vol. 2, No. 2, pp. 143–150.
- Jensen U. G.; Hoang L. C. (2012):** „Collapse mechanisms and strength prediction of reinforced concrete pile caps“. *Engineering Structures*, Vol. 35, pp. 203–214.
- Jiang D. H.; Shen J. H. (1986):** „Strength of concrete slabs in punching shear“. *Journal of Structural Engineering*, Vol. 112, No. 12, pp. 2578–2591.
- Johansen K. W. (1962):** *Yield-line Theory*. Cement and Concrete Association.
- Kordina K.; Nölting D. (1981):** *Load-carrying behaviour of eccentrically loaded isolated reinforced concrete foundations (In German: Tragverhalten von ausmittig beanspruchten Einzelfundamenten aus Stahlbeton)*. Tech. rep. DFG Research 204/27-30. Braunschweig, Germany: Technical University of Braunschweig, p. 158.
- Kuang J. S. (1991):** *An upper-bound plastic solution for punching shear failure of concrete slabs*. Tech. rep. CUED/D-Struct/TR.136. United Kingdom: Engineering Department, Cambridge University.
- Leonhardt F.; Walther R. (1962):** „Shear tests on single span beams with and without shear reinforcement (In German: Schubversuche an einfeldrigen Stahlbetonbalken mit und ohne Schubbewehrung)“. *Deutscher Ausschuss für Stahlbeton*, Vol. 151, pp. 83.
- Moe J. (1961):** *Shearing strength of reinforced concrete slabs and footings under concentrated loads*. Vol. D47. Skokie, Illinois: Portland Cement Association, Research and Development Laboratories.
- Morley C. T. (1979):** „Punching shear failure of hollow concrete spheres“. In: *Plasticity in reinforced concrete*. International Association for Bridge and Structural Engineering. IABSE colloquium, pp. 167–174.
- Müller P. (1978):** „Plastic analysis of reinforced concrete disks and beams (In German: Plastische Berechnung von Stahlbetonscheiben und-balken)“. PhD thesis. Zürich, Switzerland: ETHZ.
- Muttoni A. (1990):** „The applicability of the theory of plasticity to reinforced concrete design (In German: Die Anwendbarkeit der Plastizitätstheorie in der Bemessung von Stahlbeton)“. PhD thesis. Zürich, Switzerland: ETHZ, p. 158.
- Muttoni A.; Fernández Ruiz M. (2008):** „Shear strength of members without transverse reinforcement as function of critical shear crack width“. *ACI Structural Journal*, Vol. 105, No. 2, pp. 163–172.

- Muttoni A.; Schwartz J. (1991):** „Behavior of beams and punching in slabs without shear reinforcement“. In: *IABSE Colloquium*. Vol. 62. International Association for Bridge and Structural Engineering. Stuttgart, Germany, pp. 703–708.
- Muttoni A.; Schwartz J.; Thürlimann B. (1997):** *Design of Concrete Structures with Stress Fields*. Birkhäuser Verlag.
- Nielsen M. P.; Hoang L. C. (2011):** *Limit analysis and concrete plasticity*. 3<sup>rd</sup> edition Boca Raton. USA: CRC Press.
- Nielsen M. P.; Braestrup M. W.; Jensen B. C.; Bach F. (1978a):** *Concrete Plasticity: Beam Shear – Shear in Joints – Punching Shear*. Special Publication, Danish Society for Structural Science and Engineering.
- Nielsen M. P.; Braestrup M. W.; Bach F. (1978b):** „Rational analysis of shear in reinforced concrete beams“. In: *IABSE proceedings*. Vol. 2. International Association for Bridge and Structural Engineering, pp. 1–16.
- Richart F. E. (1948):** „Reinforced Concrete Walls and Column Footings, part 1 and 2“. *ACI Journal*, Vol. 45, pp. 97–127 & 237–260.
- Ricker M. (2006):** „Punching in RC footings considering the soil-structure-interaction“. In: *Proceedings of 6<sup>th</sup> International PhD Symposium in Civil Engineering*. Zürich.
- Ricker M. (2009):** „Reliability of punching design of isolated foundations (In German: Zur Zuverlässigkeit der Bemessung gegen Durchstanzen bei Einzelfundamenten)“. PhD thesis. RWTH, Aachen, p. 304.
- Salim W.; Sebastian W. M. (2002):** „Plasticity model for predicting punching shear strengths of reinforced concrete slabs“. *ACI Structural Journal*, Vol. 99, No. 6, pp. 827–835.
- Siburg C. (2014):** „Consistent punching design in flat slabs and foundations (In German: Zur einheitlichen Bemessung gegen Durchstanzen in Flachdecken und Fundamenten)“. PhD thesis. RWTH, Aachen, p. 197.
- Siburg C.; Hegger J. (2014):** „Experimental Investigations on Punching Behaviour of Reinforced Concrete Footings with structural dimensions“. *Structural Concrete*, Vol. 15, No. 3, pp. 331–339.
- Simões J. T.; Faria D. V.; Fernández Ruiz M.; Muttoni A. (2016):** „Strength of reinforced concrete footings without transverse reinforcement according to limit analysis“. *Engineering Structures*, Vol. 112, pp. 146–161.
- Talbot A. N. (1913):** „Reinforced Concrete Wall Footings and Column Footings“. *Engineering Experiment Station - University of Illinois*, Vol. 67, pp. 114.
- Timm M. (2003):** „Punching of foundation slabs under axisymmetric loading (In German: Durchstanzen von Bodenplatten unter rotationssymmetrischer Belastung)“. PhD thesis. Braunschweig, Germany: Technische Universität Carolo-Wilhelmina zu Braunschweig, p. 159.
- Urban T.; Goldyn M.; Krakowski J.; Krawczyk L. (2013):** „Experimental investigation on punching behaviour of thick reinforced concrete slabs“. *Archives of Civil Engineering*, Vol. 59, No. 2, pp. 157–174.
- Vecchio F. J. (2000):** „Disturbed stress field model for reinforced concrete: formulation“. *Journal of Structural Engineering*, Vol. 126, No. 9, pp. 1070–1077.
- Vecchio F. J.; Collins M. P. (1986):** „The modified compression-field theory for reinforced concrete elements subjected to shear“. *ACI Structural Journal*, Vol. 83, No. 2, pp. 219–231.

### 3.9 Notation

#### Latin characters

##### Lower Case

$a$	shear span
$b_0$	control perimeter
$c$	height of the compression zone
$d$	effective depth of bottom flexural reinforcement
$d'$	effective depth of top reinforcement
$dA$	unit of failure surface
$dA_{r,s,b}, dA_{r,s,t}$	unit of area of bottom and top tangential reinforcement
$dVol$	unit of volume
$dVol_{t,s,b}, dVol_{t,s,t}$	unit of volume of bottom and top tangential reinforcement
$dP_{i,c,FS}$	rate of internal energy dissipated in the concrete per unit of failure surface
$dP_{i,c,t}$	rate of internal energy dissipated in the concrete per unit of area due to tangential bending
$dP_{i,s,b}^{tan}, dP_{i,s,t}^{tan}$	rate of internal energy dissipated in the bottom and top reinforcement per unit of reinforcement area in the radial direction
$dP_{i,s,b}^{rad}, dP_{i,s,t}^{rad}$	rate of internal energy dissipated in the bottom and top reinforcement per unit of reinforcement area in the radial direction
$d\theta$	angle of a footing sector
$f_c$	cylinder concrete compressive strength
$f_{c0}$	reference compressive strength
$f_{c,cube}$	cube concrete compressive strength
$f_{cp}$	plastic concrete compressive strength
$f_y$	yield stress of bottom steel reinforcement
$f'_y$	yield stress of top steel reinforcement
$h$	height of the footing
$m_R$	moment capacity per unit of length
$\bar{m}_R$	reduced moment capacity per unit of length
$n, t$	normal and tangential directions in Figure 3.7
$q$	uniform soil pressure
$Q$	total load carrying capacity
$r$	radial coordinate
$r_c$	radius of a circular column
$r_{ICR}$	radial coordinate of the instantaneous centre of rotation
$r_q$	radius of the reaction resultant
$r_s$	radius of circular footing
$r_0$	radius of the failure surface at the level of the bottom flexural reinforcement
$\dot{u}$	velocity
$\dot{u}_n$	normal velocity
$\dot{u}_t$	tangential velocity
$\dot{u}_r$	radial component of velocity
$\dot{u}_{r,s,b}, \dot{u}_{r,s,t}$	radial component of velocity at the level of the bottom and top reinforcements
$z$	height coordinate
$z_c$	location of the diagonal compression strut at the column edge
$z_{ICR}$	height coordinate of the instantaneous centre of rotation

##### Upper Case

$P_e$	rate of external work
$P_i$	total rate of internal energy dissipated
$P_{i,c,FS}$	rate of internal energy dissipated in the concrete along the failure surface
$P_{i,c,t}$	rate of internal energy dissipated in the concrete due to tangential bending
$P_{i,s,b}, P_{i,s,t}$	rate of internal energy dissipated in the bottom and top reinforcements
$P_{i,s,b}^{rad}, P_{i,s,b}^{tan}$	rate of internal energy dissipated in bottom reinforcement in radial and tangential directions

$P_{i,s,t}^{rad}, P_{i,s,t}^{tan}$	rate of internal energy dissipated in the top reinforcement in radial and tangential directions
$Q_{flex}$	flexural capacity
$Q_{fs}$	flexural-shear capacity
$Q_p$	punching shear capacity
$V$	load carrying capacity
$V_{flex}$	effective flexural capacity
$V_{fs}$	effective flexural-shear capacity
$V_p$	effective punching shear capacity

## Greek characters

### Lower Case

$\alpha$	angle between failure surface and the vertical axis
$\beta$	secant inclination of the failure surface
$\dot{\gamma}_{n,t}$	deviatoric strain rate in a radial view of the plastic zone along the failure surface
$\dot{\epsilon}_n, \dot{\epsilon}_t$	normal and tangential strain rate in a radial view of the plastic zone
$\dot{\epsilon}_1, \dot{\epsilon}_2, \dot{\epsilon}_3$	principal strains rate
$\dot{\epsilon}_{c,t}$	concrete tangential strain rate in the outer portion of the footing
$\dot{\epsilon}_{s,b}^{tan}, \dot{\epsilon}_{s,t}^{tan}$	tangential strain rate in the bottom and top reinforcements
$\eta_\epsilon$	reduction factor accounting for the presence of transverse strains
$\eta_{fc}$	reduction factor accounting for the brittleness of high-strength concrete
$\eta$	global reduction factor
$\theta$	principal strain direction
$\rho$	experimental bottom reinforcement ratio
$\rho_r, \rho_t$	bottom reinforcement ratio in radial and tangential directions
$\rho'_r, \rho'_t$	top reinforcement ratio in radial and tangential directions
$\sigma_1, \sigma_3$	principal stresses
$\phi$	concrete friction angle
$\chi$	angle between failure surface and velocity
$\dot{\psi}$	relative rotation rate around the instantaneous centre of rotation
$\omega_r, \omega_t$	bottom mechanical reinforcement ratio in radial and tangential directions
$\omega_r, \omega_t$	top mechanical reinforcement ratio in radial and tangential directions

### Upper Case

$\Delta$	thickness of the plastic zone
----------	-------------------------------

## Acronyms

ICR	instantaneous centre of rotation
-----	----------------------------------

### 3.10 Appendix

#### 3.10.1 Rate of internal energy dissipated in the concrete along the failure surface

This appendix describes the calculation of the rate of internal energy dissipated in the concrete along the failure surface. As stated in Section 3.3.2, this component has already been studied by several researchers (e.g. Jensen, 1975; Braestrup *et al.*, 1976; Nielsen *et al.*, 1978a; Braestrup, 1979, 1981; Nielsen and Hoang, 2011). This dissipation of energy is investigated considering an infinitesimal region of the plastic zone occurring along the failure surface and assuming a velocity field as the one represented in Figure 3.7(b), where a radial view of this plastic zone is shown. Tangential and normal velocities as well as tangential, normal and deviatoric strains rates in this radial plane are respectively defined as:

$$\dot{u}_t = \frac{n}{\Delta} \cdot \dot{u} \cdot \cos(\chi) \quad (3.24)$$

$$\dot{u}_n = \frac{n}{\Delta} \cdot \dot{u} \cdot \sin(\chi) \quad (3.25)$$

$$\dot{\epsilon}_t = \frac{\partial \dot{u}_t}{\partial t} = 0 \quad (3.26)$$

$$\dot{\epsilon}_n = \frac{\partial \dot{u}_n}{\partial n} = \frac{\dot{u}}{\Delta} \cdot \sin(\chi) \quad (3.27)$$

$$\dot{\gamma}_{nt} = \frac{\partial \dot{u}_t}{\partial n} + \frac{\partial \dot{u}_n}{\partial t} = \frac{\dot{u}}{\Delta} \cdot \cos(\chi) \quad (3.28)$$

where  $\dot{u}$  is the velocity (refer to Eq.(3.6)) and  $\chi$  is the angle between the velocity and the failure surface (refer to Figure 3.7). As shown in Figure 3.7(c), based on Mohr's circle, the principal strains rates  $\dot{\epsilon}_1$  and  $\dot{\epsilon}_3$ , as well as the principal directions of compression  $\theta$  can be respectively determined by:

$$\dot{\epsilon}_1 = \frac{\dot{u}}{2 \cdot \Delta} \cdot \sin(\chi) + \sqrt{\frac{\dot{u}^2}{4 \cdot \Delta^2} \cdot [\sin^2(\chi) + \cos^2(\chi)]} = \frac{\dot{u}}{2 \cdot \Delta} \cdot [\sin(\chi) + 1] \quad (3.29)$$

$$\dot{\epsilon}_3 = \frac{\dot{u}}{2 \cdot \Delta} \cdot \sin(\chi) - \sqrt{\frac{\dot{u}^2}{4 \cdot \Delta^2} \cdot [\sin^2(\chi) + \cos^2(\chi)]} = \frac{\dot{u}}{2 \cdot \Delta} \cdot [\sin(\chi) - 1] \quad (3.30)$$

$$\tan(2 \cdot \theta) = \frac{\cos(\chi)}{\sin(\chi)} = \cot(\chi) = \tan\left(\frac{\pi}{2} - \chi\right) \Rightarrow \theta = \frac{\pi}{4} - \frac{\chi}{2} \quad (3.31)$$

With respect to  $\dot{\epsilon}_2$ , it varies linearly in the thickness of the plastic zone from zero (inner region) to the value of the tangential strain rate in the outer portion of the footing. Due to the fact that the thickness of the plastic zone is negligible with respect to the volume of the outer portion of the footing, the rate of internal energy dissipated in the plastic zone due to  $\dot{\epsilon}_2$  can be neglected. Using the relations defined in Eqs. (3.3), (3.4) and (3.5) for the rigid-plastic behaviour considered for the concrete (refer to Figure 3.4(b)), the rate of internal energy dissipated per unit of failure surface area  $dP_{i,c,FS}$  for the three different regimes can be computed as:

$$\begin{aligned} dP_{i,c,FS} &= (\dot{\epsilon}_1 \cdot \sigma_1 + \dot{\epsilon}_3 \cdot \sigma_3) \cdot \Delta \cdot dA \\ &= \frac{\dot{u}}{2} \cdot [\sin(\chi) + 1] \cdot \sigma_1 \cdot dA + \frac{\dot{u}}{2} \cdot [\sin(\chi) - 1] \cdot \sigma_3 \cdot dA \\ &= -\frac{1}{2} \cdot f_{cp} \cdot [\sin(\chi) - 1] \cdot \sqrt{(r - r_{ICR})^2 + (z - z_{ICR})^2} \cdot \dot{\psi} \cdot dA \end{aligned} \quad (3.32)$$

The rate of internal energy dissipated along the failure surface  $P_{i,c,FS}$  is therefore determined by:

$$P_{i,c,FS} = \int dP_{i,c,FS} \quad (3.33)$$

being the unit of area defined by:

$$dA = r \cdot d\theta \cdot \frac{dz}{\cos \alpha} \quad (3.34)$$

where  $\alpha$  refer to the angle between the failure surface and the vertical axis. Using Eqs. (3.32) and (3.34), Eq. (3.33) can be rewritten as:

$$\begin{aligned} P_{i,c,FS} &= - \int_0^{2\pi} \int_0^d \frac{1}{2} \cdot f_{cp} \cdot [\sin(\chi) - 1] \cdot \sqrt{(r - r_{ICR})^2 + (z - z_{ICR})^2} \cdot \dot{\psi} \cdot \frac{r}{\cos \alpha} \cdot dz \cdot d\theta \\ &= -\pi \cdot f_{cp} \cdot \dot{\psi} \cdot \int_0^d [\sin(\chi) - 1] \cdot \sqrt{(r - r_{ICR})^2 + (z - z_{ICR})^2} \cdot \frac{r}{\cos \alpha} \cdot dz \end{aligned} \quad (3.35)$$

### 3.10.2 Rate of internal energy dissipation in the concrete due to tangential bending

This appendix describes the rate of internal energy dissipated in the concrete due to tangential compression outside the failure surface (deformation of the footing portion outside the failure surface considered to have a conical shape). The strain rate in tangential direction within the compression zone ( $z_{ICR} < z \leq d$ ) is a function of the radial component of the velocity:

$$\dot{\epsilon}_{c,t} = -\frac{\dot{u}_r(z)}{r} = -\frac{|z - z_{ICR}|}{r} \cdot \dot{\psi} \quad (3.36)$$

where  $z$  refers to the coordinate varying along the depth of the compression zone, thus being within  $z \in [z_{ICR}; d]$ . The rate of internal energy dissipated per unit of volume  $dP_{i,c,t}$  due to this component given by:

$$dP_{i,c,t} = -\dot{\epsilon}_{c,t} \cdot f_{cp} \cdot dVol \quad (3.37)$$

Hence, the rate of internal energy dissipated in the concrete due to the tangential compression  $P_{i,c,t}$  is defined by:

$$P_{i,c,t} = - \int \dot{\epsilon}_{c,t} \cdot f_{cp} \cdot dVol \quad (3.38)$$

with

$$dVol = dA \cdot dz = r \cdot dr \cdot d\theta \cdot dz \quad (3.39)$$

where  $d\theta$  represents the angle of a footing sector. Using Eqs. (3.36), (3.37) and (3.39), Eq. (3.38) can be rewritten as:

$$\begin{aligned} P_{i,c,t} &= \int_{z_{ICR}}^d \int_0^{2\pi} \int_{r_c}^{r_s} \frac{|z - z_{ICR}|}{r} \cdot f_{cp} \cdot \dot{\psi} \cdot r \cdot dr \cdot d\theta \cdot dz \\ &= \int_{z_{ICR}}^d \int_0^{2\pi} \int_{r_c}^{r_s} |z - z_{ICR}| \cdot f_{cp} \dot{\psi} \cdot dr \cdot d\theta \cdot dz \\ &= \pi \cdot (r_s - r_c) \cdot \langle d - z_{ICR} \rangle^2 \cdot f_{cp} \cdot \dot{\psi} \end{aligned} \quad (3.40)$$

where  $\langle d - z_{ICR} \rangle$  is equal to zero when the component  $d - z_{ICR}$  is negative. These correspond to the cases where compression due to tangential bending of the outer portion of the footing does not exist. Alternatively, the same result could be obtained by considering that the continuum tangential deformation of the outer portion is replaced by assuming tangential displacement discontinuities in a number of vertical (radial) failure surfaces where plane stress conditions are assumed.

### 3.10.3 Rate of internal energy dissipation in the reinforcement

This appendix describes the rate of internal energy dissipated in both bottom flexural and top reinforcement when the radial component of the velocity is non-zero. This component of the velocity at the level of the bottom reinforcement ( $z = 0$ ) is given by:

$$\dot{u}_{r,s,b} = \dot{u}_{r(r=0)} = |z_{ICR}| \cdot \dot{\psi} \quad (3.41)$$

being the rate of internal energy dissipated in radial direction per unit of area of bottom radial reinforcement  $dP_{i,s,b}^{rad}$  defined by:

$$dP_{i,s,b}^{rad} = \dot{u}_{r,s,b} \cdot f_y \cdot dA_{r,s,b} \quad (3.42)$$

and the corresponding rate of internal energy dissipated  $P_{i,s,b}^{rad}$  is thus given by:

$$P_{i,s,b}^{rad} = \int \dot{u}_{r,s,b} \cdot f_y \cdot dA_{r,s,b} \quad (3.43)$$

where the unit of area of bottom radial reinforcement  $dA_{r,s,b}$  is determined by:

$$dA_{r,s,b} = \rho_r \cdot d \cdot r_0 \cdot d\theta \quad (3.44)$$

Replacing Eqs. (3.39), (3.40) and (3.42) in Eq. (3.41), the rate of internal energy dissipated in the bottom reinforcement in the radial direction can be defined as:

$$P_{i,s,b}^{rad} = \int_0^{2\cdot\pi} |z_{ICR}| \cdot f_y \cdot \rho_r \cdot d \cdot r_0 \cdot \dot{\psi} \cdot d\theta \quad (3.45)$$

In what respects tangential direction, the corresponding strain rate  $\dot{\epsilon}_{s,b}^{tan}$  results from the radial component of the velocity at the level of the corresponding reinforcement ( $z = 0$ ):

$$\dot{\epsilon}_{s,b}^{tan} = \frac{\dot{u}_{r,s,b}}{r} = \frac{|z_{ICR}|}{r} \cdot \dot{\psi} \quad (3.46)$$

being the rate of internal energy dissipated per unit of volume of bottom tangential reinforcement  $dP_{i,s,b}^{tan}$  defined by:

$$dP_{i,s,b}^{tan} = \dot{\epsilon}_{s,b}^{tan} \cdot f_y \cdot dVol_{t,s,b} \quad (3.47)$$

where

$$dVol_{t,s,b} = \rho_t \cdot d \cdot r \cdot dr \cdot d\theta \quad (3.48)$$

The rate of internal energy dissipated in tangential direction  $P_{i,s,b}^{tan}$  is therefore defined by:

$$P_{i,s,b}^{tan} = \int_0^{2\cdot\pi} \int_{r_0}^{r_s} |z_{ICR}| \cdot f_y \cdot \rho_t \cdot d \cdot \dot{\psi} \cdot dr \cdot d\theta \quad (3.49)$$

Taken into account the contributions of both radial and tangential directions, defined in Eqs. (3.45) and (3.49), the rate of internal energy dissipated in the bottom reinforcement can be computed as:

$$\begin{aligned} P_{i,s,b} &= P_{i,s,b}^{rad} + P_{i,s,b}^{tan} \\ &= \int_0^{2\cdot\pi} |z_{ICR}| \cdot f_y \cdot \rho_r \cdot d \cdot r_0 \cdot \dot{\psi} \cdot d\theta + \int_0^{2\cdot\pi} \int_{r_0}^{r_s} |z_{ICR}| \cdot f_y \cdot \rho_t \cdot d \cdot \dot{\psi} \cdot dr \cdot d\theta \\ &= 2 \cdot \pi \cdot d \cdot f_y \cdot [r_0 \cdot \rho_r + (r_s - r_0) \cdot \rho_t] \cdot |z_{ICR}| \cdot \dot{\psi} \end{aligned} \quad (3.50)$$

Defining respectively the bottom mechanical reinforcement ratio in radial and tangential direction as  $\omega_r = \rho_r \cdot f_y / f_{cp}$  and  $\omega_t = \rho_t \cdot f_y / f_{cp}$ , Eq. (3.50) can be rewritten:

$$P_{i,s,b} = 2 \cdot \pi f_{cp} \cdot [r_0 \cdot \omega_r + (r_s - r_0) \cdot \omega_t] \cdot |z_{ICR}| \cdot \dot{\psi} \quad (3.51)$$

The rate of internal energy dissipated in the top reinforcement can be computed in an analogous manner as for the bottom reinforcement. Hence, concerning the radial direction, the radial component of the velocity at its level  $\dot{u}_{r,s,t}^{rad}$ , the rate of internal energy dissipated per unit of area of top radial reinforcement  $dP_{i,s,t}^{rad}$  and the rate of internal energy dissipated  $P_{i,s,t}^{rad}$  are respectively given by:

$$\dot{u}_{r,s,t} = \dot{u}_{r(z=d-d')} = |z_{ICR} - (d - d')| \cdot \dot{\psi} \quad (3.52)$$

$$dP_{i,s,t}^{rad} = \dot{u}_{r,s,t} \cdot f'_y \cdot dA_{r,s,t} \quad , \quad \text{with } dA_{r,s,t} = \rho'_r \cdot d \cdot r_c \cdot d\theta \quad (3.53)$$

$$P_{i,s,t}^{rad} = \int_0^{2\pi} |z_{ICR} - (d - d')| \cdot f_y \cdot \rho_r \cdot d \cdot r_c \cdot \dot{\psi} \cdot d\theta \quad (3.54)$$

With respect to the tangential direction, the corresponding strain rate  $\dot{\epsilon}_{s,t}^{tan}$ , the rate of internal energy dissipated per unit of volume of top tangential reinforcement  $dP_{i,s,t}^{tan}$  and the rate of internal energy dissipated  $P_{i,s,t}^{tan}$  can be respectively computed as:

$$\dot{\epsilon}_{s,t}^{tan} = \frac{\dot{u}_{r,s,t}}{r} = \frac{|z_{ICR} - (d - d')|}{r} \cdot \dot{\psi} \quad (3.55)$$

$$dP_{i,s,t}^{tan} = \dot{\epsilon}_{s,t}^{tan} \cdot f'_y \cdot dVol_{t,s,t} \quad , \quad \text{with } dVol_{t,s,t} = \rho'_t \cdot d \cdot r \cdot dr \cdot d\theta \quad (3.56)$$

$$P_{i,s,t}^{tan} = \int_0^{2\pi} \int_{r_c}^{r_s} |z_{ICR} - (d - d')| \cdot f'_y \cdot \rho'_t \cdot d \cdot \dot{\psi} \cdot dr \cdot d\theta \quad (3.57)$$

The rate of internal energy dissipated in the top reinforcement  $P_{i,s,t}^{tan}$  results from the sum of both tangential and radial components, respectively given by Eqs. (3.54) and (3.57). Taking into account that top mechanical reinforcement ratio in radial and tangential directions are respectively defined by  $\omega'_r = \rho'_r \cdot f'_y / f_{cp}$  and  $\omega'_t = \rho'_t \cdot f'_y / f_{cp}$ , the rate of internal energy dissipated in the top reinforcement may be determined in accordance to Eq. (3.58):

$$P_{i,s,t} = 2 \cdot \pi \cdot d \cdot f_{cp} \cdot [r_c \cdot \omega'_r + (r_s - r_c) \cdot \omega'_t] \cdot |z_{ICR} - (d - d')| \cdot \dot{\psi} \quad (3.58)$$

# Chapter 4

## *Paper III*

### **The theoretical principles of the Critical Shear Crack Theory for punching shear failures and derivation of consistent closed-form design expressions**

This chapter is the postprint version of the journal article titled *The theoretical principles of the critical shear crack theory for punching shear failures and derivation of consistent closed-form design expressions* published in the journal *Structural Concrete* in 2017 (DOI: 10.1002/suco.201700088). The authors of the publication are Aurelio Muttoni (Professor at EPFL and thesis director), Miguel Fernández Ruiz (Senior lecturer at EPFL and thesis director) and João Tiago Simões (PhD Candidate). The complete reference is the following:

**Muttoni A., Fernández Ruiz M., and Simões J. T. (2017):** „The theoretical principles of the critical shear crack theory for punching shear failures and derivation of consistent closed-form design expressions“. *Structural Concrete*, pp. 1–17. DOI: 10.1002/suco.201700088.

The work presented in this article is an extension of a conference paper of the directors of thesis titled *Critical Shear Crack Theory for punching shear design: from the mechanical model to closed-form design expressions* presented in the ACI/fib Symposium in 2016 at Philadelphia (Muttoni and Fernández Ruiz, 2017). In the mentioned publication, the directors of this thesis proposed a new failure criterion for punching shear failures and introduce the concept of closed-form design expressions based on the Critical Shear Crack Theory. In this paper, the pertinence of the new failure criterion is theoretically justified and systematically validated with test results.

The journal article which constitutes this chapter differs from the mentioned conference article by: (i) presenting a full state-of-the art of the Critical Shear Crack Theory for punching shear failures and the basis of its development; (ii) justifying the newly proposed failure criterion with basis on mechanical models; (iii) developing closed-form solutions to calculate not only the punching strength but also the associated rotation at failure; (iv) validating the newly proposed failure criterion and the developed closed-form solutions for slender slabs and footings based on databases with recent data; (v) clarifying how different approaches of Critical Shear Crack Theory for punching shear design may be used.

The main contributions of João Tiago Simões to the creation of this article were the following:

- In charge of the review of Critical Shear Crack Theory based on the existing works of Guidotti (2010) and Simões *et al.* (2016b) (consistently with the original work of Braestrup *et al.* (1976));
- Participation in the development of the derived close-form solutions;
- Performing all the calculations;
- Comparison of the experimental results against the Critical Shear Crack Theory following the different possible approaches;
- Comparison of the results of the closed-form design expressions against recent databases and individual series of experimental tests;
- Production of the figures included in the article;
- Preparation of the manuscript of the article.

## 4.1 Abstract

The mechanical model of the critical shear crack theory (CSCT) has been used in the past to investigate a number of shear-related problems, such as punching of slab-column connections with and without transverse reinforcement. In this paper, a discussion on the differences and analogies between slender slabs and squat members (footings) without transverse reinforcement is presented on the basis of the CSCT. This discussion highlights how bending and shear deformations influence the opening of the critical shear crack and eventually its ability to transfer shear forces. On that basis, it is investigated and justified a power-law expression to characterize the failure criterion of the CSCT. This criterion, in combination with a suitable load-deformation relationship, can be used to derive closed-form expressions for punching shear design. The accuracy of these expressions is verified against databases of slender slabs (121 specimens) and footings (34 specimens) with consistent agreement.

**Keywords:** closed-form design expressions, concrete structures, critical shear crack theory, experimental verification, mechanical model, punching shear

## 4.2 Introduction

Research on punching shear and its design implications has drawn much interest of the scientific and practitioner communities (*fib*, 2001; Polak, 2005; *fib*, 2017). This has been motivated by a number of reported collapses (Fernández Ruiz *et al.*, 2010, 2013) and by the fact that many design expressions found in codes of practice still have an empirical nature (Eurocode 2, 2004; ACI 318, 2014). Following this research effort, a number of mechanically based models have been developed in the past with the aim of providing consistent design expressions for punching shear.

One of the first models with a rational basis to calculate the punching shear strength was proposed by Kinnunen and Nylander in the 1960s (Kinnunen and Nylander, 1960). This model considers that shear is carried by a conical strut whose failure in compression triggers the punching failure of the slab-column connection. Assuming that (a) failure of the strut occurs for a given level of the compressive tangential strain developing in the soffit of the slab in vicinity of the column and (b) by adopting a kinematics defined by a conical deformation in the outer region of the slab, Kinnunen and Nylander (1960) established a failure criterion as a function of the rotation of the slab (whose calculation was performed adopting a bilinear moment-curvature relationship). The rational theory of Kinnunen and Nylander (1960) was later adapted by other researchers and extended to footings, high strength concrete and to have consistent treatment of size effect (e.g. Broms, 1990; Hallgren, 1996; Broms, 2016).

Consistently with the principal ideas of Kinnunen and Nylander's model, Muttoni and Schwartz (1991) developed a rational approach to punching. The main ideas of Muttoni (2008) are that strains localize in a critical shear crack (Figure 4.1(a)) that governs the ability of a slab to transfer shear forces (as a function of the crack lips displacements and their roughness) (Muttoni and Schwartz, 1991; Muttoni, 2008, 2003). This approach was also shown to be applicable in a consistent manner to failures in shear for one-way slabs (Muttoni, 2003) and for shear-reinforced slabs (Fernández Ruiz and Muttoni, 2009) and was named as the critical shear crack theory (CSCT).

In agreement to the CSCT assumptions, and as confirmed experimentally (Muttoni, 2008; Guandalini *et al.*, 2009), larger openings of the critical shear crack reduce the capacity of transferring shear forces. Thus, the punching strength and the deformation capacity of a slab-column connection at failure can be related by means of a failure criterion (Figure 4.1(c)). By intercepting the failure criterion with

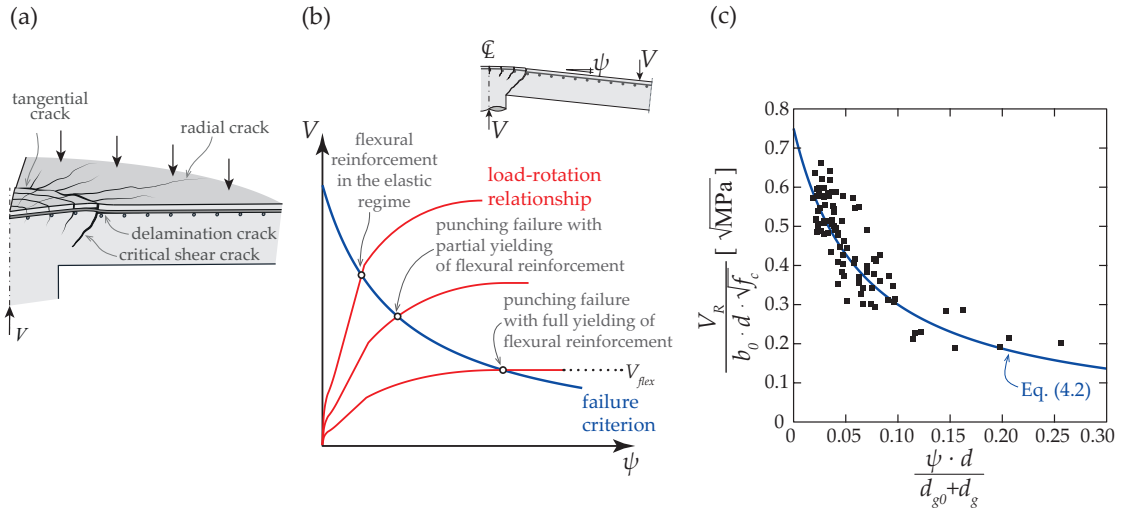


**Figure 4.1:** (a) Schematic representation of cracking at a slab-column connection; (b) potential punching failures; (c) failure criterion of critical shear crack theory (CSCT) Muttoni (2008) compared to tests according to the database of (Muttoni, 2008).

the load-deformation relationship, the punching shear strength and its associated deformation can be calculated, see Figure 4.1(b).

With respect to the load-deformation relationship for slender slabs, it can be characterized by the rotation ( $\psi$ ) of the slab (Muttoni, 2008). Such load-rotation relationship is highly nonlinear and influenced by cracking, tension-stiffening effects, and potential reinforcement yielding (Fernández Ruiz and Muttoni, 2017), thus being influenced by the reinforcement amount and properties. As a consequence, failures can occur in different regimes (Figure 4.1(b)) (Guandalini *et al.*, 2009): with all reinforcement remaining elastic, part of the reinforcement being yielded or even at the flexural capacity. Although detailed calculation of the load-rotation relationship can be performed (considering quadri-linear moment-curvature diagrams incorporating cracking and tension-stiffening effects) (Muttoni, 2008), the use of a non-linear parabolic law (derived from the quadri-linear model (Muttoni *et al.*, 2013)) has shown to be efficient for design purposes in terms of accuracy and ease of use (Muttoni, 2008):

$$\psi = k_m \cdot \frac{r_s}{d} \cdot \frac{f_y}{E_s} \cdot \left( \frac{m_s}{m_R} \right)^{3/2} \quad (4.1)$$

where  $r_s$  refers to the distance between the axis of the supported area and the line of zero radial moment,  $d$  is the effective depth,  $f_y$  and  $E_s$  are respectively the yield strength and the modulus of elasticity of flexural reinforcement,  $m_s$  is the average acting bending moment in the support strip (see, e.g., Muttoni and Fernández Ruiz (2012) for its definition),  $m_R$  is the average moment capacity in the support strip (Muttoni *et al.*, 2013), and  $k_m$  is a factor whose value depends on the level of refinement used to estimate the acting bending moment (value of 1.2 for refined analysis or 1.5 otherwise) (Muttoni *et al.*, 2013). It can be noted that an advantage of this approach is that tailored load-rotation relationships can be developed for particular cases (Maya *et al.*, 2012; Faria *et al.*, 2014; Belletti *et al.*, 2015; Einpaul *et al.*, 2015, 2016a).

With respect to the failure criterion, Muttoni and Schwartz (1991) considered that, for slender slabs, the opening of the critical shear crack ( $w$ ) could be assumed proportional to the slab rotation  $\psi$  times

the effective depth  $d$ . Thus, by assuming that  $w \propto \psi \cdot d$ , the following failure criterion was proposed (Muttoni, 2008):

$$\frac{V_{Rc}}{b_0 \cdot d \cdot \sqrt{f_c}} = \frac{3/4}{1 + 15 \cdot \frac{\psi \cdot d}{d_{g0} + d_g}} \quad (4.2)$$

where units are in SI [N, mm],  $b_0$  is the control perimeter (located at  $d/2$  from the edge of the supported area; round corners in case of square columns) and  $d_{g0}$  represents the reference aggregate size ( $d_{g0} = 16$  mm for normal weight concrete (Muttoni, 2008)). The term  $d_{g0} + d_g$  (originally introduced by Vecchio and Collins (1986)) refers in fact to a reference crack roughness accounting for the maximum aggregate size ( $d_g$ ) but also for the fact that the crack surface is not perfectly planar (Fernández Ruiz *et al.*, 2015). It can also be noted that the term  $\psi \cdot d$  actually accounts in a combined manner for the influence of size and strain effects (Fernández Ruiz *et al.*, 2015).

With respect to compact slabs or footings, the main assumptions of the CSCT have been demonstrated to be also valid (crack localization and influence of crack width and crack roughness on the capacity to transfer shear forces at the failure surface) (Simões *et al.*, 2016a). Yet, in these cases, the crack kinematics at failure is more complex and shall account for shear deformations, as also demonstrated by Simões *et al.* (2016a). In this chapter, the mechanical model of the CSCT is presented and discussed in terms of its failure mechanism and associated stresses developing on the failure surface. The calculation of the punching strength on the basis of the stresses on the failure surface is also reviewed and discussed for slender members (where flexural deformations govern) based on the work of Guidotti (2010) and for squat members (where shear deformations govern) having as basis the works of Braestrup *et al.* (1976) and Simões *et al.* (2016b). On the basis of this review, it is presented how the CSCT failure criterion can be formulated to account in a general manner for both cases. The resulting failure criterion is thereafter used in combination with the load-deformation relationship to calculate the punching strength in a closed-form manner. It is also shown that the closed-form expression derived from the mechanical model of CSCT can be extended in a very simple manner to account for other effects, as membrane action and slab continuity.

These closed-form expressions are very convenient for design and assessment purposes, allowing a direct calculation of the punching strength and providing the designer with a clear view of the role of the various parameters implied. The results obtained are compared with databases of slabs and footings showing consistent agreement.

### 4.3 The mechanical model of CSCT for punching shear

#### 4.3.1 Failure mechanism and associated internal stresses

Two-way slabs develop radial and tangential cracking due to the presence of respectively tangential and radial bending moments in the supported area (see Figure 4.1(a)). Due to the presence of shear forces, the tangential cracks in the region of the column develop in an inclined manner, disturbing the inclined compression strut carrying shear (Muttoni, 2008).

The mechanical model of the CSCT considers that crack localization occurs in a single crack (named as critical shear crack), and that the capacity of the critical shear crack to transfer shear forces depends upon the displacements between crack lips and their roughness (Muttoni and Schwartz, 1991; Muttoni, 2003, 2008).

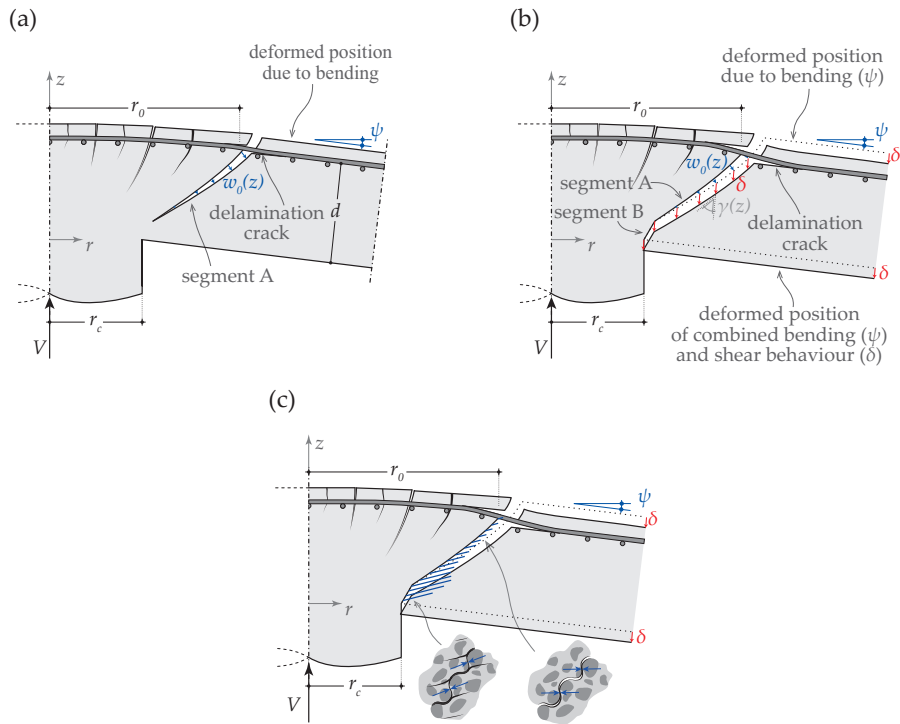


**Figure 4.2:** Mechanical approach of the critical shear crack theory (CSCT) for punching shear failures: (a) general kinematics due to flexural deformation; (b) general kinematics prior to failure; (c) schematic representation of stresses developing along failure surface with inclined strut carrying shear function of the opening  $w$  and roughness of the critical shear crack.

Calculation of the punching resistance can be performed on the basis of the assumptions by defining a critical shear crack composed of two different segments with different phenomenological behaviors, refer to Figure 4.2(a) and (b). Segment A corresponds to the crack originated by bending and segment B develops between the edge of the column and the segment A. With respect to segment A, it corresponds to a crack where a mixed-mode (opening and sliding) response occurs, while segment B behaves potentially as a shear band (with smeared cracking, eventually leading to coalescence in a single crack, Figure 4.2(b) and (c)).

The kinematics of the critical shear crack in both segments can be defined as a function of the displacements normal and parallel to the crack lips, as for instance shown in Simões *et al.* (2016b). Such kinematics results from the vector addition of the initial flexural crack opening (function of the slab rotation  $\psi$ ) and of the shear deformations (characterized by the displacement  $\delta$  occurring with a variable angle  $\gamma$  with respect to the critical shear crack, see Figure 4.1(b)). The general kinematics of the critical shear crack considers therefore a combination of both rotational and translational displacements. The extent of the two regimes developing along the critical shear crack previously mentioned, the kinematics ( $\psi$ ,  $\delta$  and  $\gamma$ ) and the shape of the critical shear crack depend significantly on mechanical and geometrical properties. As a consequence, also the resulting stresses developing along the critical shear crack are a function of the referred variables. The slenderness of the member is probably one of the most influencing parameters with this respect (Simões *et al.*, 2016a). In the following, previous works used to investigate suitable kinematics and resulting internal stresses based on the CSCT mechanical model for slender slabs and squat members (footings) are presented and discussed.

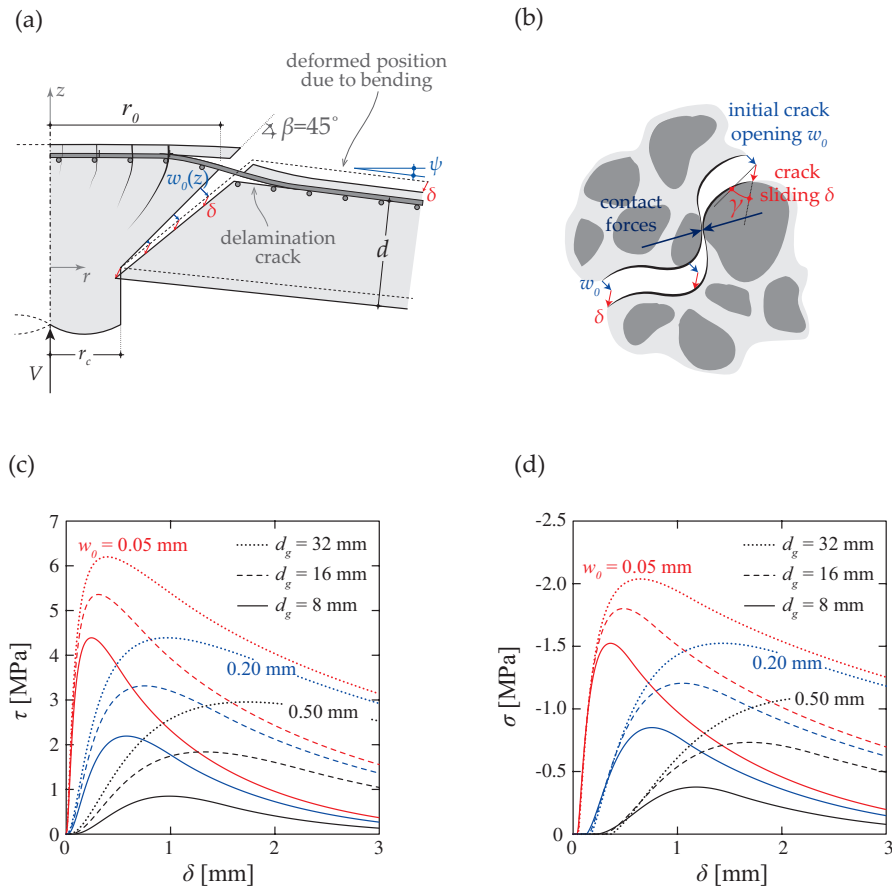


**Figure 4.3:** Mechanical model of Guidotti (2010) for the calculation of punching shear strength of slender slabs in the frame of the critical shear crack theory (CSCT): (a) shape and kinematics of the crack at failure; (b) detail of crack kinematics; (c) shear; and (d) normal stresses for different initial crack openings ( $w_0 = 0.05, 0.20, \text{ and } 0.50 \text{ mm}$ ) and aggregate sizes ( $d_g = 8, 16, \text{ and } 32 \text{ mm}$ ;  $f_c = 30 \text{ MPa}$ ;  $\gamma = 30^\circ$ ) as a function of the crack sliding calculated according to Guidotti (2010).

### 4.3.2 Application to slender members

The case of slender slabs with medium to large rotations was investigated in the frame of CSCT by Guidotti (2010). As shown in Figure 4.3(a), Guidotti (2010) considered a simplified shape for the critical shear crack developing between the edge of the column and the level of the flexural reinforcement with a constant inclination of  $\beta = 45^\circ$  (corresponding only to segment A of Figure 4.2). The resulting kinematics in this case (Guidotti, 2010) is composed of a rotation leading to a crack opening normal to the crack lips, followed by a crack sliding  $\delta$  (developing with a constant angle  $\gamma$  with respect to the crack lips), see Figure 4.3(a) and (b).

For such failure mechanism, the potential shear-transfer contributions developing along the failure surface and contributing to the punching shear strength can be calculated. They correspond to the aggregate interlock (calculated by Guidotti (2010) according to Walraven (1981)), residual tensile strength (calculated according to Hordijk (1992)) and dowelling action (that can be neglected compared to the others due to the development of the spalling cracks, according to Guidotti (2010)). With respect to the aggregate interlock contribution, Guidotti (2010) considered a consistent kinematics at failure (initial crack opening  $w_0$  developing before the crack sliding  $\delta$  taking place, refer to Figure 4.3(b) to (d) for kinematics and calculated shear and normal stresses). It should be noted that, as shown in Figure 4.3(c) and (d), crack sliding  $\delta$  is required to activate the aggregate interlock stresses.

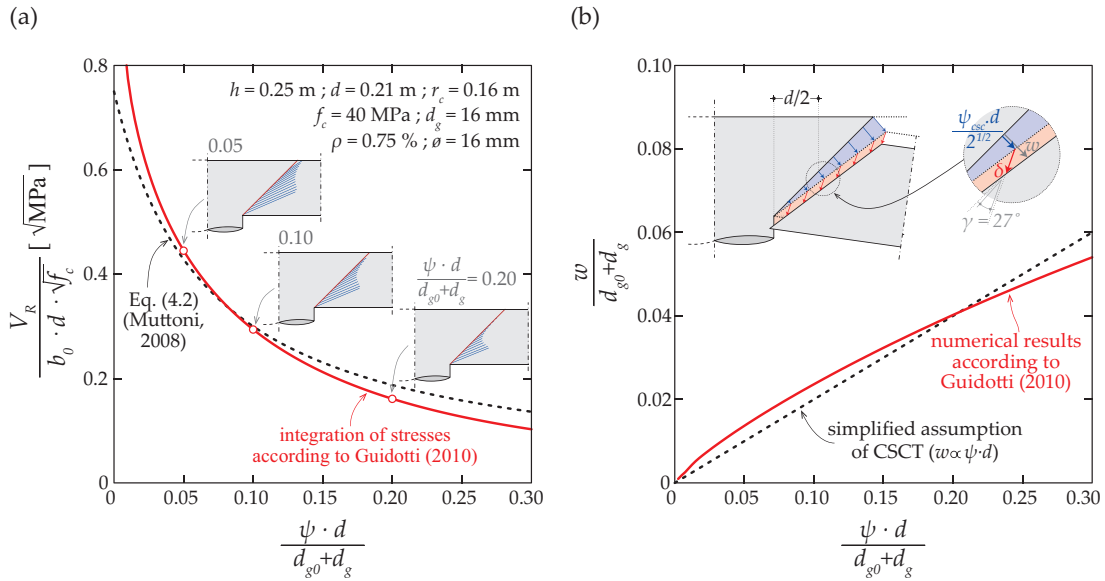


**Figure 4.4:** Numerical results of Guidotti (2010) for an example: (a) comparison of numerical failure criterion with critical shear crack theory (CSCT) hyperbolic (Eq. (4.2)) failure criterion with representation of the resultant of stresses developing along the failure surface for different rotations; (b) crack opening-rotation relationship numerically obtained and comparison to simplified assumption of Muttoni (2008).

Figure 4.4(a) shows the punching shear strength calculated under the assumptions of Guidotti (2010) for a general case ( $h = 0.25 \text{ m}$ ;  $d = 0.21 \text{ m}$ ;  $f_c = 40 \text{ MPa}$ ;  $d_g = 16 \text{ mm}$  and  $\rho = 0.75\%$ ) as a function of the rotation of the slab. Also, the resulting internal stresses developing along the critical shear crack are shown in Figure 4.4(a) for three different rotations: low, medium, and high rotations. A decay of shear strength with the increase of the crack width can be clearly observed, as a result of the decrease of the capacity of the different shear-transfer actions (due to loss of contact in the upper part of the slab and by the softening in the lower part due to increasing crack opening). It can be noted that the resulting stress state can be described by an inclined compression strut whose strength is thus strain and size dependent. This result is in agreement with the CSCT assumptions as well as those of Kinnunen and Nylander (1960). As shown in Figure 4.4(a), the hyperbolic failure criterion proposed by Muttoni (2008) and defined in Eq. (4.2) approximates fairly well the results predicted by the mechanical model of CSCT presented by Guidotti (2010).

The approach of Guidotti (2010) also allows validating the assumption of the CSCT for slender slabs that the crack width  $w$  can be assumed to be correlated to the product  $\psi \cdot d$ . This fact is shown in Figure 4.4(b) where the numerical results from Guidotti (2010) for the crack width  $w$  measured at peak load and at  $d/2$  from the edge of the column are shown. It can be noted that the crack width at failure, accounting for the development of the flexural and shear deformations ( $\psi$  and  $\delta$ ), follows a trend which is almost linear. This result is physically justified as larger crack openings require larger shear deformations  $\delta$  to mobilize aggregate interlock forces and thus both parameters are related.

### 4.3.3 Application to footings and squat members

For small rotations, the approach of Guidotti (2010) is not necessarily governing, as other shapes of the failure surface and associated kinematics may limit the punching shear strength. This topic has been investigated in the past (for instance by Braestrup *et al.* (1976) on the basis of limit analysis and more recently by Simões *et al.* (2016b) (see *Chapter 3*) showing that for footings or squat members, flexural deformations play a more secondary role (Simões *et al.*, 2016a; see *Chapter 2*). In these cases, the behaviour is mostly controlled by segment B in Figure 4.2(b), where the shear deformations are governing.

According to Braestrup *et al.* (1976), a kinematically admissible mechanism in these cases consists of a vertical translation of the outer portion of the member (Figure 4.5(a), also used by other researchers (Jiang and Shen, 1986; Bortolotti, 1990; Kuang, 1991; Salim and Sebastian, 2002)). It is interesting to note that the failure mechanism originally proposed by Braestrup *et al.* (1976) corresponds to a limit situation of the mechanical model of CSCT where only segment B develops. Also, in agreement to the CSCT assumptions, and as discussed by Simões *et al.* (2016b) (see *Chapter 3*), the capacity of the governing failure surface to transfer shear forces in these cases is affected by its state of deformations (crack opening). The punching strength calculated accounting for such failure mechanism and by adopting a rigid-plastic constitutive law for concrete (Figure 4.5(b) and (c)) can be consulted in Braestrup *et al.* (1976). It can be in a general manner expressed as (see Figure 4.5(d) using axis of ordinates on the left, neglecting the capacity of the concrete cover):

$$V_R = k_v \cdot b_0 \cdot d \cdot f_{ce} \quad (4.3)$$

where  $k_v$  is a parameter which depends upon the member slenderness (function of  $r_c$ ,  $d$ , and  $r_0$ ) and the friction angle of concrete ( $\varphi$ ). It shall be noted that in Eq. (4.3), the punching strength ( $V_R$ ) is also dependent on the effective compressive strength of concrete ( $f_{ce}$ ). This parameter accounts for the brittleness of concrete in compression and for the influence of the state of deformations as proposed by Nielsen and Hoang (2011):

$$f_{ce} = f_c \cdot \eta = f_c \cdot \eta_{f_c} \cdot \eta_w \quad (4.4)$$

where  $\eta$  is a global effectiveness factor that, for this case, can be split into two distinct ones:  $\eta_{f_c}$  and  $\eta_w$  referring to the effectiveness factors accounting for concrete brittleness and the state of deformations, respectively. With respect to the concrete brittleness in compression, previous works on the application of limit analysis for the case of punching shear (e.g. Nielsen *et al.*, 1978; Braestrup, 1979; Hoang, 2006; Nielsen and Hoang, 2011) have suggested adopting a relationship  $\eta_{f_c} = k_{f_c} / \sqrt{f_c}$ . With respect to  $\eta_w$ , its value may depend on the state of strains (Simões *et al.*, 2016b) and also on the size of the member (Nielsen and Hoang, 2011). For practical purposes, the maximum achievable punching strength can therefore be calculated as (see Figure 4.5(d) using axis of ordinates on the right):

$$V_R = k_v \cdot k_{f_c} \cdot \eta_w \cdot d \cdot b_0 \cdot \sqrt{f_c} \quad (4.5)$$

It can be noted that this equation presents the same parameters  $d$ ,  $b_0$ , and  $\sqrt{f_c}$  as that of the CSCT failure criterion (refer Eq. (4.2)). Additionally, it considers that the shear capacity is affected by the size and strains of the member, both parameters influencing the opening of the critical shear crack as considered in the CSCT mechanical model. As shown in the results of Figure 4.5(d), since the variation of the maximum achievable punching shear strength is relatively limited, the consideration of a constant value for the multiplication of the parameters  $k_v \cdot k_{f_c} \cdot \eta_w$  equal to 0.55 is a reasonable simplification for design purposes.

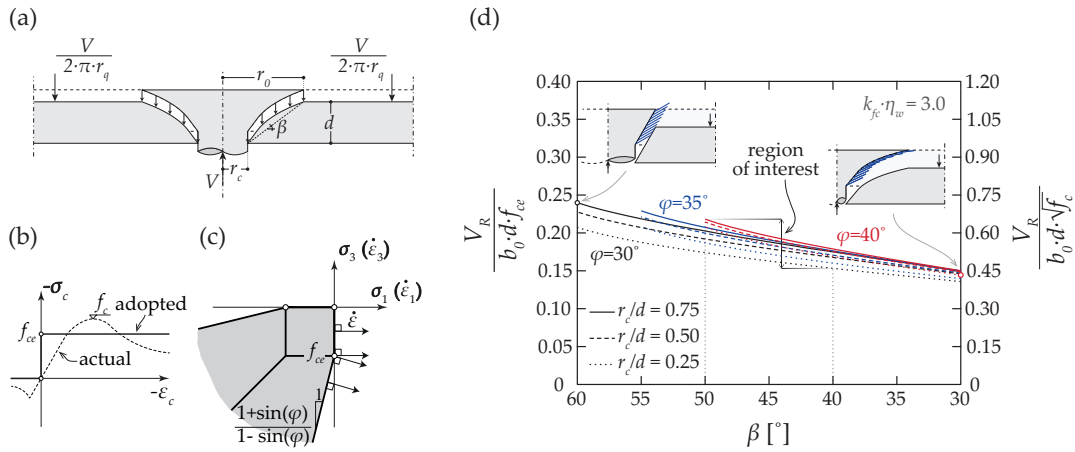


**Figure 4.5:** Punching shear strength according to upper bound theorem of limit analysis by Braestrup *et al.* (1976): (a) adopted failure mechanism; (b) rigid-plastic behaviour considered for concrete; (c) Mohr-Coulomb yield criterion adopted for concrete with tension cut-off; (d) punching shear strength as a function of secant inclination of the failure surface  $\beta$  and of the concrete friction angle  $\varphi$ .

#### 4.4 Considerations on the failure criterion of the CSCT

Calculating the punching response on the basis of the mechanical model of the CSCT by performing a numerical integration of the resulting stresses on the failure surface (Guidotti, 2010; Simões *et al.*, 2016b) is a general but not suitable approach for design purposes. To provide a simpler design approach, it can be observed that, when normalized in terms of the main physical parameters of the CSCT mechanical model, both numerical integrations (Guidotti, 2010; Simões *et al.*, 2016b) and test results remain within a narrow failure region (Figure 4.1(c)). These results indicate a decrease of the normalized strength for increasing normalized crack opening. On that basis, Muttoni (2008) proposed a simplified expression for the failure criterion with a hyperbolic shape (refer Eq. (4.2) and Figure 4.1(c)).

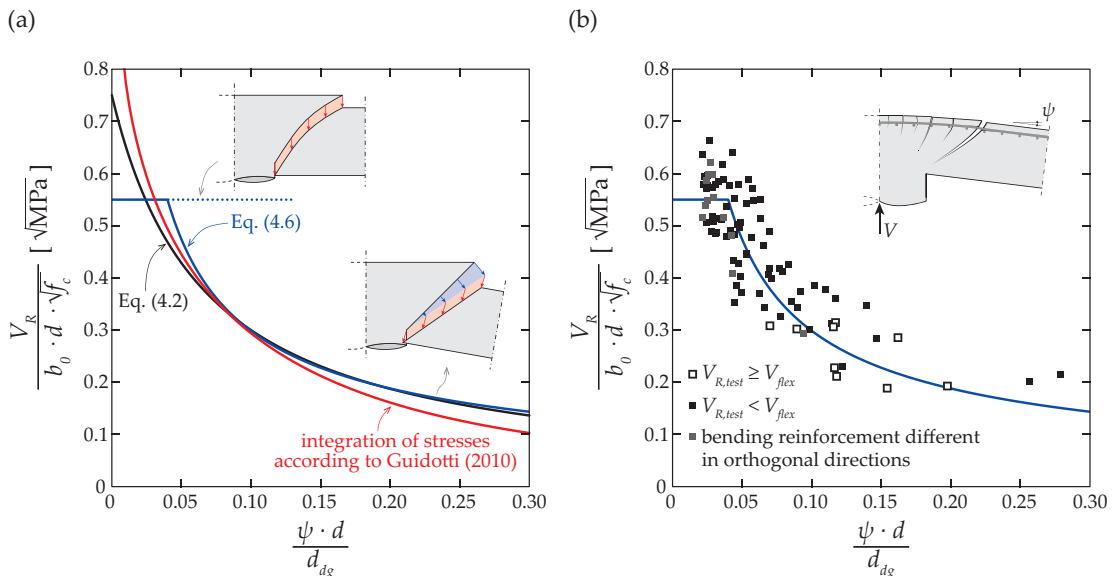


**Figure 4.6:** Comparison of power-law failure criterion of critical shear crack theory (CSCT) (Eq. (4.6)) with: (a) hyperbolic failure criterion (Equation (2)) and case of Figure 4.4; (b) with experimental results of database of Muttoni (2008).

This hyperbolic failure criterion and the parabolic load-rotation relationship (Eq. (4.1)) can be used in a simple and direct manner for design using the Levels-of-Approximation approach (Muttoni, 2008; Muttoni and Fernández Ruiz, 2010; Muttoni and Fernández Ruiz, 2012; Muttoni *et al.*, 2013; *fib* Model Code 2010, 2013; SIA 262, 2013). This design approach has proven to be general and efficient for design and to suitably account for size and strain effects (Fernández Ruiz and Muttoni, 2017). Yet, closed-form solutions (which may enhance the usability of the theory for design and assessment and also clarify the significance of the various mechanical and geometrical parameters on the punching strength) cannot be obtained by using the previous Eqs. (4.1) and (4.2).

Despite the advantages of the hyperbolic failure criterion, a more general expression could be formulated by accounting for the two relatively distinct behaviors described before (failures governed by flexural deformations (Guidotti, 2010) and failures governed by shear deformations (Simões *et al.*, 2016b)) in order to address in a more clear manner the differences between slender and squat members. A proposal with this respect has been recently presented by Muttoni and Fernández Ruiz (2017), by considering the following power-law expression:

$$V_{Rc} = V_{Rc,0} \cdot \left( \frac{d_{dg}}{25 \cdot \psi \cdot d} \right)^{2/3} \leq V_{Rc,0} \quad (4.6)$$

where units are in SI [N, mm],  $d_{dg}$  refers to the reference value of roughness of the crack and  $V_{Rc,0}$  refers to the maximum achievable punching shear strength. With respect to term  $d_{dg}$ , it can be calculated as:

$$d_{dg} = d_{g0} + d_g \cdot \min \left( \left( \frac{60}{f_c} \right)^2, 1 \right) \leq 40\text{mm} \quad (4.7)$$

where  $d_{g0}$  is the reference roughness value of the crack, which can be adopted equal to 16 mm for normal concrete. This term for the roughness is thus consistent to that previously assumed by the CSCT (refer Eq. (4.2)), but accounts additionally for two effects: (a) the limit on the positive influence of aggregate size on the shear-transfer capacity for large aggregate sizes (limit to 40 mm in accordance to Sherwood *et al.* (2007)) and (b) the reduced roughness of the surface for high strength concrete (fracture developing through the aggregates (Muttoni and Fernández Ruiz, 2008)).

With respect to term  $V_{Rc,0}$ , its value can be calculated based on Eq. (4.5) as follows:

$$V_{Rc,0} = 0.55 \cdot b_0 \cdot d \cdot \sqrt{f_c} \quad (4.8)$$

It can be noted that this value is considered constant, although according to Eq. (4.5) a dependency on the crack width may result. Such dependency allows for a smooth transition between both regimes, but will be neglected for simplicity reasons. The power-law failure criterion defined in Eqs. (4.6) and (4.8) is compared in Figure 4.6(a) to the strength calculated according to the approach by Guidotti (2010) (for the same case as presented in Figure 4.4). It can be noted that the simplified failure criterion finely agrees with the numerical integration of stresses and also yields close results to those of the hyperbolic failure criterion of Eq. (4.2). In addition, the power-law failure criterion is compared in Figure 4.6(b) with the experimental results of the database presented by Muttoni (2008). It can be seen that for low rotations, the strength limit ( $V_{Rc0}$ ) is governing whereas for large rotations the power law is limiting the strength and deformation capacity. When compared to tests, the scatter is low (comparable to that of the hyperbolic failure criterion, Figure 4.1(c)) with all experimental results concentrated within a narrow region.

## 4.5 Closed-form solution of the CSCT

### 4.5.1 Development of closed-form expressions for elements without transverse reinforcement

The failure criterion presented in Eq. (4.6) can be used to calculate the failure load in combination with the parabolic load-rotation relationship (Eq. (4.1)) yielding closed-form solutions of the punching resistance (Muttoni and Fernández Ruiz, 2017). This can be done by introducing the rotation as a function of the acting shear force Equation (4.1) into Equation (4.6) and assuming  $m_s/m_R = V_{Rc}/V_{flex}$ :

$$V_{Rc} = V_{Rc,0} \cdot \left( \frac{V_{flex}}{V_{Rc}} \right) \cdot \left( \frac{d_{dg}}{25 \cdot k_m \cdot d} \cdot \frac{d}{r_s} \cdot \frac{E_s}{f_y} \right)^{2/3} \leq V_{Rc,0} \quad (4.9)$$

which leads to:

$$V_{Rc} = \sqrt{V_{Rc,0} \cdot V_{flex}} \cdot \left( \frac{d_{dg}}{25 \cdot k_m \cdot r_s} \cdot \frac{E_s}{f_y} \right)^{1/3} \leq V_{Rc,0} \quad (4.10)$$

The punching strength results thus a function of the maximum shear capacity ( $V_{Rc,0}$ ) and the flexural strength ( $V_{flex}$ ), shear force associated with full yielding of all radial and tangential flexural reinforcement (Muttoni, 2008)) as well as of other parameters characterizing roughness, size and strain effects. In addition, the deformation capacity at failure can also be calculated from Eqs. (4.1) and (4.10) (assuming  $m_s/m_R = V_{Rc}/V_{flex}$ ):

$$\psi_{Rc} = \left( \frac{k_m}{25} \cdot \frac{r_s}{d} \cdot \frac{d_{dg}}{d} \cdot \frac{f_y}{E_s} \right)^{1/2} \cdot \left( \frac{V_{Rc,0}}{V_{flex}} \right)^{3/4} \leq k_m \cdot \frac{r_s}{d} \cdot \frac{f_y}{E_s} \cdot \left( \frac{V_{Rc,0}}{V_{flex}} \right)^{3/2} \quad (4.11)$$

For design purposes, the calculation of the flexural strength of the slab ( $V_{flex}$ ) can be simplified assuming the following relationship between the flexural strength and the moment capacity (Muttoni, 2008):

$$V_{flex} = a \cdot m_R \quad (4.12)$$

where parameter  $a$  relates the flexural strength to sectional moment capacity (it can be taken as 8 for inner columns according to Muttoni (2008)), and  $m_R$  can be calculated as:

$$m_R = d^2 \cdot \rho \cdot f_y \cdot \left( 1 - \frac{\rho \cdot f_y}{2 \cdot f_{cp}} \right) \quad (4.13)$$

where  $f_{cp}$  refers to the plastic compressive strength of concrete in uniaxial compression, calculated as  $f_{cp} = f_c \cdot (30/f_c)^{1/3} \leq f_c$  (accounting for the influence of the concrete brittleness in compression) (Muttoni, 1990). In order to develop simple closed-form design expressions, Eq. (4.13) can be approximated in the following manner (Muttoni and Fernández Ruiz, 2017):

$$m_R = k_1 \cdot d^2 \cdot (\rho \cdot f_y)^{k_2} \cdot f_c^{1-k_2} \quad (4.14)$$

with  $k_1 = 0.75$  and  $k_2 = 0.9$ . Using the relationships established in Eqs. (4.12) and (4.14), the flexural strength  $V_{flex}$  can thus be rewritten as:

$$V_{flex} = a \cdot 0.75 \cdot d^2 \cdot \rho^{0.9} \cdot f_y^{0.9} \cdot f_c^{0.1} \quad (4.15)$$

Furthermore, by replacing Eq. (4.15) into (4.10) yields:

$$\frac{V_{Rc}}{b_0 \cdot d} = (0.55 \cdot 0.75)^{0.5} \cdot b_0^{-0.5} \cdot d^{0.5} \cdot f_c^{0.25} \cdot a^{0.5} \cdot (\rho \cdot f_y)^{0.45} \cdot f_c^{0.05} \cdot (25 \cdot k_m \cdot f_y)^{-1/3} \cdot \left( \frac{d_{dg}}{r_s} \cdot E_s \right)^{1/3} \leq 0.55 \cdot \sqrt{f_c} \quad (4.16)$$

which eventually leads to:

$$\frac{V_{Rc}}{b_0 \cdot d} = k_3 \cdot \sqrt{a \cdot \frac{d}{b_0}} \cdot \left( E_s \cdot \rho \cdot f_c \cdot \frac{d_{dg}}{r_s} \right)^{1/3} \leq 0.55 \cdot \sqrt{f_c} \quad (4.17)$$

where  $k_3 = (0.55 \cdot 0.75)^{0.5} \cdot (25 \cdot k_m)^{-1/3} \cdot f_c^{-0.033} \cdot (\rho \cdot f_y)^{0.117}$  can be approximated as  $k_3 = 0.225$  ( $k_m=1.2$ ,  $f_c \approx 30$  MPa,  $\rho \cdot f_y \approx 5$  MPa; low values of the exponents of  $f_c$ ,  $\rho$ , and  $f_y$  lead to a small influence of these variables on the value of  $k_3$ ). Considering a constant modulus of elasticity  $E_s = 200\,000$  MPa, Eq. (4.17) can finally be written as:

$$V_{Rc} = k_b \cdot \left( 100 \cdot \rho \cdot f_c \cdot \frac{d_{dg}}{r_s} \right)^{1/3} \cdot b_0 \cdot d \leq 0.55 \cdot b_0 \cdot d \cdot \sqrt{f_c} \quad (4.18)$$

where the coefficient  $k_b$  can be computed as follows:

$$k_b = \sqrt{8 \cdot a \cdot \frac{d}{b_0}} \geq 1 \quad (4.19)$$

This coefficient accounts for the effective depth-to-control perimeter ratio as well as for parameter  $a$  (defined in Eq. (4.12), relationship between flexural strength and moment capacity). It enhances the unitary shear strength for small column sizes and decreases it for large column sizes. This is physically consistent, defining a transition for failures in shear in one-way slabs (very large length of the control perimeter) (Van Der Voet *et al.*, 1982; Birkle, 2004) and is acknowledged in design codes (e.g. ACI 318, 2014).

It can be noted that Eqs. (4.18) and (4.19) do not explicitly account for the level of deformation of the slab, although it can be back calculated by means of Eq. (4.11). In addition, some of the parameters implied in the equations (as  $r_s$  and  $a$ ) have a physical meaning consistently with the CSCT, and their estimate can be performed with simple geometrical rules for conventional cases, but refined by means of more detailed analyses upon necessity (for design of complex structures or for assessment of critical connections).

It shall also be noted that, as a consequence of the assumptions used to the analytical derivation of the closed-form expression of Eq. (4.18), some additional considerations have to be accounted for when using it. These considerations refer to the flexural resistance of squat members and to the location of its control perimeter and are explained in the following.

The first consideration (flexural resistance of squat members) is related with the use of Eq. (4.13) (simplified with Eq. (4.14)) to calculate the moment sectional capacity, which, together with yield-line theory (Johansen, 1962), allows calculating the flexural strength of slender slabs. However, the use of the referred theory to the case of footings has been shown to have limitations (Simões *et al.*, 2016b). Simões *et al.* (2016b) have used the upper bound theorem of limit analysis to show that the application of yield-line theory (Johansen, 1962) may lead to a significant overestimate of the flexural capacity of

compact slabs and footings without shear reinforcement. In those cases, the flexural strength has to be reduced to account for the flexure-shear interaction resulting from the presence of an inclined strut carrying shear which reduces the flexural lever arm (Simões *et al.*, 2016b). The assumption that the flexural strength can be approximated as defined in Equation (15) requires thus a reduction of the longitudinal reinforcement ratio when applying Equation (18) to the case of footings or squat slabs without shear reinforcement. A simple expression for these cases is derived in Section 4.10 (Appendix) and results in the following relationship:

$$\frac{\rho_{red}}{\rho} = \frac{1 - 0.5 \cdot \omega \cdot r_s / r_c}{1 - 0.5 \cdot \omega} \quad (4.20)$$

where  $\rho_{red}$  is the reduced longitudinal reinforcement ratio to be introduced in Eq. (4.18) when applying it to the cases of footings without transverse reinforcement;  $\omega$  is the mechanical reinforcement ratio ( $\rho \cdot f_y / f_c$ );  $r_c$  is the radius of a circular column with the equivalent perimeter.

The second consideration (location of control perimeter for squat members) results from the fact that Eq. (4.18) considers a constant distance of the control perimeter to the edge of the supported area (control perimeter located at  $d/2$  from the edge). This approach has been shown to be consistent for the case of slender slabs (Einpaul *et al.*, 2016b). For the sake of simplicity, the same distance between the column edge and the control perimeter in the case of footings is also assumed. Nevertheless, as shown by Simões *et al.* (2016b), the location of the control perimeter for squat members should rather be related to the inclination of the failure surface, which is actually a function of geometrical properties. According to this theoretical consideration, with decreasing span-to-effective depth ratio, the inclination of the failure surface tends to be steeper (Simões *et al.*, 2016b). In addition, this theoretical consideration has been confirmed also experimentally (Hegger *et al.*, 2009; Siburg and Hegger, 2014; Simões *et al.*, 2016a). For consistency, the control perimeter should be shifted to a distance closer than  $0.5 \cdot d$  in those cases, leading to lower punching resistances. To keep the control perimeter at a distance of  $0.5 \cdot d$  from the column edge, thus, a lower limit of the distance between the axis of the supported area to the line of zero radial moment  $r_s$  has to be considered. To that aim, it is suggested to adopt  $r_s \geq 2.5 \cdot d$ , corresponding to the limit case where an angle of the failure surface of approximately  $45^{circ}$  has been observed in the analysis of Simões *et al.* (2016b).

#### 4.5.2 Development of closed-form expressions for slab continuity and compressive membrane action

An interesting consideration of the CSCT and its derived expressions is that, since the theory is based on a mechanical model, it can be tailored to specific situations by suitably evaluating its mechanical parameters. This is presented in this section with reference to slab continuity and compressive membrane action. As shown by Einpaul *et al.* (2015, 2016a) this effect might have a significant influence on the punching behaviour and strength of slab-column connections. This phenomenon is relevant particularly for inner connections where compressive in-plane forces may develop around the column area.

The influence of slab continuity and compressive membrane action have been accounted for in the frame of the CSCT by Einpaul *et al.* (2015, 2016a) by modifying the load-rotation relationship of Eq. (4.1) by means of a factor named  $k_{cs}$  (Einpaul *et al.*, 2016a):

$$\psi = k_{cs} \cdot k_m \cdot \frac{r_s}{d} \cdot \frac{f_y}{E_s} \cdot \left( \frac{V}{V_{flex}} \right)^{3/2} \quad (4.21)$$

As justified by Muttoni and Fernández Ruiz (2017) factor  $k_{cs}$  can be expressed as a function of the ratio  $m_{cr}/m_R$  (supported on the evidence that the confinement at the column region is provided by the surrounding concrete during the crack development stage) in the following manner):

$$k_{cs} = \left( 0.08 \cdot \frac{m_R}{m_{cr}} \right)^{3/4} \leq 1 \quad (4.22)$$

where  $m_{cr}$  refers to the cracking moment per unit length. By intersecting the modified load-rotation relationship with the failure criterion, the punching resistance thus results:

$$V_{Rc} = k_b \cdot \left( 100 \cdot \rho \cdot f_c \cdot \frac{d_{dg}}{k_{cs} \cdot r_s} \right)^{1/3} \cdot b_0 \cdot d \leq 0.55 \cdot b_0 \cdot d \cdot \sqrt{f_c} \quad (4.23)$$

It can be noted that Eq. (4.23) is analogous to Eq. (4.18), provided that the value of  $r_s$  is corrected (reduced) to account for the compressive membrane action. Considering that the flexural capacity per unit length  $m_R$  can be calculated with Equation (14) and that the cracking moment per unit length can be computed as (assuming a ratio  $d/h \approx 0.9$ ):

$$m_{cr} = \frac{h^2}{6} \cdot f_{ct} \approx \frac{d^2}{0.9^2 \cdot 6} \cdot f_{ct} \quad (4.24)$$

The factor  $k_{cs}$  can be simplified as follows (by introducing Eqs. (4.14) and (4.24) into Eq. (4.22) and rounding exponents and constant values):

$$\begin{aligned} k_{cs} &\cong \left( 0.08 \cdot \frac{6 \cdot 0.9^2}{d^2 \cdot f_{ct}} \cdot 0.75 \cdot d^2 \cdot (\rho \cdot f_y)^{0.9} \cdot f_c^{0.1} \right)^{3/4} \\ \Rightarrow k_{cs} &= k_4 \cdot \sqrt{100 \cdot \rho} \left( \frac{f_y}{f_{ct}} \right)^{3/4} \leq 1.0 \end{aligned} \quad (4.25)$$

where the constant  $k_4 = (0.08 \cdot 6 \cdot 0.9^2 \cdot 0.75)^{3/4} \cdot (f_c/f_y)^{3/40} \cdot \rho^{7/40} \cdot 100^{-1/2}$  can finally be simplified as  $k_4 = 1/75$  ( $f_c \approx 30$  MPa,  $\rho \approx 0.0075$ , and  $f_y \approx 500$  MPa; low values of the exponents of  $f_c$ ,  $\rho$  and  $f_y$  lead to a small influence of these variables on the value of constant  $k_4$ ).

## 4.6 Comparison of closed-form expressions against experimental results

The accuracy of the CSCT (and more specifically the closed-form design expressions previously derived in Eqs. (4.10) and (4.18)) is compared in this section to available experimental data. For slender slabs, the database considered is that of Einpaul (2016) (update of database of Muttoni (2008)) but completed with some additional tests. The considered database comprises a total of 121 slender slabs without transverse reinforcement (Elstner and Hognestad, 1956; Kinnunen and Nylander, 1960; Moe, 1961; Schaeffers, 1984; Tolf, 1988; Ramdane, 1996; Hallgren, 1996; Hassanzadeh, 1996; Sistonen *et al.*, 1997; Birkle, 2004; Guandalini *et al.*, 2009; Fernández Ruiz *et al.*, 2010; Guidotti, 2010; Tassinari, 2011; Clément, 2012; Lips *et al.*, 2012; Heinzmann *et al.*, 2012; Inácio *et al.*, 2015; Einpaul *et al.*, 2016b; Drakatos *et al.*, 2016) (see Table 4.1 for details). With respect to footings, a database accounting for 34 footings without transverse reinforcement subjected to uniform loading was compiled (Dieterle and Rostásy, 1987; Hallgren *et al.*, 1998; Hegger *et al.*, 2009; Siburg and Hegger, 2014; Simões *et al.*, 2016a) (see Table 4.2). Only specimens that do not reach their flexural strength ( $V_{R,test} < V_{flex}$ ) are included in the databases, as Eqs. (4.10) and (4.18) are only addressed to the shear strength. These databases are consistent with others available in the literature (Walkner, 2014; Siburg, 2014).

#### 4. PRINCIPLES OF CSCT FOR PUNCHING FAILURES AND DERIVATION OF CLOSED-FORM DESIGN EXPRESSIONS

**Table 4.1:** Summary of database containing 121 specimens without transverse reinforcement:  $r_c$  - radius of a circular column;  $c$  - side length of a square column;  $d$  - effective depth;  $f_c$  - cylinders concrete compressive strength;  $f_y$  - yielding strength of flexural reinforcement;  $d_g$  - maximum aggregate size;  $B$  - size of the slab along orthogonal directions.

Authors	Number of tests	$B$ [m]	$d$ [m]	$r_c$ [m]	$c$ [m]	$f_c$ [MPa]	$d_g$ [mm]	$\rho$ [%]	$f_y$ [MPa]
Elstner and Hognestad (1956)	19	1.829	0.114	-	0.254	12.8	25.4	1.15	321
			0.118		0.356	50.6	38.1	3.70	409
Kinnunen and Nylander (1960)	10	1.840	0.117	0.075	-	24.2	32	0.65	434
			0.128	0.150		31.0		1.50	461
Moe (1961)	7	1.829	0.114	-	0.152	22.1	9.5	1.05	328
					0.254	26.5	38.1	1.14	482
Schaeffers (1984)	2	1.960	0.113	0.105	-	21.3	32	0.55	450
			0.170			27.1		0.83	
Tolf (1988)	8	1.270	0.098	0.063	-	22.6	16	0.34	657
		2.540	0.200	0.125		28.2	32	0.81	720
Hallgren (1996)	7	2.540	0.194	0.125	-	84.1	18	0.33	596
			0.202			108.8		1.19	643
Ramdane (1996)	12	1.700	0.098	0.075	-	26.9	10	0.58	550
			0.100			101.8	20	1.28	650
Hassanzadeh (1996)	1	2.540	0.199	0.125	-	28.4	18	0.80	493
Sistonen <i>et al.</i> (1997)	10	1.770	0.170	0.101	-	19.0	16	0.45	576
		2.470	0.177	0.451		25.8		1.17	621
Birkle (2004)	3	2.248	0.124	-	0.250	31.4	14	1.10	488
		3.911	0.260		0.350	36.2		1.51	531
Guandalini <i>et al.</i> (2009)	5	1.500	0.096	-	0.130	27.7	16	0.32	520
		6.000	0.456		0.520	34.7		1.50	577
Guidotti (2010)	11	3.000	0.194	-	0.260	31.5	8	0.76	510
			0.208		51.7	32	1.62	551	
Tassinari (2011)	2	3.000	0.196	-	0.260	66.3	16	0.82	540
			0.212		67.0	1.48		552	
Fernández Ruiz <i>et al.</i> (2010)	1	3.000	0.210	-	0.260	34.0	16	1.50	709
Clément (2012)	3	3.000	0.346	-	0.220	31.6	16	0.75	520
			0.35		0.440	33.9		1.53	541
Lips <i>et al.</i> (2012)	4	3.000	0.193	-	0.130	30.5	16	1.50	556
			0.353		0.520	36.5		1.63	583
Heinzmann <i>et al.</i> (2012)	1	4.100	0.294	0.200	-	35.5	32	1.20	577
Inácio <i>et al.</i> (2015)	3	1.650	0.101	-	0.200	35.9	13.2	1.24	523
			0.102		130.1	13.9	1.48	532	
Einpaul <i>et al.</i> (2016b)	10	1.700	0.197	0.042	0.260	34.2	16	0.74	517
		3.900	0.218	0.330		44.1		1.59	542
Drakatos <i>et al.</i> (2016)	2	3.000	0.195	-	0.390	34.3	16	0.80	507
			0.200		39.2	1.61		593	
$\Sigma$	121	1.270	0.096	0.042	0.130	12.8	8	0.32	321
		6.000	0.456	0.451	0.520	130.1	38.1	3.70	720

## Comparison of closed-form expressions against experimental results

**Table 4.2:** Summary of database with 34 footings without transverse reinforcement subjected to uniform loading;  $r_c$  - radius of a circular column;  $c$  - side length of a square column;  $d$  - effective depth;  $f_c$  - cylinders concrete compressive strength;  $f_y$  - yielding strength of flexural reinforcement;  $d_g$  - maximum aggregate size;  $B$  - size of the footing along orthogonal directions.

Authors	Number of tests	$r_c$ [m]	$c$ [m]	$d$ [m]	$B$ [m]	$f_c$ [MPa]	$d_g$ [mm]	$\rho$ [%]	$f_y$ [MPa]
Dieterle and Rostásy (1987)	12	-	0.150	0.290	1.500	20.1	30	0.21	395
			-	0.450	0.760	3.000	27.3	32	0.89
Hallgren <i>et al.</i> (1998)	2	0.125	-	0.235	0.850	20.1	8	0.41	621
			-	0.240		26.5			
Hegger <i>et al.</i> (2009)	8	-	0.200	0.295	1.200	21.1	16	0.82	528 - 566
			-	0.470	1.800	36.4		0.86	
Siburg and Hegger (2014)	8	-	0.200	0.400	1.200	19.6	16	0.29	515
			-	0.300	0.590	2.700		53.3	0.88
Simões <i>et al.</i> (2016a)	4	-	0.300	0.506	1.590	29.5	16	0.74	517
			-	0.450	0.512	2.120		32.1	0.76
$\Sigma$	34	0.125	0.150	0.235	1.200	19.6	8	0.21	395
			-	0.450	0.760	3.000	53.3	32	0.89

**Table 4.3:** Summary of the results of critical shear crack theory (experimental-to-calculated punching strengths) obtained following different approaches.

Specimens	Number of tests	Approach	Average	COV [%]
Slabs	121	Approach (1) <sup>a</sup>	1.07	8.3
		Approach (2) <sup>b</sup>	1.03	8.6
		Approach (3) <sup>c</sup>	1.04	10.0
		Approach (4) <sup>d</sup> with $a = V_{flex}/m_R$	1.03	9.7
		Approach (4) <sup>d</sup> with $a = 8$ and $r_s = B/2$	1.02	10.6
Footings	34	Approach (3) <sup>c</sup> with $V_{flex}$ calculated with $\rho_{red}$ , $r_s = B/2$	0.96	9.4
		Approach (4) <sup>d</sup> with $a = 8$ , $\rho_{red}$ and $r_s = B/2$	0.95	11.5
		Approach (4) <sup>d</sup> with $a = 8$ , $\rho_{red}$ and $r_s = B/2 \geq 2.5 \cdot d$	1.01	11.7

<sup>a</sup> Load-rotation relationship based on quadri-linear moment curvature law (Muttoni, 2008) (with the equivalent axisymmetric value of  $r_s$  calculated from the yield-line value of  $V_{flex}$ ) and hyperbolic failure criterion (Eq. (4.2)) (Muttoni, 2008) with  $d_{ag}$  of Eq. (4.7).

<sup>b</sup> Load-rotation relationship based on quadri-linear moment curvature law (Muttoni, 2008) (with the equivalent axisymmetric value of  $r_s$  calculated from the yield-line value of  $V_{flex}$ ) and the power-law failure criterion (Eq. (4.6)).

<sup>c</sup> Closed-form solution function of  $V_{flex}$  (Eq. (4.10) with  $k_m = 1.2$ ).

<sup>d</sup> Closed-form solution function of  $\rho$  (Eq. (4.18)).

Several comparisons to the tests are presented in the following (refer Table 4.3):

- The first approach (1) corresponds to the original formulation of the CSCT by Muttoni (2008), accounting for the hyperbolic failure criterion of Eq. (4.2) and the load-rotation curve calculated based on the quadri-linear moment-curvature relationship;
- The second approach (2) corresponds to the power-law failure criterion (Eq. (4.6)) and the load-rotation curve of the slab resulting from the integration of the quadri-linear moment-curvature relationship (Muttoni, 2008);
- The third one (3) refers to the closed-form solution as a function of the flexural capacity  $V_{flex}$  (Eq. (4.10);  $V_{flex,red}$  for footings), derived analytically considering the power-law failure criterion and the simplified load-rotation curve of Eq. (4.1);

- Finally, the fourth one (4), refers to the closed-form solution as a function of the flexural reinforcement ratio  $\rho$  (Eq. (4.18);  $\rho_{red}$  for footings).

The two first approaches are applied only to slender slabs, in accordance to the validity of the derivation of the load-rotation curve based on the quadri-linear moment-curvature diagrams (Muttoni, 2008).

#### 4.6.1 Detailed results for slender slabs

As shown in Table 3, the four approaches yield very similar results in terms of average measured-to-calculated strengths and coefficient of variation (COV). Particularly, very similar results are obtained if, instead of a constant value for parameter  $a$  (shear force to average strip moment ratio,  $a \approx 8$ ), this value is calculated as defined in Eq. (4.12), with  $V_{flex}$  determined on the basis of the yield-line theory (e.g. Johansen, 1962; Muttoni, 2008; Guandalini *et al.*, 2009; Einpaul, 2016).

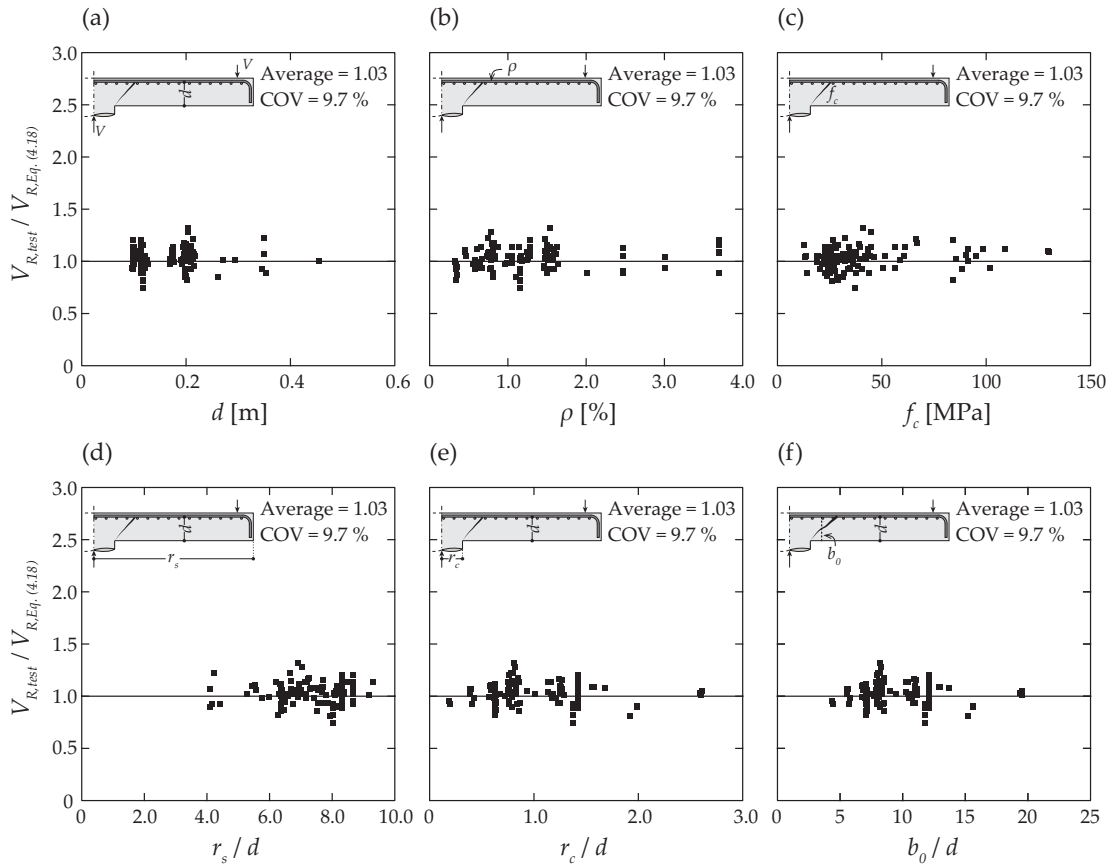


**Figure 4.7:** Ratio of experimental-to-calculated punching strength according to Eq. (4.18) with  $a = V_{flex}/m_R$  (approach (4)) as a function of: (a) effective depth; (b) flexural reinforcement ratio; (c) concrete compressive strength; (d) radius of the slab-to-effective depth ratio (equivalent  $r_s$  based on  $V_{flex}$ ); (e) column radius-to-effective depth ratio slabs (equivalent radius of a circular column with equal perimeter for square columns); (f) control perimeter-to-effective depth ratio. Database including 121 specimens without transverse reinforcement (see Table 4.1).

Figure 4.7 shows the ratio of experimental-to-predicted punching strength obtained with the closed-form expression based on the flexural reinforcement ratio derived from the CSCT (Eq. (4.18)) for the case of slabs without transverse reinforcement. For this comparison, the value of parameter  $a$  is calculated according to Eq. (4.12) (using the yield-line theory (Johansen, 1962) to determine  $V_{flex}$ ). The results show that the closed-form expression derived from the mechanical model of CSCT yields consistent results (average of measured-to-calculated values of 1.03 and COV of 9.7%), without any noticeable trend for the main geometrical and mechanical properties.

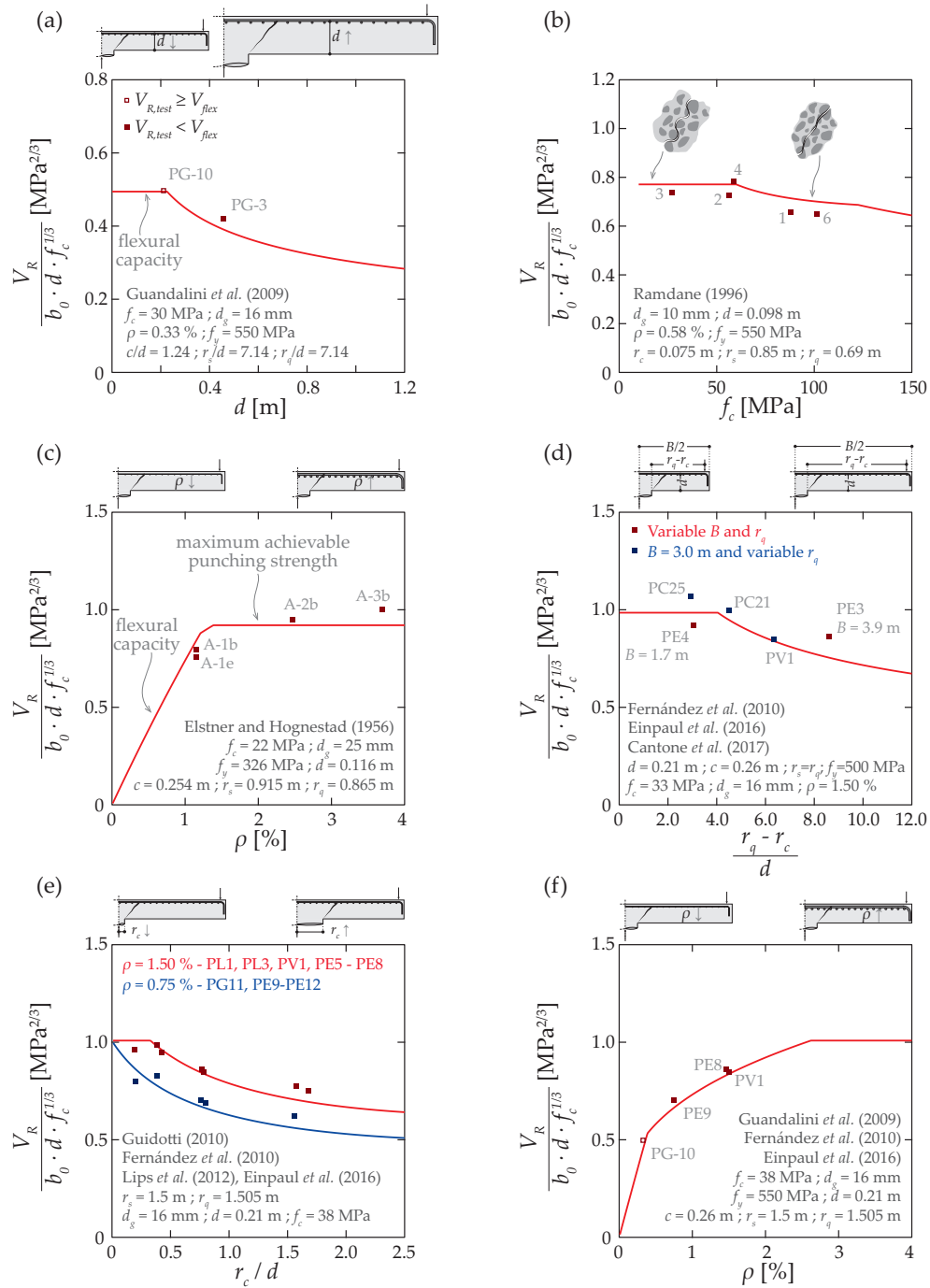


**Figure 4.8:** Comparison of punching shear resistance according to Eq. (4.18) with different series of experimental results of slabs without transverse reinforcement showing the influence of  $(a = 2 \cdot \pi \cdot r_s / (r_q - r_c))$  adopted: (a) effective depth (Guandalini *et al.*, 2009); (b) concrete compressive strength (Ramdane, 1996); (c) flexural reinforcement ratio (Elstner and Hognestad, 1956); (d) shear-slenderness as a function of the load introduction (Fernández Ruiz *et al.*, 2010; Einpaul *et al.*, 2016b; Cantone and Muttoni, 2017); (e) column radius-to-effective depth ratio (Fernández Ruiz *et al.*, 2010; Guidotti, 2010; Einpaul *et al.*, 2016b; Lips *et al.*, 2012); (f) flexural reinforcement ratio (Fernández Ruiz *et al.*, 2010; Guandalini *et al.*, 2009; Einpaul *et al.*, 2016b).

A detailed comparison with selected series is also shown in Figure 4.8 for slender slabs. The various plots refer to the influence of size effect (Figure 4.8(a)), the concrete strength (Figure 4.8(b)), the flexural reinforcement ratio (Figure 4.8(c) and (f)), the slab slenderness (Figure 4.8(d)), and the column size (Figure 4.8(e)). The results show that the various failure regimes are suitably reproduced by the closed-form expression and that the trends are finely captured.

#### 4.6.2 Detailed results for footings

With respect to footings, all results presented in Table 4.3 are, again, similar. With respect to limiting  $r_s/d$  to 2.5, it can be noted that this condition is clearly pertinent (with an average measured-to-calculated strength of 1.01). The results of the closed-form design expression as a function of the reduced flexural reinforcement ratio (Eq. (4.18)) are compared in Figure 4.9 to the test results considering the lower limit of  $r_s/d$  to 2.5 (loads applied inside the control perimeter not contributing to the acting shear force). It can be seen that the results are consistent and trend free for the main geometrical and mechanical parameters. As for the slender slabs, the various failure modes are again suitably addressed (Figure 4.10) as well as the influence of the individual parameters.

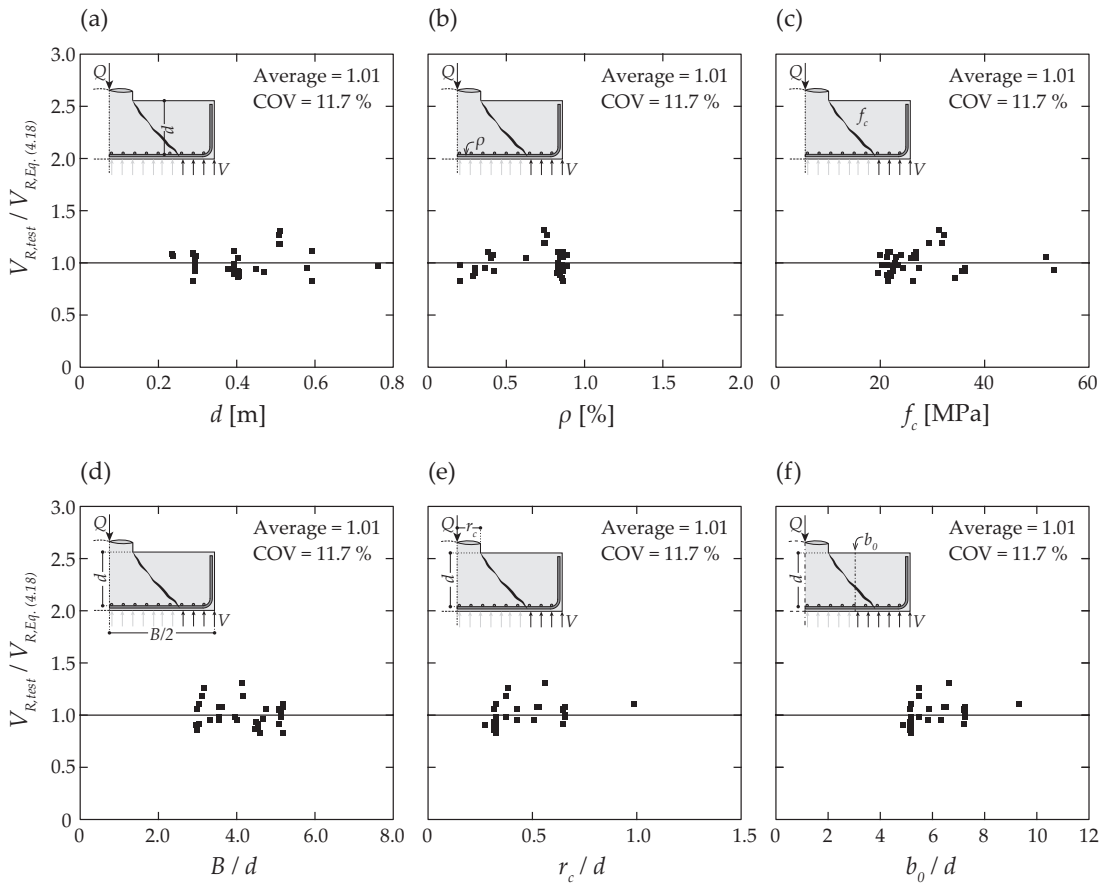


**Figure 4.9:** Ratio of experimental-to-calculated punching strength according to Eq. (4.18) as a function of ( $a = 8$ ): (a) effective depth; (b) flexural reinforcement ratio; (c) concrete compressive strength; (d) side length of the footing-to-effective depth ratio; (e) column radius-to-effective depth ratio slabs (equivalent radius of a circular column with equal perimeter for square columns); (f) specimens control perimeter-to-effective depth ratio. Database including 34 footings without transverse reinforcement (see Table 4.2).

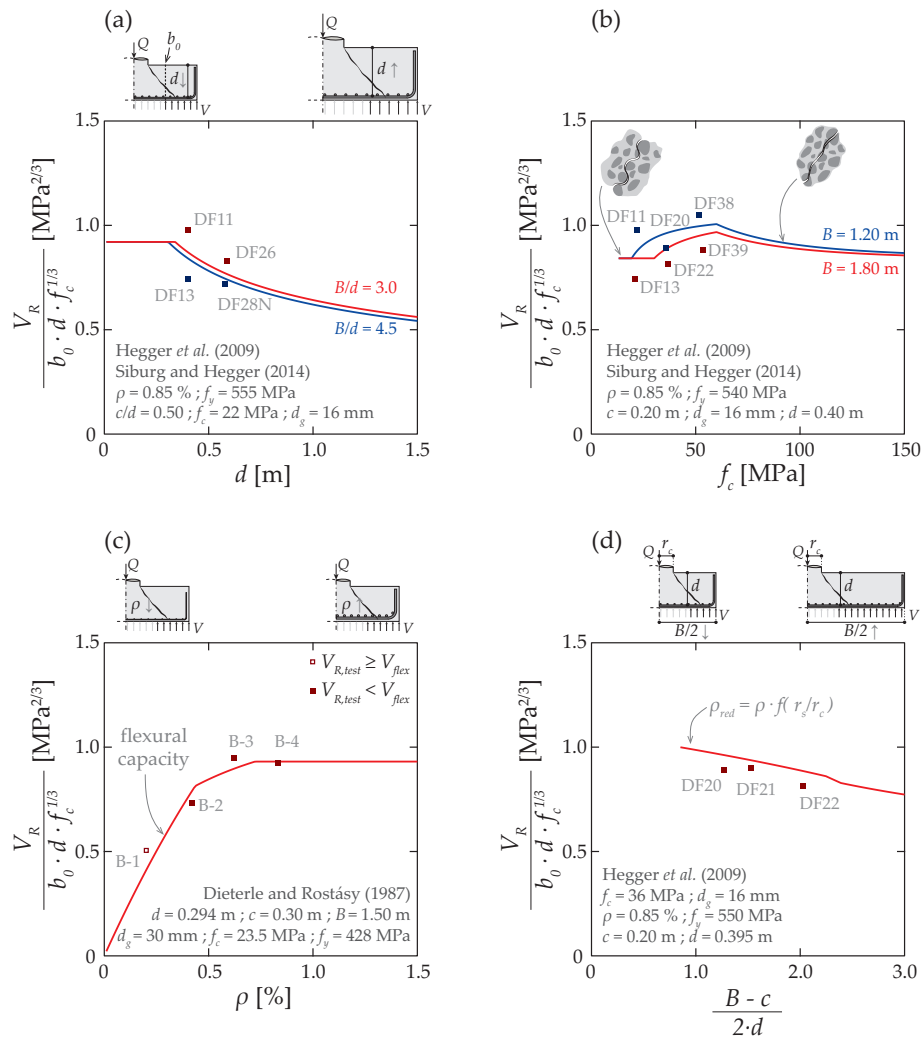


**Figure 4.10:** Comparison of punching shear resistance according to Eq. (4.18) with different series of experimental results of footings without transverse reinforcement showing the influence of ( $a = 8$ ): (a) effective depth (Hegger *et al.*, 2009; Siburg and Hegger, 2014); (b) concrete compressive strength (Hegger *et al.*, 2009; Siburg and Hegger, 2014); (c) flexural reinforcement ratio (Dieterle and Rostásy, 1987); (d) shear span-to-effective depth ratio (Hegger *et al.*, 2009).

## 4.7 Conclusions

In this paper, the CSCT is reviewed and used to derive closed-form expressions to calculate the punching shear strength of slabs and footings without transverse reinforcement. The main conclusions of this paper are listed below:

1. The mechanical model of the CSCT can account for different situations where punching failure governs the strength. At failure, localization of the strains in a critical shear crack occurs. The kinematics is governed by a rotation and a shear deformation, and the resulting stresses on the failure surface form an inclined compression strut (whose strength decays for increasing openings of the critical shear crack and lower crack roughness);
2. Slender and squat members are shown to have a different significance of the rotational and shear deformation components at failure. This also influences the failure surfaces and associated strengths. Yet, both can be consistently addressed by the CSCT mechanical model;

3. On the basis of the distinct behaviour of slender and squat members, it is justified to adopt a failure criterion characterized by a power law limited by a maximum achievable punching strength;
4. The power-law failure criterion in combination with a load-rotation relationship for the slab allows deriving closed-form expressions for calculation of the punching resistance. The derived expressions provide a clear view of the influence of every parameter and enable the calculation of the punching shear resistance in a direct manner, being therefore suitable for design purposes.
5. The closed-form design expressions can be consistently extended to special cases (as for instance the influence of membrane action), by introducing in the load-deformation relationship the necessary considerations. This allows deriving physically consistent design expressions for these cases.
6. The closed-form expressions derived based on CSCT show an excellent agreement with the experimental results both for slender slabs and squat members (footings) without transverse reinforcement. In addition, the influence of different mechanical and geometrical properties is shown to be consistently considered by the proposed expressions.

## 4.8 References

- ACI 318 (2014):** *Building Code Requirements for Reinforced Concrete (ACI 318-14)*. Farmington Hills, MI, USA.
- Belletti B.; Walraven J. C.; Trapani F. (2015):** „Evaluation of compressive membrane action effects on punching shear resistance of reinforced concrete slabs“. *Engineering Structures*, Vol. 95, pp. 25–39.
- Birkle G. (2004):** „Punching of Flat Slabs: The Influence of Slab Thickness and Stud Layout“. PhD thesis. Calgary, Canada: University of Calgary, p. 217.
- Bortolotti L. (1990):** „Punching shear strength in concrete slabs“. *ACI Structural Journal*, Vol. 87, No. 2, pp. 208–219.
- Braestrup M. W. (1979):** „Punching shear in concrete slabs“. In: *Plasticity in reinforced concrete*. International Association for Bridge and Structural Engineering. IABSE colloquium, pp. 115–136.
- Braestrup M. W.; Nielsen M. P.; Jensen B. C.; Bach F. (1976):** *Axisymmetric Punching of Plain and Reinforced Concrete*. Tech. rep. 75. Structural Research Laboratory, Technical University of Denmark, p. 33.
- Broms C. E. (1990):** „Punching of flat plates - a question of concrete properties in biaxial compression and size effect“. *ACI Structural Journal*, Vol. 87, No. 3, pp. 292–304.
- Broms C. E. (2016):** „Tangential strain theory for punching failure of flat slabs“. *ACI Structural Journal*, Vol. 113, No. 1, pp. 95–104.
- Cantone R.; Muttoni A. (2017):** *Punching Shear Tests of Flat Slabs*. Tech. rep.
- Clément T. (2012):** „Influence de la précontrainte sur la résistance au poinçonnement de dalles en béton armé“. PhD thesis. Lausanne, Switzerland: EPFL, p. 224.
- Dieterle H.; Rostásy F. (1987):** „Load-carrying behaviour of isolated reinforced concrete foundations of square columns (In German: Tragverhalten quadratischer Einzelfundamente aus Stahlbeton)“. *Deutscher Ausschuss für Stahlbeton*, Vol. 387, pp. 1–91.
- Drakatos I.-S.; Muttoni A.; Beyer K. (2016):** „Internal slab-column connections under monotonic and cyclic imposed rotations“. *Engineering Structures*, Vol. 123, pp. 501–516.
- Einpaul J. (2016):** „Punching strength of continuous flat slabs“. PhD thesis. Lausanne, Switzerland: EPFL, p. 209.
- Einpaul J.; Fernández Ruiz M.; Muttoni A. (2015):** „Influence of moment redistribution and compressive membrane action on punching strength of flat slabs“. *Engineering Structures*, Vol. 86, pp. 43–57.
- Einpaul J.; Ospina C.; Fernández Ruiz M.; Muttoni A. (2016a):** „Punching shear capacity of continuous slabs“. *ACI Structural Journal*, Vol. 113, No. 4, pp. 861–872.
- Einpaul J.; Bujnak J.; Fernández Ruiz M.; Muttoni A. (2016b):** „Study on influence of column size and slab slenderness on punching strength“. *ACI Structural Journal*, Vol. 113, No. 1, pp. 135–145.
- Elstner R. C.; Hognestad E. (1956):** „Shearing strength of reinforced concrete slabs“. *ACI Journal Proceedings*, Vol. 53, No. 2, pp. 29–58.
- Eurocode 2 (2004):** *Design of Concrete Structures - General Rules and Rules for Buildings, EN 1992-1-1*. Brussels, Belgium, p. 225.

**Faria D. M. V.; Einpaul J.; Ramos A. M. P.; Fernández Ruiz M.; Muttoni A. (2014):** „On the efficiency of flat slabs strengthening against punching using externally bonded fibre reinforced polymers“. *Construction and Building Materials*, Vol. 73, pp. 366–377.

**Fernández Ruiz M.; Muttoni A. (2009):** „Applications of the critical shear crack theory to punching R/C slabs with transverse reinforcement“. *ACI Structural Journal*, Vol. 106, No. 4, pp. 485–494.

**Fernández Ruiz M.; Muttoni A. (2017):** „Size effect on punching shear strength: Differences and analogies with shear in one-way slabs“. In: *Bulletin 81 / ACI SP-315: Punching shear test of structural concrete slabs: Honoring Neil M. Hawkins*. Ed. by Ospina C. E.; Mitchell D.; Muttoni A. Lausanne, Switzerland: International Federation for Structural Concrete, pp. 59–72.

**Fernández Ruiz M.; Muttoni A.; Kunz J. (2010):** „Strengthening of flat slabs against punching shear using post-installed shear reinforcement“. *ACI Structural Journal*, Vol. 107, No. 4, pp. 434–442.

**Fernández Ruiz M.; Mirzaei Y.; Muttoni A. (2013):** „Post-punching behavior of flat slabs“. *ACI Structural Journal*, Vol. 110, No. 5, pp. 801–812.

**Fernández Ruiz M.; Muttoni A.; Sagaseta J. (2015):** „Shear strength of concrete members without transverse reinforcement: a mechanical approach to consistently account for size and strain effects“. *Engineering Structures*, Vol. 99, pp. 360–372.

**fib (2001):** *Bulletin 12: Punching of structural concrete slabs*. Tech. rep. Lausanne, Switzerland: International Federation for Structural Concrete, p. 314.

**fib (2017):** *Bulletin 81 / ACI SP-315: Punching shear of structural concrete slabs: Honoring Neil M. Hawkins*. Tech. rep. Lausanne, Switzerland: International Federation for Structural Concrete, p. 378.

**fib Model Code 2010 (2013):** *Model Code 2010 - Final draft*. Tech. rep. Volumes 1 and 2, Bulletins 65 and 66. International Federation for Structural Concrete.

**Guandalini S.; Burdet O.; Muttoni A. (2009):** „Punching tests of slabs with low reinforcement ratios“. *ACI Structural Journal*, Vol. 106, No. 1, pp. 87–95.

**Guidotti R. (2010):** „Punching shear of slabs with column load (In French: Poinçonnement des planchers-dalles avec colonnes superposées fortement sollicitées)“. PhD thesis. Lausanne, Switzerland: EPFL, p. 189.

**Hallgren M. (1996):** „Punching Shear Capacity of Reinforced High Strength Concrete Slabs“. PhD thesis. Stockholm, Sweden: Department of Structural Engineering, Royal Institute of Technology, p. 206.

**Hallgren M.; Kinnunen S.; Nylander B. (1998):** „Punching shear tests on column footings“. *Nordic Concrete Research*, Vol. 21, pp. 1–22.

**Hassanzadeh G. (1996):** *Influence of the slab thickness on the strength of concrete slabs at punching. Tests with circular slabs (In Swedish: Förstärkning av brobanepeltor på pelaremed hänsyn till genomstansning "Redovisning av provningar")*. Tech. rep. 41. Stockholm, Sweden: Royal Institute of Technology, Department of Structural Mechanics and Engineering, p. 134.

**Hegger J.; Ricker M.; Sherif M. (2009):** „Punching Strength of Reinforced Concrete Footings“. *ACI Structural Journal*, Vol. 106, No. 5, pp. 706–716.

**Heinzmann D.; Etter S.; Villiger S.; Jaeger T. (2012):** „Punching tests on reinforced concrete slabs with and without shear reinforcement“. *ACI Structural Journal*, Vol. 109, No. 6, pp. 787–794.

- Hoang L. C. (2006):** „Punching Shear Analysis according to the Crack Sliding Model - Slabs without Shear Reinforcement“. *Proceedings of the Danish Society for Structural Science and Engineering*, Vol. 77, No. 3, pp. 69–133.
- Hordijk D. A. (1992):** „Tensile and tensile fatigue behaviour of concrete, experiments, modelling and analyses“. *HERON*, Vol. 37, No. 1, pp. 79.
- Inácio M.; Ramos A. P.; Lúcio V.; Faria D. V. (2015):** „Punching of high strength concrete flat slabs - Experimental investigation“. *Engineering Structures*, Vol. 103, pp. 275–284.
- Jiang D. H.; Shen J. H. (1986):** „Strength of concrete slabs in punching shear“. *Journal of Structural Engineering*, Vol. 112, No. 12, pp. 2578–2591.
- Johansen K. W. (1962):** *Yield-line Theory*. Cement and Concrete Association.
- Kinnunen S.; Nylander H. (1960):** *Punching of Concrete Slabs Without Shear Reinforcement*. Tech. rep. 158. Stockholm, Sweden: Transactions of the Royal Institute of Technology, p. 112.
- Kuang J. S. (1991):** *An upper-bound plastic solution for punching shear failure of concrete slabs*. Tech. rep. CUED/D-Struct/TR.136. United Kingdom: Engineering Department, Cambridge University.
- Lips S.; Fernández Ruiz M.; Muttoni A. (2012):** „Experimental Investigation on Punching Strength and Deformation Capacity of Shear-Reinforced Slabs“. *ACI Structural Journal*, Vol. 109, No. 6, pp. 896–900.
- Maya L. F.; Fernández Ruiz M.; Muttoni A.; Foster S. (2012):** „Punching shear strength of steel fibre reinforced concrete slabs“. *Engineering Structures*, Vol. 40, pp. 83–94.
- Moe J. (1961):** *Shearing strength of reinforced concrete slabs and footings under concentrated loads*. Vol. D47. Skokie, Illinois: Portland Cement Association, Research and Development Laboratories.
- Muttoni A. (1990):** „The applicability of the theory of plasticity to reinforced concrete design (In German: Die Anwendbarkeit der Plastizitätstheorie in der Bemessung von Stahlbeton)“. PhD thesis. Zürich, Switzerland: ETHZ, p. 158.
- Muttoni A. (2003):** „Shear and punching strength of slabs without shear reinforcement (In German: Schubfestigkeit und Durchstanzen von Platten ohne Querkraftbewehrung)“. *Beton- und Stahlbetonbau*, Vol. 98, No. 2, pp. 74–84.
- Muttoni A. (2008):** „Punching shear strength of reinforced concrete slabs without transverse reinforcement“. *ACI structural Journal*, Vol. 105, No. 4, pp. 440–450.
- Muttoni A.; Fernández Ruiz M. (2008):** „Shear strength of members without transverse reinforcement as function of critical shear crack width“. *ACI Structural Journal*, Vol. 105, No. 2, pp. 163–172.
- Muttoni A.; Fernández Ruiz M. (2010):** „MC2010: the critical shear crack theory as a mechanical model for punching shear design and its application to code provisions“. In: *Bulletin 57: Shear and punching shear in RC and FRC elements*. Lausanne, Switzerland: International Federation for Structural Concrete, pp. 31–60.
- Muttoni A.; Fernández Ruiz M. (2012):** „The levels-of-approximation approach in MC 2010: application to punching shear provisions“. *Structural Concrete*, Vol. 13, No. 1, pp. 32–41.
- Muttoni A.; Fernández Ruiz M. (2017):** „The Critical Shear Crack Theory for punching design: from a Mechanical Model to Closed-Form Design Expressions“. In: *Bulletin 81 / ACI SP-315: Punching shear test of structural concrete slabs: Honoring Neil M. Hawkins*. Ed. by Ospina C. E.; Mitchell D.; Muttoni A. Lausanne, Switzerland: International Federation for Structural Concrete, pp. 237–252.

- Muttoni A.; Schwartz J. (1991):** „Behavior of beams and punching in slabs without shear reinforcement“. In: *IABSE Colloquium*. Vol. 62. International Association for Bridge and Structural Engineering. Stuttgart, Germany, pp. 703–708.
- Muttoni A.; Fernández Ruiz M.; Bentz E.; Foster S.; Sigrist V. (2013):** „Background to *fib* Model Code 2010 shear provisions - Part II: punching shear“. *Structural Concrete*, Vol. 14, No. 3, pp. 204–214.
- Muttoni A.; Fernández Ruiz M.; Simões J. T. (2017):** „The theoretical principles of the critical shear crack theory for punching shear failures and derivation of consistent closed-form design expressions“. *Structural Concrete*, pp. 1–17. DOI: 10.1002/suco.201700088.
- Nielsen M. P.; Hoang L. C. (2011):** *Limit analysis and concrete plasticity*. 3<sup>rd</sup> edition Boca Raton. USA: CRC Press.
- Nielsen M. P.; Braestrup M. W.; Bach F. (1978):** „Rational analysis of shear in reinforced concrete beams“. In: *IABSE proceedings*. Vol. 2. International Association for Bridge and Structural Engineering, pp. 1–16.
- Polak M. (2005):** *SP-232: Punching Shear in Reinforced Concrete Slabs*. Tech. rep. Farmington Hills, MI, USA: American Concrete Institute, p. 302.
- Ramdane K. E. (1996):** „Punching shear of high performance concrete slabs“. In: *Proceedings of the fourth international symposium on utilization of high-strength/high performance concrete*. Paris, France, pp. 1015–1026.
- Salim W.; Sebastian W. M. (2002):** „Plasticity model for predicting punching shear strengths of reinforced concrete slabs“. *ACI Structural Journal*, Vol. 99, No. 6, pp. 827–835.
- Schaeffers U. (1984):** „Construction, Dimensioning and Safety with Respect to Punching Shear of Reinforced Concrete Flat Plates in the Vicinity of Internal Columns (In German: Konstruktion, Bemessung und Sicherheit gegen Durchstanzen von balkenlosen Stahlbetondecken im Bereich der Innenstützen)“. *Deutscher Ausschuss für Stahlbeton*, Vol. 357, pp. 83.
- Sherwood E. G.; P. E. C.B. M.; Collins (2007):** „Effect of aggregate size on beam-shear strength of thick slabs“. *ACI Structural Journal*, Vol. 104, No. 2, pp. 180–190.
- SIA 262 (2013):** *Code 262 for Concrete Structures*. Zürich, Switzerland: Swiss Society of Engineers and Architects.
- Siburg C. (2014):** „Consistent punching design in flat slabs and foundations (In German: Zur einheitlichen Bemessung gegen Durchstanzen in Flachdecken und Fundamenten)“. PhD thesis. RWTH, Aachen, p. 197.
- Siburg C.; Hegger J. (2014):** „Experimental Investigations on Punching Behaviour of Reinforced Concrete Footings with structural dimensions“. *Structural Concrete*, Vol. 15, No. 3, pp. 331–339.
- Simões J. T.; Bujnak J.; Fernández Ruiz M.; Muttoni A. (2016a):** „Punching shear on compact footings with uniform soil pressure“. *Structural Concrete*, Vol. 17, No. 4, pp. 603–617.
- Simões J. T.; Faria D. V.; Fernández Ruiz M.; Muttoni A. (2016b):** „Strength of reinforced concrete footings without transverse reinforcement according to limit analysis“. *Engineering Structures*, Vol. 112, pp. 146–161.
- Sistonen E.; Lydman M.; Huovinen S. (1997):** *The geometrical model of the calculation formula of the punching shear capacity of the reinforced concrete slab (In Finnish: Teräsbetoniilaatan lävistyskapasiteetin laskentakaa-*

---

*van geometrinen malli*). Tech. rep. 69. Helsinki University of Technology. Laboratory of Structural Engineering and Building Physics, p. 95.

**Tassinari L. (2011):** „Poinçonnement symétrique des dalles en béton armé avec armature de poinçonnement“. PhD thesis. Lausanne, Switzerland: EPFL, p. 197.

**Tolf P. (1988):** *Influence of the slab thickness on the strength of concrete slabs at punching. Tests with circular slabs (In Swedish: Plattjocklekens inverkan på betongplattors hållfasthet vid genomstansning: försök med cirkulära plattor)*. Tech. rep. 146. Stockholm, Sweden: Royal Institute of Technology, Department of Structural Mechanics and Engineering, p. 64.

**Van Der Voet A. F.; Dilger W. H.; Ghali A. (1982):** „Concrete flat plates with well-anchored shear reinforcement elements“. *Canadian Journal of Civil Engineering*, Vol. 9, No. 1, pp. 107–114.

**Vecchio F. J.; Collins M. P. (1986):** „The modified compression-field theory for reinforced concrete elements subjected to shear“. *ACI Structural Journal*, Vol. 83, No. 2, pp. 219–231.

**Walkner R. (2014):** „Critical review of EC2 regarding punching and improving the design approach (In German: Kritische analyse des durchstanznachweises nach EC2 und verbesserung des bemessungsansatzes)“. PhD thesis. Innsbruck, Austria: Innsbruck University.

**Walraven J. (1981):** „Fundamental analysis of aggregate interlock“. *Journal of Structural Engineering*, Vol. 107, No. 11, pp. 2245–2270.

## 4.9 Notation

### Latin characters

#### Lower Case

$a$	ratio between acting shear force and average moment in the support strip
$b_0$	length of control perimeter
$c$	side length of a square column
$d$	effective depth (distance from the centroid of the flexural reinforcement to the outermost compressed fiber)
$d_g$	maximum aggregate size
$d_{g0}$	reference aggregate size ( $d_{g0} = 16$ mm for normal weight concrete (Muttoni, 2008))
$d_{d_g}$	reference value of the roughness of the critical shear crack
$f_c$	concrete compressive strength measured in cylinder
$f_{ce}$	effective concrete compressive strength
$f_{cp}$	plastic compressive strength of concrete
$f_{cc}$	enhanced concrete compressive strength
$f_y$	yield strength of flexural reinforcement
$h$	slab thickness
$k_m, k_v, k_{fc}, k_1, k_2, k_3$	factors
$k_b$	shear gradient enhancement factor
$k_{cc}$	factor enhancing concrete compressive strength due to triaxial compression
$k_{cs}$	factor accounting for slab continuity and membrane action
$m_{cr}$	cracking moment
$m_R$	average unitary flexural strength in the support strip
$\overline{m_R}$	reduced sectional moment capacity
$m_s$	average unitary moment for calculation of the bending reinforcement in the support strip
$r_c$	radius of a circular column
$r_0$	radius of the failure surface at the level of the flexural reinforcement
$r_s$	distance of the column axis to the line of contraflexure of bending moments
$r_q$	distance of the column axis to the line of load introduction
$w$	crack width
$w_0$	initial crack opening due to flexural deformations
$x$	height of compression zone due to bending
$\bar{x}$	increased height of compression zone due to flexure-shear interaction

#### Upper Case

$B$	side length of a square slab
$E_s$	modulus of elasticity of flexural reinforcement
$V$	punching shear force
$V_{flex}$	shear force associated with full yielding of both radial and tangential flexural reinforcement
$V_{flex,red}$	shear force associated with full yielding of both radial and tangential flexural reinforcement considering flexural-shear interaction
$V_R$	punching shear strength
$V_{Rc}$	concrete contribution for punching shear strength
$V_{R,test}$	experimental punching shear strength
$V_{Rc,0}$	maximum achievable punching shear strength of concrete
$Q_{flex}$	flexural strength
$Q_{flex,red}$	reduced flexural strength

## Greek characters

### Lower Case

$\beta$	secant inclination of the failure surface
$\gamma$	angle between failure surface and crack sliding vector
$\delta$	crack sliding
$\eta$	global effectiveness factor
$\eta_{fc}$	effectiveness factor accounting for concrete brittleness in compression
$\eta_w$	effectiveness factor accounting for the state of deformations
$\rho$	flexural reinforcement ratio
$\rho_{red}$	reduced flexural reinforcement ratio
$\sigma$	normal stresses due to aggregate interlocking
$\tau$	shear stresses due to aggregate interlocking
$\varphi$	concrete friction angle
$\psi$	rotation
$\psi_{Rc}$	rotation at failure
$\omega$	mechanical reinforcement ratio

## Acronyms

CSCT	Critical Shear Crack Theory
------	-----------------------------

## 4.10 Appendix

A simplified expression to account for a flexure-shear interaction in squat members subjected to uniform pressure is derived in this Appendix for practical purposes. Figure 4.11(a) shows a square footing with a side length  $B$  subjected to a uniform soil pressure. A square column with a side length  $c$  is also considered. The yield-line mechanism governing in this case is considered to be characterized by the formation of a yield line along the edge of the column (see Figure 4.11(c)), where the sectional moment capacity calculated in accordance to Eq. (4.13) is reached. According to this mechanism, which corresponds to a pure flexural behavior, the height of the compression zone  $x$  is obtained by equalling the horizontal forces developing in the section:

$$\frac{x}{d} = \omega = \frac{\rho \cdot f_y}{f_{cp}} \quad (4.26)$$

where  $\omega$  represents the mechanical reinforcement ratio. Figure 4.11(b) shows a possible stress field developing along the axis of the footing (considering that tensile strength is neglected). The stress field consists only of inclined concrete struts which are horizontally equilibrated by the flexural reinforcement. With increasing flexural reinforcement ratio, the area of the inclined struts increases (as well as the region of triaxial stresses developing under the footing). The height of this region becomes very significant and can considerably decrease the lever arm between the horizontal compressive (concrete) and tensile (reinforcement) forces. In addition, provided that tensile strength is neglected, the entire horizontal tensile force has to be equilibrated by the horizontal compressive force under the column. Therefore, for practical purposes and taking into consideration the stress field illustrated in Figure 4.11(b), a sectional analysis as the one shown in Figure 4.11(d) can be adopted to calculate a reduced sectional moment capacity  $m_R$  as follows:

$$\bar{m}_R = \rho \cdot f_y \cdot d^2 \cdot \left(1 - \frac{\bar{x}}{2 \cdot d}\right) \quad (4.27)$$

where  $x$  represents an increased compression zone accounting for the flexure-shear interaction, which can be computed from the horizontal equilibrium in the section as (tensile force developing along the width of the footing  $B$  equilibrated by the compressive force developing along the width of the column  $c$  with an enhanced concrete compressive strength due to triaxial compression  $f_{cc} = k_{cc} \cdot f_c$ ):

$$\frac{\bar{x}}{d} = \frac{\rho \cdot f_y}{k_{cc} \cdot f_{cp}} \cdot \frac{B}{c} \leq 1 \quad (4.28)$$

A reduced reinforcement ratio  $\rho_{red}$  accounting for the decrease of the lever arm due to flexure-shear interaction can be calculated equalling the moment capacity established in Eq. (4.13) and the reduced moment capacity defined in Eq. (4.27) as follows:

$$\bar{m}_R = m_R \Rightarrow \rho \cdot \left(1 - \frac{\rho \cdot f_y}{2 \cdot k_{cc} \cdot f_c} \cdot \frac{B}{c}\right) = \rho_{red} \cdot \left(1 - \frac{\rho_{red} \cdot f_y}{2 \cdot f_c}\right) \quad (4.29)$$





# Chapter 5

## **PAPER IV**

### **Validation of the Critical Shear Crack Theory for punching of slabs without transverse reinforcement by means of a refined mechanical model**

This chapter is the postprint version of the journal article titled *Validation of the Critical Shear Crack Theory for punching of slabs without transverse reinforcement by means of a refined mechanical model* published in the journal *Structural Concrete* in 2018 (DOI: 10.1002/suco.201700280). The authors of the publication are João Tiago Simões (PhD Candidate), Miguel Fernández Ruiz (Senior lecturer at EPFL and thesis director), Aurelio Muttoni (Professor at EPFL and thesis director). The complete reference is the following:

**Simões J. T., Fernández Ruiz M., and Muttoni A. (2018):** „Validation of the Critical Shear Crack Theory for punching of slabs without transverse reinforcement by means of a refined mechanical model“. *Structural Concrete*, pp. 1–26. DOI: 10.1002/suco.201700280.

The work presented in this article was developed by João Tiago Simões under the supervision of Aurelio Muttoni and Miguel Fernández Ruiz. The main contributions of João Tiago Simões to the creation of this article involved:

- Reviewing the recent experimental findings available in the scientific literature;
- Developing the refined mechanical model;
- Performing all the calculations presented;
- Comparing the results of the refined mechanical model against a database and individual series of experimental tests;
- Validating theoretically the analytical failure criterion of the Critical Shear Crack Theory based on the results of the refined mechanical model;
- Production of the figures included in the article;
- Preparation of the manuscript of the article.

With respect to the postprint version of the scientific article, this chapter includes additional information in the Appendix (calculation of the neutral axis following a similar approach to that followed by Hallgren (1996), calculation of the load-rotation relationship based on the work of Muttoni (2008) and possible numerical procedure for calculation of the punching strength and its associated deformation capacity). Also the Figure 5.4 of this Chapter presents only the schematic representation of the observed cracking, while the scientific article includes also the corresponding pictures.

## 5.1 Abstract

Despite the intensive efforts dedicated in the last decades to better understanding punching shear failures, there is still no consensus on the mechanics governing this phenomenon and on how to implement it within a physical approach. In this paper, an analysis of recent detailed measurements on the kinematics and crack development associated with punching failures is presented. This allows classifying the observed cracks by their nature and to address their interaction and development on the eventual punching failure surface. On this basis, a complete mechanical model is formulated consistently with the principles of the critical shear crack theory (CSCT). This model generalizes previous approaches based on the CSCT by accounting for the various crack types and failure modes as well as for their associated kinematics. The generality of the model is verified by extensive comparisons to test data, showing accurate and consistent agreement. Its results are eventually used to investigate the role of the various potential shear-transfer actions as well as the pertinence of the assumptions adopted to simplify the CSCT by describing its failure criterion with analytical expressions.

**Keywords:** concrete structures, Critical Shear Crack Theory (CSCT), experimental verification, failure criterion, members without transverse reinforcement, punching shear strength

## 5.2 Introduction

Punching shear failures were early identified as a governing failure mode in reinforced concrete flat slabs, and their first designs accounted for this fact by introducing column capitals and mushroom-shaped columns. Intensive research performed since the second half of the 20<sup>th</sup> century led (Regan and Braestrup, 1985; *fib*, 2001; Polak, 2005; *fib*, 2017) eventually to the development of design expressions allowing to evaluate the punching shear capacity accounting for the role of some relevant mechanical and geometrical parameters (Richart, 1948; Hognestad, 1953; Elstner and Hognestad, 1956; Whitney, 1957; Moe, 1961). These expressions, with an empirical basis and at the origin of those provided still today in many codes of practice (Eurocode 2, 2004; ACI 318, 2014), had however a validity limited to the available experimental data at the time they were proposed. Theoretical approaches were later developed, on the basis of limit analysis (e.g. Braestrup *et al.*, 1976; Hoang, 2006), fracture mechanics (e.g. Bažant and Cao, 1987) or accounting for mechanical models (e.g. Kinnunen and Nylander, 1960; Shehata and Regan, 1989; Broms, 1990; Hallgren, 1996; Yankelevsky and Leibowitz, 1999; Theodorakopoulos and Swamy, 2002; Broms, 2005; Park *et al.*, 2011; Broms, 2016).

The theoretical approaches constituted a major step towards the consistent understanding of the phenomenon and the treatment of some important issues such as the size and strain effects (Fernández Ruiz and Muttoni, 2017). Among these models, one of the most notable contributions was that by Kinnunen and Nylander (1960), relating the deformation and load-carrying capacities of slab-column connections failing by punching. The model considers that the punching strength is controlled by a conical shell representing the inclined compression struts developing at the support of the column. Failure in this region was assumed to be triggered by a limit value of the tangential strain in the compression zone, calculated for a given level of load on the basis of a conically deformed shape of a slab sector (Kinnunen and Nylander, 1960). The physical principles of this model led to a notable acceptance of the research community and inspired a number of researchers that improved the original approach. For instance, Hallgren (1996) proposed an improved failure criterion to account for the influence of size effect and concrete brittleness. Broms (1990, 2005, 2016) proposed also an improvement of the theory by considering two different failure criteria based on limit tangential and radial conditions (representing different failure modes for slender and squat members). A similar approach to that of Broms (1990, 2016) was also followed by Shehata and Regan (1989), considering three failure criteria, representing

each a different failure mode (splitting of concrete strut and crushing of concrete due to high radial or tangential strains).

Inspired on the rational approach of Kinnunen and Nylander (1960), Muttoni and Schwartz (1991) developed a mechanical model for punching shear failures, named as the critical shear crack theory (CSCT) (Muttoni, 2008). According to this theory, which is also applicable to shear in beams (e.g. Muttoni and Fernández Ruiz, 2008, 2010; Fernández Ruiz *et al.*, 2015; Cavagnis *et al.*, 2015, 2017), the opening of a critical shear crack (CSC) (a crack in the shear-critical region where the compression strut carrying shear develops) reduces the ability of concrete to transfer shear forces and leads eventually to failure (Muttoni, 2008). On that basis, a failure criterion relating the maximum allowable shear force that can be transferred for a level of crack opening (related to the slab rotations) was defined (Muttoni, 2008), refer to Figure 5.1(a). The punching failure load and its associated deformation capacity can thus be calculated by intersection of the failure criterion with a load-rotation relationship (relating the opening of the cracks with the level of applied load), refer to Figure 5.1(b).

As explained by Muttoni *et al.* (2017), the opening of the CSC as a function of the acting load is associated with the rotation of the slab ( $\psi$ ) and also to its shear deformations ( $\delta_s$ ), see Figure 5.1(c). Several approaches have been proposed in the past to perform a refined calculation of the failure criterion consistently with the hypotheses of the CSCT. According to these approaches, the opening of the CSC and its associated shear capacity (resulting from the stresses developed, refer to Figure 5.1(d)) can be calculated on the basis of the shape of the failure surface and its kinematics (a detailed review can be consulted in Muttoni *et al.* (2017)).

For slender members, refined calculations of the failure criterion of the CSCT have been proposed on the basis of a simplified shape and kinematics of the failure surface. A complete approach for so doing was first developed by Guidotti (2010) and some improvements were later added by Clément (2012). As shown in Figure 5.2(a), Guidotti (2010) considered the CSC as a conical surface (inclined at  $45^\circ$ ) and a kinematics defined by a rotation around the tip of the crack (column perimeter) and a constant shear deformation. The shear strength can thus be calculated by integration of the aggregate interlock and residual tensile strength contributions. As discussed by Muttoni *et al.* (2017), the results of Guidotti (2010) show that, at failure, the shear strains ( $\delta_s$ ) are correlated to the rotations ( $\psi$ ), and thus the punching shear strength for slender members can be expressed as a function of the rotations of the slab (as proposed by the failure criterion of the CSCT, see Figure 5.1(a)). The approach of Guidotti (2010) has been observed to be more suited for slabs experiencing large rotations (thin and slender slabs with medium to low amounts of flexural reinforcement), where bending deformations govern the CSC width (Muttoni *et al.*, 2017). However, when the thickness of the compression zone is relatively large (prestressed slabs or slabs with fairly large reinforcement amounts), these assumptions need to be refined. These additional considerations were later implemented by Clément (2012), who considered the CSC composed by two conical surfaces with different responses (Figure 5.2(b)). The limit between these surfaces was considered to be given by the height of the plastic compression zone and is thus influenced by the presence of in-plane forces and the flexural reinforcement ratio. For the upper conical surface, Clément (2012) considered a similar response as Guidotti (2010). For the lower part, the contribution to the punching strength was estimated with the kinematical theorem of limit analysis based on the work of Braestrup *et al.* (1976) and considering an effective concrete compressive strength function of the bending deformations. The enhancement of the CSCT by Clément (2012) has nevertheless some limitations, as it leads to a discontinuous displacement field along the failure surface.

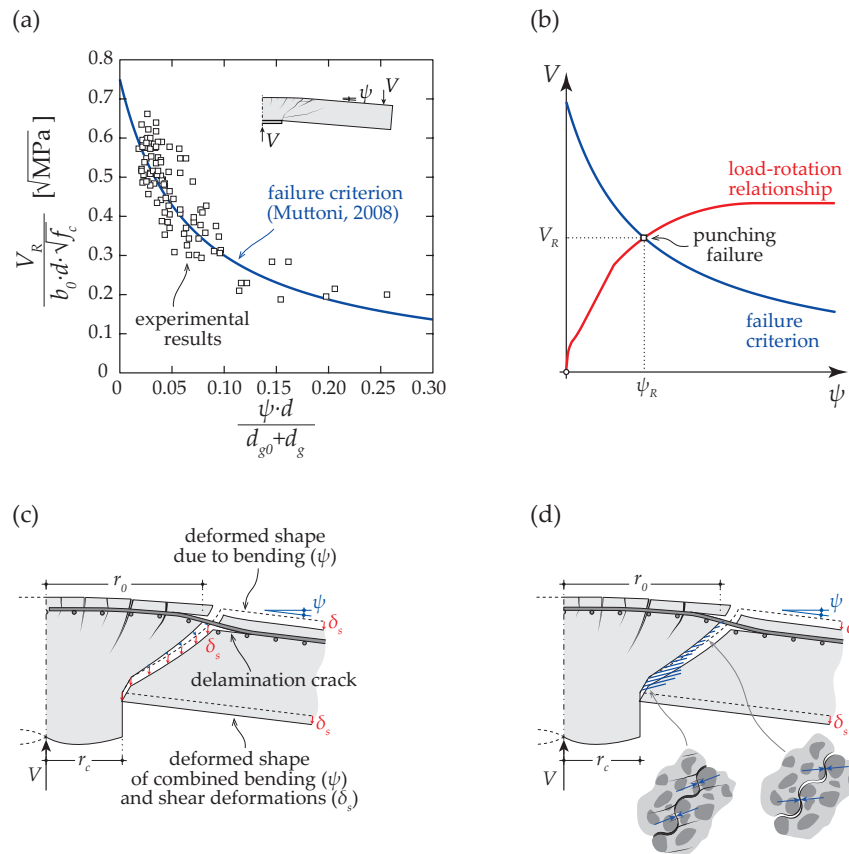


**Figure 5.1:** Mechanical model of the Critical Shear Crack Theory (CSCT): (a) experimental validation of the hyperbolic failure criterion of CSCT (experimental data from Muttoni (2008)); (b) calculation of punching shear failure by intersecting the load-rotation relationship and the failure criterion; (c) adopted kinematics at failure and (d) resulting internal forces along the critical shear crack; figure adapted from (Muttoni *et al.*, 2017).

For squat slabs or footings, where the role of the shear deformations is more dominant (Simões *et al.*, 2016a), Simões *et al.* (2016b) determined the shape of the failure surface and its associated kinematics based on limit analysis. In this case, the punching strength is calculated assuming a rigid-plastic behaviour of concrete characterized by an effective concrete compressive strength accounting for the crack opening (in agreement with the CSCT principles).

Despite the fact that all the mentioned works (Guidotti, 2010; Clément, 2012; Simões *et al.*, 2016b) share the principles of the CSCT, they were developed to address particular cases. Within this context, the present paper is aimed at introducing a comprehensive mechanical model for punching of slabs without transverse reinforcement consistent with the CSCT principles (Muttoni *et al.*, 2017) and with the crack development and kinematics measured in tests. This model generalizes the approaches of Guidotti (2010) and Clément (2012) and allows investigating members with large and low levels of flexural deformation (an extended discussion for squat members will not be presented in this paper and can be consulted elsewhere, see Chapter 6). Extensive comparisons with available data as well as detailed investigations of selected specimens validate the presented refined calculation of the failure criterion. Finally, the theoretical results are used to discuss the main assumptions and limits of applicability of the analytical failure criterion of the CSCT.

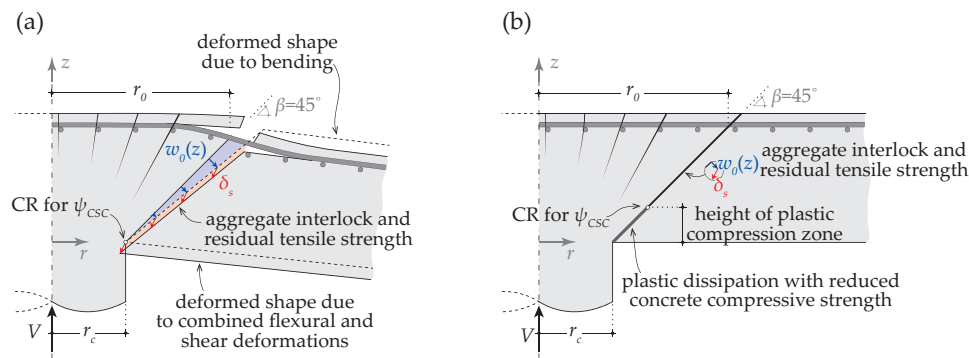


Figure 5.2: Mechanical models consistent with the theoretical principles of the CSC proposed by (a) Guidotti (2010) and (b) Clément (2012).

### 5.3 Analysis of the punching shear behaviour based on experimental observations available in the scientific literature

#### 5.3.1 Discussion on the cracking pattern observed in the saw-cuts of tested specimens

Detailed measurements on the development of cracks within reinforced concrete members have recently been performed for beams in shear (e.g. Campana *et al.*, 2013; Cavagnis *et al.*, 2015; Huber *et al.*, 2016). These measurements have shown to be instrumental for the understanding of the mechanisms leading to shear failures and the role of the various shear-transfer actions (e.g. Campana *et al.*, 2013; Cavagnis *et al.*, 2015; Huber *et al.*, 2016). As discussed by Einpaul *et al.* (2017) such measurements cannot be easily performed for punching failures and the knowledge on their crack development remains limited. An attempt to obtain direct measurements inside the slab was performed by Clément (2012), Einpaul (2016) and Einpaul *et al.* (2017) by using an innovative measuring system based on a robotic arm, reading the location of target points inside the slab (accessible by means of narrow holes). Based on these measurements, the authors could track the development of inner cracking and calculate relative crack displacements and directions at different load stages.

On that basis, Clément (2012), Einpaul (2016) and Einpaul *et al.* (2017) identified different types of cracks related to punching failures. The CSC, as previously described by Muttoni (2008) corresponds to a tangential crack with flexural origin that develops in a stable manner and whose presence disturbs the compression strut-carrying shear. As described by Clément (2012), Einpaul (2016), and Einpaul *et al.* (2017) the failure crack (eventual surface of failure) may be coincident with the CSC, partly coincident with it or completely different. In this latter case, it corresponds to a crack that propagates in an unstable manner from the compression side with a flat inclination angle (Clément, 2012; Einpaul, 2016; Einpaul *et al.*, 2017).

In addition to the CSC and failure crack, other cracking types can typically be observed in slabs failing by punching shear. Following a similar systematics and notation to the one proposed by Cavagnis *et al.* (2015) for beams in shear, the cracks that can be observed after a punching failure may be differentiated according to their location, shape, and origin (Figure 5.3):

- Cracks type A are associated with a flexural origin, originated on the tension side and propagating towards the compression side in an inclined manner due to the shear forces (as described by, for example, Moe (1961) and Muttoni (2008), refer to Figure 5.3(a)). Cavagnis *et al.* (2015) also distinguished between primary and secondary flexural cracks. While secondary flexural cracks

develop only at the height of the flexural reinforcement (controlled by bond conditions), the primary flexural cracks are those propagating towards the neutral axis (Cavagnis *et al.*, 2015);

- Cracks type B are associated with the formation of a shear band with several parallel cracks that eventually coalesce in one single crack, refer to Figure 5.3(b) (Muttoni *et al.*, 2017). This type of cracking normally develops close to failure, near the column support in the soffit of the slab (see Einpaul *et al.*, 2017). In the case represented in Figure 5.3(b), this cracking type joins the column edge to a crack type A but it can also develop only partially, followed by the propagation of a crack type F or F', see Figure 5.3(f);
- Cracks type C represent cracks with flexural origin developing in an inclined manner and that merge to a previously formed crack type A, influencing the shape of the CSC (refer to Figure 5.3(c)). This type of crack has been previously observed in one-way shear tests by Cavagnis *et al.* (2015) and in two-way shear tests by Einpaul *et al.* (2017);
- Cracks type D represented in Figure 5.3(d) result from delamination of the concrete top cover due to dowelling of the flexural reinforcement bars (cracking type previously identified by e.g. Krefeld and Thurston, 1966; Fernández Ruiz *et al.*, 2010a, 2013; Cavagnis *et al.*, 2015; Einpaul, 2016);
- Cracks type E have been originally identified by Cavagnis *et al.* (2015) to develop in one-way members originating from cracks type A, due to high local aggregate interlock stresses (when the shape of the crack is very favorable to aggregate interlock engagement, see Jacobsen *et al.*, 2012; Figure 5.3(e)).
- Cracks type F and F' correspond to unstable splitting cracks developing near the supported area and propagating towards the flexural reinforcement with a flat inclination, as described by Clément (2012), Einpaul (2016), and Einpaul *et al.* (2017) (refer to Figures 5.3(f) and (e)). Cracks type F develop from the shear band (crack type B, see Figure 5.3(f)), while cracks F' develop without the presence of a shear band (Figure 5.3(e)). Their distinction is however not neat in many cases. They also have the same origin: cracks type F result from the strain and stress state in the shear band (yielding an unstable splitting crack propagation towards the flexural reinforcement, refer to specimen PE9 in Figure 5.4), while cracks of type F' develop as a consequence of the tensile strains near the supported area (refer to specimen PF21 in Figure 5.4) which result also from the kinematics of the region of the slab at the potential location of the shear band.

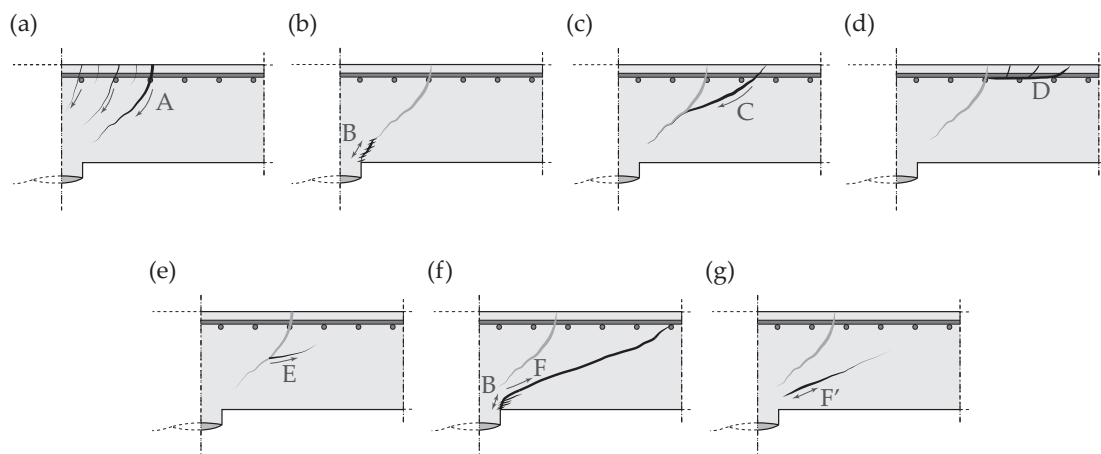
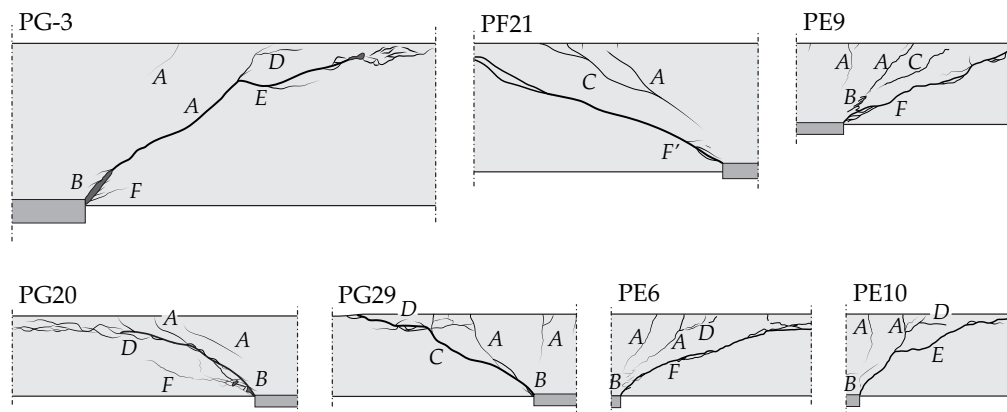


Figure 5.3: Different cracking types observed in a saw-cut of a punching test.

All types of cracks previously introduced in a qualitative manner in Figure 5.3 are generally present in a combined manner in the saw-cut of slabs failed by punching shear. Figure 5.4 (interpretation of observed cracking types) shows some instances for selected saw-cuts of slabs without in-plane forces (PG-3 of Guandalini (2005); PG20 and PG29 of Guidotti (2010); PF21 of Clément (2012); PE6, PE9 and PE10 of Einpaul (2016)). It can be noted from these figures that:

- Several cracks with flexural origin (cracks A) develop from the tension side towards the compression side (some may however have closed during unloading after failure and are hardly visible or not visible in the saw-cuts);
- Cracks with flexural origin developing further away from the column (cracks type C) are observed to govern the shape of the CSC in some cases (if merging to other flexural crack, PG29 and PF21 in Figure 5.4) but not in others (not merging, PE9 in Figure 5.4). In the latter case, the CSC is a crack type A with an average inclination of about  $45^\circ$ , whereas in the former case the CSC is composed by a crack type C merged with a crack type A, thus reducing its average inclination;
- Cracks type B (associated with the shear band) may be observed in most of the saw-cuts. In some cases, cracks type B join the edge of the column and the tip of one crack type A (PG-3 and PG20 in Figure 5.4). In other cases, cracks type B start developing, but failure is controlled by the propagation of a crack type F or F' (PE6 and PE9 in Figure 5.4). In these cases, even if a crack of type F or F' develops, a region of cracks type B can often be identified near the column;
- Cracks type B often present a steeper inclination than cracking type A and C, see PG-3, PG20 and PE6 in Figure 5.4;
- Specimen PE10 in Figure 5.4 shows an example of a crack type E, which probably developed due to the shape of the upper part of the CSC (quasi-vertical branch favorable to engage aggregate interlock forces). Similar observations have already been made by Cavagnis *et al.* (2015) in one-way shear tests.
- Cracks type D can often be recognized at the level of the flexural reinforcement (associated with delamination of the thereof; see PG20 and PG29 in Figure 5.4).



**Figure 5.4:** Interpretation of observed cracking of saw-cuts of tested slabs ( $B/d=8.6-14.9$ ;  $r_g/d=4.3-7.5$ ;  $d=0.201-0.456$  m;  $c=0.22-0.52$  m;  $r_c=0.083-0.166$  m): PG3 of Guandalini (2005); PG20 and PG29 of (Guidotti, 2010); PF21 of Clément (2012); PE6, PE9 and PE10 of Einpaul (2016).

According to the analysis of the cracking pattern of the saw-cuts, and as already discussed by Einpaul *et al.* (2017) on the basis of the internal cracking tracked, the punching failure may occur by a localization of the strains in the CSC (thus the CSC being coincident with the failure crack) or by the development of a splitting crack (the CSC and the failure crack thus not being necessarily coincident). In the former case, a crack type B joining the edge of the column and a crack type A or C develop (see, e.g., PG20 in Figure 5.4). In the case failure occurs by development of a splitting crack, both the CSC (developing from the tension reinforcement up to a certain height) and a failure crack (developing with a flatter inclination, PE9 in Figure 5.4) can be observed (Einpaul *et al.*, 2017). In this latter case, the failure crack may develop from the shear band (crack type F, PG20, and PE9 in Figure 5.4) or may also develop within a region near to the supported area without the complete development of the shear band (crack type F', PF21 in Figure 5.4).

### 5.3.2 Discussion on the distribution of tangential cracks with flexural origin

Another interesting aspect refers to the development of the tangential cracking in the vicinity of the column. Figure 5.5 shows for instance the radial strains (related to tangential cracking) on the top surface (tension side) of slabs PG-1 and PG-3 measured by Guandalini (2005). The results clearly show that, as the level of load increases, the extent of the slab where tangential cracking occurs also increases. It is interesting to note that this region may extend beyond the location of the CSC, normally assumed to develop at a distance  $d$  from the column edge (Muttoni, 2008; Guidotti, 2010; Clément, 2012). This fact is consistent with the observation that others cracks (type C) may potentially develop beyond the CSC for higher shear forces without merging with it (thus not governing the shape of the CSC).

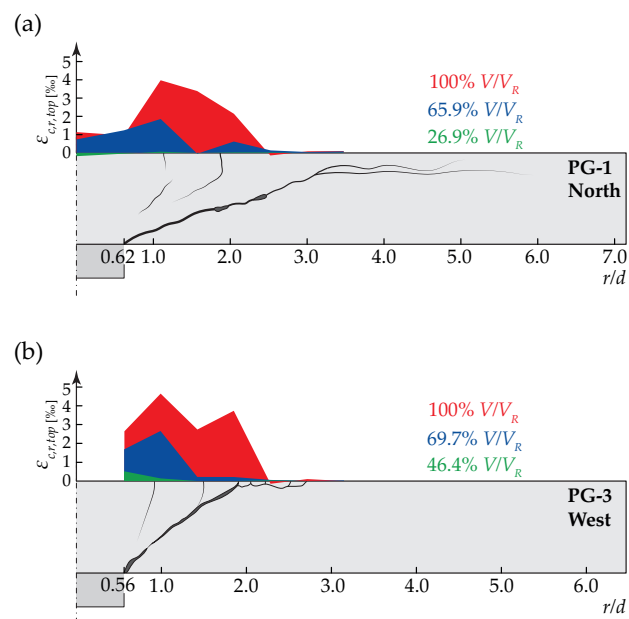


**Figure 5.5:** Experimental results of Guandalini (2005): radial strains measured at the concrete top surface for specimens (a) PG1 ( $B=3.0$  m;  $d=0.21$  m;  $c=0.26$  m;  $\rho=1.5\%$ ; measures performed along the east direction) and (b) PG3 ( $B=6.0$  m;  $d=0.456$  m;  $c=0.52$  m;  $\rho=0.33\%$ ; measures performed along the west direction); figure adapted from Guandalini (2005).

### 5.3.3 Discussion on the kinematics of the critical shear crack

As previously introduced, Clément (2012), Einpaul (2016), and Einpaul *et al.* (2017) measured the displacements of points inside of the slab using a robotic arm. Figure 5.6(a) shows the radial location of the center of rotation of the CSC calculated by Clément (2012) at different load levels for test PF21. In addition, Figure 5.6(b) plots the radial strains in the soffit of the slab as a function of the applied load (Clément, 2012). These results show that the radial location of the center of rotation of the CSC varies during loading (Clément, 2012). First, in the stage where the crack may be forming, the center of rotation is located near the axis of the column. As the load increases, the crack probably develops and the center of rotation shifts towards the edge of the column, but eventually moves back near failure. The results also show that when the center of rotation starts moving back, a reduction of the radial strains in the soffit of the slab is observed (refer to Figure 5.6(b)). As suggested by Clément (2012), this may indicate that both the movement of the center of rotation and the changes in the behaviour of the concrete strains measured on the soffit of the slab are a result of the shear deformations occurring close to failure. This observation is also supported by other researchers (Hallgren, 1996; Einpaul, 2016) that reach a similar conclusion relating the decompression of concrete strains observed in the soffit of the slab to the shear deformations occurring near failure.

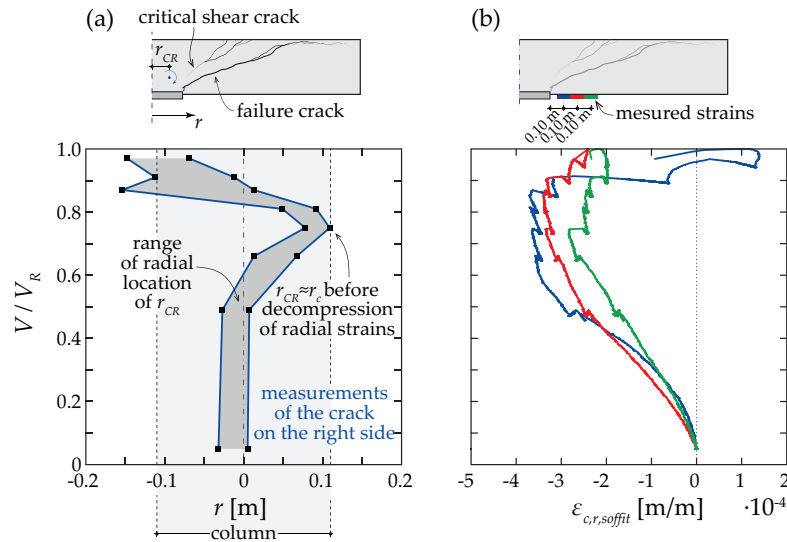


**Figure 5.6:** Results of Clément (2012) for slab PF21 ( $B=3.0$  m;  $c=0.22$  m;  $d=0.35$  m;  $\rho=0.75\%$ ): (a) radial location of centre of rotation (east-west axis); (b) concrete radial strains measured in the soffit of the slab; figure adapted from Clément (2012).

With the help of several measuring points placed inside of the slab, Einpaul *et al.* (2017) also identified the CSC and measured its crack width at an height  $z/d \approx 0.8$ . These results are presented in Figure 5.7 for six slabs with three different columns sizes ( $r_c/d \approx 0.4, 0.8$  and  $1.6$ ) and two different reinforcement ratios ( $\rho \approx 0.75\%$  and  $1.50\%$ ). The results show that for a given level of rotation (Einpaul *et al.*, 2017): (a) smaller crack widths are observed for larger column sizes (i.e., the crack width is a function of the number of cracks, with higher number of cracks for larger column sizes; refer to the average slope of Figure 5.7(a) to 5.7(c)); (b) for a given rotation, the crack width does not seem to be dependent on the flexural reinforcement ratio in the investigated range of cases (negligible differences between red and blue curves of Figure 5.7) but on the column size. Furthermore, Einpaul *et al.* (2017) also observed that the relative displacement of the crack lips in the upper part of the CSC is approximately normal to the crack surface. Eventually, based on the measured displacements of points in the interior of the slab, Einpaul *et al.* (2017) concluded that the center of rotation of the CSC in the tested specimens is inside the slab in terms of height.

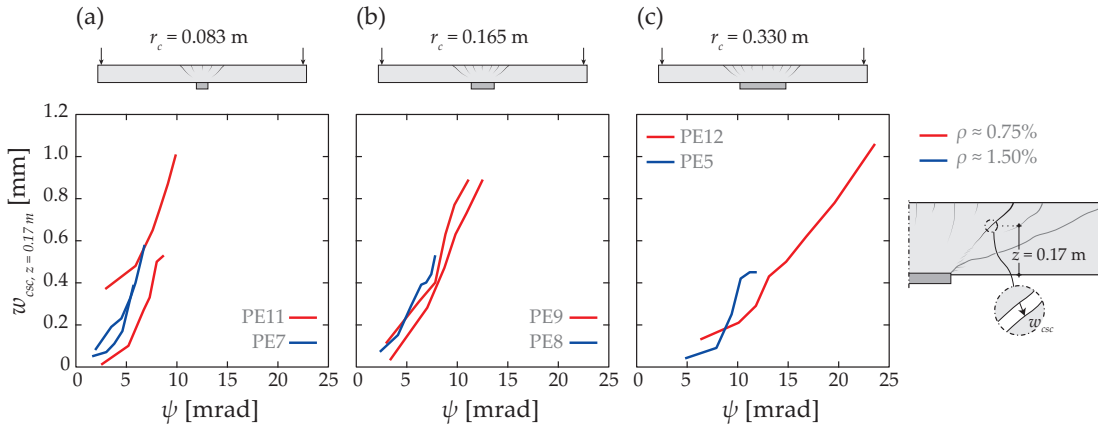


**Figure 5.7:** Experimental results of Einpaul (2016) and Einpaul *et al.* (2017): width of the critical shear crack as a function of the rotation of the slab for different column sizes and reinforcement ratios for six slender slabs ( $B=3.0$  m;  $d=0.210$ - $0.218$  m;  $f_c=36.7$ - $44.1$  MPa); figure adapted from Einpaul (2016).

## 5.4 Mechanical model for punching shear failures

### 5.4.1 Basis of the mechanical model

Based on the previously discussed experimental findings, a comprehensive mechanical model is presented in this section describing the kinematics and load-transfer capacity of slabs failing in punching. The principles of the model are shown in Figure 5.8(a) and described in the following:

- Primary and secondary tangential cracks due to bending develop in the tension side of the slab after the analysis of the cracking development in Section 5.3. The primary tangential flexural cracks are assumed to develop within a radius  $r_{\chi r}$  (measured from the axis of the column) where radial curvature is considered to be non-negligible (in accordance with the results of Guandalini (2005) and Guandalini *et al.* (2009)). The spacing of such cracks is assumed to be constant ( $s_f$ );
- A CSC develops from the tension to the compression side (Figure 5.8) after Muttoni (2008). According to Muttoni *et al.* (2017), this crack is assumed to be composed of an inclined tangential crack (cracks type A and C developing from the tension side) and a shear band (smeared crack type B developing on the compression side). The extent of each cracking type is considered to be a function of the associated displacement field. On the tension side, a mixed-mode opening-sliding occurs (localized cracking), while on the theoretical compression side, deformations may localize in a shear band (smeared cracking, eventually followed by coalescence), see Figure 5.8(a) (Muttoni *et al.*, 2017);
- The kinematics of the CSC accounts for two components. The first one refers to the rotation around the center of rotation due to flexural deformations (CR with coordinates  $(r_{CR}, z_{CR})$ ). The second one refers to the shear deformation and consists of a constant displacement between both faces of the CSC. First, the behaviour is governed by the flexural response (rotations) and, near failure, shear deformations develop (Muttoni *et al.*, 2017). Such kinematics is consistent with the behaviour experimentally observed by Clément (2012) (Figure 5.6) and to previous assumptions of the CSCT (Guidotti, 2010; Clément, 2012; Muttoni *et al.*, 2017);
- The location of the CSC at the level of the flexural reinforcement ( $r_0$ ) is considered to be variable, in agreement with the experimental observations on the radial deformations of Guandalini (2005), see Figure 5.5.

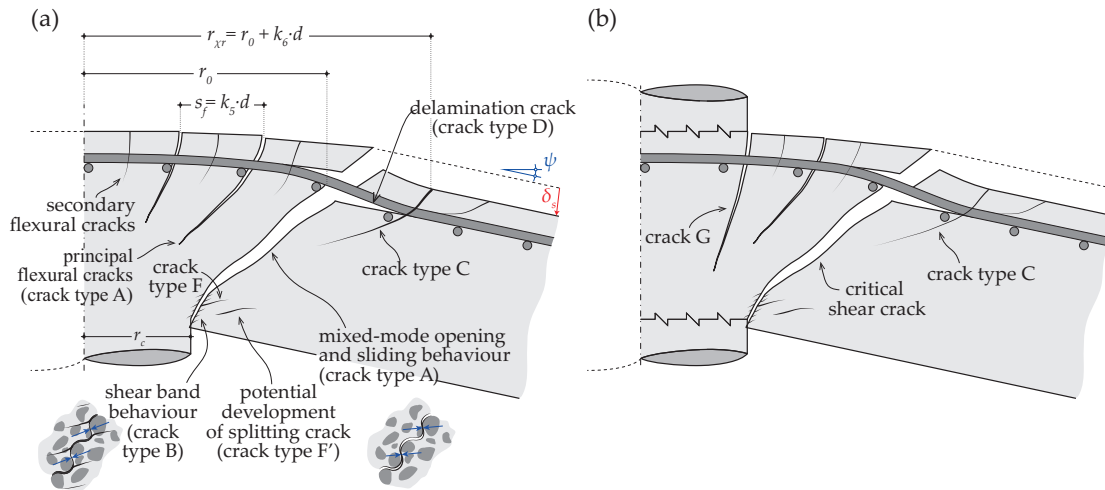


**Figure 5.8:** Punching shear of slab-column connection: (a) hypotheses of the mechanical model and description of potentially different phenomenological behaviors and cracking types; (b) case of column extending above the slab.

As described by Einpaul *et al.* (2017) and according to the experimental result observations, the failure may occur by a localization of the strains in the CSC (thus the CSC being coincident with the failure crack, Figure 5.8(a)) or by the development of a new splitting crack (also shown in Figure 5.8(a) and discussed by Einpaul *et al.* (2017)). For the latter case, the failure crack may propagate from the shear band (crack type F') or at its vicinity (crack type F'), but in both cases, its development is assumed to be governed by the kinematics, shape, and stresses transferred by the CSC. Thus, despite the fact that the failure crack may not be coincident with the critical one, the punching strength is still governed by the properties and response of the CSC (Einpaul *et al.*, 2017) (as the splitting crack develops when the strength is attained in the shear band region). For all cases, thus, it is assumed that the punching strength can be calculated on the basis of the capacity of the CSC to transfer forces, by integration of the internal stresses developing along it based on the adopted kinematics and considering suitable fundamental laws for the shear-transfer actions.

It shall be noted that in the case of columns extending above the slab, see Figure 5.8(b), the cracks develop mostly outside of the column region. However, the crack developing at the edge of the column (crack G in Figure 5.8(b)) concentrates a significant fraction of the rotation, which is related otherwise to the cracks type A developing inside the column region in the absence of an upper column. Consequently, the rotation concentrated at the CSC, governing the punching strength, is not significantly influenced by the presence of a column above the slab, as confirmed by examination and comparison of punching models to test results based on setups presenting both types of support conditions (Muttoni, 2008).

#### 5.4.2 Geometrical definition of regions of the slab with different behaviour

Following the experimental evidences discussed in Section 5.3 and based on the hypotheses of the mechanical model established in Section 5.4.1, different regions of the slab with distinct deformations have to be defined. As shown in Figure 5.9(a), the mechanical model here presented considers that the slab is divided into three different portions: the inner and outer portions of the slab and a wedge-shaped region between them. Similarly to Kinunnen and Nylander's approach (Kinunnen and Nylander, 1960), it is considered that the inner portion of the slab deforms in a spherical manner (due to the develop-

ment of principal and secondary flexural cracks) and that the outer portion of the slab behaves as a rigid body following a conical deformation (experimentally validated by several researchers (e.g. Kinnunen and Nylander, 1960; Hallgren, 1996; Guandalini, 2005)). The wedge-shaped region is considered as a deformable body (whose height is equal to the neutral axis depth) ensuring compatibility conditions associated with the rotations of the slab. This region accommodates the radial displacements due to bending, consistently to the approach of Kanellopoulos (1986) for beams. Above the neutral axis, the CSC separates the inner and outer portions of the slab while, below the neutral axis, the CSC separates the inner portion of the slab and the wedge element.

### 5.4.3 Shape of the Critical Shear Crack

As discussed in Muttoni *et al.* (2017) and Einpaul *et al.* (2017) as well as previously introduced based on the analysis of the cracking types (A or C compared to cracks type B in Section 5.3), the CSC presents two regions with different phenomenological behaviors. The slope of the CSC is also typically different in these regions, with an often steeper inclination of the shear band (near to the supported area). This assumption is consistent with other experimental observations (Guandalini, 2005) and theoretical approaches available in the scientific literature (Braestrup *et al.*, 1976; Yankelevsky and Leibowitz, 1999).

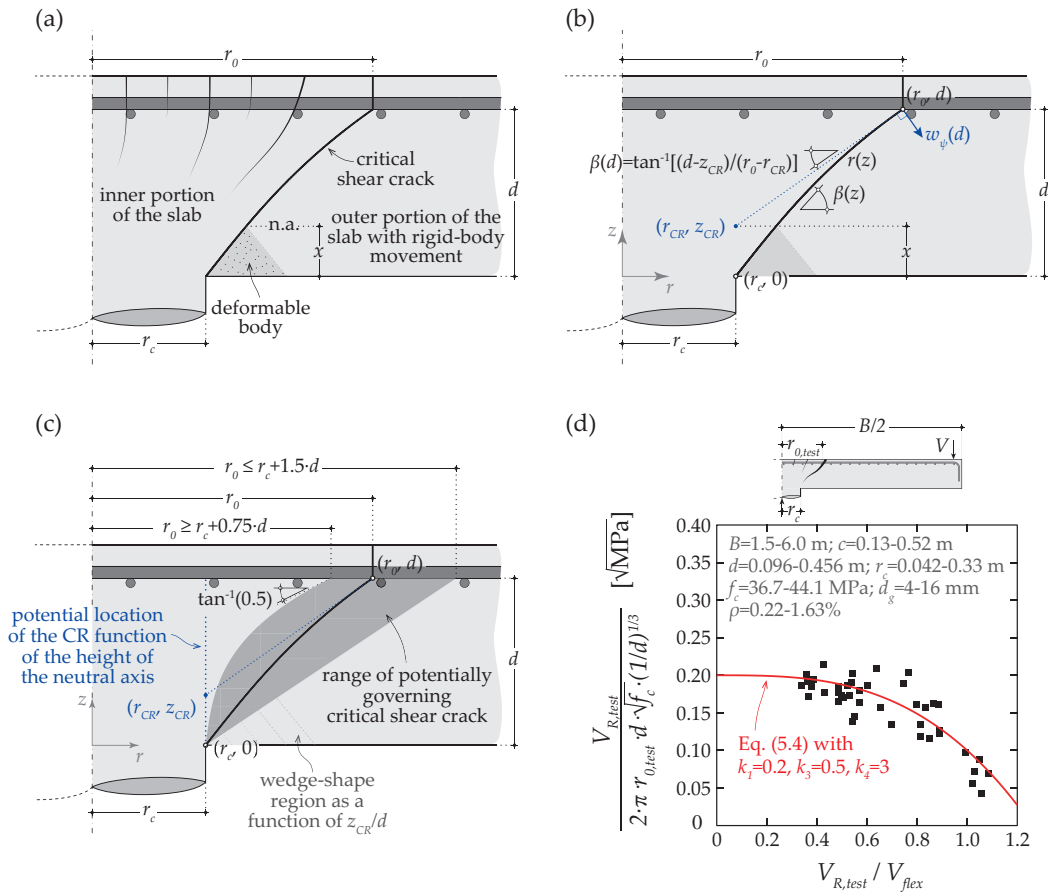


**Figure 5.9:** Definition of the geometry of the CSC: (a) definition of portions of the slab and description of adopted behaviours; (b) assumptions adopted to define geometry of CSC; (c) representation of range of  $r(z)$  as a function of  $r_0$  and corresponding potential locations of the CR for a given CSC; (d) values of  $\tau_i$  calculated based on experimental results of Guandalini (2005), Guidotti (2010), Tassinari (2011), Fernández Ruiz *et al.* (2010b), Clément (2012), Lips (2012), Einpaul (2016), and Drakatos (2016).

In order to account for the varying slope of the CSC, a third-degree polynomial is used to characterize the geometry of the investigated CSC ( $r(z)$ ) as:

$$r(z) = a_0 + a_1 \cdot z + a_3 \cdot z^3 \quad (5.1)$$

where  $a_0$ ,  $a_1$  and  $a_3$  are constants which can be calculated based on the following assumptions (Figure 5.9(b)):

1. The CSC develops between the edge of the column and the level of the flexural reinforcement, that is,  $r(0) = r_c$ ;
2. The radial distance between the axis of column and the CSC at the level of the flexural reinforcement is equal to  $r_0$ , that is  $r(d) = r_0$ ;
3. The tangent to the CSC at the level of the flexural reinforcement passes through the centre of rotation ( $r_{CR}$ ,  $z_{CR}$ ) and is equal to  $r'(d) = 1/\tan(\beta(d))$ , where  $\beta(d)$  refers to the slope of the CSC at  $z = d$ . This assumption means that the displacement due to the rotation at the level of the flexural reinforcement has a direction normal to the crack lips (consistently with the experimental observations of Einpaul *et al.* (2017)).

Based on these assumptions, Eq. (5.1) becomes:

$$r(z) = r_c + \frac{3}{2} \cdot \frac{(r_0 - r_c)}{d} \cdot z - \frac{z}{2 \cdot \tan(\beta(d))} + \frac{z^3}{2 \cdot d^2 \cdot \tan(\beta(d))} - \frac{(r_0 - r_c) \cdot z^3}{2 \cdot d^3} \quad (5.2)$$

where  $\tan(\beta(d)) = (d - z_{CR})/(r_0 - r_{CR}) \geq 0.5$ , the lower limit representing the minimal inclination of the CSC at  $z = d$ . It shall be noted that the punching shear resistance is not very sensitive to the function adopted for the CSC (reasonable variations of the shape of the CSC yielding similar results).

With respect to the location of the CSC at the level of the flexural reinforcement ( $r_0$ ), it has been discussed in Section 5.3 that the region where tangential cracks develops progresses with the increase of the load level. In addition, it has also been shown that the potential development of cracks type C merging with cracks type A for higher load levels might govern the shape of the CSC. To account for this effect, the location of the CSC at the level of the flexural reinforcement is considered to vary between  $r_c + 0.75 \cdot d$  and  $r_c + 1.5 \cdot d$  (in agreement with the experimental observations in the saw-cuts of tested specimens) according to the following expression:

$$\frac{r_0}{d} = \frac{V}{2 \cdot \pi \cdot d^2 \cdot \tau_l} \quad (5.3)$$

This expression accounts for the parameter  $\tau_l$  which refers to a reference value of the nominal shear stress causing flexural cracks to become inclined flexural-shear cracks and thus governing the shape of the CSC. The value of  $\tau_l$  is assumed to be correlated to the shear strength of uncracked concrete (normally depending upon the square root of the compressive strength of concrete (Vecchio and Collins, 1986)) and accounting also for the size of the member (Nielsen and Hoang, 2011). In addition, the value of  $\tau_l$  is also considered to depend on the degree of utilization of the flexural reinforcement, in the sense that larger deformations lead to wider flexural cracks reducing the effective height of the section enabling the transmission of shear stresses and thus leading to stress concentrations. As a first estimate, the value of  $\tau_l$  at failure is proposed to be calculated as:

$$\tau_l = \sqrt{f_c} \cdot k_1 \cdot \left(\frac{k_0}{d}\right)^{k_2} \cdot \left[1 - k_3 \cdot \left(\frac{V_R}{V_{flex}}\right)^{k_4}\right] \quad (5.4)$$

where  $f_c$  refers to the concrete compressive strength (in [MPa]);  $V_R$  is the punching strength;  $V_{flex}$  is the flexural strength;  $d$  is the effective depth (in m);  $k_0$  is a constant reference size taken equal to  $k_0 = 1.0$  m;  $k_1$  is constant value with unit ( $\text{MPa}^{1/2}$ ) and  $k_2$  to  $k_4$  are dimensionless constant values. With respect to the exponent governing size effect ( $k_2$ ), its value is taken as  $1/3$  in agreement to Nielsen and Hoang (2011) for phenomena governed by the tensile strength of concrete. A suitable value for the coefficient  $k_1$ ,  $k_3$  and  $k_4$  can be derived by comparison to test results where information on the saw cuts can be observed. On the basis of available test data (Guandalini, 2005; Guidotti, 2010; Fernández Ruiz *et al.*, 2010b; Tassinari, 2011; Clément, 2012; Lips, 2012; Einpaul, 2016; Drakatos, 2016), it is proposed to consider  $k_1 = 0.2$ ,  $k_3 = 0.5$ , and  $k_4 = 3$  (refer to Figure 5.9(d)). The calculation of  $\tau_l$  in this work is based on experimental values, but further work may be required in view of understanding the potential influence of other non-considered parameters. It can be noted that by calculating the value of  $r_0$  as a function of a nominal reference value  $\tau_l$ , one considers that, for larger values of the applied shear stresses, the inclined flexure-shear cracks can develop at larger distances from the edge of the column and the value of  $r_0$  becomes larger (Guandalini, 2005).

#### 5.4.4 Kinematics and displacement field along the critical shear crack

According to the CSCT, the kinematics of the CSC at failure consists of two components (see Figure 5.10(a)):

1. a flexural deformation defined by a rotation  $\psi_{csc}$  around the centre of rotation ( $r_{CR}, z_{CR}$ );
2. a shear deformation characterized by a sliding  $\delta_s$  with an angle  $\gamma_0$  with respect to the steepest region of the CSC.

Hereafter, the following notations will be used (see Figure 5.10(b)):

- $w$  refers to a crack opening, that is, displacement normal to the face of the CSC;
- $\Delta$  is a displacement parallel to the face of the CSC;
- $\delta$  represents a vector sum of the displacements normal and parallel to the face of the CSC;
- $\gamma$  defines the angle between the face of the CSC and the displacements vector sum;
- $u$  and  $v$  are respectively the radial and vertical components of  $\delta$ ;
- $\alpha$  is the angle between the vertical axis and the displacement vector  $\delta$ .

This notation is used in combination with the subscripts: ' $\psi$ ' to describe the displacements associated with the rotation; ' $s$ ' referring to the components due to the shear deformation and ' $T$ ' when referring to the vector sum of both contributions of rotation and shear deformation.

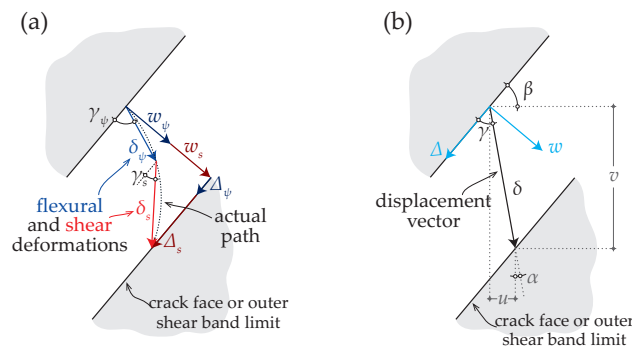


Figure 5.10: Definition of displacements: (a) flexural and shear deformations; (b) notation.

#### 5.4.4.1 Flexural deformations

The displacement field along the CSC due to flexural deformations is a function of the location of the center of rotation ( $r_{CR}$ ,  $z_{CR}$ ) and of the rotation developing in this crack ( $\psi_{csc}$ ). Considering that the rotation of the slab  $\psi$  is equally divided in the primary tangential flexural cracks without any contribution of the secondary flexural cracks, the rotation concentrated in the CSC  $\psi_{csc}$  can be calculated as follows as (similarly to Guidotti (2010) and in accordance with the experimental results of Clément (2012) and Einpaul *et al.* (2017)):

$$\psi_{csc} = \frac{\psi}{n_{cr}} \quad (5.5)$$

where  $n_{cr}$  represents the number of primary tangential flexural cracks, which can be calculated as (similarly to Guidotti (2010)):

$$n_{cr} = 0.5 + \frac{r_{\chi r}}{s_f} \quad (5.6)$$

where  $s_f$  refers to the distance between the primary flexural cracks and  $r_{\chi r}$  is the extent of the region where these cracks develop (where the term 0.5 refers to the crack forming at the axis of symmetry), see Figure 5.8(a). Scanty information has been reported regarding this spacing ( $s_f$ ) in punching tests. However, this parameter has been experimentally investigated for beams failing in shear (e.g. Khaja and Sherwood, 2013; Cavagnis *et al.*, 2015), where it has been shown that this value is mainly proportional to the effective depth  $s_f \propto k_5 \cdot d$ , with  $k_5$  varying from 0.50 to 0.60 (e.g. Khaja and Sherwood, 2013; Cavagnis *et al.*, 2015). Consistently with these observations, a value  $k_5 = 0.50$  will be adopted in this work. With respect to the distance  $r_{\chi r}$ , it will be estimated as  $r_c + k_6 \cdot d$ , where  $k_6 = 0.25$  will be considered. This is physically consistent with the discussion of cracking observed in saw-cuts presented in Section 5.3.1 (development of crack type A or C further away from the column that only merge at higher shear stresses) and with the experimental measurements of Guandalini (2005) presented in Figure 5.5.

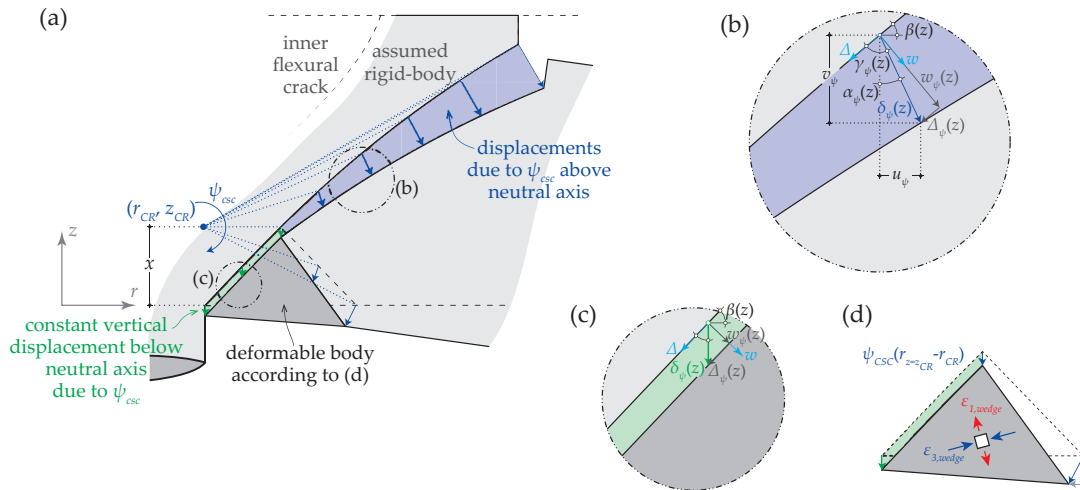


**Figure 5.11:** (a) Adopted kinematics and corresponding displacements along the critical shear crack due to rotation  $\psi_{csc}$ ; details of resulting displacement field in the (b) lower and (c) upper portion of CSC; (d) wedge element and corresponding displacements associated with  $\psi_{csc}$ .

With respect to the center of rotation associated with  $\psi_{csc}$  (Figure 5.9(b)), it is assumed that it is radially located at the edge of the column (in accordance to the experimental results of Clément (2012) before shear deformations take place, Figure 5.8) and at the height of the neutral axis ( $z_{CR} = x$ ) associated with the tangential bending moment at  $r_0$  (curvature calculated as  $\chi = \psi/r_0$  corresponding to the assumption of a spherical deformed shape inside  $r_0$  consistently with the works of Kinnunen and Nylander (1960) and others (Hallgren, 1996; Broms, 1990, 2016)). In this paper, the calculation of the height of

the neutral axis is performed in a similar manner as Hallgren (1996), that is, adopting an elastic-plastic behaviour of concrete and reinforcement. The uniaxial behaviour of concrete is considered to be characterized by the ascending branch given by the modulus of elasticity ( $E_c$ ; calculated based on the value of the uniaxial concrete compressive strength as Muttoni (2008)) and by a plastic plateau at a stress of  $\eta_{f_c} \cdot f_c$  (where the factor  $\eta_{f_c}$  accounts for the brittleness of high-strength concrete and is calculated according to Muttoni (1990) as  $\eta_{f_c} = (30/f_c)^{1/3} \leq 1$  with  $f_c$  in [MPa]). The elastic-plastic behaviour of the reinforcement is also described by its modulus of elasticity ( $E_s$ ) and yield strength ( $f_y$ ) (see Section 5.10.1 for details on the calculation of  $x$ ).

Figure 5.9(c) shows the shape adopted for the CSC and the associated tangent inclination for a given  $r_0$  and height of the neutral axis. Also the range of potentially governing critical shear cracks is shown in Figure 5.9(c).

Finally, the displacement field along the CSC due to the rotation  $\psi_{csc}$  can be calculated assuming that (Figure 5.11):

- Above the neutral axis, all displacements localize in the CSC;
- Below the neutral axis, only the vertical displacements (equal to the one at  $z = z_{CR}$ ) localize at the CSC, while the wedge-shape region accommodates the radial displacements (in accordance to the approach of Kanellopoulos (1986) for beams in bending).

The radial ( $u_\psi$ ) and vertical ( $v_\psi$ ) components of the displacements resulting from the rotation  $\psi_{csc}$  around the CR localizing in the CSC are given by (see Figures 5.11(b) and (c)):

$$u_\psi(z) = \begin{cases} \psi_{csc} \cdot (z - z_{CR}) & \text{if } z \geq z_{CR} \\ 0 & \text{if } z < z_{CR} \end{cases} \quad (5.7)$$

$$v_\psi(z) = \begin{cases} \psi_{csc} \cdot (r_{CR} - r) & \text{if } z \geq z_{CR} \\ \psi_{csc} \cdot (r_{CR} - r_{z=z_{CR}}) & \text{if } z < z_{CR} \end{cases} \quad (5.8)$$

The vector of displacements due to the rotation localizing in the CSC can be computed as:

$$\delta_\psi(z) = \sqrt{u_\psi(z)^2 + v_\psi(z)^2} \quad (5.9)$$

and the angle between the vertical axis and this vector is given by:

$$\alpha_\psi(z) = \tan^{-1} \left( -\frac{u_\psi}{v_\psi} \right) \quad (5.10)$$

The angle between the CSC and the vector of displacement due to the rotation is finally computed as:

$$\gamma_\psi(z) = \frac{\pi}{2} - \beta(z) + \alpha_\psi(z) \quad (5.11)$$

and the corresponding displacements parallel  $\Delta_\psi(z)$  and normal  $w_\psi(z)$  to the CSC are calculated as follows (Figure 5.11):

$$w_\psi(z) = \delta_\psi(z) \cdot \sin(\gamma_\psi(z)) \quad (5.12)$$

$$\Delta_\psi(z) = \delta_\psi(z) \cdot \cos(\gamma_\psi(z)) \quad (5.13)$$

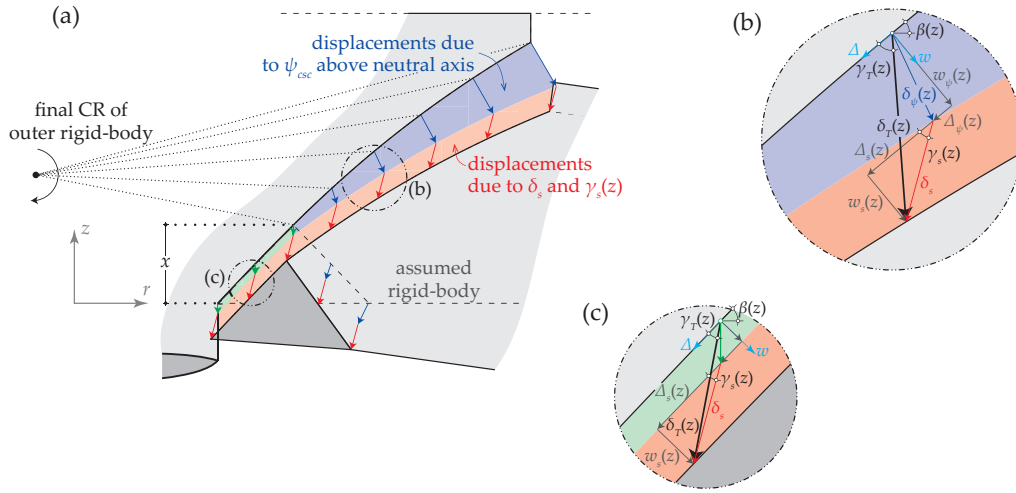


**Figure 5.12:** (a) Adopted kinematics and corresponding displacements along the critical shear crack due to combined effects of rotation  $\psi_{csc}$  and shear deformation  $\delta_s$ ; details of resulting displacement field in the (b) lower and (c) upper portion of CSC.

#### 5.4.4.2 Shear deformations

Considering that the shear deformations fully localize at the CSC, the resulting displacement field along it is characterized only by the total constant displacement  $\delta_s$  (corresponding to a translation) and angle of sliding  $\gamma_s(z)$  (variable due to the potentially variable tangent inclination of the CSC). With respect to the angle of sliding, it can be considered that the lowest angle measured between the CSC and the direction of the vector of shear deformations is related to the angle of dilatancy observed in push-off tests of concrete members (following the approach of Guidotti (2010) based on the results of Walraven (1980)). As the point with steepest inclination along the failure surface is located at  $z = 0$  (edge of the column), the lowest angle of dilatancy occurs at this location and is equal to  $\gamma_s(0) = \gamma_0$ . Based on the analysis of experimental results and theoretical considerations (Mattock, 1974; Walraven, 1980; Walraven, 1981; Mansur *et al.*, 2008), Clément (2012) concluded that this angle should vary from  $25^\circ$  to  $30^\circ$ . A value of  $\gamma_0 = 27^\circ$  is adopted in this work (consistently with Guidotti (2010), but limited to the value  $90^\circ - \beta(0)$  corresponding to a vertical translation of the slab in the phase of shear deformations). Thereby, the angle between the CSC and the vector of shear deformations  $\gamma_s(z)$  can be calculated as a function  $\beta(z)$  as follows:

$$\gamma_s(z) = \gamma_0 + (\beta(0) - \beta(z)) \quad (5.14)$$

Considering a shear deformation (characterized by a constant displacement  $\delta_s$  with and angle  $\gamma_s(z)$ ), the corresponding displacements parallel  $\Delta_s(z)$  and normal  $w_s(z)$  to the CSC are computed as follows (Figure 5.12):

$$\Delta_s(z) = \delta_s \cdot \cos(\gamma_s(z)) \quad (5.15)$$

$$w_s(z) = \delta_s \cdot \sin(\gamma_s(z)) \quad (5.16)$$

Finally, the displacements parallel  $\Delta_T(z)$  and normal  $w_T(z)$  to the CSC associated with the combined effect of rotation and shear deformation are respectively given by:

$$\Delta_T(z) = \Delta_\psi(z) + \Delta_s(z) \quad (5.17)$$

$$w_T(z) = w_\psi(z) + w_s(z) \quad (5.18)$$

and its vector sum  $\delta_T(z)$  and corresponding direction  $\gamma_T(z)$  with respect to the CSC plan can be obtained as (Figure 5.12):

$$\delta_T(z) = \sqrt{w_T(z)^2 + \Delta_T(z)^2} \quad (5.19)$$

$$\gamma_T(z) = \tan^{-1} \left( \frac{w_T(z)}{\Delta_T(z)} \right) \quad (5.20)$$

It should be noted that, following the development of the shear deformation, the CR moves away from the column edge (compare location of CR in Figures 5.11 and 5.12). This is in agreement with the results of Clément (2012) shown in Figure 5.6.

#### 5.4.5 Internal stresses along the critical shear crack

As discussed by Muttoni *et al.* (2017), different phenomenological responses occur along the CSC. The zone in the tension side presents a mixed-mode opening-sliding response due to the development of a discrete crack (localizing strains, representing a localized cracking behaviour) caused by flexural deformations. The zone in the compression side may in its turn behave as a shear band, where deformations smear in a narrow region (representing a smeared cracking behaviour) eventually leading to coalesce in one single crack (see Figure 5.8). These two different phenomenological responses will be considered in this work by calculating the internal stresses along the CSC in accordance to the expected crack kinematics.

##### 5.4.5.1 Transition between single crack behaviour and shear band behaviour

The transition between these two distinct regimes (localized and smeared cracking) is a complex phenomenon and depends upon the opening and direction of the crack displacement vector, the loading path, and the concrete properties (Jacobsen *et al.*, 2012). With this respect, some interesting results have been reported by Jacobsen *et al.* (2012), who performed an experimental program with double-notched concrete specimens where an initial crack opening was applied (imposed displacement normal to the notched surface) followed by a shear displacement at a given angle (mixed-mode opening and sliding). Based on the experimental results, Jacobsen *et al.* (2012) concluded that a clear localized cracking behaviour (aggregate interlock along the notched surface) could only be obtained if: (a) a discrete crack caused by an initial opening displacement occurs (initial crack opening corresponding to a decrease on the normal stress of 30-50% of the tensile strength) and (b) a shear displacement with an opening-to-sliding angle sufficiently large is applied (limit value of  $40^\circ$  suggested by the author).

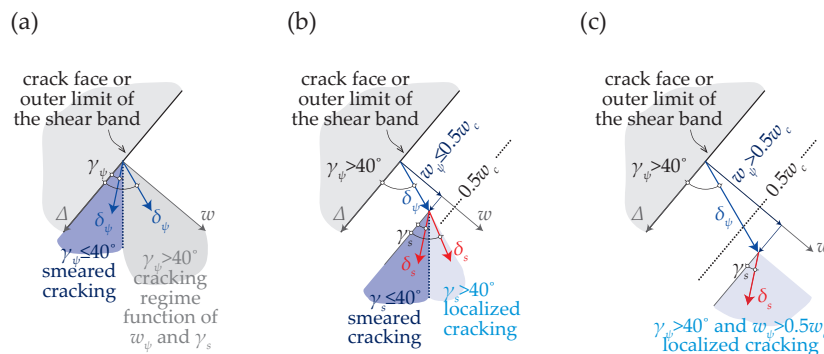


**Figure 5.13:** Adopted transition between localized and smeared cracking regimes function of the displacement field: (a) transition criterion based on the angle of the displacement vector associated with flexural deformations; (b) transition criterion based on the crack opening-to-crack sliding angle associated with shear deformations; (c) transition criterion based on the crack opening due to the flexural behavior.

The transition between these two distinct regimes (localized and smeared cracking) is a complex phenomenon and depends upon the opening and direction of the crack displacement vector, the loading path and the concrete properties. With this respect, some interesting results have been reported by , who performed an experimental programme with double-notched concrete specimens where an initial crack opening was applied (imposed displacement normal to the notched surface) followed by a shear displacement at a given angle (mixed mode opening and sliding). Based on the experimental results, concluded that a clear localized cracking behaviour (aggregate interlock along the notched surface) could only be obtained if: (i) a discrete crack caused by an initial opening displacement occurs (initial crack opening corresponding to a decrease on the normal stress of 30% to 50% of the tensile strength) and (ii) a shear displacement with an opening-to-sliding angle large enough is applied (value of  $40^\circ$  suggested by the author).

In this work, based on the experimental observations of Jacobsen *et al.* (2012), the transition between the localized and the smeared cracking regions will be defined on the basis of the initial crack opening ( $w_\psi$ ) and on the crack opening-to-crack sliding angles associated with flexural ( $\gamma_\psi$ ) and shear ( $\gamma_s$ ) deformations. The transition is thus defined according to the following criteria:

- The region of the CSC with  $\gamma_\psi \leq 40^\circ$  will be assumed to have a smeared cracking response (Figure 5.13(a));
- The response (localized or smeared cracking) of the region of the CSC with  $\gamma_\psi > 40^\circ$  is assumed to depend on the initial crack opening ( $w_\psi$ ) and on the crack opening-to-crack sliding angle associated with the shear displacement vector ( $\gamma_s$ ). In this case, the region of the CSC with  $w_\psi \leq 0.5 \cdot w_c$  and  $\gamma_s \leq 40^\circ$  is assumed to behave with a smeared cracking response as shown in Figure 5.13(b) (where  $w_c$  is the crack opening corresponding to a zero tensile stress). On the contrary, localized cracking behaviour is assumed to be governing in other cases ( $\gamma_\psi > 40^\circ$  and  $\gamma_s > 40^\circ$ , independently of  $w_\psi$  as shown in Figure 5.13(c); or  $\gamma_\psi > 40^\circ$  and  $w_\psi > 0.5 \cdot w_c$  independently of  $\gamma_s$ , corresponding to a full localization of the strains).

Mathematically, the vertical coordinate where the transition between both regimes occurs ( $z_{tr}$ ) can be expressed as follows:

$$z_{tr} = \min \left( z_{\gamma_s=40^\circ}, z_{w_\psi=0.5 \cdot w_c} \right) \geq z_{\gamma_\psi=40^\circ} \quad (5.21)$$

where  $z_{\gamma_s=40^\circ}$  refers to the vertical coordinate where  $\gamma_s = 40^\circ$ ,  $z_{w_\psi=0.5 \cdot w_c}$  to the vertical coordinate where  $w_\psi = 0.5 \cdot w_c$  and  $z_{\gamma_\psi=40^\circ}$  is the vertical coordinate where  $\gamma_\psi = 40^\circ$ . It can be noted that in the previous condition it is assumed (consistently with the governing kinematics) that  $\gamma_s \leq \gamma_\psi$ .

#### 5.4.5.2 Internal stresses developing in the segment with localized cracking

In the region of the CSC where deformations localize in a single crack (opening-sliding mixed-mode behaviour), it is considered that the shear-transfer capacity is governed by the residual tensile strength and the aggregate interlock stresses, leading to the following normal ( $\sigma_{agg}$ ) and shear ( $\tau_{agg}$ ) interlocking stresses as a function of the crack opening ( $w_T$ ) and sliding ( $\Delta_T$ ) (according to Cavagnis *et al.* (2017)):

$$\sigma_{agg}(w_T, \Delta_T) = \sigma_{fct}(w_T) + \sigma_{agg,0}(w_T, \Delta_T, f_c, d_g) \quad (5.22)$$

$$\tau_{agg}(w_T, \Delta_T) = \tau_{agg,0}(w_T, \Delta_T, f_c, d_g) \quad (5.23)$$

where  $\sigma_{fct}$  refers to the residual tensile strength,  $\tau_{agg,0}$  and  $\sigma_{agg,0}$  are the shear and normal stresses due to aggregate interlocking engagement. According to Hordijk (1992), the residual tensile strength can

be calculated as:

$$\sigma_{fct} = f_{ct} \cdot \left[ 1 + \left( t_1 \cdot \frac{w_T}{w_c} \right)^3 \right] \cdot e^{(-t_2 \cdot \frac{w_T}{w_c})} - \frac{w_T}{w_c} \cdot (1 + t_1^3) \cdot e^{(-t_2)} \geq 0 \quad (5.24)$$

where  $f_{ct}$  refers to the tensile strength of concrete,  $w_c$  is the crack opening corresponding to a zero tensile stress and  $t_1 = 3$  and  $t_2 = 6.93$  are constants (Hordijk, 1992). The tensile strength of concrete is computed according to the following relationships ( $f_c$  in [MPa]) (Cavagnis *et al.*, 2017):

$$f_{ct} = \begin{cases} 0.3 \cdot f_c^{2/3} & \text{if } f_c \leq f_{c0,t} \\ 0.3 \cdot f_{c0,t}^{1/3} \cdot f_c^{1/3} & \text{if } f_c \geq f_{c0,t} \end{cases} \quad (5.25)$$

with  $f_{c0,t} = 50$  MPa and the crack opening  $w_c$  is computed as follows (Hordijk, 1992):

$$w_c = 5.14 \cdot \frac{G_F}{f_{ct}} \quad (5.26)$$

where the total fracture energy  $G_F$  is calculated in accordance to the (*fib* Model Code 2010, 2013):

$$G_F = 73 \cdot f_c^{0.18} \quad (f_c \text{ in [MPa], } G_F \text{ in [N/m]}) \quad (5.27)$$

With respect to the aggregate interlock engagement stresses, the simplified formulation of Cavagnis *et al.* (2017) will be used in this work ( $f_c$  in [MPa]):

$$\sigma_{agg,0} = -c_1 \cdot \sqrt{f_c} \cdot \frac{\bar{\Delta}^{-7/3}}{(c_3 \cdot \bar{w})^{3+c_3 \cdot \bar{\Delta}}} \quad (5.28)$$

$$\tau_{agg,0} = c_2 \cdot \sqrt{f_c} \cdot \frac{\bar{\Delta}^{-4/3}}{(c_3 \cdot \bar{w})^{1.8+c_3 \cdot \bar{\Delta}}} \quad (5.29)$$

where  $c_1 = 400$  (unit of  $\sqrt{\text{MPa}}$ ),  $c_2 = 35$  (unit of  $\sqrt{\text{MPa}}$ ) and  $c_3 = 40$  are constant values;  $\bar{\Delta} = \Delta_T/d_{dg}$  and  $\bar{w} = w_T/d_{dg}$  are the normalized displacements parallel and normal to the crack surface;  $d_{dg}$  is the reference value of the crack roughness and is calculated according to Cavagnis *et al.* (2017) as:

$$d_{dg} = 16 + d_g \cdot \min \left( \left( \frac{60}{f_c} \right)^2, 1 \right) \leq 40 \text{mm} \quad (5.30)$$

with  $d_{dg}$  and  $d_g$  in [mm] and  $f_c$  in [MPa]. According to Cavagnis *et al.* (2017) the reduction of  $d_g$  for high concrete grades is related to a reduction of the roughness of the crack associated with the development of cracks through the aggregates described by Collins and Kuchma (1999). Cavagnis *et al.* (2017) proposed also the consideration of an upper limit of  $d_{dg}$  related to the limited increased of transferred stresses across a crack for higher aggregate sizes as experimentally observed by Sherwood *et al.* (2007) for shear in beams (limit of 40 mm in Equation 5.30). It should be mentioned that Eqs. (5.28) and (5.29) have been proposed by Cavagnis *et al.* (2017) based on the model of aggregate interlock of Walraven (1981) but adopting the kinematics at failure of Guidotti (2010) (defined by an initial crack opening and a sliding with a given angle with respect to the crack; see Guidotti (2010) for details). It is also important to note that other approaches could also be used to calculate the aggregate interlock engagement stresses (e.g. Walraven, 1980; Guidotti, 2010) but the approach of Cavagnis *et al.* (2017) is kept because of its simplicity and validation against the recent experimental results of Jacobsen *et al.* (2012).

### 5.4.5.3 Internal stresses developing in the segment with smeared cracking

A shear band behaviour is considered for calculating the internal stresses in the region of the CSC where deformations are considered to develop in a band of finite thickness. The concept of shear band introduced by Jensen (1975) is used in this work to calculate the strains developing in a band where a given displacement field is assumed to occur. Figure 14a shows the typical cracking pattern observed locally near the column edge (refer also to Figure 5.8). A shear band with a width  $\lambda$  together with a displacement field characterized by a total displacement  $\delta_T(z)$  and a direction  $\gamma_T(z)$  with respect to its axis (calculated in Section 5.4.4) is shown in Figure 5.14(b), where the principal strains result (Figure 5.14(c) and (d); Jensen, 1975):

$$\varepsilon_{1,sb}(z) = \frac{\delta_T(z)}{2 \cdot \lambda} \cdot (\sin(\gamma_T(z)) + 1) \quad (5.31)$$

$$\varepsilon_{3,sb}(z) = \frac{\delta_T(z)}{2 \cdot \lambda} \cdot (\sin(\gamma_T(z)) - 1) \quad (5.32)$$

where  $\varepsilon_{1,sb}$  and  $\varepsilon_{3,sb}$  refer to the principal tensile and compressive strains respectively in the shear band. The principal direction of compression with respect to the shear band axis is given by (refer to Figure 5.14(c) and (d)):

$$\theta_{sb}(z) = \frac{\pi}{4} - \frac{\gamma_T(z)}{2} \quad (5.33)$$

The width of the band  $\lambda$  will be considered to be related to the size of the aggregate ( $\lambda = d_{dg}$ ). This simplification is consistent with other approaches, based on the concept of localization on a crack band (Bažant and Xiang, 1997) and supported on the following considerations: (i) the width of the band is considered to have a finite size even in the case of a zero aggregate size ( $\lambda = 16$  mm) and (ii) the influence of the aggregate size on the width of the band decreases in the case of high-strength concrete due to the development of smeared cracking through the aggregates (Collins and Kuchma, 1999; Angelakos *et al.*, 2001; Bentz *et al.*, 2006; Muttoni and Fernández Ruiz, 2008) (thus reducing the influence of this parameter on the width of the shear band).

In order to determine the associated state of stresses (Figure 5.14(g)), a strain-stress relationship adapted from the work of Guidotti *et al.* (2011) will be used in this work. The formulae presented by Guidotti *et al.* (2011) allows determining the axial stress ( $\sigma_3$ ) and the radial strains ( $\varepsilon_1$ ) of a concrete cylinder as a function of the axial strain ( $\varepsilon_3$ ) and confining pressure.

The original formulation of Guidotti *et al.* (2011) is nevertheless valid for concrete cylinders, whereas the state of strains in the investigated axisymmetric element (Figure 5.14(e)) is more complex (in most cases two compressive and one tensile strains, Figure 5.14(f)). In fact, in addition to the principal tensile and compressive strains (developing in a radial plane,  $\varepsilon_{1,sb}$  and  $\varepsilon_{3,sb}$ ), also a state of tangential strains in the shear band ( $\varepsilon_{2,sb}$  in Figure 5.14(f)) results from the flexural deformations in the inner portion of the slab inside (inside  $r_0$ ) and from the radial displacement field occurring in the shear band. The former component induces a constant state of tangential strains in the band, whereas the latter leads to a discontinuity of tangential strains along its thickness (Jensen, 1975; Figure 5.14(c)).

When analysing the behaviour of a concrete panel representing an element of shear band (Figures 5.14(e) to (g)), two distinct effects have thus to be distinguished: (i) the favourable effect of a potential tangential compression ( $\varepsilon_{2,sb}$ ) on the peak stress and deformation capacity of the  $\varepsilon_3 - \sigma_3$  relationship and (ii) the potential unfavourable influence of imposed tensile strains ( $\varepsilon_{1,sb}$ ) on the  $\varepsilon_3 - \sigma_3$  relationship (strain softening). In the following, these phenomena are briefly presented as well as their consideration in the constitutive law adopted for concrete in this region.

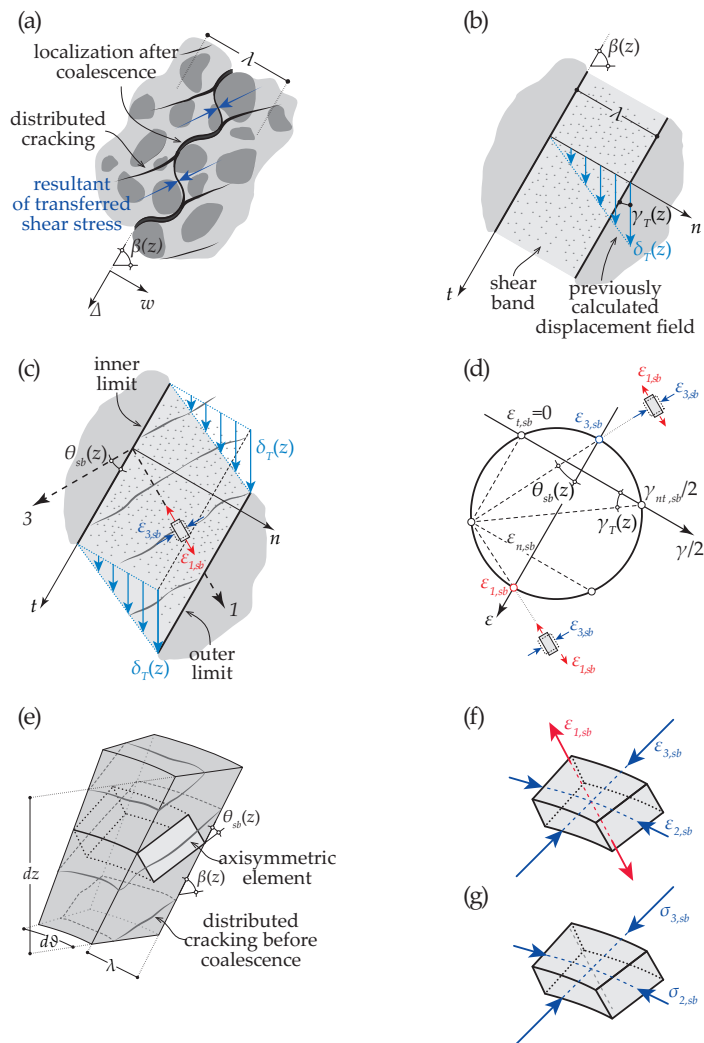


**Figure 5.14:** Model assuming the formation of a shear band: (a) cracking; (b) geometrical definition and relative radial displacement field; (c) strains field; (d) Mohr's circle; (e) axisymmetric element; (f) strain and (g) stress state of an element of the shear band.

### Influence of compressive tangential strain

As schematically represented in Figure 5.15(a), the behaviour of a panel in biaxial compression is actually in-between the behaviour of an unconfined and confined concrete element (Kupfer *et al.*, 1969; Kupfer and Gerstle, 1973). The behaviour of concrete panels under biaxial compression has been investigated by numerous researchers (e.g. Kupfer *et al.*, 1969; Kupfer and Gerstle, 1973). The original experimental research presented by Kupfer *et al.* (1969) showed that concrete compressive strength and deformation capacity increase in the case of biaxial compression. On that basis, Kupfer and Gerstle (1973) proposed an envelope in the stress-space for concrete panels under biaxial loading conditions. Furthermore, Kupfer *et al.* (1969) have also shown that the increased peak stress in the case of biaxial compression may increase up to approximately 20% of the uniaxial compression strength.

In this work, the favourable effect of biaxial compression due to tangential strains developing in the region with smeared cracking will be considered in a simplified manner. This will be performed by considering that the strain-stress relationship of the region with smeared cracking corresponds to the one of a cylinder with a confining pressure leading to a peak stress of  $\kappa_b \cdot f_c$ . As previously discussed,

the value of  $\kappa_b$ , representing the enhancement of the peak strength and deformation capacity of concrete (see differences between dotted black and blue curves in Figure 5.15(a) and (c)), may have values between 1 and approximately 1.2 depending on the level of transverse compression (Kupfer *et al.*, 1969). In this work, a constant value of  $\kappa_b = 1.1$  is considered, representing the case where moderate values of the tangential compression develop in the region with smeared cracking (in agreement with the results of the mechanical model).

### Influence of imposed tensile transverse radial strain $\varepsilon_2$

When investigating the shear strength of reinforced concrete panels, Vecchio and Collins (1986) identified a decrease of the concrete compressive strength (compression softening) in presence of transverse tensile strains. Consistently to these observations, Muttoni (1990) suggested that, for the case of unreinforced concrete members, the influence of imposed transverse tensile strains can be investigated on the basis of the  $\varepsilon_1 - \sigma_3$  relationship (as for instance done by Guidotti *et al.* (2011)). This approach is represented in Figure 5.15(b), where  $f_{c,eff}$  corresponds to the value of  $\sigma_3$  associated with the imposed transverse tensile strain  $\varepsilon_1^*$ . In addition, a softer strain-stress relationship (green line in Figure 5.15(b)) accounting for the presence of large tensile strains can thus be derived considering that its peak occurs at the point with coordinates  $(\varepsilon_1^*, f_{c,eff})$ .

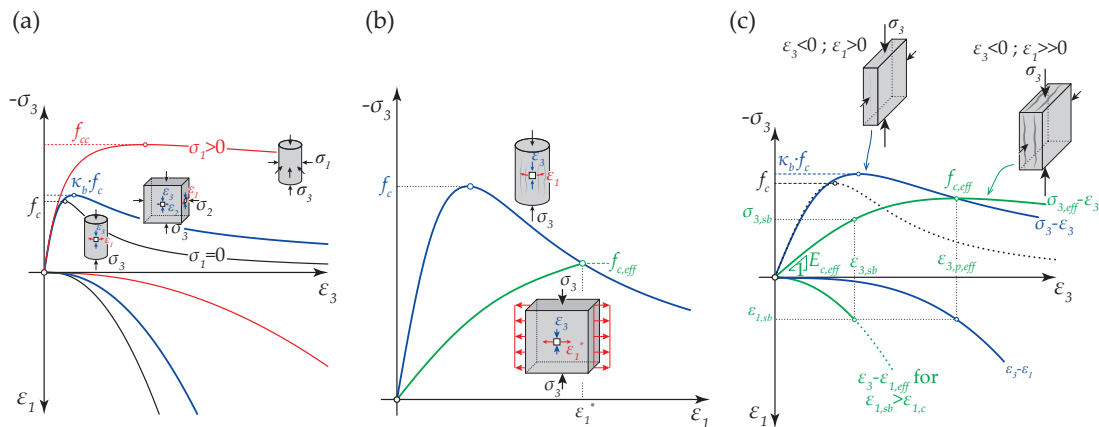


**Figure 5.15:** Adopted behaviour of concrete in the shear band: (a) influence of confining pressure ( $\sigma_1$ ) on the compression resistance ( $\sigma_3$ ) and deformation capacity ( $\varepsilon_1$  and  $\varepsilon_3$ ) of different concrete elements (based on Guidotti *et al.* (2011) and Kupfer *et al.* (1969)); (b) reduction of concrete compressive strength due to imposed transverse strain (adapted from Muttoni (1990)); (c) procedure to calculate the stresses developing in the shear band.

### Calculation of normal and shear stresses in the region of smeared cracking

The stresses acting in the axisymmetric element of shear band can be calculated accounting for the potential effects of biaxial compression and imposed transverse tensile strains based on the principles described above. The procedure followed to calculate the stress  $\sigma_{3,sub}$  in the shear band is shown in Figure 5.15(c), where both  $\varepsilon_3 - \sigma_3$  and  $\varepsilon_3 - \varepsilon_1$  relationships are plotted for concretes under different conditions. The dotted black curve represents the behaviour of an unconfined concrete cylinder. The blue curves  $\varepsilon_3 - \sigma_3$  and  $\varepsilon_3 - \varepsilon_1$  represent the behaviour of a concrete cylinder with a confining pressure leading to a peak strength equal to  $\kappa_b \cdot f_c$ . The difference between the black dotted and blue curves represents the considered beneficial effect of biaxial compression on the concrete behaviour. However, the behaviour of the concrete in the shear band is still not represented by the blue curves in Figure 5.15(c), as they do not consider the imposed tensile strain  $\varepsilon_{1,sub}$ . To account for it, a softer  $\varepsilon_3 - \sigma_{3,eff}$  relationship (green curve in Figure 5.15(c)) is derived considering that its peak occurs at the stress  $f_{c,eff}$

corresponding to the imposed transverse tensile strain  $\varepsilon_{1, sb}$  (by introducing  $\varepsilon_{1, sb}$  in the blue curve  $\varepsilon_3 - \varepsilon_1$  and calculating the corresponding  $\sigma_3$ , consistently with the procedure proposed by Muttoni (1990)) and assuming  $\varepsilon_3 - \sigma_{3, eff}$  (green curve) to be an homothetic curve of  $\varepsilon_3 - \sigma_3$  (blue curve). Finally, the stress  $\sigma_{3, sb}$  in the shear band can be computed by introducing  $\varepsilon_{3, sb}$  in the green curve  $\varepsilon_3 - \sigma_{3, eff}$ .

By considering the  $\varepsilon_3 - \sigma_3$  relationship proposed by Guidotti *et al.* (2011) and a simplified  $\varepsilon_1 - \varepsilon_3$  relationship, the previously described steps can be analytically solved, leading to the following expression to calculate the principal compressive stress in the smeared cracking region (see Appendix for detailed analytical derivation):

$$\sigma_{3, sb} = (\bar{\alpha} - 1) \cdot \frac{\varepsilon_{3, sb} \cdot E_{c, eff}}{\bar{\alpha} - 1 + \left( \frac{\varepsilon_{3, sb}}{\varepsilon_{3, p, eff}} \right)^{\bar{\alpha}}} \quad (5.34)$$

where  $\bar{\alpha}$  is a factor of the  $\varepsilon_3 - \sigma_3$  relationship accounting for the brittleness of concrete (Eq. (5.66) (Guidotti *et al.*, 2011);  $E_{c, eff}$  is the effective modulus of elasticity of the concrete, whose value is a function of the imposed transverse tensile strain in the shear band  $\varepsilon_{1, sb}$  (Equation (5.70) derived in the Appendix);  $\varepsilon_{3, p, eff}$  is the strain at the peak of the  $\varepsilon_3 - \sigma_{3, eff}$  relationship, whose value is also a function of the imposed transverse tensile strain in the shear band  $\varepsilon_{1, sb}$  (Equation (5.69)).

Figure 5.16 shows the  $\varepsilon_3 - \sigma_{3, sb}$  according to Eq. (5.34) obtained for different values of the imposed transverse tensile strain ( $\varepsilon_{1, sb}$ ) adopting two different concrete compressive strengths. This figures clearly shows the effects of brittleness and strain softening (due to imposed transverse tensile strains).

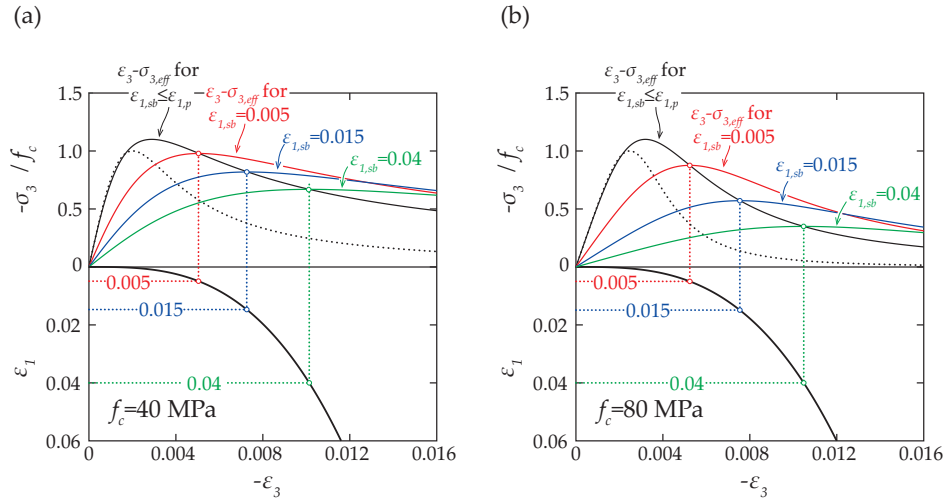


**Figure 5.16:** Calculated  $\varepsilon_3 - \sigma_{3, sb}$  relationship as a function of the imposed transverse tensile strain in the shear band  $\varepsilon_{1, sb}$  for two concrete compressive strengths: (a)  $f_c = 40$  MPa and (b)  $f_c = 80$  MPa.

Still with respect to the calculation of the stress state in the shear band, it will additionally be assumed that the principal directions of stresses are parallel to the principal directions of deformations  $\theta_{sb}(z)$  (Fernández Ruiz and Muttoni, 2007) and that the stress in the principal tensile direction is equal to  $\sigma_{1, sb} = 0$ . In these conditions, the normal and shear stresses parallel to the axis of the shear band can be respectively calculated as:

$$\sigma_{sb}(z) = \sigma_{3, sb}(z) \cdot \sin^2(\theta_{sb}(z)) \quad (5.35)$$

$$\tau_{sb}(z) = -\sigma_{3, sb}(z) \cdot \sin(\theta_{sb}(z)) \cdot \cos(\theta_{sb}(z)) \quad (5.36)$$

#### 5.4.5.4 Contribution of dowel action

As shown in Figure 5.17(a), dowelling of flexural reinforcement bars may potentially develop at failure contributing to the shear strength (e.g. Rasmussen, 1963; Krefeld and Thurston, 1966; Millard and Johnson, 1984; Fernández Ruiz *et al.*, 2010a, 2013; Campana *et al.*, 2013; Fernández Ruiz *et al.*, 2015; Einpaul, 2016). In this work, a similar approach to that followed by Einpaul (2016) is considered, consisting on a combination of the approaches of Millard and Johnson (1984) (yield criterion), Fernández Ruiz *et al.* (2010a, 2015) (reduced capacity of spalled concrete to carry tensile stresses), Cavagnis *et al.* (2017) (expression to calculate the spalled concrete tensile stresses) and Randl (2013) (activation of the dowel action) as explained in the following.

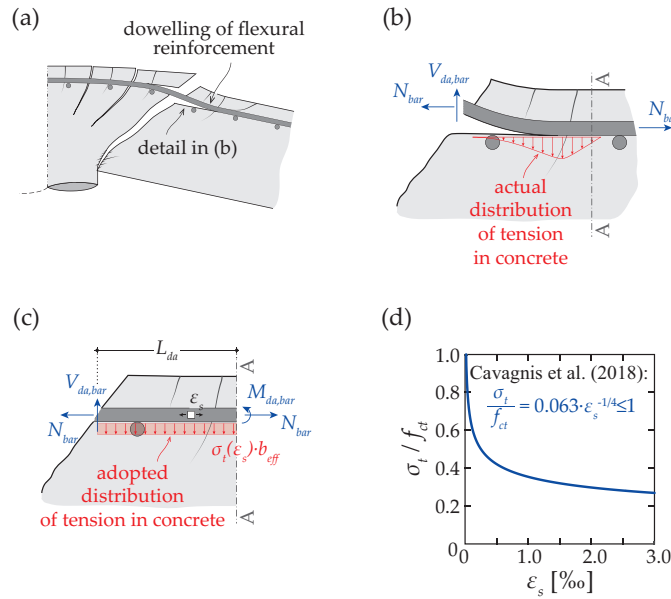


**Figure 5.17:** Calculation of shear transfer contribution due to dowelling of flexural reinforcement: (a) investigated phenomenon; (b) localized deformation of the bar and associated distribution of tensile stresses in the spalled concrete; (c) representation of the equilibrium of local free-body of the bar and surrounding concrete according to Einpaul (2016); (d) reduction of tensile stresses in the bar as a function of the state of strains in bar according to Cavagnis *et al.* (2017).

According to Fernández Ruiz *et al.* (2015), the ability of a dowelled bar to transfer shear forces when spalling of the concrete cover is governing can be investigated based on the equilibrium of the dowelling forces of the bar with the surrounding concrete tensile stresses (Figure 5.17(b)). The stresses in the concrete can be evaluated assuming a reduced tensile strength developing in a given area (length  $L_{da}$ , width  $b_{eff}$ ) (Fernández Ruiz *et al.*, 2015). The vertical and moment equilibrium conditions of the free body (previously adopted by e.g. Einpaul (2016)) shown in Figure 5.17(c) allows thus for calculating the acting shear force ( $V_{da,bar}$ ) as a function of the acting moment ( $M_{da,bar}$ ):

$$\begin{cases} V_{da,bar} = \sigma_t \cdot b_{eff} \cdot L_{da} \\ M_{da,bar} = V_{da,bar} \cdot \frac{L_{da}}{2} \end{cases} \Rightarrow V_{da,bar} = \sqrt{2 \cdot \sigma_t \cdot b_{eff} \cdot M_{da,bar}} \quad (5.37)$$

where the effective width of spalled concrete  $b_{eff}$  (Figure 5.21(c)) can be calculated as (Fernández Ruiz *et al.*, 2010a):

$$b_{eff} = s_b - \phi \leq \min(4 \cdot c; 6 \cdot \phi) \quad (5.38)$$

whose parameter  $s_b$  refers to the bar spacing,  $\phi$  to the bar diameter and  $c$  to the concrete cover.

The maximum capacity of the bar to carry a moment ( $M$ ) in the presence of normal forces ( $N$ ) is nevertheless limited by the yield conditions of the bar and can be expressed as (parabolic yield criterion of a bar with an equivalent square section; Millard and Johnson, 1984; Sorensen *et al.*, 2016):

$$\frac{M}{M_p} + \left(\frac{N}{N_p}\right)^2 = 1 \quad \Rightarrow \quad M = M_p \cdot \left(1 - \left(\frac{N}{N_p}\right)^2\right) \quad (5.39)$$

where  $N_p$  and  $M_p$  are the plastic normal force ( $N_p = \pi \cdot \phi^2/4 \cdot f_y$ ) and plastic moment ( $M_p = \phi^3/6 \cdot f_y$ ). By combining Eqs. (5.37) and (5.39) ( $M_{da,bar} = M$ ), the maximum available dowelling contribution of one bar can eventually be calculated as (similar equations have been previously derived or proposed by other researchers as e.g. Rasmussen (1963), Millard and Johnson (1984), Randl (2013), and Einpaul (2016)):

$$V_{da,bar} = \sqrt{\frac{1}{3}} \cdot \sqrt{\phi^3 \cdot b_{eff}} \cdot \sqrt{\sigma_t \cdot f_y \cdot \left(1 - \left(\frac{\sigma_s}{f_y}\right)^2\right)} \quad (5.40)$$

where the normal force in the bar is replaced by  $N = \pi \cdot \phi^2/4 \cdot \sigma_s$ , with  $\sigma_s$  representing the stress in the flexural reinforcement considering only the effect of the rotation  $\psi$  based on the previously introduced assumption of a spherical deformation inside  $r_0$ , that is, shear deformation not affecting the strain and stress of the flexural reinforcement:

$$\sigma_s = \varepsilon_s \cdot E_s = \frac{\psi \cdot (d - z_{CR})}{r_0} \cdot E_s \leq f_y \quad (5.41)$$

With respect to the tensile capacity of the concrete cover (spalling strength), it shall be noted that the tensile strains in the reinforcement reduce the ability of the spalled concrete to carry tensile stresses (Fernández Ruiz *et al.*, 2010a). Based on the works of Fernández Ruiz *et al.* (2010a, 2015), Cavagnis *et al.* (2017) proposed the following expression to calculate the tensile stresses in the spalled concrete as a function of the state of strains in the flexural reinforcement (Figure 5.17(d)):

$$\frac{\sigma_t}{f_{ct}} = 0.063 \cdot \varepsilon_s^{-1/4} \leq 1 \quad (5.42)$$

where the strains in the flexural reinforcement  $\varepsilon_s$  are computed in accordance to Eq. (5.41). According to Randl (2013), the contribution of dowel action of a bar ( $V_{da,bar}$ ) can be calculated as a function of the slip following a parabolic function as follows:

$$V_{da,bar} = V_{da,max,bar} \cdot \min\left(\sqrt{\frac{s}{s_{max}}}, 1\right) \quad (5.43)$$

where  $s_{max}$  refers to the slip required to activate the maximum dowel contribution, which can be assumed as  $0.10\phi$  to  $0.20\phi$  (Randl, 2013) (a value of  $0.20\phi$  is adopted in this work). The slip of the bar refers to the vertical projection of the vector sum of flexural and shear deformations at the level of the flexural reinforcement, which can be calculated on the basis of the adopted kinematics as:

$$s = (r_0 - r_{CR}) \cdot \psi_{csc} + \delta_s \cdot \cos\left(\frac{\pi}{2} - \beta(0) - \gamma_0\right) \quad (5.44)$$

The contribution of dowel action of the flexural reinforcement to the punching shear strength can finally be calculated by multiplying the contribution of one bar by the number of bars intersected by the CSC ( $n_b = 2 \cdot \pi \cdot r_0/s_b$  with the bar spacing given by  $s_b = \pi \cdot \phi^2/(4 \cdot d \cdot \rho)$  considering one layer of flexural

reinforcement in each direction) (Fernández Ruiz *et al.*, 2013, 2015; Einpaul, 2016):

$$V_{DA} = n_b \cdot V_{da,bar} = 8 \cdot \frac{r_0 \cdot d}{\phi^2} \cdot \rho \cdot V_{da,bar} \quad (5.45)$$

With respect to dowelling action of the compression reinforcement, this effect is neglected in this work.

#### 5.4.6 Calculation of the punching shear strength

The punching strength can be calculated in a similar manner as performed in the CSCT (Figure 5.1(b); Muttoni (2008)), by intersecting a failure criterion (providing the shear strength for a given opening of the CSC) with a load-deformation relationship (providing the rotations and associated crack openings for a given level of applied load).

The load-rotation relationship can be calculated as described by Muttoni (2008) using a quadri-linear moment-curvature relationship (briefly reviewed in Section 5.10.3). The failure criterion is obtained by numerical integration of the internal stresses (calculated in Section 5.4.5) along the CSC (whose geometry was defined in Section 5.4.3) as follows:

$$\begin{aligned} V_c(\psi, \delta_s) = & \overbrace{2 \cdot \pi \cdot \int_0^{z_{tr}} \frac{r(z)}{\sin(\beta(z))} \cdot [\tau_{sb}(z) \cdot \sin(\beta(z)) + \sigma_{sb}(z) \cdot \cos(\beta(z))] dz}^{\text{shear-transfer due to smeared cracking}} \\ & + \overbrace{2 \cdot \pi \cdot \int_{z_{tr}}^d \frac{r(z)}{\sin(\beta(z))} \cdot [\tau_{agg}(z) \cdot \sin(\beta(z)) + \sigma_{agg}(z) \cdot \cos(\beta(z))] dz}^{\text{shear-transfer due to localized cracking}} \\ & + \underbrace{V_{DA}}_{\text{dowel action}} \end{aligned} \quad (5.46)$$

Each point of the failure criterion is numerically determined calculating the resistance associated with a given rotation  $\psi$  by searching for the applied shear deformation  $\delta_s$  that maximizes the shear strength of the CSC (Section 5.10.4 presents a possible numerical procedure to calculate the punching strength).

Failure, defined as the intersection of the failure criterion and the load-rotation relationship, provides thus not only the punching strength  $V_{R,calc}$  but also the associated deformation capacity characterized by the rotation  $\psi_R$  and shear deformation at failure  $\delta_{s,R}$ .

### 5.5 Comparison against experimental results

The model presented in Section 5.4 is compared with a database of experimental tests in this section. The database presented by Muttoni *et al.* (2017) (including 121 experimental tests) is completed with tests from other authors (Elstner and Hognestad, 1956; Kinnunen and Nylander, 1960; Moe, 1961; Guandalini, 2005; Inácio *et al.*, 2015), leading to a total of 133 specimens (where  $B = 1.27 - 6.00$  m,  $d = 0.096 - 0.456$  m,  $r_c = 0.042 - 0.451$  m,  $c = 0.130 - 0.520$  m,  $f_c = 12.8 - 130.1$  MPa,  $d_g = 4 - 38.1$  mm,  $\rho = 0.32 - 3.70\%$ ,  $f_y = 321 - 720$  MPa; see 5.1).

The model shows an excellent agreement with the experimental results, leading to an average measured-to-calculated punching strength of 1.08 and a coefficient-of-variation (COV) of 7.9%. The main results are plotted in Figure 5.18 as a function of the effective depth, flexural reinforcement ratio, concrete compressive strength, equivalent slab radius-to-effective depth ratio, column radius-to-effective depth ratio and maximum aggregate size. Figure 5.18 shows that the model captures in a systematic manner the influence of the main geometrical and mechanical properties, without any noticeable trend.

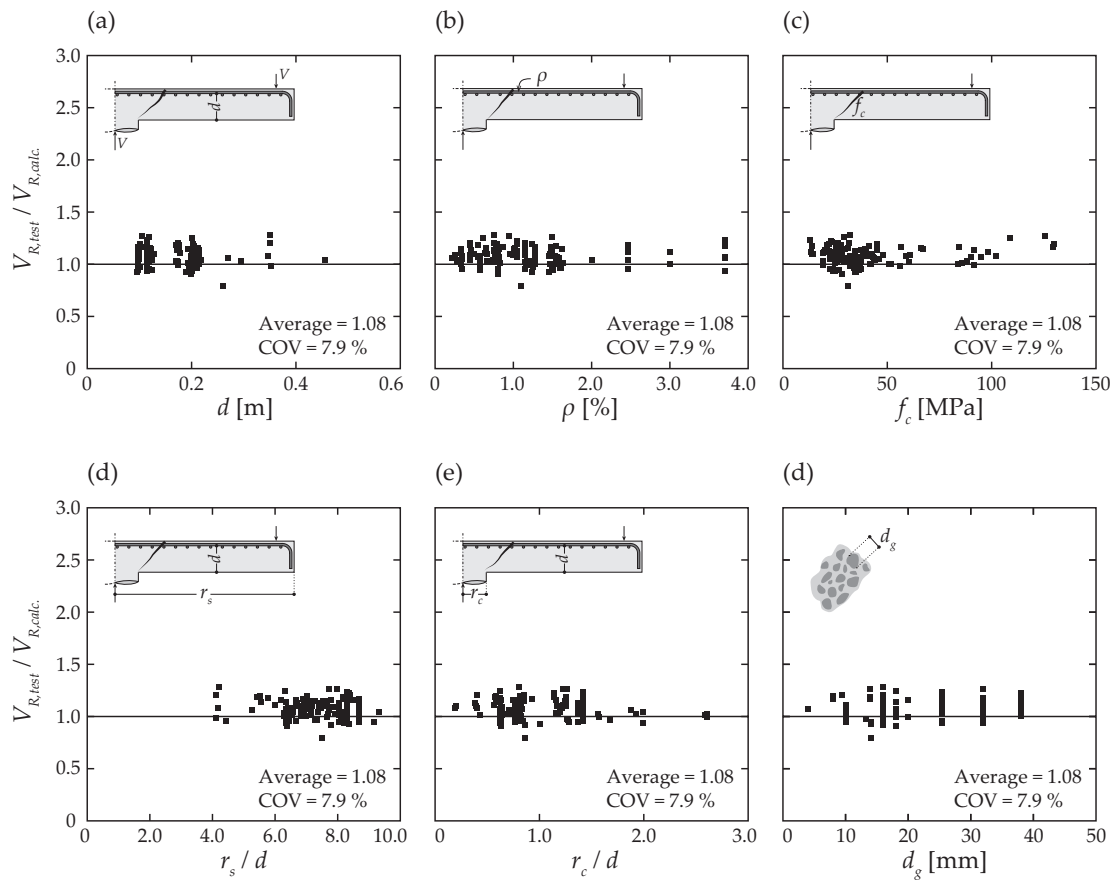


**Figure 5.18:** Ratio of experimental to calculated resistance as a function of (total of 133 specimens; see Table 5.1): (a) effective depth; (b) flexural reinforcement ratio; (c) concrete compressive strength; (d) equivalent radius of the slab-to-effective depth ratio (equivalent radius of an axisymmetric slab calculated ensuring equal flexural capacity); (e) column radius-to-effective depth ratio; (f) maximum aggregate size.

The model is also compared with some selected series of experimental tests in Figure 5.19, showing that the influence of all investigated parameters is consistently addressed. In addition, the contributions of dowel action, localized and smeared cracking are also presented in Figure 5.19. It should be noted that the relative contributions of the smeared and localized cracking regions depend upon the definition of the transition between the two regimes. Other criteria for defining the transition will have little influence on the total strength but would influence the relative contributions of each region.

Figure 5.19(b) shows that the decrease of the normalized punching strength with the increase of concrete compressive strength is mainly related to the decrease of the shear-transfer contribution in the region with smeared cracking. This result is a consequence of the increased brittleness of the compressive behaviour of high-strength concrete, which leads to an increased gradient of stresses along the CSC at failure.

Figures 5.19(c) and (d) show a decrease of the normalized punching strength with increasing column size, resulting also mainly from the decrease of the contribution in the smeared cracking region. This is a consequence of the larger rotations at failure, which lead to larger crack openings and, consequently, to smaller extents of the region governed by smeared cracking.

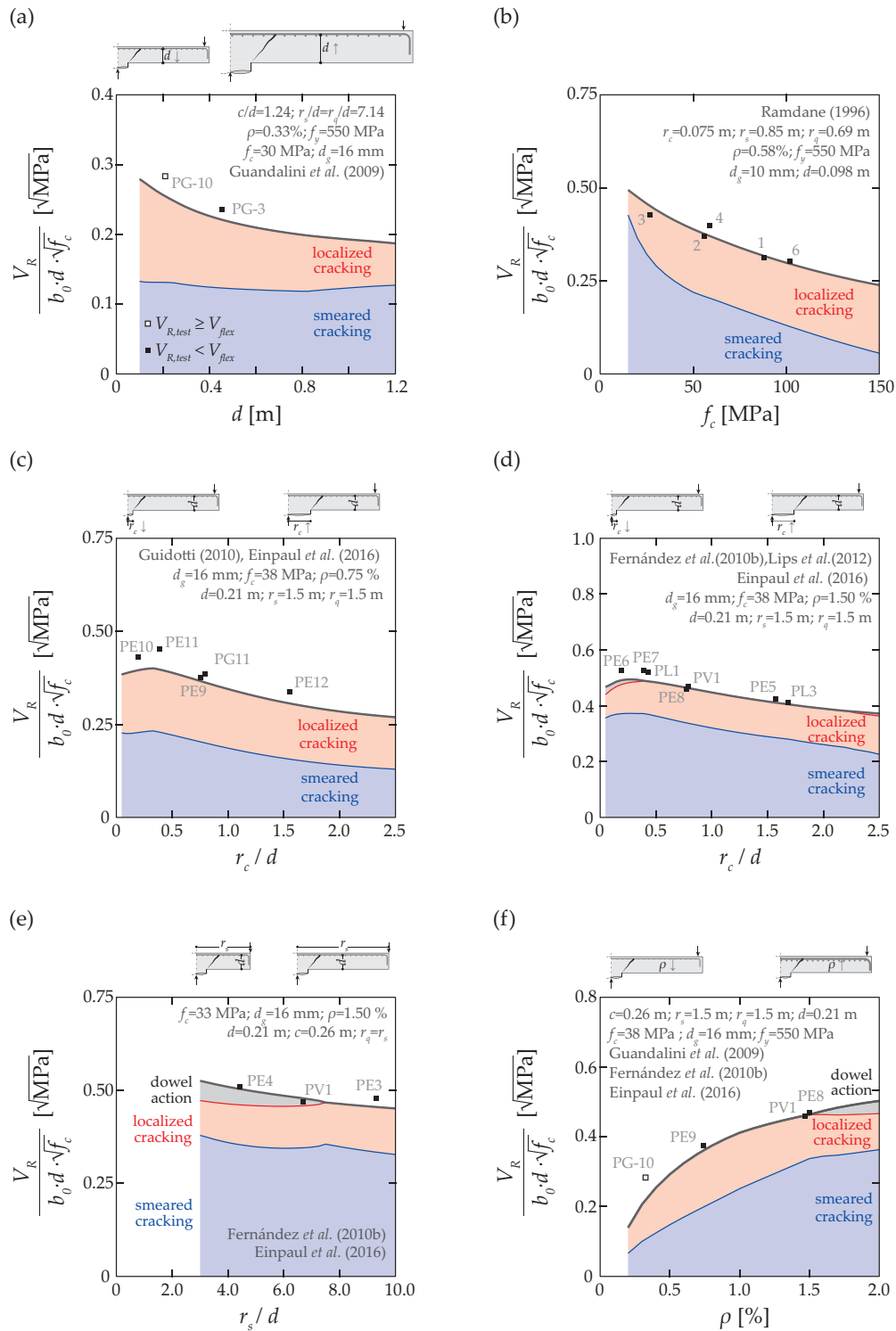


**Figure 5.19:** Comparison of the punching strength calculated with the mechanical model against experimental test series where the following parameters were varied: (a) effective depth (Guandalini *et al.*, 2009); (b) concrete compressive strength (Ramdane, 1996); (c) and (d) column radius-to-effective depth ratio (Guidotti, 2010; Fernández Ruiz *et al.*, 2010b; Lips *et al.*, 2012; Einpaul *et al.*, 2016); (e) slab radius-to-effective depth ratio (Fernández Ruiz *et al.*, 2010b; Einpaul *et al.*, 2016); (f) flexural reinforcement ratio (Guandalini *et al.*, 2009; Fernández Ruiz *et al.*, 2010b; Einpaul *et al.*, 2016).

Conversely, it can be noted that the contribution of the smeared cracking region to the strength increases at a higher rate than the contribution related to localized cracking with increasing flexural reinforcement ratio (Figure 5.19(f)). This can be justified by the decrease of the rotations at failure for increasing flexural reinforcement ratio, which leads to lower crack openings and, consequently, to larger extents of the region with smeared cracking behaviour.

It should also be noted that the contribution of dowel action of flexural reinforcement bars is null or negligible in most of cases due to yielding of the flexural reinforcement at  $r_0$ . Thus, dowel action can only be activated in failures with small rotations, that is, members with reduced slenderness (Figure 5.19(e)) or members with large flexural reinforcement ratios (Figure 5.19(f)).

## 5.6 Validation of the failure criterion of the Critical Shear Crack Theory

As discussed by Muttoni *et al.* (2017), the calculation of the punching strength by integration of stresses along the CSC is not suitable for design purposes. For that reason, assuming that the width of the CSC ( $w$ ) is proportional to the product of the slab rotation ( $\psi$ ) times the effective depth ( $d$ ) for the case of slender slabs ( $w \propto \psi \cdot d$ ), Muttoni (2008) proposed the following simplified failure criterion (see Figure 5.1(a) for agreement with experimental results):

$$\frac{V_R}{b_0 \cdot d \cdot \sqrt{f_c}} = \frac{0.75}{1 + 15 \cdot \frac{\psi \cdot d}{d_{g0} + d_g}} \quad (5.47)$$

where units are in SI [N, mm],  $V_R$  is the punching shear strength,  $f_c$  the cylinders concrete compressive strength,  $b_0$  the control perimeter located at  $d/2$  from the supported area,  $d_g$  the aggregate size and  $d_{g0}$  the reference aggregate size ( $d_{g0}=16$  mm for normal weight concrete (Muttoni, 2008)).

Some refinements (Muttoni and Fernández Ruiz, 2017) based on theoretical considerations (transition from slender slabs to footings (Muttoni *et al.*, 2017)) have recently been proposed leading to a power-law failure criterion (that can be used additionally to derive closed-form design expressions (Muttoni and Fernández Ruiz, 2017; Muttoni *et al.*, 2017)):

$$\frac{V_R}{b_0 \cdot d \cdot \sqrt{f_c}} = 0.55 \cdot \left( \frac{d_{dg}}{25 \cdot \psi \cdot d} \right)^{2/3} \leq 0.55 \quad (5.48)$$

where units are in SI [N, mm],  $d_{dg}$  represents the reference value of roughness of the failure surface, whose value was defined in Eq. (5.30).

The hyperbolic (Eq. (5.47)) and power-law (Eq. (5.48)) failure criteria of CSCT are depicted in Figure 5.20(a) together with the numerical results of the model presented in Section 5.4 corresponding to the experimental tests of the database. It is interesting to note that all points (every point representing the numerical result of an experimental test) concentrate in a narrow band with a clear trend of decreasing punching shear strength with increasing rotation. In the refined mechanical model, the decay of the contributions of the different shear-transfer actions with increasing rotation results mainly from the: (i) larger crack openings associated with flexural deformations which decrease the extent of the region with smeared cracking (thus decreasing its contribution); (ii) strain softening in the shear band; (iii) larger crack opening along the CSC which reduces its capacity to transfer stresses due to aggregate interlock (localized cracking); (iv) increased stresses in the flexural reinforcement decreasing the capacity of transferring shear forces by dowel action. It can also be seen that both simplified failure criteria approximate fairly well the numerical results (a detailed comparison is presented in Table 5.2).

Validation of the failure criterion of the Critical Shear Crack Theory

**Table 5.1:** Summary of database containing 133 specimens without transverse reinforcement:  $r_c$  - radius of a circular column;  $c$  - side length of a square column;  $d$  - effective depth;  $f_c$  - cylinders concrete compressive strength;  $f_y$  - yielding strength of flexural reinforcement;  $d_g$  - maximum aggregate size;  $B$  - size of the slab along orthogonal directions.

Authors	Number of tests ( $V_{R,test} \geq V_{flex}$ )	$B$ [m]	$d$ [m]	$r_c$ [m]	$c$ [m]	$f_c$ [MPa]	$d_g$ [mm]	$\rho$ [%]	$f_y$ [MPa]
Elstner and Hognestad (1956)	22 (3)	1.829	0.114	-	0.254	12.8	25.4	0.50	303
			-	-	-	-	-	-	-
Kinnunen and Nylander (1960)	12 (2)	1.840	0.117	0.075	-	24.2	-	0.44	434
			-	-	-	-	-	-	-
Moe (1961)	8 (1)	1.829	0.114	-	0.152	22.1	9.5	1.05	328
			-	-	-	-	-	-	-
Schaeffers (1984)	2	1.960	0.113	0.105	-	21.3	32	0.55	450
			-	-	-	-	-	-	-
Tolf (1988)	8	1.270	0.098	0.063	-	22.6	16	0.34	657
		-	-	-	-	-	-	-	-
Hallgren (1996)	7	2.540	0.194	0.125	-	84.1	18	0.33	596
			-	-	-	-	-	-	-
Ramdane (1996)	12	1.700	0.098	0.075	-	26.9	10	0.58	550
			-	-	-	-	-	-	-
Hassanzadeh (1996)	1	2.540	0.199	0.125	-	28.4	18	0.8	493
			-	-	-	-	-	-	-
Sistonen <i>et al.</i> (1997)	10	1.770	0.170	0.101	-	19.0	16	0.45	576
		-	-	-	-	-	-	-	-
Birkle (2004)	3	2.248	0.124	-	0.250	31.4	14	1.10	488
		-	-	-	-	-	-	-	-
Guandalini <i>et al.</i> (2009)	10 (5)	1.500	0.096	-	0.130	27.7	4	0.22	520
		-	-	-	-	-	-	-	-
Guidotti (2010)	11	3.000	0.194	-	0.260	31.5	8	0.76	510
			-	-	-	-	-	-	-
Tassinari (2011)	2	3.000	0.196	-	0.260	66.3	16	0.82	540
			-	-	-	-	-	-	-
Fernández Ruiz <i>et al.</i> (2010b)	1	3.000	0.210	-	0.260	34.0	16	1.500	709
			-	-	-	-	-	-	-
Clément (2012)	3	3.000	0.346	-	0.220	31.6	16	0.75	520
			-	-	-	-	-	-	-
Lips <i>et al.</i> (2012)	4	3.000	0.193	-	0.130	30.5	16	1.50	556
			-	-	-	-	-	-	-
Heinzmann <i>et al.</i> (2012)	1	4.100	0.294	0.200	-	35.5	32	1.200	577
			-	-	-	-	-	-	-
Inácio <i>et al.</i> (2015)	4 (1)	1.650	0.101	-	0.200	35.9	13.2	0.98	523
			-	-	-	-	-	-	-
Einpaul <i>et al.</i> (2016)	10	1.700	0.197	0.042	-	34.2	-	0.74	517
		-	-	-	-	-	-	-	-
Drakatos <i>et al.</i> (2016)	2	3.000	0.195	-	0.390	34.3	16	0.80	507
			-	-	-	-	-	-	-
$\Sigma$	133 (12)	1.270	0.096	0.042	0.130	12.8	4	0.22	303
		-	-	-	-	-	-	-	-
		6.000	0.456	0.451	0.520	130.1	38.1	3.70	720

**Table 5.2:** Summary of obtained experimental-to-calculated resistance  $V_{R,test}/V_{R,calc.}$  of 133 specimens combining the load-rotation relationship according to Muttoni (2008) and the different failure criteria of CSCT.

Failure Criterion	Average	COV [%]
Numerical integration of the refined model	1.08	7.9
Hyperbolic failure criterion (Eq. (5.47)) (Muttoni, 2008) with $d_{dg}$ of Eq. (5.30) (Muttoni <i>et al.</i> , 2017)	1.08	8.0
Power-law failure criterion (Eq.(5.48)) (Muttoni <i>et al.</i> , 2017)	1.03	8.4

With respect to the original assumption of Muttoni (2008) that the crack opening is correlated to the product of the effective depth times the rotation of the slab ( $w \propto \psi \cdot d$ ), its validity can also be verified with the refined mechanical model. At failure, the opening of the CSC depends on the rotation of the slab ( $\psi$ ) and on its shear deformations ( $\delta_s$ ). As shown in Figure 5.20(b), where the normalized crack opening at failure calculated at  $d/2$  from the soffit of the slab is plotted as a function of the normalized rotation, a clear correlation between both parameters appears. As suggested by Muttoni *et al.* (2017), this is justified by the fact that a larger initial crack opening (associated with larger rotations) also requires a larger crack sliding to activate the shear-transfer actions. It can be noted that for slabs whose failure load is governed by bending (empty squares in Figure 5.20(b)) this assumption seems to be conservative in cases where very large rotations are experienced.

The mechanical model can also be used to parametrically verify the simplified failure criteria (hyperbolic and power-law expressions), refer to Figure 5.21. The influence of the concrete compressive strength, column size and slenderness is investigated separately in that figure, where the internal stresses developing along the CSC are also represented for small, moderate and large rotation conditions (smeared and localized cracking represented in dark and light blue, respectively). The parametric study shows overall consistent results with suitable predictions of the trends.

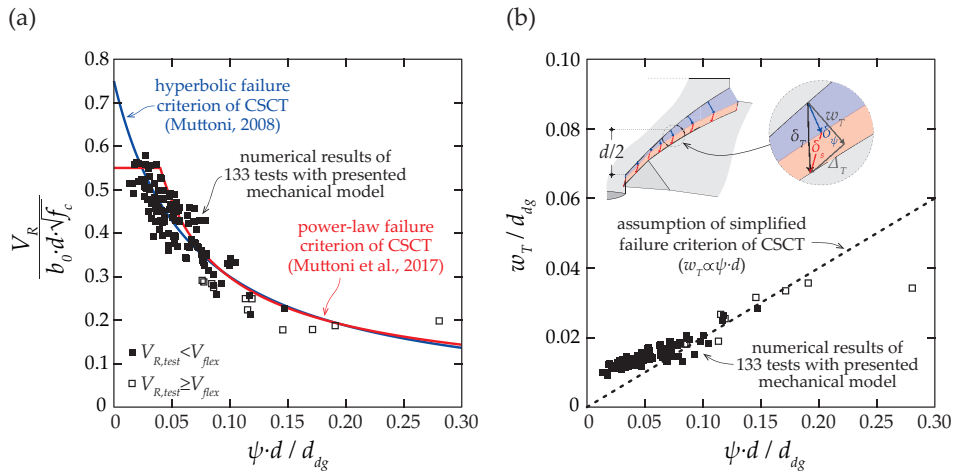


**Figure 5.20:** Results of the refined calculation of the failure criterion of CSCT: (a) calculated punching shear strength as a function of the rotation and comparison with hyperbolic (Muttoni, 2008) and power-law failure criteria (Muttoni *et al.*, 2017); (b) calculated crack opening at  $d/2$  from the soffit of the slab as a function of normalized rotation and comparison with assumption of simplified criteria of CSCT.

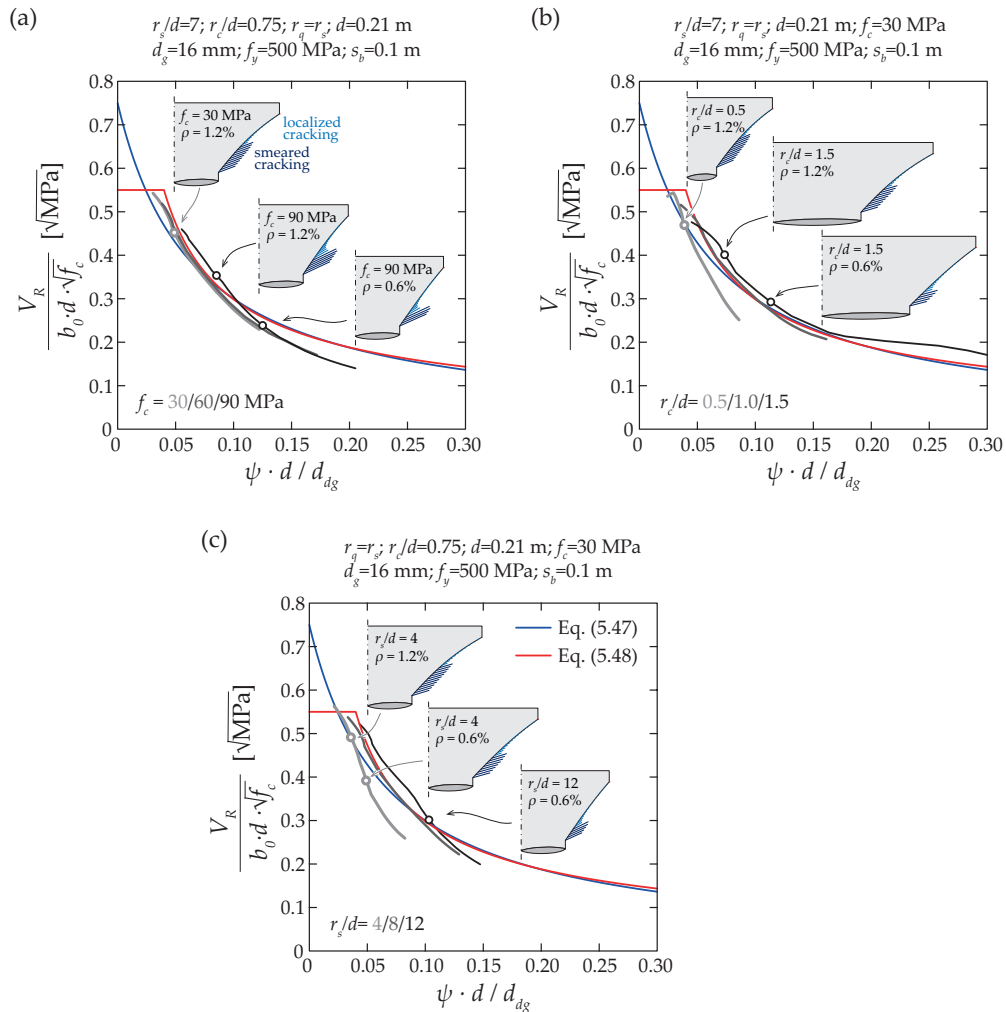


**Figure 5.21:** Comparison of the normalized punching strength calculated with the mechanical model against the hyperbolic (Muttoni, 2008) and power-law (Muttoni *et al.*, 2017) failure criteria of CSCT for  $\rho = 0.3 - 3.0\%$  with varying: (a) concrete compressive strength; (b) column radius-to-effective depth ratio; (c) slab radius-to-effective depth ratio.

With respect to size-effect, the results of the numerical integration of internal stresses are shown in Figure 5.22(a), where three different cases (corresponding to different flexural reinforcement ratios) are represented and compared to the analytical failure criteria of the CSCT. The results show again fine agreement. In fact, a more detailed analysis shows that the size-effect predicted by the numerically calculated failure criterion leads to a slope of approximately  $-1/3$  in a double-log scale (Figure 5.22(b)). Thus, the size-effect law predicted by the refined mechanical model is milder when compared to the size-effect law resulting from the application of Linear Elastic Fracture Mechanics (LEFM), which is of  $-1/2$  in a double-log scale (Bažant and Cao, 1987). This result is consistent with the theoretical works of Fernández Ruiz and Muttoni (2017) and is justified by the fact that the slab behaviour in terms of the load-deformation response is not linear (but highly non-linear).

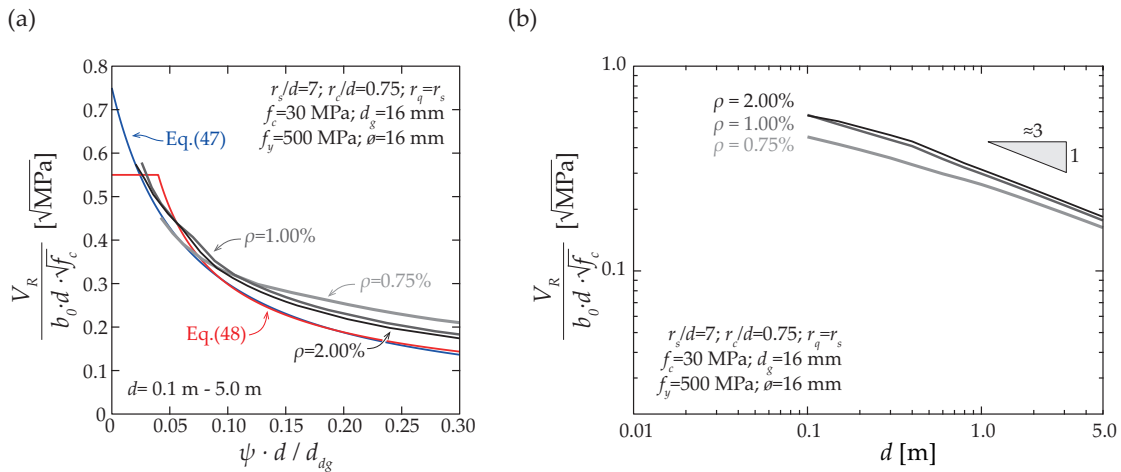


Figure 5.22: Investigation of size-effect with the numerical integration of the failure criterion (calculated by varying only the effective depth  $d$ ): (a) comparison with the analytical failure criteria of CSCT; (b) calculated size-effect law represented in a double logarithmic scale.

### 5.7 Conclusions

This paper validates the principles of the Critical Shear Crack Theory (CSCT) for punching shear failures of members without transverse reinforcement by means of a refined mechanical model. The refined mechanical model is supported on the analysis of recent experimental results available in the scientific literature, which show that:

1. The development of a critical shear crack governs the punching strength of flat slabs as its opening disturbs the compression struts carrying shear. Failure may occur by localization of the strains in this crack or by the opening of a new one (failure crack) due to the transverse tensile (splitting) stresses developed near the supported area. This is also consistent with the experimental measurements of Einpaul *et al.* (2017) based on measurements of internal cracking in punching tests.
2. The kinematics of a slab sector is governed at failure by the rotations of the slab as well as by the shear deformations developing in the critical shear crack according to the experimental results of Clément (2012);
3. Two different regions can be distinguished in the critical shear crack: a region where localized cracking occurs and a region where smeared cracking develops (in agreement with Muttoni *et al.* (2017)). This latter region is considered as a shear band, eventually failing by coalescence of cracks;

Based on the three previously described experimental evidences, a refined mechanical model is developed considering that the shear transfer capacity of the region with localized cracking is mostly governed by aggregate interlock, while in the shear band, an inclined compression strut allows for the transfer of shear forces. In addition, it is considered that dowelling of the flexural reinforcement may develop. The main results of the refined mechanical model are listed below:

1. All the shear-transfer actions decay with increasing rotation as a consequence of larger crack openings. This is justified by the fact that larger crack openings reduce the aggregate interlock action, soften concrete in compression and limit the dowelling capacity of bars (by a reduction of the tensile strength of the concrete cover and due to yielding of the bars);

2. A parametric study based on the refined mechanical model confirms the validity of the simplified failure criteria proposed by the CSCT;
3. The assumption of a crack opening correlated to the multiplication of the rotation by the effective depth ( $w \propto \psi \cdot d$ ) considered by Muttoni (2008) when proposing the simplified failure criterion of the CSCT can be justified on the basis of the proposed refined mechanical model, as there exists a correlation at failure between the rotations of the slab and the opening of the critical shear crack;
4. The refined mechanical model predicts a size-effect law with a slope of approximately  $-1/3$  in a double-logarithmic scale. This results is in agreement with the theoretical work of Fernández Ruiz and Muttoni (2017);
5. The results of the model show a good agreement with experimental results when compared to a database of tested specimens as well as individual series of tests where only one parameter is varied.

## 5.8 References

- ACI 318 (2014):** *Building Code Requirements for Reinforced Concrete (ACI 318-14)*. Farmington Hills, MI, USA.
- Angelakos D.; Bentz E. C.; Collins M. P. (2001):** „Effect of Concrete Strength and Minimum Stirrups on Shear Strength of Large Members“. *ACI Structural Journal*, Vol. 98, No. 3, pp. 290–300.
- Bažant Z. P.; Cao Z. (1987):** „Size Effect in Punching shear Failure of Slabs“. *ACI Structural Journal*, Vol. 84, No. 1, pp. 44–53.
- Bažant Z. P.; Xiang Y. (1997):** „Size effect in compression fracture: splitting crack band propagation“. *Journal of Engineering Mechanics*, Vol. 123, No. 2, pp. 162–172.
- Bentz E. C.; Vecchio F. J.; Collins M. P. (2006):** „Simplified Modified Compression Field Theory for Calculating Shear Strength of Reinforced Concrete Elements“. *ACI Structural Journal*, Vol. 103, No. 4, pp. 614–624.
- Birkle G. (2004):** „Punching of Flat Slabs: The Influence of Slab Thickness and Stud Layout“. PhD thesis. Calgary, Canada: University of Calgary, p. 217.
- Braestrup M. W.; Nielsen M. P.; Jensen B. C.; Bach F. (1976):** *Axisymmetric Punching of Plain and Reinforced Concrete*. Tech. rep. 75. Structural Research Laboratory, Technical University of Denmark, p. 33.
- Broms C. E. (1990):** „Punching of flat plates - a question of concrete properties in biaxial compression and size effect“. *ACI Structural Journal*, Vol. 87, No. 3, pp. 292–304.
- Broms C. E. (2005):** „Concrete flat slabs and footings: Design method for punching and detailing for ductility“. PhD thesis. Stockholm, Sweden: Department of Structural Engineering, Royal Institute of Technology, p. 114.
- Broms C. E. (2016):** „Tangential strain theory for punching failure of flat slabs“. *ACI Structural Journal*, Vol. 113, No. 1, pp. 95–104.
- Campana S.; Anastasi A.; Fernández Ruiz M.; Muttoni A. (2013):** „Analysis of shear-transfer actions on one-way RC members based on measured cracking pattern and failure kinematics“. *Magazine of Concrete Research*, Vol. 65, No. 6, pp. 386–404.
- Cavagnis F.; Fernández Ruiz M.; Muttoni A. (2015):** „Shear failures in reinforced concrete members without transverse reinforcement - An analysis of the critical shear crack development on the basis of test results“. *Engineering Structures*, Vol. 103, pp. 157–173.
- Cavagnis F.; Fernández Ruiz M.; Muttoni A. (2017):** „A mechanical model for failures in shear of members without transverse reinforcement based on development of a critical shear crack“. *Engineering Structures*. (accepted for publication).
- Clément T. (2012):** „Influence de la précontrainte sur la résistance au poinçonnement de dalles en béton armé“. PhD thesis. Lausanne, Switzerland: EPFL, p. 224.
- Collins M. P.; Kuchma D. (1999):** „How Safe Are Our Large, Lightly Reinforced Concrete Beams, Slabs, and Footings?“ *ACI Structural Journal*, Vol. 96, No. 4, pp. 482–490.
- Drakatos I. S. (2016):** „Seismic behaviour of slab-column connections without transverse reinforcement“. PhD thesis. Lausanne, Switzerland: EPFL, p. 196.
- Drakatos I.-S.; Muttoni A.; Beyer K. (2016):** „Internal slab-column connections under monotonic and cyclic imposed rotations“. *Engineering Structures*, Vol. 123, pp. 501–516.

- Einpaul J. (2016):** „Punching strength of continuous flat slabs“. PhD thesis. Lausanne, Switzerland: EPFL, p. 209.
- Einpaul J.; Bujnak J.; Fernández Ruiz M.; Muttoni A. (2016):** „Study on influence of column size and slab slenderness on punching strength“. *ACI Structural Journal*, Vol. 113, No. 1, pp. 135–145.
- Einpaul J.; Fernández Ruiz M.; Muttoni A. (2017):** „Measurements of internal cracking in punching test slabs without shear reinforcement“. *Magazine of Concrete Research*. DOI: 10.1680/jmacr.16.00099.
- Elstner R. C.; Hognestad E. (1956):** „Shearing strength of reinforced concrete slabs“. *ACI Journal Proceedings*, Vol. 53, No. 2, pp. 29–58.
- Eurocode 2 (2004):** *Design of Concrete Structures - General Rules and Rules for Buildings, EN 1992-1-1*. Brussels, Belgium, p. 225.
- Fernández Ruiz M.; Muttoni A. (2007):** „On development of suitable stress fields for structural concrete“. *ACI Structural Journal*, Vol. 104, No. 4, pp. 495–502.
- Fernández Ruiz M.; Muttoni A. (2017):** „Size effect in shear and punching shear failures: differences between statically determinate members and redundant structures“. *Structural Concrete*, pp. 1–11. DOI: 10.1002/suco.201700059.
- Fernández Ruiz M.; Muttoni A. (2017):** „Size effect on punching shear strength: Differences and analogies with shear in one-way slabs“. In: *Bulletin 81 / ACI SP-315: Punching shear test of structural concrete slabs: Honoring Neil M. Hawkins*. Ed. by Ospina C. E.; Mitchell D.; Muttoni A. Lausanne, Switzerland: International Federation for Structural Concrete, pp. 59–72.
- Fernández Ruiz M.; Plumey S.; Muttoni A. (2010a):** „Interaction between bond and deviation forces in spalling failures of arch-shaped members without transverse reinforcement“. *ACI Structural Journal*, Vol. 107, No. 3, pp. 346–354.
- Fernández Ruiz M.; Muttoni A.; Kunz J. (2010b):** „Strengthening of flat slabs against punching shear using post-installed shear reinforcement“. *ACI Structural Journal*, Vol. 107, No. 4, pp. 434–442.
- Fernández Ruiz M.; Mirzaei Y.; Muttoni A. (2013):** „Post-punching behavior of flat slabs“. *ACI Structural Journal*, Vol. 110, No. 5, pp. 801–812.
- Fernández Ruiz M.; Muttoni A.; Sagaseta J. (2015):** „Shear strength of concrete members without transverse reinforcement: a mechanical approach to consistently account for size and strain effects“. *Engineering Structures*, Vol. 99, pp. 360–372.
- fib (2001):** *Bulletin 12: Punching of structural concrete slabs*. Tech. rep. Lausanne, Switzerland: International Federation for Structural Concrete, p. 314.
- fib (2017):** *Bulletin 81 / ACI SP-315: Punching shear of structural concrete slabs: Honoring Neil M. Hawkins*. Tech. rep. Lausanne, Switzerland: International Federation for Structural Concrete, p. 378.
- fib Model Code 2010 (2013):** *Model Code 2010 - Final draft*. Tech. rep. Volumes 1 and 2, Bulletins 65 and 66. International Federation for Structural Concrete.
- Guandalini S. (2005):** „Symmetric punching shear of reinforced concrete slabs (In French: Poinçonnement symétrique des dalles en béton armé)“. PhD thesis. Lausanne, Switzerland: EPFL, p. 289.
- Guandalini S.; Burdet O.; Muttoni A. (2009):** „Punching tests of slabs with low reinforcement ratios“. *ACI Structural Journal*, Vol. 106, No. 1, pp. 87–95.

- Guidotti R. (2010):** „Punching shear of slabs with column load (In French: Poinçonnement des planchers-dalles avec colonnes superposées fortement sollicitées)“. PhD thesis. Lausanne, Switzerland: EPFL, p. 189.
- Guidotti R.; Fernández Ruiz M.; Muttoni A. (2011):** „Crushing and Flexural Strength of Slab-Column Joints“. *Engineering Structures*, Vol. 33, No. 3, pp. 855–867.
- Hallgren M. (1996):** „Punching Shear Capacity of Reinforced High Strength Concrete Slabs“. PhD thesis. Stockholm, Sweden: Department of Structural Engineering, Royal Institute of Technology, p. 206.
- Hassanzadeh G. (1996):** *Influence of the slab thickness on the strength of concrete slabs at punching. Tests with circular slabs (In Swedish: Förstärkning av brobanep Plattor på pelare med hänsyn till genomstansning "Redovisning av provningar")*. Tech. rep. 41. Stockholm, Sweden: Royal Institute of Technology, Department of Structural Mechanics and Engineering, p. 134.
- Heinzmann D.; Etter S.; Villiger S.; Jaeger T. (2012):** „Punching tests on reinforced concrete slabs with and without shear reinforcement“. *ACI Structural Journal*, Vol. 109, No. 6, pp. 787–794.
- Hoang L. C. (2006):** „Punching Shear Analysis according to the Crack Sliding Model - Slabs without Shear Reinforcement“. *Proceedings of the Danish Society for Structural Science and Engineering*, Vol. 77, No. 3, pp. 69–133.
- Hognestad E. (1953):** „Shearing Strength of Reinforced Concrete Column Footings“. *ACI Journal*, Vol. 25, No. 3, pp. 189–208.
- Hordijk D. A. (1992):** „Tensile and tensile fatigue behaviour of concrete, experiments, modelling and analyses“. *HERON*, Vol. 37, No. 1, pp. 79.
- Huber P.; Huber T.; Kolleger J. (2016):** „Investigation of the shear behavior of RC beams on the basis of measured crack kinematics“. *Engineering Structures*, Vol. 113, pp. 41–58.
- Inácio M.; Ramos A. P.; Lúcio V.; Faria D. V. (2015):** „Punching of high strength concrete flat slabs - Experimental investigation“. *Engineering Structures*, Vol. 103, pp. 275–284.
- Jacobsen J. S.; Olesen J. F.; Poulsen P. N. (2012):** *Constitutive Mixed Mode Behavior of Cracks in Concrete: Experimental Investigations of Material Modeling*. BYGDTU Report. Kgs. Lyngby: Technical University of Denmark.
- Jensen B. C. (1975):** „Lines of discontinuity for displacements in the theory of plasticity of plain and reinforced concrete“. *Magazine of Concrete Research*, Vol. 2, No. 2, pp. 143–150.
- Kanellopoulos A. (1986):** „On the inelastic behavior and fracture of reinforced concrete (In German: Zum unelastischen Verhalten und Bruch von Stahlbeton)“. PhD thesis. Zürich, Switzerland: ETHZ, p. 86.
- Khaja M. N.; Sherwood E. G. (2013):** „Does the shear strength of reinforced concrete beams and slabs depend upon the flexural reinforcement ratio or the reinforcement strain?“ *Canadian Journal of Civil Engineering*, Vol. 40, pp. 1068–1081.
- Kinnunen S.; Nylander H. (1960):** *Punching of Concrete Slabs Without Shear Reinforcement*. Tech. rep. 158. Stockholm, Sweden: Transactions of the Royal Institute of Technology, p. 112.
- Krefeld W. J.; Thurston C. W. (1966):** „Contribution of longitudinal steel to shear resistance of reinforced concrete beams“. *ACI Journal*, Vol. 63, No. 3, pp. 325–344.
- Kupfer H.; Gerstle H. (1973):** „Behavior of Concrete under Biaxial Stresses“. *Journal of Engineering Mechanics*, Vol. 99, No. 4, pp. 853–866.

- Kupfer H.; Hubert K. H.; Rusch H. (1969):** „Behavior of concrete under biaxial stresses“. *ACI Journal Proceedings*, Vol. 66, No. 52, pp. 656–666.
- Lips S. (2012):** „Punching of Flat Slabs with Large Amounts of Shear Reinforcement“. PhD thesis. EPFL, p. 217.
- Lips S.; Fernández Ruiz M.; Muttoni A. (2012):** „Experimental Investigation on Punching Strength and Deformation Capacity of Shear-Reinforced Slabs“. *ACI Structural Journal*, Vol. 109, No. 6, pp. 896–900.
- Mansur M. A.; Vinayagam T.; Tan K. H. (2008):** „Shear Transfer across a crack in reinforced high-strength concrete“. *Journal of Materials in Civil Engineering*, Vol. 20, No. 4, pp. 294–302.
- Mattock A. H. (1974):** *Effect of aggregate type on single direction shear transfer in monolithic concrete*. Tech. rep. 2, SM74. Seattle, Washington.
- Millard S. G.; Johnson R. P. (1984):** „Shear transfer across cracks in reinforced concrete due to aggregate interlock and to dowel action“. *Magazine of Concrete Research*, Vol. 36, No. 126, pp. 9–21.
- Moe J. (1961):** *Shearing strength of reinforced concrete slabs and footings under concentrated loads*. Vol. D47. Skokie, Illinois: Portland Cement Association, Research and Development Laboratories.
- Muttoni A. (1990):** „The applicability of the theory of plasticity to reinforced concrete design (In German: Die Anwendbarkeit der Plastizitätstheorie in der Bemessung von Stahlbeton)“. PhD thesis. Zürich, Switzerland: ETHZ, p. 158.
- Muttoni A. (2008):** „Punching shear strength of reinforced concrete slabs without transverse reinforcement“. *ACI structural Journal*, Vol. 105, No. 4, pp. 440–450.
- Muttoni A.; Fernández Ruiz M. (2008):** „Shear strength of members without transverse reinforcement as function of critical shear crack width“. *ACI Structural Journal*, Vol. 105, No. 2, pp. 163–172.
- Muttoni A.; Fernández Ruiz M. (2010):** „Shear in slabs and beams: should they be treated in the same way?“ In: *Bulletin 57: Shear and punching shear in RC and FRC elements*. Lausanne, Switzerland: International Federation for Structural Concrete, pp. 105–128.
- Muttoni A.; Fernández Ruiz M. (2017):** „The Critical Shear Crack Theory for punching design: from a Mechanical Model to Closed-Form Design Expressions“. In: *Bulletin 81 / ACI SP-315: Punching shear test of structural concrete slabs: Honoring Neil M. Hawkins*. Ed. by Ospina C. E.; Mitchell D.; Muttoni A. Lausanne, Switzerland: International Federation for Structural Concrete, pp. 237–252.
- Muttoni A.; Schwartz J. (1991):** „Behavior of beams and punching in slabs without shear reinforcement“. In: *IABSE Colloquium*. Vol. 62. International Association for Bridge and Structural Engineering. Stuttgart, Germany, pp. 703–708.
- Muttoni A.; Fernández Ruiz M.; Simões J. T. (2017):** „The theoretical principles of the critical shear crack theory for punching shear failures and derivation of consistent closed-form design expressions“. *Structural Concrete*, pp. 1–17. doi: 10.1002/suco.201700088.
- Nielsen M. P.; Hoang L. C. (2011):** *Limit analysis and concrete plasticity*. 3<sup>rd</sup> edition Boca Raton. USA: CRC Press.
- Park H. G.; Choi K. K; Chung L. (2011):** „Strain-based strength model for direct punching shear of interior slab-column connections“. *Engineering Structures*, Vol. 33, No. 3, pp. 1062–1073.
- Polak M. (2005):** *SP-232: Punching Shear in Reinforced Concrete Slabs*. Tech. rep. Farmington Hills, MI, USA: American Concrete Institute, p. 302.

- Ramdane K. E. (1996):** „Punching shear of high performance concrete slabs“. In: *Proceedings of the fourth international symposium on utilization of high-strength/high performance concrete*. Paris, France, pp. 1015–1026.
- Randl N. (2013):** „Design recommendations for interface shear transfer in fib Model Code 2010“. *Structural Concrete*, Vol. 14, No. 3, pp. 230–241.
- Rasmussen B. H. (1963):** „Betonindstøbte, tvæbelastede boltes og dornes bæeevne (in Danish)“. *Bygningsstatistiske Meddelelser*, Vol. 34, No. 2, pp. 39–55.
- Regan P.; Braestrup M. W. (1985):** *Punching shear in reinforced concrete*. Tech. rep. 168. Comité Euro-International du Béton (CEB), p. 232.
- Richart F. E. (1948):** „Reinforced Concrete Walls and Column Footings, part 1 and 2“. *ACI Journal*, Vol. 45, pp. 97–127 & 237–260.
- Schaefers U. (1984):** „Construction, Dimensioning and Safety with Respect to Punching Shear of Reinforced Concrete Flat Plates in the Vicinity of Internal Columns(In German: Konstruktion, Bemessung und Sicherheit gegen Durchstanzen von balkenlosen Stahlbetondecken im Bereich der Innenstützen)“. *Deutscher Ausschuss für Stahlbeton*, Vol. 357, pp. 83.
- Shehata I. A.E. M.; Regan P. E. (1989):** „Punching in R. C. Slabs“. *Journal of Structural Engineering*, Vol. 115, No. 7, pp. 1726–1740.
- Sherwood E. G.; P. E. C.B. M.; Collins (2007):** „Effect of aggregate size on beam-shear strength of thick slabs“. *ACI Structural Journal*, Vol. 104, No. 2, pp. 180–190.
- Simões J. T.; Bujnak J.; Fernández Ruiz M.; Muttoni A. (2016a):** „Punching shear on compact footings with uniform soil pressure“. *Structural Concrete*, Vol. 17, No. 4, pp. 603–617.
- Simões J. T.; Faria D. V.; Fernández Ruiz M.; Muttoni A. (2016b):** „Strength of reinforced concrete footings without transverse reinforcement according to limit analysis“. *Engineering Structures*, Vol. 112, pp. 146–161.
- Simões J. T.; Fernández Ruiz M.; Muttoni A. (2018):** „Validation of the Critical Shear Crack Theory for punching of slabs without transverse reinforcement by means of a refined mechanical model“. *Structural Concrete*, pp. 1–26. DOI: 10.1002/suco.201700280.
- Sistonen E.; Lydman M.; Huovinen S. (1997):** *The geometrical model of the calculation formula of the punching shear capacity of the reinforced concrete slab (In Finnish: Teräsbetoniilaatan lävistyskapasiteetin laskentakaavan geometrinen malli)*. Tech. rep. 69. Helsinki University of Technology. Laboratory of Structural Engineering and Building Physics, p. 95.
- Sorensen J. H.; Hoand L. H.; Olesen J. F.; Fischer G. (2016):** „Catenary action in rebars crossing a casting joint loaded in shear“. In: *11<sup>th</sup> fib International PhD Symposium in Civil Engineering*. Ed. by Maekawa K.; Kasuga A.; Yamazaki J., pp. 735–742.
- Tassinari L. (2011):** „Poinçonnement symétrique des dalles en béton armé avec armature de poinçonnement“. PhD thesis. Lausanne, Switzerland: EPFL, p. 197.
- Theodorakopoulos D. D.; Swamy R. N. (2002):** „Ultimate punching shear strength analysis of slab-column connections“. *Cement and Concrete Composites*, Vol. 24, No. 6, pp. 509–521.
- Tolf P. (1988):** *Influence of the slab thickness on the strength of concrete slabs at punching. Tests with circular slabs (In Swedish: Plattjocklekens inverkan på betongplattors hållfasthet vid genomstansning: försök med*

- 
- cirkulära plattor*). Tech. rep. 146. Stockholm, Sweden: Royal Institute of Technology, Department of Structural Mechanics and Engineering, p. 64.
- Vecchio F. J.; Collins M. P. (1986):** „The modified compression-field theory for reinforced concrete elements subjected to shear“. *ACI Structural Journal*, Vol. 83, No. 2, pp. 219–231.
- Walraven J. (1981):** „Fundamental analysis of aggregate interlock“. *Journal of Structural Engineering*, Vol. 107, No. 11, pp. 2245–2270.
- Walraven J. C. (1980):** „Aggregate interlock: a theoretical and experimental analysis“. PhD thesis. Delft, Netherlands: Delft University of Technology, Faculty of Civil Engineering, p. 197.
- Whitney C. S. (1957):** „Ultimate Shear Strength of Reinforced Concrete Flat Slabs, Footings, Beams, and Frame Members Without Shear Reinforcement“. *ACI Journal Proceedings*, Vol. 54, No. 10, pp. 265–298.
- Yankelevsky D. Z.; Leibowitz O. (1999):** „Punching shear in concrete slabs“. *International Journal of Mechanical Sciences*, Vol. 41, No. 1, pp. 1–15.

## 5.9 Notation

### Latin characters

#### Lower Case

$a_0, a_1, a_3$	parameters characterizing the shape of the critical shear crack
$a_\varepsilon, b_\varepsilon, c_\varepsilon$	parameters characterizing the $\varepsilon_1$ - $\varepsilon_3$ relationship proposed by Guidotti <i>et al.</i> (2011)
$b_0$	length of control perimeter located at $d/2$ from the column edge
$b_1, b_2, b_3$	constants
$b_{eff}$	effective width of spalled concrete involved in the dowelling of a bar
$c$	side length of a square column
$c_1, c_2, c_3$	constants to calculate the aggregate interlock engagement stresses
$d$	effective depth (distance from the centroid of the flexural reinforcement to the outermost compressed fiber)
$d_g$	maximum aggregate size
$d_{g0}$	reference aggregate size
$d_{dg}$	reference value of the roughness of the critical shear crack (limited to 40 mm)
$d_{dg}^*$	reference value of the roughness of the critical shear crack (not limited)
$d\theta$	angle of slab sector (also angle of shear band sector)
$f_c$	concrete compressive strength measured in cylinders
$f_{cc}$	confined concrete compressive strength
$f_{c,eff}$	peak of concrete compressive strength accounting for imposed transverse tensile strain
$f_{cp}$	plastic concrete compressive strength
$f_{ct}$	concrete tensile strength
$f_{c0,t}$	reference value of concrete compressive strength to calculate concrete tensile strength
$f_y$	yielding strength of reinforcement
$h$	height of reinforced concrete section
$h_c, h_s$	force per unit width in the concrete and in the reinforcement, respectively
$k_0, k_1, k_2, k_3, k_4, k_5, k_6$	constants
$m$	moment
$m_{cr}$	cracking moment per unit width
$m_r$	radial moment per unit width
$m_R$	moment capacity per unit width
$m_t$	tangential moment per unit width
$n, t$	axis normal a parallel to the shear and
$n_E$	ratio of the modulus of elasticity of the reinforcement and concrete
$n_b$	number of bars
$n_{cr}$	number of cracks
$n_p$	in-plane force per unit width
$r, z$	radial and vertical coordinates
$r_{CR}, z_{CR}$	radial and vertical coordinates of the centre of rotation
$r_c$	radius of a circular column
$r_{cr}$	radius of cracked region
$r_q$	radial location of the resultant of vertical applied load
$r_s$	radius of isolated axisymmetric member
$r_y$	radius of the region in which reinforcement is yielding
$r_1$	radius of the region with stabilized cracking
$r_0$	radial distance between the axis of the column and the critical shear crack at the level of the flexural reinforcement
$r_{0,test}$	radial distance between the axis of the column and the critical shear crack at the level of the flexural reinforcement experimentally measured
$r_{\chi r}$	radial distance with non-negligible radial deformation measured from the axis of the column
$s$	slip of the bar
$s_{max}$	slip required to activate the maximum dowel action contribution

$s_b$	bar spacing
$s_f$	distance between primary flexural cracks
$t_1, t_2$	constants to calculate the stresses associated with residual tensile strength
$u_\psi, v_\psi$	radial and vertical components of vector of displacement due to rotation, respectively
$w$	crack opening
$w_c$	crack opening associated with a zero normal stress due to residual tensile strength
$w_\psi, w_s, w_T$	crack opening (displacement normal to the critical shear crack) due to rotation, shear deformation and combined effect (vector sum), respectively
$w_{CSC,z}$	width of the critical shear crack at the vertical coordinate $z$
$\bar{w}$	normalized displacement normal to the crack surface
$w_0$	initial crack opening due to flexural deformations
$x$	depth of neutral axis
$x_{el}$	depth of the compression zone assuming an linear-elastic behaviour of both concrete and reinforcement
$z_{Tr}$	vertical coordinate where transition from localized and smeared cracking occurs
$z_{\gamma_T=35^\circ}$	vertical coordinates where $\gamma_T = 35^\circ$
$z_{\gamma_s=40^\circ}$	vertical coordinate where $\gamma_s = 40^\circ$
$z_{w_\psi=0.5 \cdot w_c}$	vertical coordinate where $w_\psi = 0.5 \cdot w_c$
$z_{\gamma_\psi=40^\circ}$	vertical coordinate where $\gamma_\psi = 40^\circ$

### Upper Case

$B$	side length of a square slab
$C$	force in the concrete conical shell
$E_c, E_s$	modulus of elasticity of concrete and reinforcement, respectively
$E_{cc}$	modulus of elasticity of confined concrete
$E_{c,eff}$	effective modulus of elasticity of concrete accounting for the presence of imposed transverse tensile strains
$EI_0$	uncracked stiffness of reinforced concrete section
$EI_1$	cracked stiffness of reinforced concrete section
$G_F$	total fracture energy
$L_{da}$	length of the bar where dowel action is assumed to develop
$M$	acting moment
$M_{da,bar}$	acting moment in the bar due to dowel action
$M_p$	plastic moment
$N$	acting normal force
$N_{bar}$	acting normal force in the bar
$N_p$	plastic normal force
$V$	punching shear force
$V_{da,max,bar}$	maximum shear force in the bar due to dowel action
$V_{da,bar}$	shear force in the bar due to dowel action
$V_{DA}$	contribution of dowel action to the punching strength
$V_c$	strength associated with a given rotation and shear deformation
$V_{fc}$	punching strength associated with a given rotation (failure criterion)
$V_{flex}$	flexural strength of an isolated specimen
$V_{LR}$	punching force associated with given rotation (load-rotation relationship)
$V_R$	punching shear strength
$V_{R,calc}$	calculated punching shear strength
$V_{R,test}$	experimental punching shear strength

## Greek characters

### Lower Case

$\alpha$	angle between vertical axis and the displacement vector sum
$\alpha_\psi, \alpha_s, \alpha_T$	angle between vertical axis and vector of displacement due to rotation, shear deformation and combined effect (vector sum), respectively
$\alpha_c$	factor accounting for the brittleness of concrete on the $\varepsilon_3$ - $\sigma_3$ relationship
$\alpha_{cc}$	factor accounting for the brittleness of confined concrete on the $\varepsilon_3$ - $\sigma_3$ relationship
$\bar{\alpha}$	modified concrete brittleness factor
$\beta$	tangent angle of the critical shear crack
$\gamma$	angle between the crack surface and the displacements vector sum
$\gamma_0$	angle between critical shear crack and vector of displacement due to shear deformation at $z = 0$
$\gamma_\psi, \gamma_s, \gamma_T$	angle between critical shear crack and vector of displacement due to rotation, shear deformation and combined effect (vector sum), respectively
$\delta$	vector sum of the displacement normal and parallel to the crack face
$\delta_{s,R}$	sliding due to shear deformation at failure
$\delta_\psi, \delta_s, \delta_T$	sliding due to rotation, shear deformation and combined effect (vector sum), respectively
$\varepsilon_0$	reference strain
$\varepsilon_{1,sb}, \varepsilon_{3,sb}$	principal tensile and compressive radial strains in the shear band
$\varepsilon_{2,sb}$	tangential strain in the outer limit of the shear band
$\varepsilon_1, \varepsilon_2, \varepsilon_3$	strains in directions 1, 2 and 3, respectively
$\varepsilon_1^*$	imposed transverse tensile strain
$\varepsilon_{1,p}$	strain at the peak of the $\varepsilon_1$ - $\sigma_3$ relationship
$\varepsilon_{3,p}$	strain at the peak of the $\varepsilon_3$ - $\sigma_3$ relationship
$\bar{\varepsilon}_{3,p}$	modified peak strain
$\varepsilon_{1,c}$	strain of the $\varepsilon_1$ - $\sigma_3$ relationship corresponding to $\sigma_3 = 0.8 \cdot f_c$
$\varepsilon_{3,c}$	strain at the peak of the $\varepsilon_3$ - $\sigma_3$ relationship corresponding to $\sigma_3 = 0.8 \cdot f_c$
$\varepsilon_{3,p,eff}$	strain at the peak of the $\varepsilon_3$ - $\sigma_{3,eff}$ relationship accounting for the presence of imposed transverse strains
$\varepsilon_c$	concrete strain
$\varepsilon_{c0}$	strain at the beginning of the plastic plateau when considering an elastic-plastic behaviour of concrete
$\varepsilon_{c,r,top}, \varepsilon_{c,r,soffit}$	radial strain at the concrete top and bottom (soffit) surface of the slab
$\varepsilon_{n,sb}, \varepsilon_{t,sb}, \gamma_{nt,sb}$	normal, shear and distortional strains in the shear band, respectively (Figure 5.14)
$\varepsilon_s$	strain in the flexural reinforcement bars at $r_0$
$\varepsilon_y$	yielding strain of flexural reinforcement
$\eta_{fc}$	reduction factor accounting for the brittleness of concrete in compression
$\kappa_b$	factor accounting for the increase of the peak stress in the $\varepsilon_3 - \sigma_3$ due to biaxial compression
$\theta_{sb}$	direction of principal compressive strain
$\lambda$	thickness of the shear band
$\nu_c$	modulus of Poisson of concrete
$\xi$	efficiency factor accounting for orthogonal reinforcement
$\rho$	flexural reinforcement ratio
$\sigma_1, \sigma_2, \sigma_3$	principal stresses in directions 1, 2 and 3
$\sigma_{1,sb}, \sigma_{3,sb}$	principal tensile and compressive stresses in the shear band, respectively
$\sigma_{3,eff}$	effective concrete compressive strength
$\sigma_{lat}$	lateral confining pressure
$\sigma_s$	stress in the flexural reinforcement bars at $r_0$
$\sigma_{agg,0}, \tau_{agg,0}$	normal and shear stresses due to aggregate interlock engagement, respectively
$\sigma_{agg}, \tau_{agg}$	normal and shear stresses associated with aggregate interlock, respectively
$\sigma_{sb}, \tau_{sb}$	normal and shear stresses developing in the shear band, respectively
$\sigma_{fct}$	normal stress due to residual tensile strength
$\sigma_c$	concrete strain
$\sigma_t$	reduced tensile resistance of spalled concrete

$\tau_l$	shear stresses causing a flexural crack to become an inclined flexural crack governing the shape of the critical shear crack
$\phi$	diameter of the bar
$\varphi$	concrete friction angle
$\chi$	curvature
$\chi_r, \chi_t$	radial and tangential curvatures, respectively
$\chi_{cr}$	curvature at cracking
$\chi_1$	curvature at stabilizing cracking
$\chi_y$	curvature associated with yielding of the reinforcement
$\chi_{TS}$	reduction of curvature associated with tension-stiffening effect due to reinforcement bond
$\psi$	rotation of the slab
$\psi_{csc}$	rotation of the slab at the critical shear crack
$\psi_R$	rotation of the slab at failure

**Upper Case**

$\Delta$	displacement parallel to the CSC
$\Delta_\psi, \Delta_s, \Delta_T$	displacement parallel to the CSC due to rotation, shear deformation and combined effect (vector sum), respectively
$\bar{\Delta}$	normalized displacement parallel to the crack surface

**Acronyms**

CSCT	Critical Shear Crack Theory
CSC	critical shear crack
CR	centre of rotation

## 5.10 Appendix

### 5.10.1 Calculation of the depth of the neutral axis

This appendix describes the calculation of the height of the neutral axis due to tangential bending (calculated at  $r_0$  as  $\chi = \psi/r_0$  (Muttoni, 2008)). This calculation is performed in a similar manner as that proposed by Hallgren (1996). An elastic-plastic behaviour is adopted for both reinforcement and concrete (refer to Figure 5.23(a) and (b)). The uniaxial behaviour of concrete is considered to be entirely described by the modulus of elasticity ( $E_c$ ) and the uniaxial plastic concrete compressive strength ( $f_{cp} = f_c \cdot \eta_{fc}$ ), which is obtained by multiplying the concrete compressive strength measured in cylinders ( $f_c$ ) by the factor accounting for the brittleness of high-strength concrete ( $\eta_{fc}$ ) according to (Muttoni, 1990). The modulus of elasticity of concrete is calculated based on the value of the uniaxial concrete compressive strength measured in cylinders as proposed by Muttoni (2008):

$$E_c = 10'000 \cdot f_c^{1/3} \quad (5.49)$$

With respect to the elastic-plastic behaviour of the reinforcement, it is also described by its modulus of elasticity ( $E_s$ ) and the yield strength ( $f_y$ ). Different expressions to calculate the height of the neutral axis  $x$  result from the various potentially governing regimes (refer to Figure 5.23(c) to (f)):

1. Concrete and reinforcement in elastic regime ( $\chi \cdot x \leq \varepsilon_{c0}; \chi \cdot (d - x) \leq \varepsilon_y$ ):

$$x = d \cdot \rho \cdot n_E \cdot \left( \sqrt{1 + \frac{2}{\rho \cdot n_E} \cdot \left( 1 - \frac{n_p}{\rho \cdot n_E \cdot d^2 \cdot \chi \cdot E_c} \right)} - 1 \right) \quad (5.50)$$

2. Concrete in elastic regime and reinforcement in plastic regime ( $\chi \cdot x \leq \varepsilon_{c0}; \chi \cdot (d - x) \geq \varepsilon_y$ ):

$$x = \sqrt{\frac{2}{\chi \cdot E_c} \cdot (f_y \cdot \rho \cdot d - n_p)} \quad (5.51)$$

3. Concrete in elastic-plastic regime and reinforcement in elastic regime ( $\chi \cdot x \geq \varepsilon_{c0}; \chi \cdot (d - x) \leq \varepsilon_y$ ):

$$x = \frac{2 \cdot (\chi \cdot d)^2 \cdot n_E \cdot \rho + \varepsilon_{c0}^2 - 2 \cdot \chi \cdot \frac{n_p}{E_c}}{2 \cdot \chi^2 \cdot d \cdot n_E \cdot \rho + 2 \cdot \chi \cdot \varepsilon_{c0}} \quad (5.52)$$

4. Concrete in elastic-plastic regime and reinforcement in plastic regime ( $\chi \cdot x \geq \varepsilon_{c0}; \chi \cdot (d - x) \geq \varepsilon_y$ ):

$$x = \frac{\rho \cdot f_y \cdot d - n_p}{f_{cp}} + \frac{1}{2} \cdot \frac{\varepsilon_{c0}}{\chi} \quad (5.53)$$

where  $n_p$  is the normal force applied in the section,  $n_E = E_s/E_c$  is the ratio of the modulus of elasticity of reinforcement and concrete,  $\varepsilon_{c0} = f_{cp}/E_c$  and  $\varepsilon_y = f_y/E_s$ .

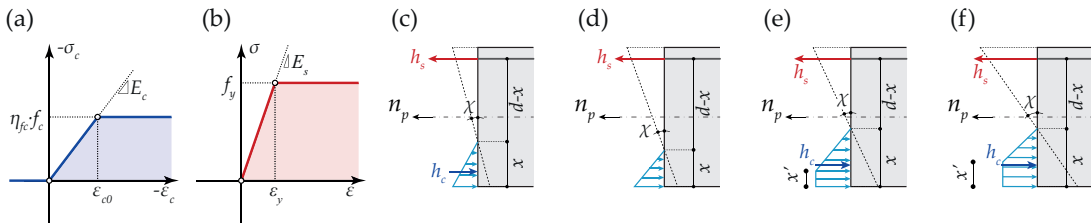


**Figure 5.23:** Calculation of the depth of the neutral axis  $x$  assuming and elastic-plastic behaviour of reinforcement and concrete: (a) uniaxial elastic-plastic behaviour of concrete; (b) uniaxial elastic-plastic behaviour of reinforcement; (c) elastic behaviour of both reinforcement and concrete; (d) elastic behaviour of concrete and plastic behaviour of reinforcement; (e) elastic behaviour of reinforcement and elastic-plastic behaviour of concrete; (f) plastic behaviour of reinforcement and elastic-plastic behaviour of concrete.

## 5.10.2 Constitutive relationships adopted for concrete

### 5.10.2.1 Triaxial behaviour of concrete according to Guidotti *et al.* (2011)

This appendix describes the calculation of the longitudinal stress ( $\sigma_3$ ) and transverse strain ( $\varepsilon_1$ ) of a concrete cylinder associated with a longitudinal strain ( $\varepsilon_3$ ) and confining pressure. For that purpose, the strain-stress relationship presented and experimentally validated by Guidotti *et al.* (2011) is used in this work. The formulae of the mentioned relationship are briefly described in the following (please refer to Guidotti *et al.* (2011) for further details).

According to the relationship proposed by Guidotti *et al.* (2011), the compressive stress  $\sigma_3$  is calculated as a function of the compressive strain  $\varepsilon_3$  as follows:

$$\sigma_3 = (\alpha_{cc} - 1) \cdot \frac{\varepsilon_3 \cdot E_{cc}}{\alpha_{cc} - 1 + \left(\frac{\varepsilon_3}{\varepsilon_{3,p}}\right)^{\alpha_{cc}}} \quad (5.54)$$

where  $E_{cc}$  refers to the modulus of elasticity of confined concrete and  $\varepsilon_{3,p}$  is the strain corresponding to the peak of the stress-strain relationship, whose values can be respectively computed as:

$$E_{cc} = \frac{E_c}{1 - 2 \cdot \nu_c \cdot \frac{\sigma_{lat}}{f_c}} \quad (5.55)$$

$$\varepsilon_{3,p} = -\frac{\alpha_{cc}}{\alpha_{cc} - 1} \cdot \frac{f_{cc}}{E_{cc}} \quad (5.56)$$

where,

$$\alpha_{cc} = \frac{\alpha_c + 40 \cdot \frac{\sigma_{lat}}{f_c}}{\zeta + \alpha_c \cdot (1 - \zeta) + 40 \cdot \frac{\sigma_{lat}}{f_c}} \quad (5.57)$$

$$\zeta = \frac{f_{cc}}{f_c} \cdot \frac{E_c}{E_{cc}} \quad (5.58)$$

$$\alpha_c = 1.5 + \frac{f_c}{75} + \frac{f_c^2}{4500} \quad \text{with } f_c \text{ in [MPa]} \quad (5.59)$$

with the  $\sigma_{lat}$  representing a lateral confining pressure,  $\nu_c$  representing the Poisson's coefficient (adopted equal to 0.2 in the linear elastic regime) and  $f_{cc}$  referring to the concrete compressive strength under confined conditions, which can be calculated based on a Mohr-Coulomb yield criterion as  $f_{cc} = f_c + k \cdot \sigma_{lat}$  with  $k = (1 + \sin(\varphi)) / (1 - \sin(\varphi)) \approx 4$  for a concrete friction angle of  $\varphi = 37^\circ$  (Nielsen and Hoang, 2011). Guidotti *et al.* (2011) also proposed formulae to calculate the transverse strain ( $\varepsilon_1$ ) associated with a given longitudinal strain ( $\varepsilon_3$ ):

$$\varepsilon_1 = \begin{cases} \nu_c \cdot \varepsilon_3 - \frac{\sigma_{lat}}{E_{cc}} \cdot (1 - \nu_c) & \text{if } \varepsilon_3 \leq \varepsilon_{3,c} \\ a_\varepsilon \cdot \varepsilon_3^2 + b_\varepsilon \cdot \varepsilon_3 + c_\varepsilon & \text{if } \varepsilon_3 > \varepsilon_{3,c} \end{cases} \quad (5.60)$$

where  $\varepsilon_{3,c} = \varepsilon_3(\sigma_3 = 0.8 \cdot f_c)$  represents the strain in the beginning of the nonlinear behaviour. The parameters  $a_\varepsilon$ ,  $b_\varepsilon$  and  $c_\varepsilon$  are obtained establishing a smooth transition between the phases and assuming that the lateral strain  $\varepsilon_1$  at the peak is obtained assuming a Poisson modulus of 0.5 (Guidotti *et al.*, 2011):

$$a_\varepsilon = \frac{\varepsilon_{1,p} - \varepsilon_{1,c} + \nu_c \cdot (\varepsilon_{3,c} - \varepsilon_{3,p})}{(\varepsilon_{3,p} - \varepsilon_{3,c})^2} \quad (5.61)$$

$$b_\varepsilon = \nu_c - 2 \cdot a_\varepsilon \cdot \varepsilon_{3,c} \quad (5.62)$$

$$c_\varepsilon = \varepsilon_{1,c} - a_\varepsilon \cdot \varepsilon_{3,c}^2 - b_\varepsilon \cdot \varepsilon_{3,c} \quad (5.63)$$

with  $\varepsilon_{1,c}$  referring to the transverse strain corresponding to a longitudinal stress of  $\sigma_3 = 0.8 \cdot f_c$ .

### 5.10.2.2 Strain-stress relationship adopted for concrete in the smeared cracking region

The strain-stress relationship proposed by Guidotti *et al.* (2011) is adopted in this work in order to calculate the stress  $\sigma_3$  in the smeared cracking region. As shown by Kupfer *et al.* (1969), the peak stress and the deformation capacity of concrete increase in the case of biaxial compression. As discussed in Section 5.4.5.3, the region with smeared cracking is subjected to tangential compression due to both flexural and shear deformations. For this reason, the stress-strain relationship adopted for this region has to account for an increased peak stress and associated deformation. In this work, it is considered that the stress-strain relationship of the region with smeared cracking corresponds to the one of a cylinder with a lateral confining pressure leading to a peak stress of  $\kappa_b \cdot f_c$  with  $\kappa_b = 1.1$  (see Section 5.4.5.3 for discussion on the value). With this respect, the formulae of Guidotti *et al.* (2011) are simplified in order to: (a) to include a single parameter ( $\kappa_b$ ) increasing the peak strength and deformation capacity of the  $\varepsilon_3$ - $\sigma_3$  relationship; and (b) to have a  $\varepsilon_1$ - $\varepsilon_3$  relationship given by a single function. Therefore, the  $\varepsilon_3$ - $\sigma_3$  relationship adopted in this work consists on the one of Guidotti *et al.* (2011) (Equation (5.54)) as follows:

$$\sigma_3 = (\bar{\alpha} - 1) \cdot \frac{\varepsilon_3 \cdot E_c}{\bar{\alpha} - 1 + \left(\frac{\varepsilon_3}{\bar{\varepsilon}_{3,p}}\right)^{\bar{\alpha}}} \quad (5.64)$$

where  $\bar{\varepsilon}_{3,p}$  is the modified peak strain and  $\bar{\alpha}$  is the modified brittleness factor of the strain-stress relationship. The modified peak strain can be obtained based on Eq. (5.56) considering  $f_{cc} = \kappa_b \cdot f_c$ ,  $E_{cc} \approx E_c$  (low confinement pressures) and  $\alpha_{cc} = \bar{\alpha}$  as:

$$\bar{\varepsilon}_{3,p} = \kappa_b \cdot \frac{\bar{\alpha}}{(\bar{\alpha} - 1)} \cdot \frac{f_c}{E_c} \quad (5.65)$$

The value of the modified brittleness factor  $\bar{\alpha}$  can be approximated from Eq. (5.57) for a constant value of the ratio  $f_{cc}/f_c = \kappa_b$  only as a function of the value of  $\alpha_c$ . In this case, for  $\kappa_b = 1.1$ , the value of  $\bar{\alpha}$  can be reasonably estimated as:

$$\bar{\alpha} = \frac{1 + \alpha_c}{2 - 0.05 \cdot \alpha_c} \quad (5.66)$$

with  $\alpha_c$  calculated according to Eq. 5.59.

With respect to the  $\varepsilon_1$ - $\varepsilon_3$  relationship, a satisfactory agreement can be found with the parabola proposed by Guidotti *et al.* (2011) in the range of strains of interest (descending branch of  $\varepsilon_1$ - $\sigma_3$  relationship) by considering the following third-degree parabola:

$$\varepsilon_1 = 0.5 \cdot \frac{\varepsilon_3^3}{\varepsilon_0 \cdot \bar{\varepsilon}_{3,p}} \quad (5.67)$$

where  $\varepsilon_0$  refers to a reference strain taken equal to 0.0045 (fitting parameter to approximate the numerical results of Guidotti *et al.* (2011) for the case of  $f_{cc}/f_c = \kappa_b = 1.1$ ).

### 5.10.2.3 Calculation of $\varepsilon_{3, sb} - \sigma_{3, sb}$ relationship accounting for imposed transverse strains

In the case where the imposed transverse tensile strain in the shear band  $\varepsilon_{1, sb}$  does not exceed the transverse strain corresponding to the peak of the  $\varepsilon_1 - \sigma_3$  relationship ( $\bar{\varepsilon}_{1, p}$ , back calculated with Eq.(5.67) and  $\varepsilon_3 = \bar{\varepsilon}_{3, p}$ ), it is assumed that any effect of strain softening occurs. In this case, the  $\varepsilon_{3, sb} - \sigma_{3, sb}$  relationship is assumed to be equal to the  $\varepsilon_3 - \sigma_3$  relationship.

On the other hand, if the imposed transverse tensile strain in the shear band  $\varepsilon_{1, sb}$  exceeds the transverse strain expected at the peak of the  $\varepsilon_1 - \sigma_3$  relationship ( $\bar{\varepsilon}_{1, p}$ ), the peak stress  $\kappa_b \cdot f_c$  is replaced by an effective concrete compressive strength  $f_{c, eff}$ . The value of  $f_{c, eff}$  corresponds to the value of the stress  $\sigma_3$  obtained introducing the value of the imposed strain  $\varepsilon_{1, sb}$  in the strain-stress  $\varepsilon_1 - \sigma_3$  relationship.

On that basis, the  $\varepsilon_{3, sb} - \sigma_{3, sb}$  relationship can be mathematically computed in a general manner as follows:

$$\sigma_{3, sb} = (\bar{\alpha} - 1) \cdot \frac{\varepsilon_{3, sb} \cdot E_{c, eff}}{\bar{\alpha} - 1 + \left( \frac{\varepsilon_{3, sb}}{\varepsilon_{3, p, eff}} \right)^{\bar{\alpha}}} \quad (5.68)$$

where the effective peak strain  $\varepsilon_{3, p, eff}$  and the effective modulus of elasticity of the concrete  $E_{c, eff}$  are calculated as a function of the value of the imposed transverse tensile strain ( $\varepsilon_{1, sb}$ ). The effective peak strain is calculated with Eq. (5.67) by knowing that the point  $(\varepsilon_1, \varepsilon_3) = (\varepsilon_{1, sb}, \varepsilon_{3, p, eff})$ :

$$\varepsilon_{3, p, eff} = \begin{cases} \bar{\varepsilon}_{3, p} & \text{if } \varepsilon_{1, sb} \leq \bar{\varepsilon}_{1, p} \\ \sqrt[3]{2 \cdot \varepsilon_0 \cdot \bar{\varepsilon}_{3, p} \cdot \varepsilon_{1, sb}} & \text{if } \varepsilon_{1, sb} > \bar{\varepsilon}_{1, p} \end{cases} \quad (5.69)$$

The effective modulus of elasticity of the concrete is calculated with Eq. (5.68) knowing that the curve passes through the point with coordinates at the peak  $(\varepsilon_{3, p, eff}, f_{c, eff})$ :

$$E_{c, eff} = \begin{cases} E_c & \text{if } \varepsilon_{1, sb} \leq \bar{\varepsilon}_{1, p} \\ \frac{\bar{\alpha}}{\bar{\alpha} - 1} \cdot \frac{f_{c, eff}}{\varepsilon_{c, eff}} & \text{if } \varepsilon_{1, sb} > \bar{\varepsilon}_{1, p} \end{cases} \quad (5.70)$$

where  $f_{c, eff}$  is calculated by replacing  $\varepsilon_{3, p, eff}$  directly in Eq. (5.60):

$$f_{c, eff} = (\bar{\alpha} - 1) \cdot \frac{\varepsilon_{3, p, eff} \cdot E_c}{\bar{\alpha} - 1 + \left( \frac{\varepsilon_{3, p, eff}}{\bar{\varepsilon}_{3, p}} \right)^{\bar{\alpha}}} \quad (5.71)$$

### 5.10.3 Load-rotation relationship according to Muttoni (2008)

As previously described, the punching shear strength and associated deformation capacity calculated in this work are given by the intersection of the load-rotation relationship with the refined failure criterion. The calculation of the latter is described in detail in Section 5.4.

The calculation of the load-rotation relationship of slender slabs in Chapters 4 and 5 was performed as proposed by Muttoni (2008) for isolated axisymmetric specimens. The calculation of the load-rotation relationship and the corresponding main assumptions are briefly described in the following based on the work of Muttoni (2008).

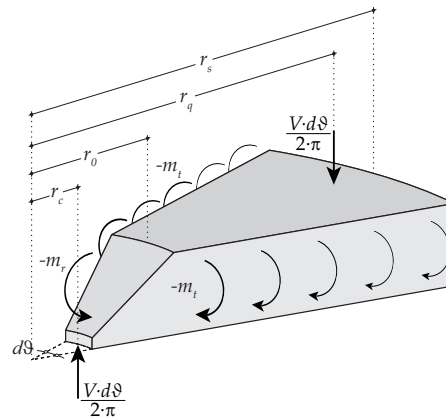


Figure 5.24: Equilibrium of a slab sector with the acting vertical loads and radial and tangential moments; figure adapted from Muttoni (2008).

The load-rotation relationship can be calculated on the basis of the equilibrium of a slab sector (refer to Figure 5.26) which can be written in a general manner as:

$$V \cdot \frac{d\theta}{2 \cdot \pi} \cdot (r_q - r_c) = -m_r \cdot d\theta \cdot r_0 - d\theta \cdot \int_{r_0}^{r_s} m_t \cdot dr \quad (5.72)$$

The radial and tangential moments (resulting from the couple of forces given by the tension in the reinforcement and compression in the concrete) acting in the slab sector for a given rotation are a function of the kinematics of the slab and of the moment-curvature relationship of the reinforced concrete section. With respect to the kinematics, Muttoni (2008) considered that (Figure 5.25): (i) inner and outer portions of the slab are divided by a critical shear crack located at  $r_0 = r_c + d$  at the level of the flexural reinforcement; (ii) as the tangential cracks concentrate in the vicinity of the column, radial curvature is negligible in the outer portion of the slab; (iii) as the vertical load in the column is equilibrated by an inclined concrete strut, strains in the flexural reinforcement in the inner portion of the slab are constant. Based on the previously mentioned observations, Muttoni (2008) considered that the inner and outer portion of the slab deform respectively in a spherical and conical shape (consistently with Kinunen and Nylander (1960)). As a result, radial and tangential curvatures inside the critical shear crack (located at  $r = r_0$ ) are equal and their value at  $r = r_0$  is given by:

$$\chi_r = \chi_t = -\frac{\psi}{r_0} \quad (5.73)$$

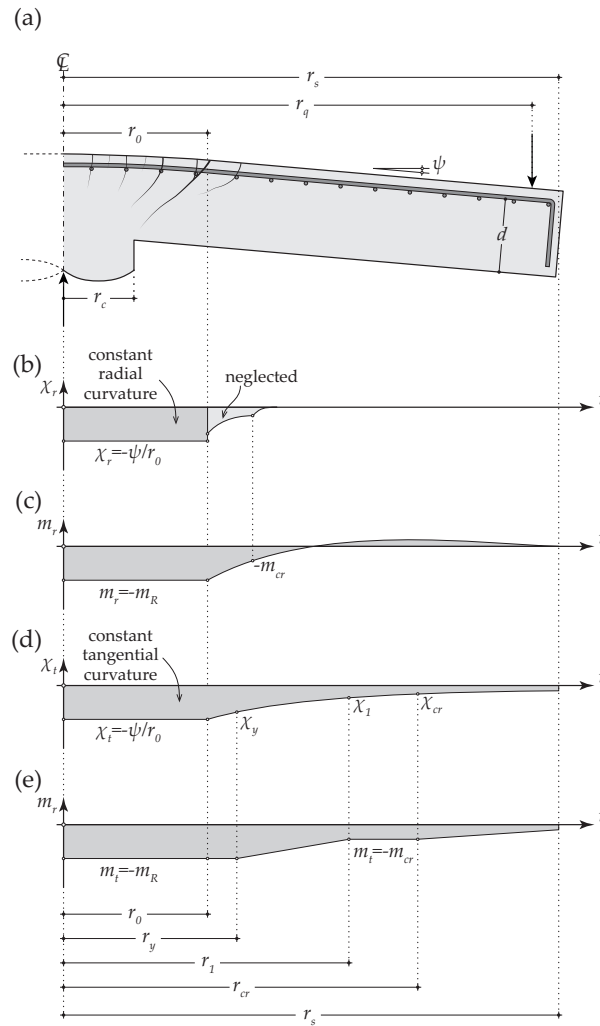


**Figure 5.25:** Calculation of load-rotation relationship of an axisymmetric slab according to Muttoni (2008): (a) slab in deformed position and associated geometrical parameters; (b) radial curvature along the radial coordinate; (c) radial moment along the radial coordinate; (d) tangential curvature along radial coordinate; (e) tangential moment along radial coordinate; figure adapted from Muttoni (2008).

Based on the considered conical deformation of the outer portion of the slab, the tangential curvature at a given radial location can be computed as follows:

$$\chi_t = -\frac{\psi}{r} \quad (5.74)$$

To calculate the acting moment associated with a given curvature, Muttoni (2008) proposed a quadri-linear moment-curvature relationship with (refer to Figure 5.26(a)): (i) an uncracked linear-elastic behaviour; (ii) cracking plateau; (iii) cracked linear-elastic behaviour accounting for tension-stiffening and (iv) yielding of flexural reinforcement (plastic moment capacity). This quadri-linear relationship is fully defined by the uncracked stiffness ( $EI_0$ ), cracked stiffness ( $EI_1$ ), cracking moment ( $m_{cr}$ ), plastic moment capacity ( $m_R$ ) and differential of curvature due to tension-stiffening effect  $\chi_{TS}$ . The uncracked stiffness and the cracking moment may be calculated in a simple manner by neglecting the effect of reinforcement before cracking as:

$$m_{cr} = \frac{h^2}{6} \cdot f_{ct} \quad (5.75)$$

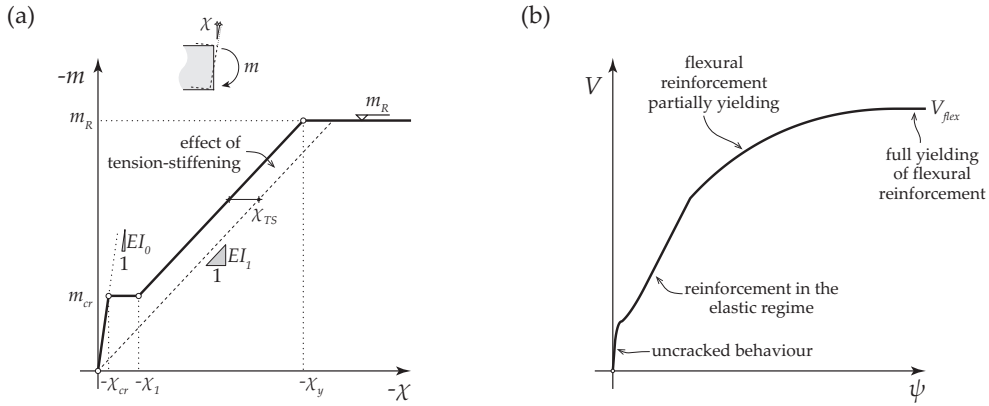


Figure 5.26: (a) Quadri-linear moment-curvature relationship proposed by Muttoni (2008); (b) calculated load-rotation relationship according to Muttoni (2008) and indication of the resulting regimes (Fernández Ruiz and Muttoni, 2017).

$$EI_0 = \frac{E_c \cdot h^3}{12} \quad (5.76)$$

The cracked stiffness can be calculated by considering a linear-elastic behaviour for both concrete and reinforcement (Muttoni, 2008):

$$EI_1 = \rho \cdot \zeta \cdot E_s \cdot d^3 \cdot \left(1 - \frac{x_{el}}{d}\right) \cdot \left(1 - \frac{x_{el}}{3 \cdot d}\right) \quad (5.77)$$

where  $x_{el}$  refers to the depth of the compression zone assuming an linear-elastic behaviour of both concrete and reinforcement:

$$x_{el} = \rho \cdot \zeta \cdot \frac{E_s}{E_c} \cdot d \cdot \left(\sqrt{1 + \frac{2 \cdot E_c}{\rho \cdot \zeta \cdot E_s}} - 1\right) \quad (5.78)$$

with  $\zeta$  representing a efficiency factor accounting for the fact that orthogonal reinforcement presents a reduced stiffness compared to reinforcement placed in radial and tangential directions (as considered in this axisymmetric model). As introduced in Section 5.10.1, Muttoni (2008) suggested a value of  $\zeta = 0.6$  for this factor (used in this work). Regarding the moment capacity, it can be calculated adopting a perfectly plastic behaviour of both reinforcement and concrete and by neglecting the influence of reinforcement in the compression zone:

$$m_R = \rho \cdot f_y \cdot d^2 \cdot \left(1 - \frac{\rho \cdot f_y}{2 \cdot \eta_{fc} \cdot f_c}\right) \quad (5.79)$$

where the factor  $\eta_{fc}$  accounts for the brittleness of concrete in compression (a stress  $\eta_{fc} \cdot f_c$  is adopted for the rectangular stress block) and is calculated as  $\eta_{fc} = (30/f_c)^{1/3} \leq 1$  Muttoni (1990). Muttoni (2008) suggested that tension stiffening effects may be accounted by adopting a constant decrease in the curvature given by:

$$\chi_{TS} = \frac{f_{ct}}{\rho \cdot \zeta \cdot E_s} \cdot \frac{1}{6 \cdot h} \quad (5.80)$$

The curvature at crack ( $\chi_{cr}$ ), at the beginning of stabilized cracking ( $\chi_1$ ) and at yielding of the flexural reinforcement ( $\chi_y$ ) are thus calculated as follows (Muttoni, 2008):

$$-\chi_{cr} = \frac{m_{cr}}{EI_0} = \frac{2 \cdot f_{ct}}{E_c \cdot h} \quad (5.81)$$

$$-\chi_1 = \frac{m_{cr}}{EI_1} - \chi_{TS} \quad (5.82)$$

$$-\chi_y = \frac{m_R}{EI_1} - \chi_{TS} \quad (5.83)$$

Finally, a closed-form solution of the applied load  $V$  as a function of the rotation  $\psi$  can be obtained based on Eq. (5.72) by considering the previously introduced deformation shape (spherical inside the critical shear crack and conical outside; curvatures given by Eqs. (5.73) and (5.74)) and the quadri-linear moment curvature relationship as (Muttoni, 2008):

$$V = \frac{2 \cdot \pi}{r_q - r_c} \cdot \left( \begin{array}{l} -m_r \cdot r_0 + m_R \cdot \langle r_y - r_0 \rangle + EI_1 \cdot \psi \cdot \langle \ln(r_1) - \ln(r_y) \rangle + \\ EI_1 \cdot \chi_{TS} \cdot \langle r_1 - r_y \rangle + m_{cr} \cdot \langle r_{cr} - r_1 \rangle + EI_0 \cdot \psi \cdot \langle \ln(r_s) - \ln(r_{cr}) \rangle \end{array} \right) \quad (5.84)$$

where  $\langle \Delta r \rangle$  is equal to zero when  $\Delta r < 0$ ,  $r_{cr}$ ,  $r_1$  and  $r_y$  are the radii defining the extents of the regions where concrete is cracked, cracks are stable and reinforcement is yielding, respectively. Their values can be calculated based on the rotation and corresponding curvatures:

$$r_{cr} = -\frac{\psi}{\chi_{cr}} = \frac{\psi \cdot EI_0}{m_{cr}} \leq r_s \quad (5.85)$$

$$r_1 = -\frac{\psi}{\chi_1} = \frac{\psi}{\frac{m_{cr}}{EI_1} - \chi_{TS}} \leq r_s \quad (5.86)$$

$$r_y = -\frac{\psi}{\chi_y} = \frac{\psi}{\frac{m_R}{EI_1} - \chi_{TS}} \leq r_s \quad (5.87)$$

Figure 5.26(b) shows an example of a calculated load-rotation relationship, where the different regimes where a punching failure can occur are indicated (Guandalini *et al.*, 2009; Fernández Ruiz and Muttoni, 2017): flexural reinforcement in the elastic regime; flexural reinforcement partly yielded and full yielding of flexural reinforcement. In the latter case ( $r_y = r_s$  with Eq. (5.87)), the applied load ( $V$ ) corresponds to the flexural capacity ( $V_{flex}$ ) of an isolated axisymmetric element, which is given by:

$$V_{flex} = \frac{2 \cdot \pi \cdot r_s}{r_q - r_c} \cdot m_R \quad (5.88)$$

### 5.10.4 Numerical procedure to calculate the punching shear strength

The numerical calculation of the punching strength according to the refined mechanical model presented in this chapter can be performed following different procedures. One possibility is shown in Figure 5.27 and consists on the following steps:

1. Calculation of the load-rotation relationship ( $\psi - V_{LR}$ ) describing the response of the slab-column connection in a wide range of rotations  $[0; \psi_{final}]$  (performed in this work following the approach proposed by Muttoni (2008), see Section 5.10.3);
2. Calculation of the punching shear strength associated with different values of the rotation. For a given value of the rotation  $\psi_k$ :
  - 2.1. Calculation of the value of  $r_{0,k}$  function of the acting shear force  $V_{LR,k}$  (associated with the rotation  $\psi_k$  based on the load-rotation relationship) with Eqs. (5.3) and (5.4);
  - 2.2. Calculation of the depth of the neutral axis  $x_k$  at  $r_{0,k}$  with Eqs. (5.50) to (5.53);
  - 2.3. Definition of the location of the centre of rotation associated with flexural deformations at  $(r_{CR}, z_{CR}) = (r_c, x)$ ;
  - 2.4. Calculation of the rotation localized at the critical shear crack  $\psi_{csc}$  with Eqs. (5.5) and (5.6);
  - 2.5. Calculation of the shape of the critical shear crack with Eq. (5.2);
  - 2.6. Vary incrementally the value of  $\delta_s$  in a wide range of values  $[0; \delta_{final}]$ . Repetition of the following steps for each value of  $\delta_{s,j}$  (light gray box in Figure 5.27):
    - 2.6.1. Calculation of the displacement field along the CSC associated with the vector sum of the flexural and shear deformations based on Eqs. (5.17) to (5.18);
    - 2.6.2. Calculation of the vertical coordinate corresponding to the transition between smeared and localized cracking (Eq. (5.21));
    - 2.6.3. Calculation of the normal and shear stresses along the region of the CSC with a localized cracking response based on Eqs. (5.22) and (5.23);
    - 2.6.4. Calculation of the normal and shear stresses along the region of the CSC with a smeared cracking response based on Eqs. (5.35) and (5.36);
    - 2.6.5. Calculation of the dowelling action of the flexural reinforcement (Eq. (5.45));
    - 2.6.6. Calculation of the punching strength associated with the rotation  $\psi_k$  and shear deformation  $\delta_{s,j}$  by summing the different contributions ( $V_{c,k,j}$  with Eq. (5.46));
  - 2.7. Calculation of the punching shear strength associated with  $\psi_k$  as the  $V_{fc,k} = \max(V_{c,k,j})$ . This is justified by the assumption that the critical shear crack forms due to the flexural behaviour and thereafter starts sliding until reaching the maximum strength;
  - 2.8. Calculation of the punching strength  $V_R$  and deformation capacity  $(\psi_R, \delta_{s,R})$  by intersection of the load-rotation relationship  $\psi - V_{LR}$  and the failure criterion  $\psi - V_{fc}$ . It is important to note that the calculated failure criterion as previously described is only valid at the intersection with the load-rotation relationship  $(\psi_R, V_R)$  as only at this rotation the value of  $r_0$  (Eqs. (5.3) and (5.4)) is calculated with the value of  $V_{LR} = V_R$ .

It is important to note that the part of the numerical procedure inside the light gray box of Figure 5.27 consists on the calculation of the punching strength for a given rotation concentrated at the CSC ( $\psi_{csc}$ ) considering a given location of the CSC at the level of the flexural reinforcement ( $r_0$ ). The procedure (inside the light gray box) is thus based on the theoretical principles of the CSCT by calculating a shape of the CSCT, the displacement field and the associated internal stresses along it.

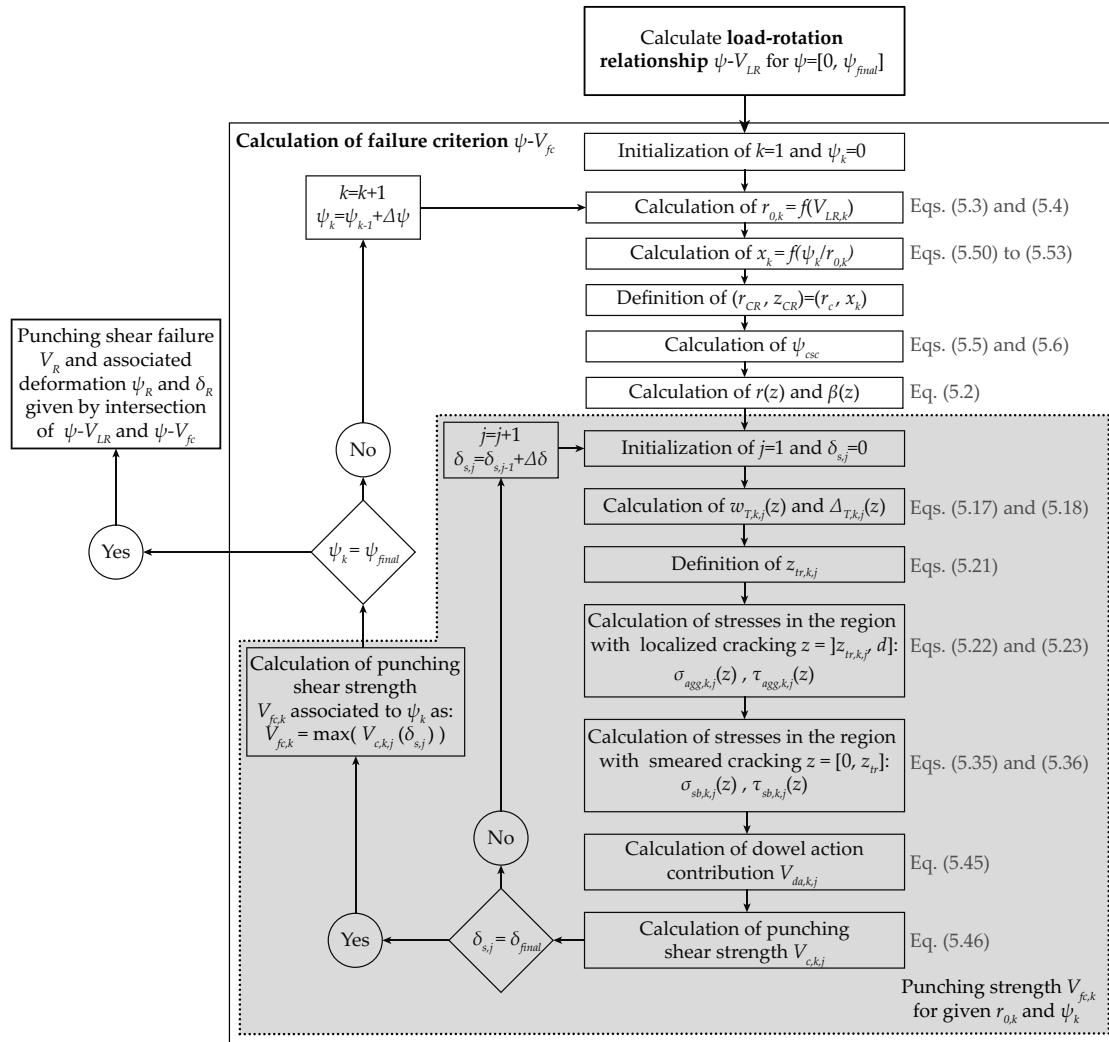


Figure 5.27: Numerical procedure followed to calculate the punching shear strength and associated deformation capacity.



# Chapter 6

## **A discussion on the extension of the mechanical model for punching failures of prestressed slabs and footings**

This chapter was prepared by João Tiago Simões and compiles an additional work which is not included in none of the journal articles composing the previous chapters. This chapter discusses the extension of the refined mechanical model presented in *Chapter 5* to prestressed slabs and reinforced concrete footings.

### **6.1 Introduction**

It is widely recognized that one of the significant advantages of a mechanical model with respect to the empirically based equations is their possible extension to other cases than those initially investigated. In that regard, this chapter presents a discussion on the extension of the mechanical model presented in *Chapter 5* for the cases of prestressed slabs and reinforced concrete footings. An exhaustive review of other existing models for prestressed slabs and footings, as well as their validation and comparison with databases is out of the scope of this chapter. This chapter aims only at showing that the mechanical model presented in *Chapter 5*, which is based on the theoretical principles of the Critical Shear Crack Theory (CSCT), is general enough to be extended to other cases such as prestressed slabs and reinforced concrete footings.

This chapter is divided in three sections and presents some preliminary results of a work under development. In the first section, a potential extension of the mechanical model to deal with the case of prestressed slabs is discussed and a brief comparison against experimental results is shown. The second section presents a possible extension of the mechanical model for punching shear failures of reinforced concrete footings, together with a comparison of the theoretical results against a database and selected series of experimental tests. Finally, the third section summarizes the main conclusions.

## 6.2 Potential extension of the mechanical model to prestressed slabs

### 6.2.1 Introduction

The punching shear strength of prestressed reinforced concrete slabs has been the object of numerous studies along the last decades (e.g. Kinnunen *et al.*, 1977; Regan and Braestrup, 1985; *fib*, 2001; Ramos, 2003; Silva *et al.*, 2005, 2007; Ramos *et al.*, 2011; Clément, 2012; Ramos *et al.*, 2014; Clément *et al.*, 2014). The influence of in-plane and deviation forces as well as moments due to prestressing has been experimentally investigated and some theoretical approaches have been proposed (e.g. Regan and Braestrup, 1985; *fib*, 2001; Silva, 2005; Silva *et al.*, 2005, 2007; Ramos *et al.*, 2011; Clément, 2012; Ramos *et al.*, 2014; Clément *et al.*, 2014). With respect to the punching shear verification according to codes of practice (e.g. Eurocode 2, 2004), they tend to treat this case on an empirical basis, normally allowing for an increase of the punching strength as a function of the in-plane stresses and a deduction of the deviation forces inside the control perimeter (e.g. Ramos, 2003; Silva *et al.*, 2007; Ramos *et al.*, 2011; Clément *et al.*, 2014; Ramos *et al.*, 2014). Detailed descriptions of the experimental programmes focusing on this topic, available analytical models as well as an evaluation of the suitability of the codes of practice to calculate the punching strength of prestressed slab-column connections is not an objective of the present document (works dealing with these issues have been recently published by, among others, Silva (2005), Silva *et al.* (2007), Clément (2012), Clément *et al.* (2013), Clément *et al.* (2014), and Ramos *et al.* (2014)). This section aims only at discussing the potential of the mechanical model presented in *Chapter 5* (calculation of a refined failure criterion) to be applied to investigate the punching shear failures of prestressed slabs.

As discussed in the previous chapters (refer also to Muttoni *et al.* (2017)), the calculation of the punching shear strength and associated deformation capacity of a slab-column connection in the framework of the CSCT is performed determining the intersection of a suitable load-rotation relationship (relating the applied load and the crack opening) with the failure criterion (representing the maximum shear force that can be carried for a given crack opening), refer to Figure 6.1 (Muttoni, 2008; Clément *et al.*, 2014). In this section, the punching strength will be calculated using the load-rotation relationship of prestressed slabs proposed by Clément *et al.* (2014) and the failure criterion calculated according to the mechanical model of *Chapter 5*.

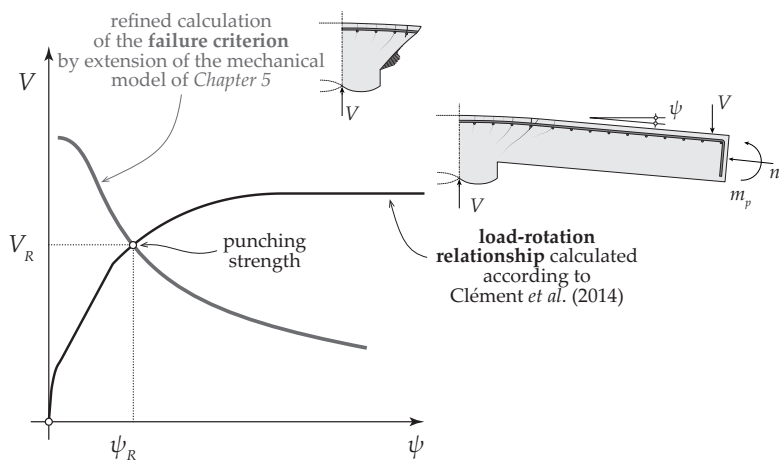


**Figure 6.1:** Punching failures of prestressed slabs without transverse reinforcement according to the principles of the CSCT (Muttoni, 2008; Clément *et al.*, 2014; Muttoni *et al.*, 2017): calculation of the punching strength by intersecting the load-rotation relationship proposed by Clément *et al.* (2014) with the refined failure criterion calculated on the basis of the model presented in *Chapter 5*.

As mentioned in *Chapter 5*, the mechanical model presented in this thesis may be considered as an enhancement of the model previously developed by Clément (2012), who also proposed the calculation of a refined failure criterion for prestressed slabs based on the principles of the CSCT. With respect to the mentioned work, the mechanical model presented in this document differs on the calculation of the refined failure criterion by (Simões *et al.*, 2018):

- considering of a continuous displacement field along the critical shear crack (CSC);
- considering the shape of the CSC to be a function of an acting nominal shear stress (based on cracking development, see Section 5.3) and in-plane stresses;
- including different assumptions to define the location of the centre of rotation associated with the flexural deformations (at the edge of the column and at the height of the neutral axis, which is calculated adopting a linear elastic-plastic behaviour of the reinforcement and concrete);
- defining the extents of the regions with different phenomenological behaviours along the CSC as a function of the crack shape and displacement field along the CSC (based on experimental measurements at the material level by Jacobsen *et al.* (2012));
- enabling a realistic calculation of the strain and stress states along the entire extent of the CSC, including the region of the CSC with a smeared cracking behaviour;
- considering different fundamental material laws for the aggregate interlock engagement stresses (Cavagnis *et al.* (2017) instead Guidotti (2010)) and smeared cracking region;
- being based on a general theoretical framework, which is applicable to a wide range of cases (including slabs with and without in-plane forces as well as footings).

The calculation of the load-rotation relationship proposed by Clément *et al.* (2014) is briefly presented in Section 6.2.2. The influence of the in-plane forces in the calculation of the refined failure criterion according to the mechanical model of *Chapter 5* is discussed in Section 6.2.3. Finally, a comparison of the mechanical model against the experimental results of Clément *et al.* (2014) is shown.

## 6.2.2 Load-rotation relationship of prestressed slabs according to Clément *et al.* (2014)

As discussed by Clément *et al.* (2014), the calculation of the load-rotation relationship of a prestressed slab has to account for the effects of prestressing on the equilibrium of the slab sector and on the moment-curvature relationship. As also explained by the mentioned authors, two different approaches may be followed to deal with these effects. On the one hand, effects of prestressing may be considered as an auto-equilibrated state of stresses. On the other hand, a set of equivalent forces replacing the effects of prestressing (anchorage and deviation forces) may be considered as external loads, still accounting for an additional reinforcement which is a function of the prestressing level (Clément *et al.*, 2014). The easiness of each approach depends upon the situation, but both approaches lead evidently to an equivalent result (Clément *et al.*, 2014).

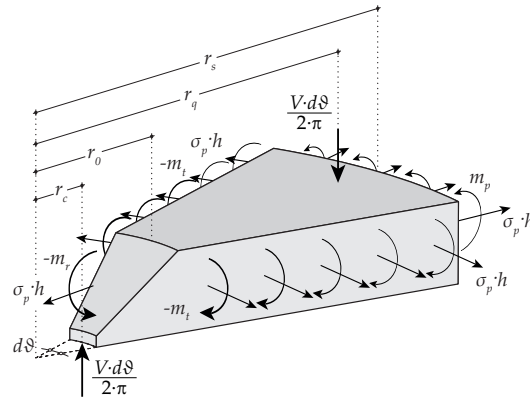
In this work, the calculation of the load-rotation relationship of prestressed slabs is performed as proposed by Clément *et al.* (2014), who have considered the effects of prestressing as a set of equivalent forces. The calculation of this relationship is briefly described in the following based on the work of Clément *et al.* (2014), which should be consulted for further details.

Figure 6.2 shows a slab sector with the applied vertical load ( $V$ ), radial ( $m_r$ ) and tangential ( $m_t$ ) moments as well as in-plane forces ( $\sigma_p \cdot h$ ) and moments ( $m_p$ ) due to prestressing effects. The equilibrium of

moments in the slab sector yields (Clément *et al.*, 2014):

$$V \cdot \frac{d\vartheta}{2 \cdot \pi} \cdot (r_q - r_c) = -m_r \cdot d\vartheta \cdot r_0 - d\vartheta \cdot \int_{r_0}^{r_s} m_t \cdot dr + m_p \cdot r_m \quad (6.1)$$

where  $r_c$  is the column radius,  $r_s$  is the radius of the slab,  $r_q$  is the radial distance between the axis of the column and the location of the resultant of the vertical applied load,  $r_0$  refers to the radial distance between the axis of the column and the location of the inclined surface dividing the inner and outer portions of the slab at the level of the flexural reinforcement,  $r_m$  is the radial location where the moment due to prestressing effects is acting. An analytical integration of Eq. (6.1) can be obtained (for instance, as performed by Muttoni (2008)) provided that some hypotheses are adopted for the kinematics of the slab and sectional response (moment-curvature relationship).



**Figure 6.2:** Equilibrium of a slab sector with the acting vertical loads, in-plane forces and moments due to prestressing effects, radial and tangential moments (normal tension positive in the adopted sign convention; figure adapted from Clément *et al.* (2014)).

With respect to the kinematics of the slab, similarly to Kinnunen and Nylander (1960) and Muttoni (2008), Clément *et al.* (2014) considered that an inclined shear crack develops (at  $r_0 = r_c + d$  at the level of the flexural reinforcement) and separates the inner and outer portions of the slab, whose deformations follow respectively a spherical and a conical shapes. It thus results that the radial and tangential curvatures for  $r \leq r_0$  are equal to  $\chi_r = \chi_t = -\psi/r_0$ , while the tangential curvature in the outer portion of the slab is given by  $\chi_t = -\psi/r$ .

Regarding the sectional response, Clément *et al.* (2014) proposed a simplified multi-linear moment-curvature relationship including the effect of in-plane stresses. As shown in Figure 6.3(a), this relationship is characterized by a linear elastic uncracked response of the concrete, cracking plateau (which may not develop for large in-plane compressive stresses), linear elastic cracked response of the section and moment capacity. From a mathematical point of view, this relationship is a function of the cracking moment ( $m_{cr}$ ), moment capacity ( $m_R$ ), uncracked stiffness ( $EI_0$ ), cracked stiffness ( $EI_1$ ), curvature reduction associated with tension stiffening ( $\chi_{TS}$ ) and, eventually, the variation of curvature accounting for the effect of normal stresses ( $\Delta\chi_N$ ). The cracking moment and the corresponding curvature can be calculated neglecting the effect of reinforcement as follows:

$$m_{cr} = \frac{h^2}{6} \cdot (f_{ct} - \sigma_p) \quad (6.2)$$

$$-\chi_{cr} = \frac{m_{cr}}{EI_0} = \frac{2}{E_c \cdot h} \cdot (f_{ct} - \sigma_p) \quad (6.3)$$

where the stiffness of the uncracked section  $EI_0$  is calculated with Eq. (5.76),  $f_{ct}$  is the concrete tensile strength,  $E_c$  is the modulus of elasticity of concrete,  $h$  is the height of the section and  $\sigma_p$  is the in-plane stress (tension positive). In the phase of stabilized cracking, two different effects have to be considered. The first refers to the tension stiffening effect due to the reinforcement bond, which, according to Muttoni (2008), can be accounted by reducing the curvature by a constant value  $\chi_{TS}$  (Eq. (5.80)). The second effect influencing the stiffness of the response in the cracked phase results from the presence of in-plane stresses (Clément *et al.*, 2014). As discussed by Clément *et al.* (2014), the depth of the compression zone in the presence of in-plane stresses can be calculated by solving a non-linear equation, provided that a linear-elastic behaviour is adopted for the reinforcement and concrete. However, a simplified formulation to consider such effect was proposed by Clément *et al.* (2014). It consists on neglecting the change of the depth of the compression zone due to the in-plane stresses (calculation of cracked stiffness ( $EI_1$ ) and height of the compression zone ( $x_{el}$ ) with Eqs. (5.77) and (5.78), respectively) but considering an additional variation of the curvature according to the following expression (see Clément *et al.* (2014) for complete derivation):

$$\Delta\chi_N = -\frac{n_p}{(d - x_{el}/3)^2} \cdot \left( \frac{h/2 - x_{el}/3}{\rho \cdot d \cdot \xi \cdot E_s} - \frac{2 \cdot (d - h/2)}{x_{el} \cdot E_c} \right) \quad (6.4)$$

where  $\rho$  is the flexural reinforcement ratio,  $E_s$  is the modulus of elasticity of the reinforcement,  $\xi$  represents the reduction factor accounting for the reduced stiffness of flexural reinforcement placed orthogonally with respect to reinforcement placed in radial and tangential directions, and  $n_p$  refers to the in-plane force. The curvature at the end of the cracking plateau is given by:

$$-\chi_1 = \frac{m_{cr}}{EI_1} - \chi_{TS} - \Delta\chi_N < \chi_{cr} \quad (6.5)$$

The development of a cracking plateau is a function of the level of in-plane compressive stresses. For large values of this variable, the cracking plateau does not occur ( $\chi_{cr} \geq \chi_1$ ) and the tension stiffening effect associated with the normal force is governed by the condition  $\chi_1 = \chi_{cr}$ :

$$\Delta\chi_N = \frac{m_{cr}}{EI_1} - \frac{m_{cr}}{EI_0} - \chi_{TS} \quad (6.6)$$

The moment capacity can be calculated adopting a plastic behaviour of the reinforcement and concrete and still accounting for the presence of in-plane stresses as:

$$m_R = \rho \cdot d \cdot f_y \cdot \left( d - \frac{h}{2} \right) + f_{cp} \cdot x_{pl} \cdot \left( \frac{h}{2} - \frac{x_{pl}}{2} \right) \quad (6.7)$$

with  $x_{pl}$  representing the depth of the plastic compression zone, which is calculated as follows (neglecting again the influence of compression reinforcement):

$$x_{pl} = \frac{\rho \cdot d \cdot f_y - \sigma_p \cdot h}{f_{cp}} \quad (6.8)$$

where the factor  $\eta_{fc}$  considers the brittle behaviour of concrete in compression (calculated according to Muttoni (1990) and *fib* Model Code 2010 (2013)). The curvature defining the transition between the cracked phase and plastic strength  $\chi_y$  is given by the following expression:

$$-\chi_y = \frac{m_R}{EI_1} - \chi_{TS} - \Delta\chi_N \quad (6.9)$$

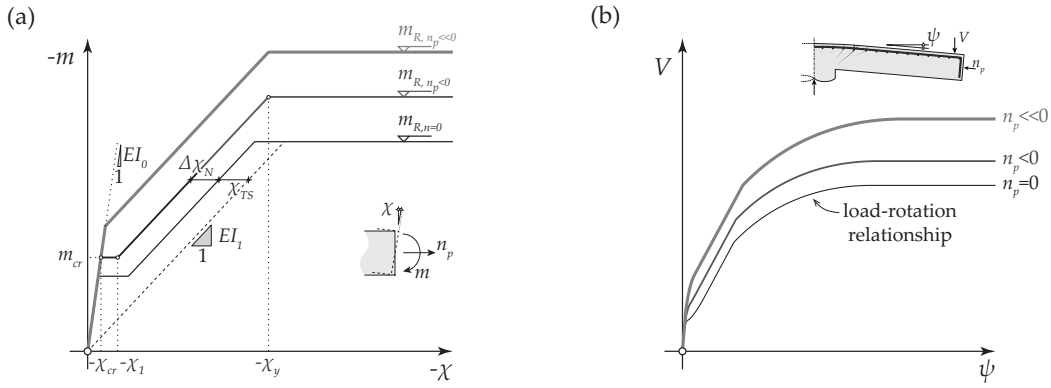


**Figure 6.3:** Calculation of load-rotation relationship accounting for in-plane forces according to Clément *et al.* (2014): (a) multi-linear moment-curvature relationship proposed; (b) influence of in-plane forces in the calculated load-rotation relationship.

Eventually, a closed-form solution of Eq. (6.1) can be obtained by analytical integration based on the adopted kinematics and on the multi-linear moment-curvature relationship (Clément *et al.*, 2014):

$$V = \frac{2 \cdot \pi}{r_q - r_c} \cdot \left( -m_r \cdot r_0 + m_R \cdot \langle r_y - r_0 \rangle + EI_1 \cdot \psi \cdot \langle \ln(r_1) - \ln(r_y) \rangle + \right. \\ \left. EI_1 \cdot \chi_{TS} \cdot \langle r_1 - r_y \rangle + m_{cr} \cdot \langle r_{cr} - r_1 \rangle + EI_0 \cdot \psi \cdot \langle \ln(r_s) - \ln(r_{cr}) \rangle + m_p \cdot r_m \right) \quad (6.10)$$

where  $r_{cr}$ ,  $r_1$  and  $r_y$  are the radii defining the end of the region where concrete is cracked, cracks are stable and reinforcement is yielding. These values are calculated as follows (Clément *et al.*, 2014):

$$r_{cr} = -\frac{\psi}{\chi_{cr}} = \frac{\psi \cdot EI_0}{m_{cr}} \leq r_s \quad (6.11)$$

$$r_1 = -\frac{\psi}{\chi_1} = \frac{\psi}{\frac{m_{cr}}{EI_1} - \chi_{TS} - \Delta\chi_N} \leq r_s \quad (6.12)$$

$$r_y = -\frac{\psi}{\chi_y} = \frac{\psi}{\frac{m_R}{EI_1} - \chi_{TS} - \Delta\chi_N} \leq r_s \quad (6.13)$$

### 6.2.3 Calculation of the refined failure criterion accounting for in-plane stresses

The failure criterion defines the maximum shear force associated with a given crack opening (see *Chapter 4* and *Chapter 5*; (Muttoni *et al.*, 2017; Simões *et al.*, 2018)). The calculation of the punching strength for a given rotation according to the mechanical model of *Chapter 5* is performed by integration of the internal stresses developing along the CSC for a given state of deformations, refer to Figure 6.1. The basis of the mechanical model are recalled in the following (refer to Figure 5.9 in *Chapter 5*; Simões *et al.*, 2018)

- Primary tangential flexural cracks with a spacing equal to  $s_f$  develop on the tension side of the slab within a radius  $r_{\chi r}$ , in accordance with the analysis of the cracking development presented in Section 5.3;
- A CSC propagates from the tension to the compression side (Muttoni, 2008). This crack is composed of two regions with different phenomenological behaviours after the analysis of the cracking pattern shown in Section 5.3 and in agreement with Muttoni *et al.* (2017) (mixed-mode opening-sliding behaviour on the tension side and shear band behaviour on the compression side);
- The kinematics of the CSC is described by two components, consistently with the experimental observations of Clément (2012) and models based on the principles of the CSCT (Guidotti, 2010; Clément, 2012; Muttoni *et al.*, 2017): flexural and shear deformations;

- The location of the CSC at the level of the flexural reinforcement ( $r_0$ ) is considered as a variable (in accordance with the experimental observations discussed in Section 5.3).

All the hypotheses stated above are assumed to be also valid for punching shear failure of prestressed slabs. Again, punching failure may occur by localization of the strains along the CSC or by the development of a splitting failure crack (Clément, 2012; Einpaul, 2016; Einpaul *et al.*, 2017). The development of a splitting crack at failure is assumed to be correlated to the formation and development of the CSC and its associated displacement field (Einpaul *et al.*, 2017). For this reason, the punching shear strength is assumed herein to be governed in both cases by the development of the CSC (Einpaul *et al.*, 2017). Consequently, the punching strength can be evaluated by analysing the state of strains and stresses along it (Einpaul *et al.*, 2017).

The introduction of in-plane forces is considered to be the main effect of prestressing influencing the calculation of the failure criterion (Clément, 2012; Clément *et al.*, 2014). In the following, it is discussed how the introduction of in-plane stresses may be accounted for in the calculation of the refined failure criterion according to the mechanical model presented in Chapter 5 (Simões *et al.*, 2018).

### Influence of in-plane stresses on the definition of the regions of the slab with different behaviour

It is assumed in Chapter 5 (Simões *et al.*, 2018) that the slab is divided in three different regions: an inner and an outer portions of the slab, together with a wedge-shaped region. The inner and outer portions of the slab are assumed to deform respectively according to a spherical and conical shapes. The wedge-shaped region is considered to accommodate the radial displacements below the neutral axis resulting from the rotation concentrated at the CSC (following the approach of Kanellopoulos (1986) for beams in bending). It is considered in this section that the division of the slab in the regions established in Chapter 5 (Simões *et al.*, 2018) is not affected by the presence of in-plane stresses, refer to Figure 6.4.

### Influence of in-plane stresses on the shape of the CSC

In Chapter 5 (Simões *et al.*, 2018), the shape of the CSC is defined by a third-degree polynomial (without second order term) based on the three following conditions (refer to Figure 6.4): (i) it passes through the root of the column ( $r_c, 0$ ); (ii) its radial coordinate at the level of the flexural reinforcement is equal  $r_0$ ; (iii) the tangent to the CSC at the level of the flexural reinforcement passes through the centre of rotation associated with the flexural deformations. All conditions are assumed still to be valid for the case of slabs with in-plane stresses.

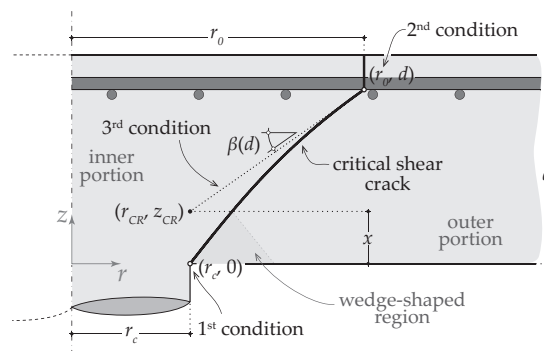
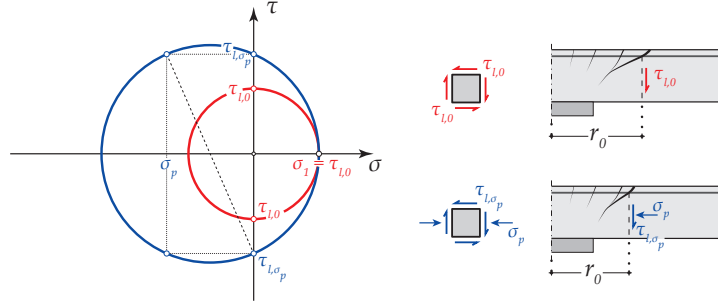


Figure 6.4: Regions of the slab with different behaviour and conditions for establishing the shape of the critical shear crack; figure adapted from Chapter 5 (Simões *et al.*, 2018).

The location of the critical shear crack at the level of the flexural reinforcement ( $r_c + 0.75 \cdot d \leq r_0 \leq r_c + 1.5 \cdot d$ ) is computed as a function of a nominal shear stress ( $\tau_l$ ) in Chapter 5, referring to the nominal

shear stress causing flexural cracks to become inclined flexural-shear cracks governing the shape of the CSC. It is considered that the same procedure can be followed for the case of slabs with in-plane stresses, provided that the value of this nominal shear stress is modified to account for the presence of in-plane stresses.



**Figure 6.5:** Variation of  $\tau_{l,\sigma}$  as a function of in-plane stresses acting on the slab according to an analysis based on Mohr's circle.

A possible approach is to calculate the value of the nominal shear stress analysing the state of nominal stresses in a radial plan of slabs with and without in-plane stresses. This is shown in Figure 6.5, where the red circle represents the case of a slab without in-plane stresses, whereas the blue circle refers to the case of a slab with in-plane compressive stresses. Limiting the value of the principal tensile stress to the nominal shear stress defined for the case without in-plane stresses ( $\sigma_1 = \tau_{l,0}$ ), the value of the nominal shear stress causing vertical cracks to become inclined and governing the critical shear crack in the presence of in-plane stresses ( $\tau_{l,\sigma}$ ) can be defined with the help of the Mohr's circle as follows:

$$\tau_{l,\sigma} = \frac{\sigma_p}{2} + \sqrt{\frac{\sigma_p^2}{4} + \tau_{l,0}^2} \quad (6.14)$$

where  $\sigma_p$  is the nominal in-plane stress and  $\tau_{l,0}$  refers to the nominal shear stress leading flexural cracks to become inclined and governing the shape of the critical shear crack with zero in-plane stresses (calculated with Eq. (5.4)). Thus, the nominal shear stress  $\tau_{l,\sigma}$  turns to be:

$$\frac{\tau_{l,\sigma}}{\tau_{l,0}} = \sqrt{1 - \frac{\sigma_p}{\tau_{l,0}}} \quad (6.15)$$

It is worth to mention that  $\tau_{l,\sigma} = \tau_{l,0}$  in the case of a zero in-plane stress ( $\sigma_p = 0$ ), thus defining a smooth transition between slabs without and with in-plane stresses. Indeed, Eq. (5.4) may be seen as a particular case of Eqs. (6.14) and (6.15). Finally, the location of the critical shear crack at the level of the flexural reinforcement is computed analogously to Eq. (5.3) as:

$$\frac{r_0}{d} = \frac{V}{2 \cdot \pi \cdot d^2 \cdot \tau_{l,\sigma}} \quad (6.16)$$

The pertinence of Eq. (6.15) can be verified with the experimental results of Clément *et al.* (2014), where the value of the in-plane compressive stress was one of the investigated variables (for two different flexural reinforcement ratios). Similarly to the procedure followed and presented in Section 5.3 for slabs without in-plane forces, the location of the critical shear crack at the level of the flexural reinforcement  $r_{0,test}$  was controlled in the specimens PC5 to PC10, whose saw-cuts are shown in Figure 6.6(a) (red crack considered as critical shear crack). The shear stress leading a flexural crack to become an

inclined flexural-shear crack was estimated by calculating the experimental nominal shear stress as  $\tau_{l,\sigma, test} = V_R / (b_{0,r_{0,test}} \cdot d)$ , where  $b_{0,r_{0,test}}$  refers to the perimeter calculated at the section located at  $r_{0,test}$  from the axis of the column (average of values measured in both sides of the available saw-cut). The experimental results of  $\tau_{l,\sigma, test}$  of specimens PC5 and PC10 are shown as a function of the in-plane compressive stresses (both normalized by  $\tau_{l,0}$  calculated with Eq. (5.4)) in Figure 6.6(b), where a consistent agreement with Eq. (6.15) can be observed.

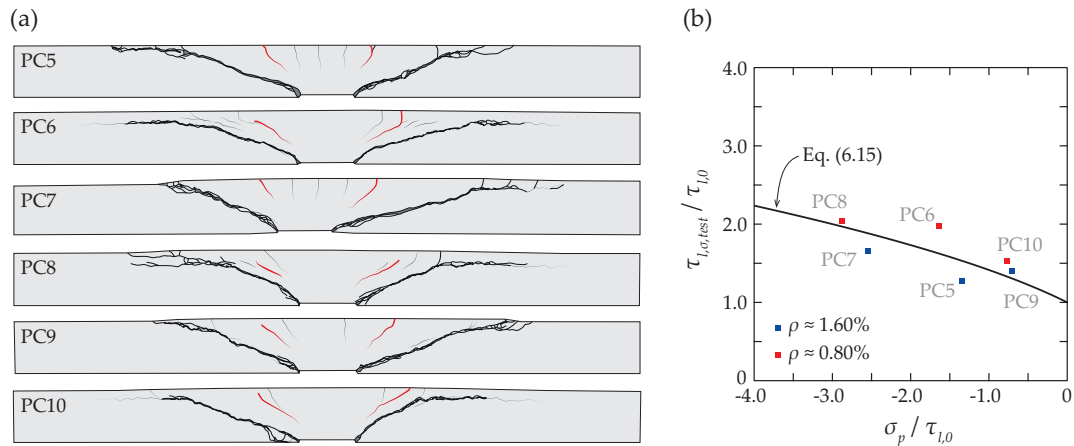


**Figure 6.6:** Influence of in-plane compressive stresses on the location of the critical shear crack: (a) saw-cuts of Clément *et al.* (2014) with indication of critical shear crack considered (red color) in the calculation of  $\tau_{l,\sigma}$ ; (b) calculated and experimental shear stress  $\tau_{l,\sigma}$  as a function of normalized in-plane stresses.

In addition to the calculation of  $r_0$ , the in-plane stresses also influence the calculation of the neutral axis (defining the location of the centre of rotation associated with flexural deformations) and, consequently, the value of the tangent inclination of the CSC at  $z = d$  (as a consequence of the third assumption adopted to define the shape of the CSC; see Figure 6.4). It thus results that, according to the mechanical model, in-plane stresses may change the shape of the critical shear crack by influencing its location at the level of the flexural reinforcement and the location of the centre of rotation associated with flexural deformations.

#### Influence of in-plane stresses on the kinematics and displacement field along the CSC

It has been shown in Section 5.4 that the displacement field along the CSC is composed by the vector sum of flexural and shear deformations (Figure 5.12). With respect to the component due to the flexural deformation, it is characterized by the rotation  $\psi_{csc}$  around a centre of rotation with coordinates  $(r_{CR}, z_{CR})$ . The value of the rotation developing at the CSC ( $\psi_{csc}$ , calculated with Eqs. (5.5) and (5.6)) for a given total rotation ( $\psi$ ) is influenced by the introduction of in-plane stresses, as a consequence of a potentially different radial extent of the region where primary tangential cracks develop ( $r_{\chi r}$ ). Also the location of the centre of rotation associated with the flexural deformation is influenced by the presence of in-plane stresses, notably by means of the depth of the neutral axis (corresponding to the height of the centre of rotation; calculated according to Section 5.10.1).

Regarding the shear deformation occurring along the CSC, it is described by a constant crack sliding  $\delta_s$  with an angle  $\gamma_s(z)$  with respect to the crack face (representing the crack opening-to-crack sliding angle associated with the shear deformation). This angle has its minimum value (defined as  $\gamma_0$ ) at the steepest region of the CSC, located by definition at the vicinity of the column edge, refer to Figure 5.12. As discussed in Section 5.4, Guidotti (2010) and Clément (2012) suggested that the value of  $\gamma_0$  may vary between  $25^\circ$  and  $30^\circ$  on the basis of the works of Mattock (1974), Walraven (1980), and Mansur

*et al.* (2008). In addition, based on an analysis of the experimental results of Walraven (1980) (push-off specimens with external restraint bars), Clément (2012) also suggested that the value of  $\gamma_0$  is also a function of the in-plane compressive stresses. This effect is nevertheless not considered in this work. A constant value equal to  $\gamma_0 = 27^\circ$  is used herein also for the case of prestressed slabs (consistently with the value used in *Chapter 5* (Simões *et al.*, 2018); still limited by the kinematical condition corresponding to a vertical translation of the outer portion of the slab  $\beta(0) + \gamma_0 \leq 90^\circ$ ).

#### **Influence of in-plane forces on the internal stresses along the CSC**

The presence of in-plane stresses does not require any modification in the procedure described in Section 5.4.5 to calculate the internal stresses developing along the CSC. Both localized and smeared cracking regimes may still occur along the CSC and the transition between these two regimes is still considered to occur under the conditions defined in Section 5.4.5.1 (Eq. (5.21)). The normal and shear stresses developing in the region responding in localized and smeared cracking conditions are computed as defined in Section 5.4.5 (Eqs. (5.22) and (5.23) for localized cracking and Eqs. (5.35) and (5.36) for smeared cracking). Also the contribution of dowel action of the flexural reinforcement is performed as described in Section 5.4.5.4.

#### **Calculation of the refined failure criterion and the punching shear strength**

Again, the punching strength and associated deformation capacity result from the intersection of the load-rotation relationship and the calculated failure criterion (Muttoni, 2008; Clément *et al.*, 2014; Muttoni *et al.*, 2017; Simões *et al.*, 2018). In the case of slabs with in-planes stresses, the load-rotation relationship can be calculated according to the approach of Clément *et al.* (2014) briefly presented in Section 6.2.2.

With respect to the calculation of the refined failure criterion, the only difference comparing to *Chapter 5* (Simões *et al.*, 2018) is the inclusion of the influence of the in-plane stresses on the calculation of the depth of the neutral axis ( $x$ ) and of the nominal shear stresses leading flexural cracks to become inclined and governing the shape of the CSC ( $\tau_{l,\sigma}$ ). A smooth transition occurs in the calculation of both parameters in the case of slabs with and without in-plane stresses. The calculation of the refined failure criterion is thus performed as described in *Chapter 5* (Simões *et al.*, 2018) by summing the contributions of the dowelling action, localized and smeared cracking regions (resulting from the integration of the internal stresses), i.e. according to Eq. (5.46). The numerical procedure described in detail in Section 5.10.4 may thus be applied to calculate the punching strength and the associated deformation capacity, with the exception of the calculation of  $r_0$ , which is computed on the basis of Eqs. (6.15) and (6.16).

#### **6.2.4 Brief comparison with experimental results**

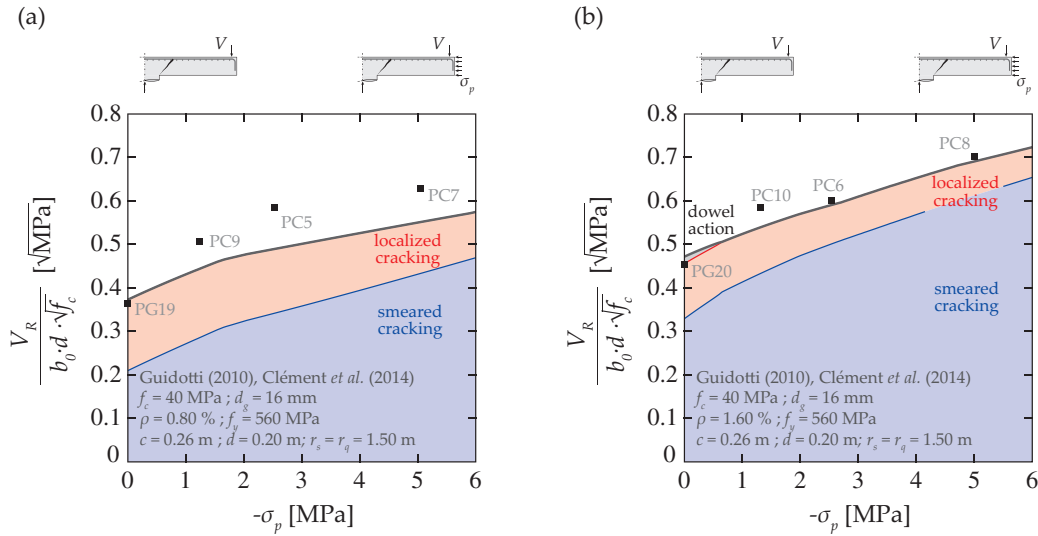
Among the numerous experimental campaigns investigating the punching strength of prestressed slabs available in scientific literature (e.g. Kinnunen *et al.*, 1977; Silva, 2005; Silva *et al.*, 2005, 2007; Ramos *et al.*, 2011, 2014; Clément *et al.*, 2014), the work of Clément *et al.* (2014) is particularly interesting because the effects of in-plane forces and external moments due to prestressing are individually varied. For this reason, the results of the mentioned experimental programme (Clément *et al.*, 2014) are used in this section to investigate the consistency of the mechanical model to evaluate the punching strength of prestressed slabs. A summary of the main properties and experimental results of the specimens tested by Clément *et al.* (2014) and Guidotti (2010) (reference specimens) is given in Table 6.1 (square specimens 0.25 m thick, with a side length of 3.0 m and supported on a 0.26 m square column).

**Table 6.1:** Overview of the experimental programme of Clément *et al.* (2014) together with the reference specimens of Guidotti (2010) (table adapted from Clément *et al.* (2014)).

Reference	Specimen	$d$ [m]	$f_c$ [MPa]	$\rho$ [%]	$f_y$ [MPa]	$\sigma_p$ [MPa]	$m_p$ [kNm/m]	$V_R$ [MN]
Guidotti (2010)	PG19	0.206	46.2	0.78	510	0	0	0.860
	PG20	0.201	51.7	1.56	551	0	0	1.094
Clément <i>et al.</i> (2014)	PC1	0.192	44.0	0.84	583	0	78	1.202
	PC2	0.192	45.3	1.64	549	0	77	1.397
	PC3	0.194	43.8	0.83	591	0	152	1.338
	PC4	0.190	44.4	1.65	602	0	152	1.431
	PC5	0.201	33.8	0.80	560	-2.53	0	1.141
	PC6	0.203	34.7	1.55	586	-2.53	0	1.205
	PC7	0.204	40.5	0.79	580	-5.04	0	1.370
	PC8	0.198	41.9	1.59	528	-5.00	0	1.494
	PC9	0.210	37.2	0.77	601	-1.24	0	1.105
	PC10	0.208	37.5	1.51	548	-1.32	0	1.260

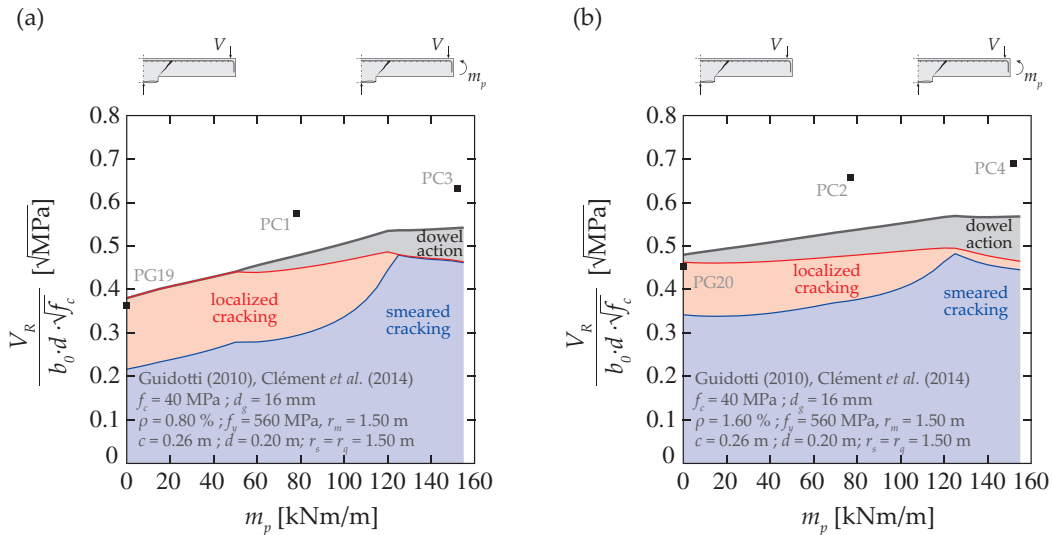
The results of the mechanical model presented in *Chapter 5* (with the development discussed in Section 6.2.3) are compared in Figure 6.7 to specimens where only the in-plane compressive stresses were varied (for two different flexural reinforcement ratios: (a) for  $\rho = 0.8\%$  and (b) for  $\rho = 1.6\%$ ). A good agreement is obtained between the theoretical and the experimental results, where a clear trend corresponding to the increase of the punching strength with increasing in-plane compressive stresses can be observed for both series of tests with regular and large flexural reinforcement ratios. According to the results of the mechanical model, this occurs due to a reduction of the crack opening along the CSC, as well as due to a more favourable shape of the CSC. The reduction of the crack opening along the CSC is caused by the stiffer response of the slab (accounted for in the load-rotation relationship of Clément *et al.* (2014)) and by the by increased depth of the neutral axis. Both the stiffness of the slab response and the depth of the neutral axis rise with the increase of in-plane compressive stresses, leading to a reduction of the crack opening along the CSC and, consequently, enlarging the extent of the region with smeared cracking which increases significantly the contribution of this region. Even if the extent of the CSC with localized cracking reduces, the smaller crack opening increases the shear-transfer in this region and thus compensates its shorter extent. It thus remains clear that the increase of punching strength with increasing compressive in-plane stresses observed in Figure 6.7 is partly due to the load-rotation relationship proposed by Clément *et al.* (2014) and partly due to the refined calculation of the failure criterion discussed in this section.

Figure 6.8 shows a comparison between the results of the mechanical model and the experimental results of Clément *et al.* (2014) where the applied external moment (representing a moment due to prestressing) was varied. The theoretical results show a satisfactory agreement with the experimental results, following the increase of the punching strength experimentally observed for increasing values of the external moment (with a sign opposite to the moment resulting from the applied vertical load). The increase of the external moment leads to a stiffer load-rotation relationship (Clément *et al.*, 2014), which is associated with smaller crack openings along the critical shear crack and, consequently, larger contributions of the regions responding in both localized and smeared cracking conditions. For very large external moments, rotations at failure are very limited and almost the entire CSC responds in smeared cracking conditions. In this case, the punching shear resistance reaches a maximum punching strength which remains approximately constant with the increase of the external moment. It is important to mention that, even if the theoretical results follow the experimentally observed trend, the results of the extended mechanical model seem to underestimate the experimental punching shear resistances in the case of a large applied external moment.



**Figure 6.7:** Influence of in-plane compressive stresses on the punching strength: comparison of the mechanical model with the experimental results of Guidotti (2010) (reference specimens: PG19 and PG20) and Clément *et al.* (2014) (specimens with in-plane compressive stresses: PC5 to PC10) for reinforcement ratio of (a)  $\rho \approx 0.8\%$  and of (b)  $\rho \approx 1.60\%$ .

The satisfactory agreement between theoretical and experimental results shows the potential of the mechanical model presented in *Chapter 5* (Simões *et al.*, 2018) to be extended to investigate the case of prestressed slab-column connections. However, accounting that only a brief comparison against the experimental results is performed in this section, additional experimental validation is required in order to assess whether the influence of the in-plane stresses and external moments is correctly predicted. Additional theoretical research may also be required in order to investigate if the in-plane forces and external moments play a role in other variables of the mechanical model.



**Figure 6.8:** Influence of moment due to prestressing effects on the punching strength: comparison of the mechanical model with the experimental results of Guidotti (2010) (reference specimens: PG19 and PG20) and Clément *et al.* (2014) (specimen with acting moment: PC1 to PC4) for reinforcement ratios of (a)  $\rho \approx 0.8\%$  and of (b)  $\rho \approx 1.60\%$ .

The CSCT was extended to deal with the case of prestressed slabs by Clément (2012) and Clément *et al.* (2014). For that purpose, Clément *et al.* (2014) suggested to combine the load-rotation relationship considering the effects of prestressing (briefly presented in Section 6.2.2) and the hyperbolic failure criterion of the CSCT proposed by Muttoni (2008) using a corrected rotation accounting for the influence of in-plane stresses. According to Clément *et al.* (2014), considering a reduced rotation in the presence of in-plane compressive stresses is mechanically justified by the increase of the depth of the compression chord and consequent decrease of the depth of cracked concrete, thus leading to a decrease of the width of the critical shear crack. The preliminary results presented in this section with the extended mechanical model (refined calculation of the failure criterion) confirm this hypothesis (in an analogous manner as for slabs with high reinforcement ratios presented in *Chapter 5* (Simões *et al.*, 2018)). However, a full validation of the extended mechanical model presented in this section is still required in order to investigate the suitability of the approach proposed by Clément *et al.* (2014).

## 6.3 Potential extension of the mechanical model to footings

### 6.3.1 Introduction

Even though one of the first experimental programmes focusing on the punching strength of reinforced concrete members was carried out on footings (Talbot, 1913), most research efforts have been dedicated to the case of slender slabs thereafter. Consequently, methods to calculate the punching strength have been historically tailored to slabs and extrapolated or adapted to footings (Hognestad, 1953; Whitney, 1957; Moe, 1961; Hegger *et al.*, 2009) in an attempt to have a consistent design method for both types of members (Kueres *et al.*, 2017).

However, experimental measurements (e.g. Dieterle and Rostásy, 1987; Hallgren *et al.*, 1998; Urban *et al.*, 2013; Hegger *et al.*, 2009; Siburg and Hegger, 2014; Simões *et al.*, 2016a), numerical calculations (e.g. Hallgren and Bjerke, 2002; Kueres *et al.*, 2013) and theoretical considerations (e.g. Hallgren and Bjerke, 2002; Broms, 2005; Simões *et al.*, 2016b) suggest that some of the parameters governing the punching capacity may have a different influence for slabs and for footings. It is thus of interest to extend the mechanical model presented in *Chapter 5* (Simões *et al.*, 2018) to deal with the case of reinforced concrete footings without transverse reinforcement.

A review of the available models or approaches of the codes to calculate the punching shear strength of reinforced concrete footings, as well as their comparison with available experimental data is out of the scope of this document. This section aims only at presenting a possible approach to extend the mechanical model presented in *Chapter 5* (based on the principles of the CSCT) to the case of isolated compact footings without transverse reinforcement and subjected to a uniform soil pressure.

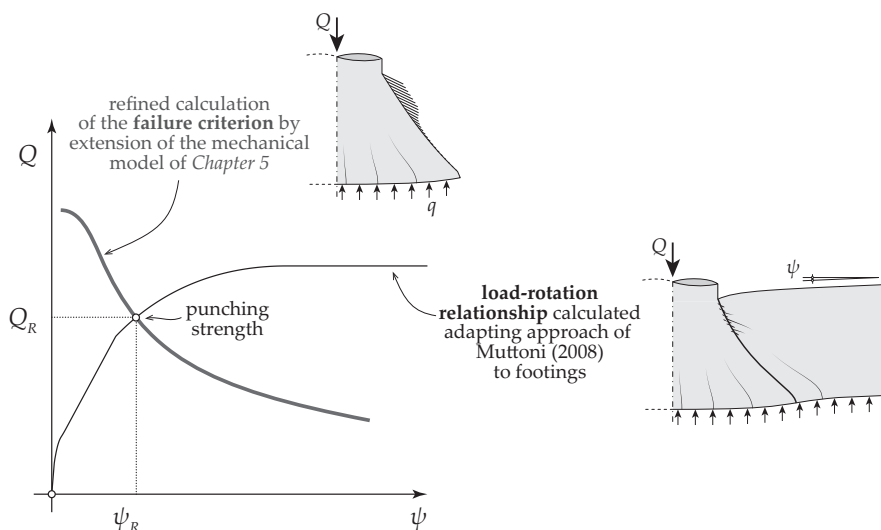


**Figure 6.9:** Punching shear failures of reinforced concrete footings without transverse reinforcement on the basis of the principles of the CSCT (Muttoni, 2008; Muttoni *et al.*, 2017): calculation of the total punching strength by intersecting the load-rotation relationship with the refined failure criterion calculated on the basis of the model presented in *Chapter 5*.

Following the principles of the CSCT (Muttoni, 2008; Muttoni *et al.*, 2017), punching failure is considered to occur at the intersection of the load-rotation relationship and the failure criterion, refer to Figure 6.9. As for slender slabs, the former law relates the applied load and the deformation of the member, while the latter relationship defines the maximum allowable shear force associated with a given state of deformation of the member.

With respect to the calculation of the load-rotation relationship of footings, the approach of Muttoni (2008) for slabs is slightly adapted and compared with the experimental results presented in *Chapter 2* (Simões *et al.*, 2016a). Regarding to the calculation of the refined failure criterion, the differences compared to the method presented in *Chapter 5* are discussed and mechanically grounded modifications are suggested at the level of the definition of the shape of the critical shear crack. Finally, the punching strengths calculated with the refined mechanical model are compared against a database of experimental results and selected series of tests.

### 6.3.2 Adaptation of load-rotation relationship of Muttoni (2008) to footings

Contrary to the case of slender flat slabs (Muttoni, 2008), no generally accepted analytical calculation of the load-rotation relationship of reinforced concrete footings is available in the scientific literature to the author's knowledge. Muttoni (2008) proposed the calculation of this relationship for slender slabs based on the equilibrium of a slab sector by considering a simplified kinematics and a quadri-linear moment-curvature relationship (see Section 5.10.3). In this section, the approach of Muttoni (2008) is adapted to allow its application to footings without transverse reinforcement, notably by modifying the geometry of the considered sector (to account for the lower slenderness of the member) and the moment-curvature relationship (to consider a reduced flexural capacity, see *Chapter 3*).

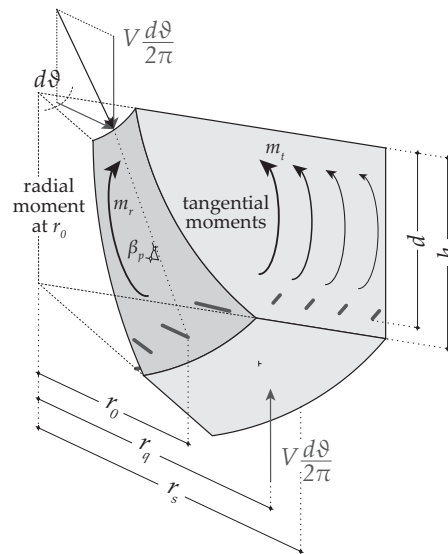


Figure 6.10: Geometrical definition of an axisymmetric sector of footing.

As shown in Figure 6.10, the axisymmetric sector of the footing under investigation is geometrically defined by its effective depth ( $d$ ), height ( $h$ ) as well as the column ( $r_c$ ) and footing radius ( $r_s$ ). Similarly to the works of Kinnunen and Nylander (1960) and Muttoni (2008), it is considered that an inclined failure surface separates an inner and an outer portions of the footing. This surface is considered to be described by its secant inclination ( $\beta_p$ ), which enables the calculation of its radial coordinate at the level of the flexural reinforcement ( $r_0$ ). Based on experimental tests, Hegger *et al.* (2009) and Siburg and Hegger (2014) suggested that the inclination of this surface (and thus of the value of  $r_0$ ) is a function of the span-to-effective depth ratio in the case investigated in this section (footings without transverse reinforcement and subjected to a uniformly distributed loading). In addition, the theoretical results based on the application of the kinematical theorem of limit analysis presented in *Chapter 3* (Simões *et al.*, 2016b) indicate that the inclination of the failure surface in the punching shear regime depends

mainly on the span-to-effective depth ratio of the footing. Based on these experimental and theoretical findings, it will be assumed in the following that  $r_0$  can be estimated with Eqs. (3.19) and (3.20) derived in *Chapter 3* (Simões *et al.*, 2016b):

$$r_0 = r_c + d \cdot \cot(\beta_p) \leq r_c + 1.5 \cdot d \quad \text{with} \quad \beta_p = \frac{90^\circ}{0.8 + 0.5 \cdot a/d} \quad (6.17)$$

where  $\beta_p$  is the secant inclination of the failure surface and  $a$  represents the radial distance from the edge of the column to the edge of the footing ( $a = r_s - r_c$ ;  $a/d$  representing the span-to-effective depth ratio).

It should be noted that only the load acting at the bottom surface of the outer portion of the footing is considered as acting shear force ( $V$ ). The relationship between the acting shear force ( $V$ ) and the total load ( $Q$ ) is thus the following:

$$Q = V \cdot \frac{r_s^2}{r_s^2 - r_0^2} \quad (6.18)$$

With respect to the kinematics of the footing, by analogy with the assumption adopted by Kinnunen and Nylander (1960) and Muttoni (2008) for slabs, it is assumed that the deformation of the inner and outer portions of the footing follow spherical and conical shapes, respectively. The equilibrium of the axisymmetric sector of footing shown in Figure 6.10 yields (analogously to slender slabs as considered by Muttoni, 2008):

$$V \cdot \frac{d\vartheta}{2 \cdot \pi} \cdot (r_q - r_c) = -m_r \cdot d\vartheta \cdot r_0 - d\vartheta \cdot \int_{r_0}^{r_s} m_t \cdot dr \quad (6.19)$$

where  $r_q$  is the radius where the resultant of the vertical load is applied,  $m_r$  the radial moment acting at  $r_0$  and  $m_t$  the tangential moment. The analytical integration of Eq. (6.19) can be performed by adopting a multi-linear moment-curvature diagram (Muttoni, 2008), as for instance the one shown in Figure 6.11. This relationship differs from the one originally proposed by Muttoni (2008) (see Section 5.10.3) only by including a reduced moment capacity ( $m_{R,red}$ ). As shown in *Chapter 3* (Simões *et al.*, 2016b), a significant flexural-shear interaction occurs in footings without transverse reinforcement due to the presence of an inclined concrete strut carrying shear in the vicinity of the column (Figure 3.12). This concrete strut increases the depth of the compression zone, thus decreasing the lever arm between tensile and compressive forces (and consequently the moment capacity). The reduced moment capacity ( $m_{R,red}$ ) proposed in *Chapter 3* (Simões *et al.*, 2016b) to account for the flexural-shear interaction is used in this section (Eq. (3.18)):

$$m_{R,red} = \rho \cdot f_y \cdot d^2 \cdot \left(1 - \frac{z_c}{d}\right) \quad (6.20)$$

where  $\rho$  represents the flexural reinforcement ratio,  $f_y$  the yield strength of the reinforcement and  $z_c$  the vertical distance between the top surface of the footing and the point of application of the diagonal concrete strut (representing an augmented compression zone; see Figure 3.12), which is computed according to (Eq. (3.17)):

$$\frac{z_c}{d} = \frac{\rho \cdot f_y}{2 \cdot \eta_{fc} \cdot f_c} \cdot \left(1 + 0.4 \cdot \frac{r_s}{r_c} \cdot \frac{d}{r_{q,0} - r_c}\right) \leq 0.5 \quad (6.21)$$

where  $r_{q,0}$  refers to the radial location of the resultant of the vertical load applied in the case of vertical yield line developing at the edge of the column (Figure 3.12; Eq. (3.10) with  $r_0 = r_c$ ) and where the upper limit of  $z_c/d$  represents the maximum strut width. It should be mentioned that the reduction factor accounting for the state of deformations ( $\eta_\epsilon$ ) in Eq. (3.18) ( $f_{cp} = \eta_\epsilon \cdot \eta_{fc} \cdot f_c$ ) is assumed equal to  $\eta_\epsilon = 1$  for the analysis but it could eventually be considered as a function of the state of deformations (as it will be discussed later in this section).

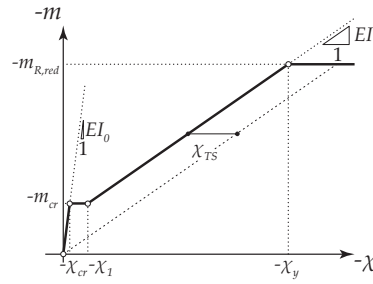


**Figure 6.11:** Tailored quadri-linear moment-curvature relationship to footings without transverse reinforcement subjected to a uniform soil pressure (relationship adapted from Muttoni (2008)).

In addition to the value of the reduced moment capacity, the moment-curvature relationship shown in Figure 6.11 is characterized by the uncracked stiffness ( $EI_0$ ), cracking moment ( $m_{cr}$ ), tension stiffening effect ( $\chi_{TS}$ ) and cracked stiffness ( $EI_1$ ). These parameters can be calculated as suggested by Muttoni (2008) (Eqs. (5.76), (5.75), (5.80) and (5.77) respectively for  $EI_0$ ,  $m_{cr}$ ,  $\chi_{TS}$  and  $EI_1$ ).

Based on the adopted kinematics and quadri-linear moment-curvature relationship, Eq. (6.19) can be expressed in a closed-form format as follows:

$$V = \frac{2 \cdot \pi}{r_q - r_c} \cdot \left( \begin{array}{l} -m_r \cdot r_0 + m_{R,red} \cdot \langle r_y - r_0 \rangle + EI_1 \cdot \psi \cdot \langle \ln(r_1) - \ln(r_y) \rangle + \\ EI_1 \cdot \chi_{TS} \cdot \langle r_1 - r_y \rangle + m_{cr} \cdot \langle r_{cr} - r_1 \rangle + EI_0 \cdot \psi \cdot \langle \ln(r_s) - \ln(r_{cr}) \rangle \end{array} \right) \quad (6.22)$$

where  $\langle \Delta r \rangle$  is equal to zero when  $\Delta r < 0$ ,  $r_{cr}$ ,  $r_1$  and  $r_y$  are the radii defining respectively the extent of the region where concrete is cracked, cracks are stable and reinforcement is yielding, whose values can be calculated according to Eqs.(5.85), (5.86) and (5.87) (adopting  $m_R = m_{R,red}$ ).

### Definition of an equivalent axisymmetric footing

The analytical calculation of the load-rotation relationship above presented applies for axisymmetric members. Footings are rarely axisymmetric and, for that reason, equivalent values for the radii of the column ( $r_c$ ), footing ( $r_s$ ) and load application  $r_q$  have to be considered. The radius of an equivalent circular column ( $r_c$ ) may be calculated assuming an equal perimeter ( $r_c = 2 \cdot c / \pi$  for square columns). With respect to the radius of the equivalent axisymmetric member ( $r_s$ ), it may be estimated in a first approach ensuring an equal area of the bottom surface of the footing, thus implying an equal load applied in both actual and axisymmetric members for an equal soil pressure (which turns to be  $r_s = B / \sqrt{2}$  for square footings). Finally, the radius of the application of the resultant of vertical loads applied at the bottom surface of the outer portion of the footing in the axisymmetric member ( $r_q$ ) may be estimated ensuring an equal flexural capacity calculated according to yield-line theory for the investigated and axisymmetric cases (plateau in the load-rotation relationship at the same load level in both cases). For square footings with square columns,  $r_q$  turns to be:

$$Q_{flex} = Q_{flex,axis} \Rightarrow \frac{8}{\left(1 - \frac{c}{B}\right)^2} = \frac{2 \cdot \pi \cdot r_s}{r_q - r_c} \cdot \frac{r_s^2}{r_s^2 - r_0^2} \quad (6.23)$$

$$r_q = r_c + r_s \cdot \frac{2 \cdot \pi}{8} \cdot \left(1 - \frac{c}{B}\right)^2 \cdot \frac{r_s^2}{r_s^2 - r_0^2}$$

where  $c$  refers to the size of a square column,  $Q_{flex}$  is the flexural capacity of a square footing with a square column based on yield-line theory (Johansen, 1962) assuming a cantilever mechanism (Gesund, 1983),  $Q_{flex,axis}$  is the flexural capacity of a circular footing with a circular column (axisymmetric member) based on yield-line theory (Johansen, 1962). It should be noted that the (reduced) moment capacity multiplying in both sides of Eq. (6.23) (and thus accounting for the flexural-shear interaction) cancels.

### Experimental validation of proposed load-rotation relationship

Figure 6.12 depicts a comparison between the calculated and the experimental load-rotation relationships of the four specimens without transverse reinforcement presented in *Chapter 2* (Simões *et al.*, 2016a), where the amount of top reinforcement, the column and the specimen side lengths were varied (PS11 to PS14). The satisfactory agreement between the theoretical and the experimental results demonstrates that the approach proposed by Muttoni (2008) to slabs may be adapted to footings by considering a consistent sector of the member (modifying  $r_0$ ) and a tailored moment-curvature relationship (incorporating a reduced moment capacity  $m_{R,red}$ ).

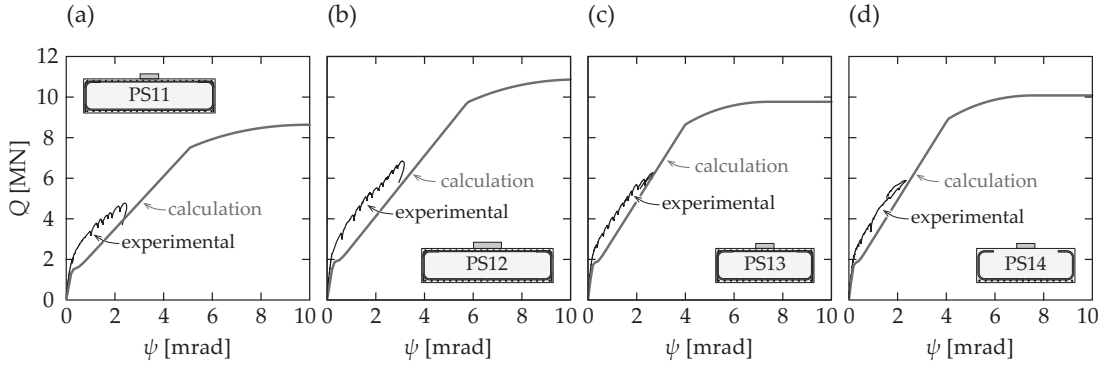


**Figure 6.12:** Comparison of calculated and experimental load-rotation relationships of reinforced concrete footings under uniform soil pressure: (a) PS11; (b) PS12; (c) PS13; (d) PS14; specimens by Simões *et al.* (2016a).

However, it can be noted from Figure 6.12 that the calculated relationship seems to underestimate the contribution of concrete in tension (cracking load and tension-stiffening effects). Therefore, a possible adaptation of the sectional response of the member to obtain a better agreement with the experimental results remains to be investigated as future work.

In addition, although the calculation of  $r_0$  and  $m_{R,red}$  according to Eqs. (6.17) and (6.20) appears to be reasonable for the four specimens used for comparison, its general application also requires further experimental validation. The calculation of the reduced moment capacity ( $m_{R,red}$ ) deserves particular attention in future works as it represents the flexural-shear interaction experimentally observed in *Chapter 2* (Simões *et al.*, 2016a) and theoretically described in *Chapter 3* (Simões *et al.*, 2016b). It is of interest to understand whenever a reduction factor function of the state of deformations ( $\eta_\epsilon$ ) should be included in the calculation of the reduced moment capacity by means of the plastic concrete compressive strength ( $f_{cp}$  in Eq. (6.21)). From the mechanical point of view, the weakening of the concrete strength with increasing deformations (Vecchio and Collins, 1986) leads to an augmented height of the compression zone and, consequently, to a decrease of the lever arm and of the moment capacity. An approach including such effect can be carried out by including a factor  $\eta_\epsilon$  in the calculation of  $m_{R,red}$ . A similar approach has already been previously proposed by Lips (2012) to calculate the load-rotation relationship of slabs with large amounts of transverse reinforcement.

### 6.3.3 Calculation of the refined failure criterion for isolated footings

The calculation of the refined failure criterion presented in *Chapter 5* (Simões *et al.*, 2018) can also be applied in order to study the punching strength of isolated reinforced concrete footings. The basis of the mechanical model are recalled in the following (Figure 6.13; Simões *et al.*, 2018):

- Primary tangential flexural cracks develop on the tension side within a radius  $r_{\chi r}$ . The spacing between such cracks is considered to be equal to  $s_f$ ;

- The CSC is a primary tangential flexural crack that develops from the tension to the compression side (Muttoni, 2008). Two regions with different phenomenological behaviour develop along it (Muttoni *et al.*, 2017). A mixed-mode opening-sliding behaviour governs the response on the tension side, whereas a shear band response takes place on the compression side;
- The displacement field along the CSC results from the vector sum of flexural and shear deformations, consistently with the experimental observations of Clément (2012) for slabs and Simões *et al.* (2016a, Chapter 2) for footings, as well as in agreement with previous models based on the principles of the CSCT (Guidotti, 2010; Clément, 2012; Muttoni *et al.*, 2017).
- A variable location of the CSC at the level of the flexural reinforcement is adopted.

Comparing to the slender slabs investigated in Chapter 5 (Simões *et al.*, 2018), footings with a uniformly distributed loading applied at the bottom surface differ mainly due to their low slenderness and loading conditions. The influence of such differences on the calculation of the refined failure criterion is discussed in the following.

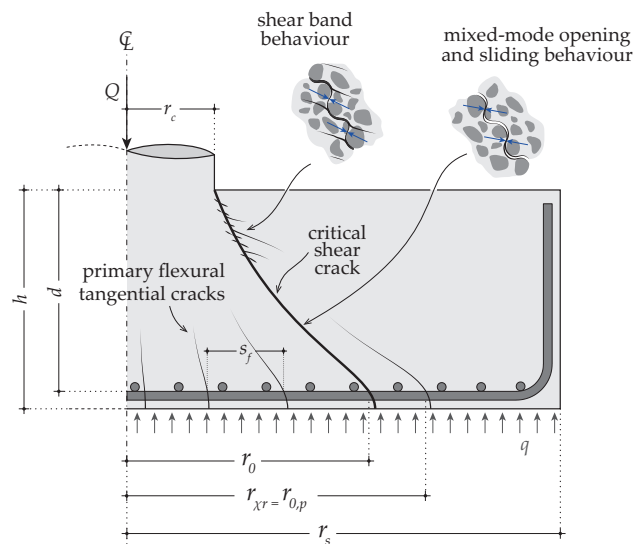


Figure 6.13: Punching shear of isolated footings: hypotheses of the mechanical model of Chapter 5 (Simões *et al.*, 2018) and description of potentially different phenomenological (Muttoni *et al.*, 2017) applied to footings.

### Influence of slenderness and loading conditions on the definition of the different regions

The three regions of the slab with different behaviour defined in Chapter 5 (Simões *et al.*, 2018) for slender slabs are also considered to be valid in the case of footings. As shown in Figure 6.14, the footing is divided in an inner and an outer portions, together with a wedge-shaped region. Similarly to the case of slender slabs and in agreement with the approach of Kanellopoulos (1986) for beams in bending, the wedge-shaped region is considered to accommodate the radial displacements associated with the flexural deformations below the neutral axis (according to the axis convention of Figure 6.14).

### Influence of the slenderness and loading conditions on the shape of the CSC

The geometry of the CSC of footings will be considered as defined in Chapter 5 (Simões *et al.*, 2018) for slender slabs, i.e. by adopting a third-degree polynomial degree parabola (without second order term) together with the three following conditions (see Figure 6.14): (i) the CSC passes by the root of the column and (ii) joins the level of the flexural reinforcement at  $r_0$ ; (iii) the tangent to the CSC at the level of the flexural reinforcement passes by the centre of rotation associated with the flexural

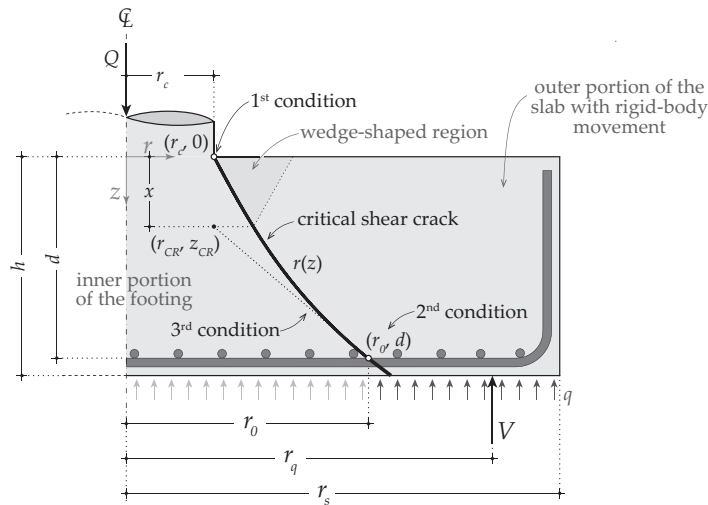


**Figure 6.14:** Extension of the mechanical model of Chapter 5 to footings without transverse reinforcement: regions of the footing with different behaviour and adopted hypotheses for definition of the shape of the critical shear crack.

deformations (hypothesis established on the basis of the experimental observations of Einpaul (2016) and Einpaul *et al.* (2017) in slender slabs). This geometry was defined based on the analysis of the cracking development of punching tests of slender slabs (Chapter 5; Simões *et al.*, 2018) but is considered in a first attempt to suitably describe the geometry of the CSC of footings as well. In addition, the shapes of the CSC obtained with such approach agree fairly well with the shapes of the failure surfaces of footings experimentally observed in Chapter 2 (Simões *et al.*, 2016a) and theoretically calculated based on limit analysis in Chapter 3 (Simões *et al.*, 2016b).

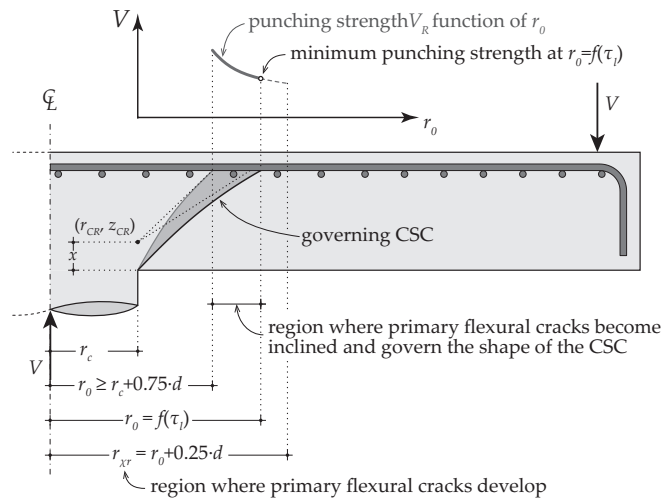


**Figure 6.15:** Punching shear resistance  $V_R$  as a function of  $r_0$  in the case of slender slabs.

Even if the slenderness and loading conditions are considered not to influence the geometry of the CSC, they may influence the governing shape of the CSC by modifying the radial coordinate of the CSC at the level of the flexural reinforcement ( $r_0$ ).

Based on the analysis of experimental results, a verification on the basis of a nominal shear stress was proposed to determine the location of the CSC at the level of the flexural reinforcement in slender

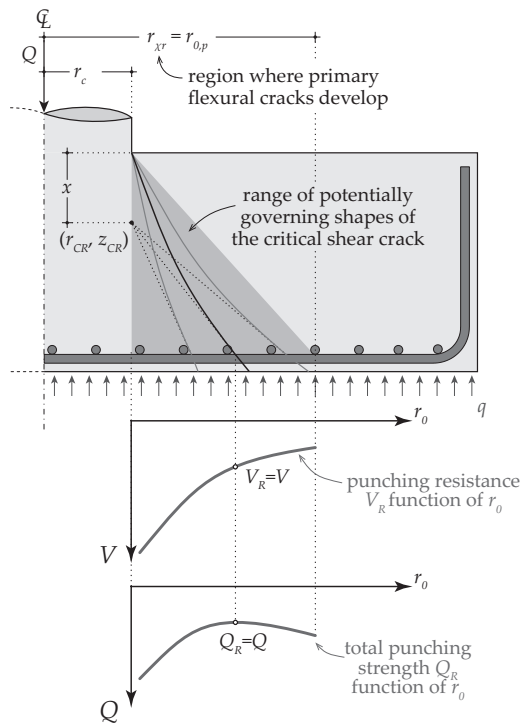


**Figure 6.16:** Punching shear resistance  $V_R$  as a function of  $r_0$  against acting shear force: definition of governing shape of the CSC in the case of footings with uniformly distributed loading applied on the bottom surface.

slabs (Chapter 5; Simões *et al.*, 2018). Therefore, although the CSC could theoretically develop between  $r_c + 0.75 \cdot d$  and the calculated value of  $r_0$  (function of the nominal shear stress  $\tau_j$ ; defining the region where inclined-flexural cracks develop and may progress towards the compression side, Figure 6.15), the shape of the CSC governing the punching strength was always assumed to be located at  $r_0$ . This is theoretically justified by the fact that the punching strength reduces with decreasing the secant inclination of the CSC (larger value of  $r_0$ ; see  $V$  as a function of  $r_0$  in Figure 6.15), while the acting shear force in the case investigated in Chapter 5 (Simões *et al.*, 2018) remains constant between the support and the load introduction. For these reasons, in Chapter 5 (Simões *et al.*, 2016b), the governing shape of the CSC corresponds to the crack reaching the flexural reinforcement at the value of  $r_0$ . In the case of footings subjected to an uniformly distributed loading applied at the bottom surface, even if a flatter secant inclination of the CSC (larger value of  $r_0$ ) may lead to a lower effective punching strength ( $V_R$ ), it does not necessarily lead to a lower total punching shear capacity ( $Q_R$ ), refer to Figure 6.16. With increasing values of  $r_0$ , the amount of load acting inside the CSC and being equilibrated by direct support action increases. It thus results that the location of the CSC at the level of the flexural reinforcement  $r_0$  has to be found by minimization of the total punching shear strength. This difference with respect to the case of slender slabs previously dealt in Chapter 5 (Simões *et al.*, 2016b) is a consequence of the different loading conditions.

Even if the location of  $r_0$  is determined by minimizing the total punching shear capacity, the extent of the region in which primary flexural cracks develop and, consequently, where the CSC may form has to be defined. An expression to calculate the location of the failure surface at the level of the flexural reinforcement ( $r_{0,p}$ ) has been proposed in Chapter 3 (Eqs. (3.19) and (3.20); Simões *et al.*, 2016b) on the basis of the application of the upper bound theorem of limit analysis for footings without transverse reinforcement subjected to a uniform loading. As a first estimate, it will be considered in the following

that the CSC at the level of the flexural reinforcement may vary between the edge of the column and the location of the failure surface calculated based on the application of limit analysis ( $r_c \leq r_0 \leq r_{0,p}$ ). Consistently, it is thus considered that primary flexural cracks develop within a radius corresponding to the furthest possible location of the CSC at the level of the flexural reinforcement ( $r_{\chi r} = r_{0,p}$  with  $r_{0,p}$  calculated with Eq. (6.17)), refer to Figures 6.13 and 6.16.

In summary, the shape of the CSC in footings will be estimated in the following based on Eq. (5.2) where the value of  $r_0$  results from the minimization of the total punching shear strength ( $r_c \leq r_0 \leq r_{0,p}$ ). Consequently, it is considered that primary flexural cracks develop within the region where the critical shear crack may form ( $r_{\chi r} = r_{0,p}$ ).

#### **Influence of the slenderness and loading conditions on the kinematics and displacement field**

In the following, it will be considered that the kinematics of the CSC is equivalent in both slabs and footings, i.e. composed by a rotation and a shear deformation (Figure 5.12), even if their relative contributions to the displacement field along the CSC may differ in both cases (Simões *et al.*, 2016a; Muttoni *et al.*, 2017). The contribution of the flexural deformations to the displacement field along the critical shear crack is a function of the centre of rotation ( $r_{CR}, z_{CR}$ ) and of the rotation developing at the CSC ( $\psi_{csc}$ ). The assumptions adopted in the case of slender slabs are also considered in the case of footings to determine both the centre of rotation (located at the edge of the column and at the depth of the neutral axis) and the rotation concentrated in the critical shear crack (total rotation equally divided in the number of primary tangential crack developing within  $r_{\chi r}$ ). With respect to the shear deformation, it is characterized by the shear displacement  $\delta_s$  and the minimum angle  $\gamma_0$  occurring between the CSC and the vector associated with the shear deformation. With respect to the later parameter, similarly to the case of slender slabs, it is again assumed equal to  $\gamma_0 = 27^\circ \leq 90^\circ - \beta(0)$ , where  $\beta(0)$  refers to the tangent inclination of the CSC at  $z = 0$  (steepest region of the CSC). The limit value of  $\gamma_0$  represents the case of a shear deformation corresponding to a vertical translation of the outer portion of the footing. It is important to note that, although this limitation is hardly governing in slender slabs, it may be governing in the case of footings due to the low value of  $r_0$  (steep inclination of the CSC).

In summary, as the same kinematics and assumptions are adopted for both slender slabs and footings, the displacement field along the CSC in the latter case can also be calculated on the basis of the equations presented in Section 5.4.4.

#### **Influence of the slenderness and loading conditions on the internal stresses along the CSC**

The fundamental material laws do not depend on the slenderness and loading conditions of the member. The internal stresses developing in the region with localized cracking are therefore given by Eqs. (5.22) and (5.23). In the region with smeared cracking, the internal stresses are obtained by means of Eqs. (5.35) and (5.36). With respect to the dowel action, it is calculated according to Eq. (5.45). Finally, also the transition between localized and smeared cracking regimes is considered as defined for slender slabs (Eq. (5.21)). Although the internal stresses are calculated on the basis of the same equations for slender slabs and footings, their value may differ as a consequence of the different shape of the CSC (different secant inclination) and displacement field along it (different relative contributions of flexural and shear deformations).

#### **Calculation of the refined failure criterion and punching shear strength**

Analogously to the procedure followed in slender slabs without and with in-plane forces (Muttoni, 2008; Clément *et al.*, 2014; Muttoni *et al.*, 2017; Simões *et al.*, 2018), the punching shear strength and its associated deformation capacity are calculated by intersecting the load-rotation relationship and

the refined failure criterion. The load-rotation relationship ( $Q_{LR} - \psi$ ) of isolated reinforced concrete footings is calculated here as explained in Section 6.3.2 (Eqs. (6.18) and (6.22)).

The refined failure criterion is obtained calculating the total punching shear strength as a function of the rotation. The effective punching strength  $V_c$  associated with a given value of the rotation and of the shear deformation is calculated as described in Section 5.4.6, i.e. by summing the contribution of localized and smeared cracking (integration of internal stresses) as well as the contribution of the dowel action of the flexural reinforcement. The total punching strength is obtained adding the load equilibrated by direct support (uniformly distributed load inside  $r_0$ ):

$$Q_c = \underbrace{\text{localized cracking} + \text{smeared cracking} + \text{dowel action}}_{V_c} + \underbrace{\text{load equilibrated by direct support}}_{V_c \cdot \frac{r_0^2}{r_s^2 - r_0^2}} = V_c \cdot \frac{r_s^2}{r_s^2 - r_0^2} \quad (6.24)$$

with  $V_c$  calculated according to Eq. (5.46). A similar procedure to the one followed for slabs (and described in Section 5.10.4) may be adopted to calculate the refined failure criterion and the punching strength. As previously discussed, the only difference refers to the determination of the value  $r_0$  by minimization of the total punching shear strength. Thus, for a given rotation, the value of the total punching shear strength is minimized by varying the value of  $r_0$  between  $r_c$  and  $r_{0,p}$ .

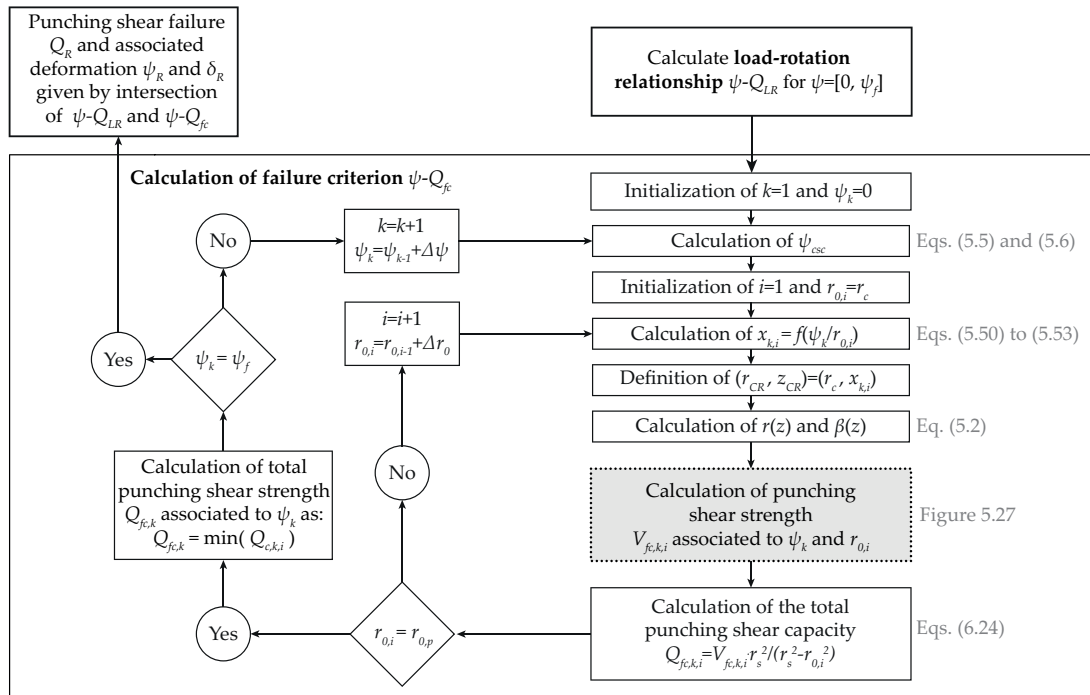
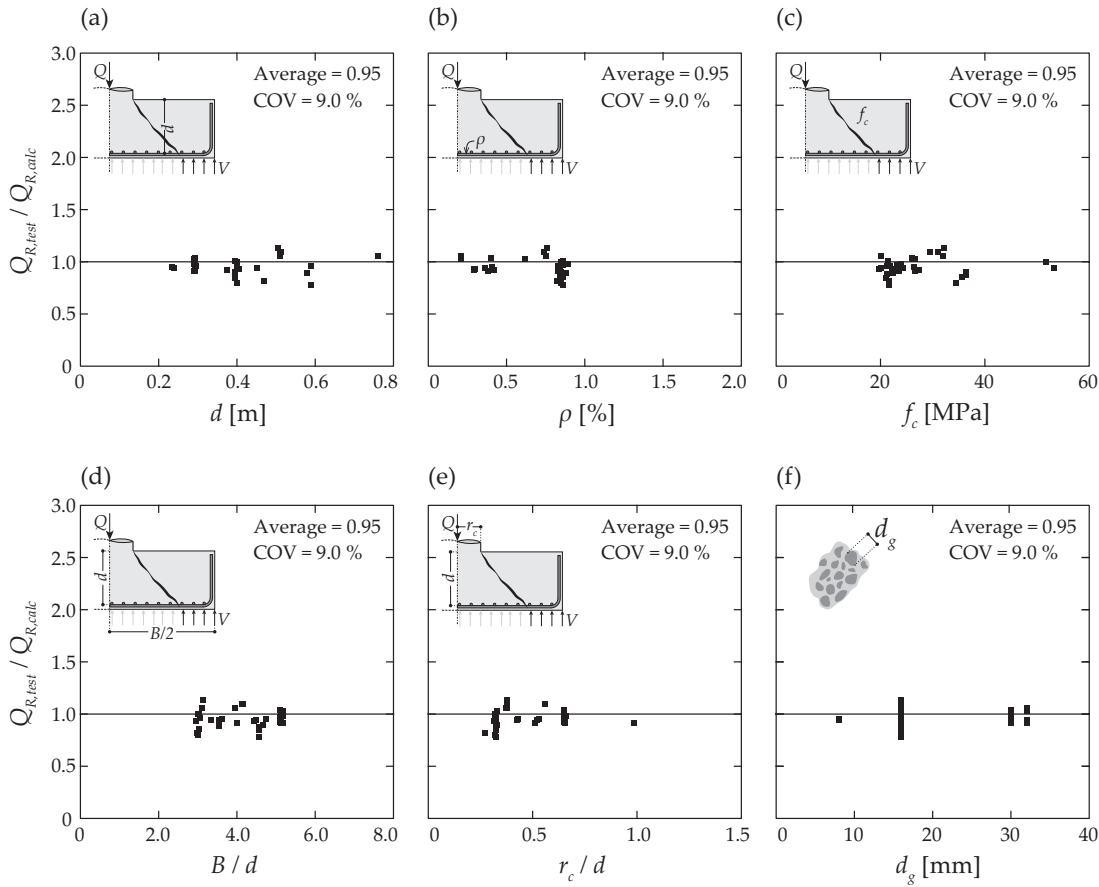


Figure 6.17: Numerical procedure followed to calculate the punching shear strength and associated deformation capacity of footings without transverse reinforcement subjected to a uniform soil pressure.

A possible numerical procedure to calculate the total punching shear strength of a footing is shown in Figure 6.17 (analogous to the one presented in Section 5.10.4). In the numerical procedure presented in Figure 6.17, both the load-rotation relationship and the failure criterion are first calculated in a wide range of rotations, followed by the calculation of their intersection. Another numerical procedure could consist on determining iteratively the value of the rotation at failure (calculating the value of the applied load -based on the load-rotation relationship- and of the maximum shear strength -failure criterion- for a given rotation until reaching an equal value).

### 6.3.4 Validation and comparison against experimental results

A comparison against experimental results is presented in this section in order to verify the consistency of the extension of the mechanical model to footings without transverse reinforcement subjected to a uniform loading. The database of reinforced concrete footings without transverse reinforcement presented in *Chapter 4* (Muttoni *et al.*, 2017) with a total of 34 specimens is considered for that purpose (refer to Table 4.2 for details). The experimental-to-calculated punching strength ratios are shown as a function of the main geometrical and mechanical properties in Figure 6.18, where a fine agreement between experimental and theoretical results may be observed (average of 0.95 and coefficient of variation equal to 9.0%).



**Figure 6.18:** Ratio of experimental-to-calculated punching resistance applying the refined mechanical model of *Chapter 5* (Simões *et al.*, 2016b) extended to footings as a function of: (a) effective depth; (b) flexural reinforcement ratio; (c) concrete compressive strength; (d) side length of the footing-to-effective depth ratio; (e) column radius-to-effective depth ratio slabs (equivalent radius of a circular column with equal perimeter for square columns); (f) aggregate size. Database including 34 footings without transverse reinforcement subjected to a uniform loading (see Table 4.2 for details; Muttoni *et al.*, 2017).

The average value of the experimental-to-calculated strength ratios is slightly below one, indicating an overestimate of the predicted punching strength. This result can be justified by different factors. Firstly, some of the assumptions of the extended model may require further theoretical work and experimental validation to be applied to footings, such as for example the geometry of the CSC, the region where tangential cracking is considered to develop or still the adopted crack spacing. Other possible factors may include the consideration of square footings loaded with point loads applied in a limited number of locations (whose distance may become significantly large in some cases) as axisymmetric specimens with a uniformly distributed loading. Finally, also the transformation of a real case to an

axisymmetric problem may influence the obtained results. Thus, further work is needed to understand if the rather low average value of the experimental-to-calculated punching strength ratios is a consequence of limitations of the model or if it is a consequence of the extrapolation of an actual footing to an axisymmetric specimens. On the other hand, it is worth to mention that the rather low coefficient of variation obtained in the comparison against the database of experimental tests shows the model accuracy to correctly predict the influence of the main geometrical and mechanical properties.

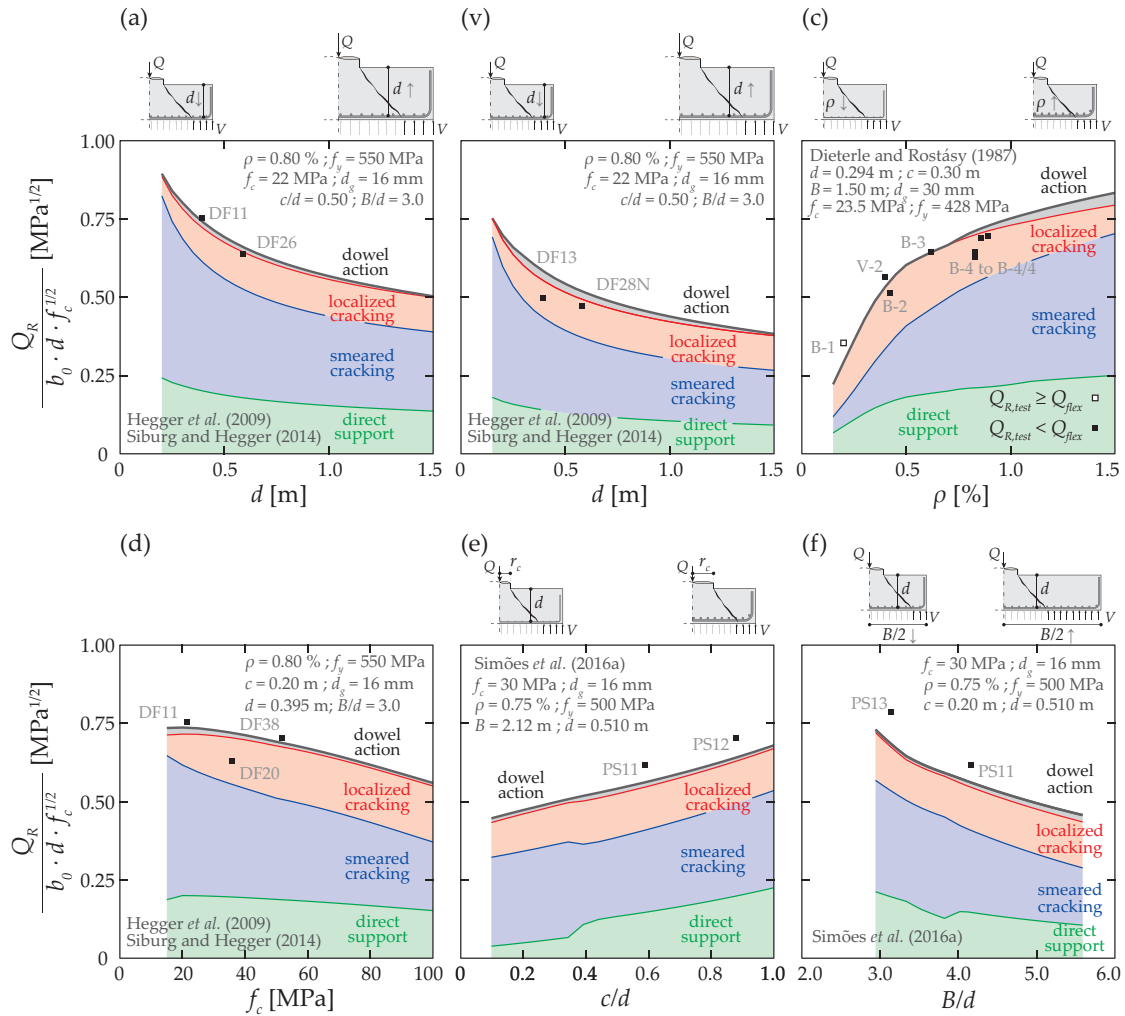


**Figure 6.19:** Comparison of calculated punching resistance applying the refined mechanical model of Chapter 5 (Simões et al., 2016b) (extended to footings) with different series of experimental tests: (a) effective depth with  $B/d = 3.0$  (Hegger et al., 2009; Siburg and Hegger, 2014); (b) effective depth with  $B/d = 4.5$  (Hegger et al., 2009; Siburg and Hegger, 2014); (c) flexural reinforcement ratio (Dieterle and Rostásy, 1987); (d) concrete compressive strength with  $B/d = 3.0$  (Hegger et al., 2009; Siburg and Hegger, 2014); (e) side length of the column-to-effective depth ratio (Simões et al., 2016a); (f) side length of the footing-to-effective depth ratio (Simões et al., 2016a).

The theoretical results are also compared against selected series of tests in Figure 6.19, where it is shown that the influence of the main parameters governing the punching strength of footings is captured in a systematic manner by the model. Figure 6.19 also shows the contributions of the different shear-transfer actions. The relative contribution of the region with localized cracking seems to be slightly smaller in footings than in slender slabs (compare relative contribution of localized cracking in Figures 5.19 and 6.19). This result may be justified based on the: (i) different loading conditions that lead to a not negligible amount of load equilibrated by direct support in the case of footings; (ii) smaller

rotations at failure of footings compared to slabs, thus leading to larger extents of the region with smeared cracking in the former case; (iii) low slenderness of footings with respect to the slabs, which leads to a more favourable shape of the CSC in the former case (due to the low value of  $r_0$ ). These are also the reasons why the relative contribution of localized cracking to the total punching strength reduces for decreasing the slenderness of the footing (Figure 6.19(f)). With this respect, it is interesting to observe that the refined mechanical model consistently captures the increase of the total punching shear strength with decreasing the span-to-effective depth ratio of the footings (Figure 6.19(f)), which corresponds to a trend experimentally observed and reported by, for example, Hegger *et al.* (2006, 2009), Urban *et al.* (2013), Siburg and Hegger (2014), and Simões *et al.* (2016b).

As shown in Figures 6.19(a) and (b), a fine agreement is also found between the results of the mechanical model and the experimental results of Hegger *et al.* (2009) and Siburg and Hegger (2014) in the series where the effective depth of the footings is varied, corroborating the experimental observations of Dieterle and Rostásy (1987) and Siburg and Hegger (2014) with respect to the existence of a size-effect in the punching strength of footings.

Figure 6.19(d) additionally shows that the influence of the concrete compressive strength is well captured by the mechanical model. It is interesting to mention that the influence of the concrete compressive strength in footings seems to be slightly larger than the one obtained in slender slabs in the investigated case (compare Figure 5.19(b) to Figure 6.19(d)), specially in the range of concrete compressive strengths lower than approximately 40 MPa. According to the mechanical model, in this range of concrete compressive strengths, the influence of this parameter in the case footings seems to be consistently described by a square root, while in the case of slender slabs seems to be rather correlated to the cubic root. This result in agreement with the experimental observations of Hallgren *et al.* (1998), Hegger *et al.* (2009), and Bonić *et al.* (2017), who suggested that the influence of the concrete compressive strength on the punching strength may be larger in footings than in slender slabs. Finally, Figures 6.19(e) and (f) show that the extended mechanical model captures consistently the experimental trends observed in *Chapter 2* (Simões *et al.*, 2016a), corresponding to an increase of the total punching strength with the decrease of the span-to-effective depth ratio and the increase of the column size.

The comparison of the theoretical and experimental results presented in this section shows that the theoretical principles of the CSCT can be successfully applied to investigate the punching strength of footings provided that an adequate shape of the CSC is adopted. However, it remains also clear that the extension of the mechanical model here presented requires further theoretical work and experimental validation.

## 6.4 Conclusions

This chapter discusses the extension of the mechanical model presented in *Chapter 5* (Simões *et al.*, 2018) to prestressed slabs and to reinforced concrete footings without transverse reinforcement.

With respect to the extension of the mechanical model to the case of prestressed slabs, the main conclusions are presented below:

1. The mechanical model accounts for the influence of in-plane stresses on the calculation of the depth of the neutral axis and of the nominal shear stress leading flexural cracks to become inclined flexural-shear cracks thus governing the shape of the critical shear crack (CSC). These parameters influence the shape of the CSC and the displacement field along it. Consequently, the introduction of in-plane stresses plays a role on the development of internal stresses along the CSC;
2. The results of the extended mechanical model show a satisfactory agreement with the experimental results of prestressed slabs of Clément *et al.* (2014). According to the results of the mechanical model, the increase of the punching strength with increasing in-plane compressive stresses is a result of the decrease of the crack opening along the CSC. This leads to an increase of the extent of the CSC contribution under smeared cracking conditions (increasing the contribution of this region), while the contribution of the region with localized cracking remains approximately constant (smaller extent of this region compensated by smaller crack opening leading to the development of higher internal stresses);
3. The preliminary results suggest that the theoretical principles of the CSC, which form the basis of the refined mechanical model, can be successfully applied to perform a refined calculation of the punching shear strength and deformation capacity of prestressed slab-column connections;
4. Even if the preliminary results seem to be physically consistent, an extensive validation of the mechanical model to deal with the case of prestressed slabs is still required;
5. The results of the refined mechanical model confirm the ideas of Clément (2012) and Clément *et al.* (2014), who suggested that the crack opening of the CSC decreases for increasing in-plane compressive stresses.

Regarding the extension of the mechanical model presented in *Chapter 5* (Simões *et al.*, 2018) to footings without transverse reinforcement subjected to a uniformly distributed loading, the following conclusions can be drawn:

1. The refined mechanical model presented Chapter 5 (Simões *et al.*, 2018) may be applied to investigate the punching strength and associated state of deformations at failure of footings provided that an adequate shape of the CSC is adopted;
2. The calculation of the load-rotation relationship slabs proposed by Muttoni (2008) may be adapted to the case of footings subjected to a uniformly distributed loading considering an appropriate sector of the footing and a tailored moment-curvature relationship;
3. The mechanical model shows a fine agreement when compared to a database and selected series of experimental tests, being able to capture consistently the role of the main parameters governing the punching strength of footings;
4. The agreement between theoretical and experimental results shows that the theoretical principles of the CSCT (on which the model is based) are valid to investigate the punching strength and the associated deformation capacity of reinforced concrete footings. However, some aspects of this extension of the theory still deserve some future work.

## 6.5 References

- Bonić Z.; Davidović N.; Vacev T.; Romić N.; Zlatanović E.; Savic J. (2017):** „Punching Behaviour of Reinforced Concrete Footings at Testing and According to Eurocode 2 and *fib* Model Code 2010“. *International Journal of Concrete Structures and Materials*, Vol. 11, No. 4, pp. 657–676.
- Broms C. E. (2005):** „Concrete flat slabs and footings: Design method for punching and detailing for ductility“. PhD thesis. Stockholm, Sweden: Department of Structural Engineering, Royal Institute of Technology, p. 114.
- Cavagnis F.; Fernández Ruiz M.; Muttoni A. (2017):** „A mechanical model for failures in shear of members without transverse reinforcement based on development of a critical shear crack“. *Engineering Structures*. (accepted for publication).
- Clément T. (2012):** „Influence de la précontrainte sur la résistance au poinçonnement de dalles en béton armé“. PhD thesis. Lausanne, Switzerland: EPFL, p. 224.
- Clément T.; Ramos A. M. P.; Fernández Ruiz M.; Muttoni A. (2013):** „Design for punching of prestressed concrete slabs“. *Structural Concrete*, Vol. 14, No. 2, pp. 157–167.
- Clément T.; Ramos A. P.; Fernández Ruiz M.; Muttoni A. (2014):** „Influence of prestressing on the punching strength of post-tensioned slabs“. *Engineering Structures*, Vol. 72, pp. 56–69.
- Dieterle H.; Rostásy F. (1987):** „Load-carrying behaviour of isolated reinforced concrete foundations of square columns (In German: Tragverhalten quadratischer Einzelfundamente aus Stahlbeton)“. *Deutscher Ausschuss für Stahlbeton*, Vol. 387, pp. 1–91.
- Einpaul J. (2016):** „Punching strength of continuous flat slabs“. PhD thesis. Lausanne, Switzerland: EPFL, p. 209.
- Einpaul J.; Fernández Ruiz M.; Muttoni A. (2017):** „Measurements of internal cracking in punching test slabs without shear reinforcement“. *Magazine of Concrete Research*. doi: 10.1680/jmacr.16.00099.
- Eurocode 2 (2004):** *Design of Concrete Structures - General Rules and Rules for Buildings, EN 1992-1-1*. Brussels, Belgium, p. 225.
- fib (2001):** *Bulletin 12: Punching of structural concrete slabs*. Tech. rep. Lausanne, Switzerland: International Federation for Structural Concrete, p. 314.
- fib Model Code 2010 (2013):** *Model Code 2010 - Final draft*. Tech. rep. Volumes 1 and 2, Bulletins 65 and 66. International Federation for Structural Concrete.
- Gesund H. (1983):** „Flexural Limit Analysis of Concentrically Loaded Column Footings“. *ACI Journal Proceedings*, Vol. 80, No. 3, pp. 223–228.
- Guidotti R. (2010):** „Punching shear of slabs with column load (In French: Poinçonnement des planchers-dalles avec colonnes superposées fortement sollicitées)“. PhD thesis. Lausanne, Switzerland: EPFL, p. 189.
- Hallgren M.; Bjerke M. (2002):** „Non-linear finite element analyses of punching shear failure of column footings“. *Cement and Concrete Composites*, Vol. 24, No. 6, pp. 491–496.
- Hallgren M.; Kinnunen S.; Nylander B. (1998):** „Punching shear tests on column footings“. *Nordic Concrete Research*, Vol. 21, pp. 1–22.
- Hegger J.; Sherif A.; Ricker M. (2006):** „Experimental Investigations on Punching Behaviour of Reinforced Concrete Footings“. *ACI Structural Journal*, Vol. 103, No. 4, pp. 604–613.

- Hegger J.; Ricker M.; Sherif M. (2009):** „Punching Strength of Reinforced Concrete Footings“. *ACI Structural Journal*, Vol. 106, No. 5, pp. 706–716.
- Hognestad E. (1953):** „Shearing Strength of Reinforced Concrete Column Footings“. *ACI Journal*, Vol. 25, No. 3, pp. 189–208.
- Jacobsen J. S.; Olesen J. F.; Poulsen P. N. (2012):** *Constitutive Mixed Mode Behavior of Cracks in Concrete: Experimental Investigations of Material Modeling*. BYGDTU Report. Kgs. Lyngby: Technical University of Denmark.
- Johansen K. W. (1962):** *Yield-line Theory*. Cement and Concrete Association.
- Kanellopoulos A. (1986):** „On the inelastic behavior and fracture of reinforced concrete (In German: Zum unelastischen Verhalten und Bruch von Stahlbeton)“. PhD thesis. Zürich, Switzerland: ETHZ, p. 86.
- Kinnunen S.; Nylander H. (1960):** *Punching of Concrete Slabs Without Shear Reinforcement*. Tech. rep. 158. Stockholm, Sweden: Transactions of the Royal Institute of Technology, p. 112.
- Kinnunen S.; Nylander H.; Ingvarsson H. (1977):** *Genomstansning av pelarunderstödd plattbro av betong med spänd och ospänd armering*. Tech. rep. 123. Stockholm, Sweden, p. 56.
- Kueres D.; Siburg C.; Reissen K.; Hegger J. (2013):** „Experimental and numerical investigations on the punching behavior of thick footings with and without shear reinforcement“. In: *Research and Applications in Structural Engineering, Mechanics and Computation*. Ed. by Zingoni A. London: Taylor & Francis Group, pp. 1543–1548.
- Kueres D.; Siburg C.; Herbrand M.; Clasen M.; Hegger J. (2017):** „Uniform Design Method for punching shear in flat slabs and column bases“. *Engineering Structures*, Vol. 136, pp. 149–164.
- Lips S. (2012):** „Punching of Flat Slabs with Large Amounts of Shear Reinforcement“. PhD thesis. EPFL, p. 217.
- Mansur M. A.; Vinayagam T.; Tan K. H. (2008):** „Shear Transfer across a crack in reinforced high-strength concrete“. *Journal of Materials in Civil Engineering*, Vol. 20, No. 4, pp. 294–302.
- Mattock A. H. (1974):** *Effect of aggregate type on single direction shear transfer in monolithic concrete*. Tech. rep. 2, SM74. Seattle, Washington.
- Moe J. (1961):** *Shearing strength of reinforced concrete slabs and footings under concentrated loads*. Vol. D47. Skokie, Illinois: Portland Cement Association, Research and Development Laboratories.
- Muttoni A. (1990):** „The applicability of the theory of plasticity to reinforced concrete design (In German: Die Anwendbarkeit der Plastizitätstheorie in der Bemessung von Stahlbeton)“. PhD thesis. Zürich, Switzerland: ETHZ, p. 158.
- Muttoni A. (2008):** „Punching shear strength of reinforced concrete slabs without transverse reinforcement“. *ACI structural Journal*, Vol. 105, No. 4, pp. 440–450.
- Muttoni A.; Fernández Ruiz M.; Simões J. T. (2017):** „The theoretical principles of the critical shear crack theory for punching shear failures and derivation of consistent closed-form design expressions“. *Structural Concrete*, pp. 1–17. DOI: 10.1002/suco.201700088.
- Ramos A. M. P.; Lúcio V. J. G.; Regan P. E. (2011):** „Punching of slabs with in-plane forces“. *Engineering Structures*, Vol. 33, pp. 894–902.

- Ramos A. M. P.; Lúcio V. J. G.; Faria D. M. V. (2014):** „The effect of the vertical component of prestress forces on the punching strength of flat slabs“. *Engineering Structures*, Vol. 76, pp. 90–98.
- Ramos A. P. (2003):** „Punching of prestressed slabs (In Portuguese: Punçoamento em lajes fungiformes pré-esforçadas)“. PhD thesis. Lisbon, Portugal: Universidade Técnica de Lisboa, Instituto Superior Técnico, p. 203.
- Regan P.; Braestrup M. W. (1985):** *Punching shear in reinforced concrete*. Tech. rep. 168. Comité Euro-International du Béton (CEB), p. 232.
- Siburg C.; Hegger J. (2014):** „Experimental Investigations on Punching Behaviour of Reinforced Concrete Footings with structural dimensions“. *Structural Concrete*, Vol. 15, No. 3, pp. 331–339.
- Silva R. J. C. (2005):** „Punção em lajes cogumelo protendidas com cordoalhas não aderentes e pilares de diferentes dimensões“. PhD thesis. Brasília, Brasil: Universidade de Brasília, Faculdade de Tecnologia, Departamento de Engenharia civil e Ambiental, p. 224.
- Silva R. J. C.; Regan P. E.; Melo G. S.S. A. (2005):** „Punching resistances of unboded post-tensioned slabs by decompression methods“. *Structural Concrete*, Vol. 6, pp. 9–21.
- Silva R. J. C.; Regan P. E.; Melo G. S.S. A. (2007):** „Punching of Post-Tensioned Slabs - Tests and Codes“. *ACI Structural Journal*, Vol. 104, No. 2, pp. 123–132.
- Simões J. T.; Bujnak J.; Fernández Ruiz M.; Muttoni A. (2016a):** „Punching shear on compact footings with uniform soil pressure“. *Structural Concrete*, Vol. 17, No. 4, pp. 603–617.
- Simões J. T.; Faria D. V.; Fernández Ruiz M.; Muttoni A. (2016b):** „Strength of reinforced concrete footings without transverse reinforcement according to limit analysis“. *Engineering Structures*, Vol. 112, pp. 146–161.
- Simões J. T.; Fernández Ruiz M.; Muttoni A. (2018):** „Validation of the Critical Shear Crack Theory for punching of slabs without transverse reinforcement by means of a refined mechanical model“. *Structural Concrete*, pp. 1–26. DOI: 10.1002/suco.201700280.
- Talbot A. N. (1913):** „Reinforced Concrete Wall Footings and Column Footings“. *Engineering Experiment Station - University of Illinois*, Vol. 67, pp. 114.
- Urban T.; Krakowski J.; Goldyn M.; Krawczyk L. (2013):** *Punching of RC thick plates*. Tech. rep. 19. Poland: Department of Concrete Structures, Technical University of Lodz.
- Vecchio F. J.; Collins M. P. (1986):** „The modified compression-field theory for reinforced concrete elements subjected to shear“. *ACI Structural Journal*, Vol. 83, No. 2, pp. 219–231.
- Walraven J. C. (1980):** „Aggregate interlock: a theoretical and experimental analysis“. PhD thesis. Delft, Netherlands: Delft University of Technology, Faculty of Civil Engineering, p. 197.
- Whitney C. S. (1957):** „Ultimate Shear Strength of Reinforced Concrete Flat Slabs, Footings, Beams, and Frame Members Without Shear Reinforcement“. *ACI Journal Proceedings*, Vol. 54, No. 10, pp. 265–298.

## 6.6 Notation

### Latin characters

#### Lower Case

$a$	shear span
$b_{0,r_{0,exp}}$	perimeter of the section located at $r_{0,exp}$ from the axis of the column
$b_0$	length of control perimeter located at $d/2$ from the column edge
$c$	side length of a square column
$d$	effective depth (distance from the centroid of the flexural reinforcement to the outermost compressed fiber)
$d_g$	maximum aggregate size
$d_{g0}$	reference aggregate size
$d\theta$	angle of slab sector (also angle of shear band sector)
$f_c$	concrete compressive strength measured in cylinders
$f_{cp}$	plastic concrete compressive strength
$f_{ct}$	concrete tensile strength
$f_y$	yielding strength of reinforcement
$h$	height of reinforced concrete section
$m$	moment
$m_{cr}$	cracking moment per unit width
$m_p$	external moment per unit width
$m_r$	radial moment per unit width
$m_R$	moment capacity per unit width
$m_{R,red}$	reduced moment capacity per unit width
$m_t$	tangential moment per unit width
$n_p$	in-plane force per unit width
$q$	uniformly distributed load
$r, z$	radial and vertical coordinates
$r_{CR}, z_{CR}$	radial and vertical coordinates of the centre of rotation
$r_c$	radius of a circular column
$r_{cr}$	radius of cracked region
$r_m$	radial location where the external moment is applied
$r_q$	radial location of the resultant of vertical applied load
$r_{q,0}$	radial location of the resultant of the vertical load applied in the case of vertical yield line developing at the edge of the column
$r_s$	radius of isolated axisymmetric member
$r_y$	radius of the region in which reinforcement is yielding
$r_0$	radial distance between the axis of the column and the critical shear crack at the level of the flexural reinforcement
$r_{0,p}$	radial distance between the axis of the column and the failure surface at the level of the flexural reinforcement calculated by applying the upper bound theorem of limit analysis
$r_{0,exp}$	radial distance between the axis of the column and the critical shear crack at the level of the flexural reinforcement experimentally measured
$r_1$	radius of the region in which cracking is stabilized
$r_{\chi r}$	radial distance with non-negligible radial deformation measured from the axis of the column
$s_f$	distance between primary flexural cracks
$w$	crack opening
$w_0$	initial crack opening
$x$	depth of neutral axis
$x_{el}$	depth of the compression zone assuming an linear-elastic behaviour of both concrete and reinforcement
$x_{pl}$	depth of the plastic compression zone
$z_c$	location of the diagonal compression strut at the column edge

**Upper Case**

$B$	side length of a square slab
$E_c, E_s$	modulus of elasticity of concrete and reinforcement, respectively
$EI_0$	uncracked stiffness of reinforced concrete section
$EI_1$	cracked stiffness of reinforced concrete section
$Q$	total applied load
$Q_c$	total punching strength associated with a given rotation and shear deformation
$Q_{fc}$	total punching strength associated with a given rotation (failure criterion)
$Q_{flex}$	total flexural strength of an actual isolated footing
$Q_{flex,axis}$	total flexural strength of an axisymmetric isolated footing
$Q_{LR}$	total punching force associated with given rotation (load-rotation relationship)
$Q_R$	total punching shear strength
$Q_{R,test}$	experimental total punching shear strength
$Q_{R,calc}$	calculated total punching shear strength
$V$	punching shear force
$V_c$	strength associated with a given rotation and shear deformation
$V_{fc}$	punching strength associated with a given rotation (failure criterion)
$V_{flex}$	flexural strength of an isolated specimen
$V_{LR}$	punching force associated with given rotation (load-rotation relationship)
$V_R$	punching shear strength
$V_{R,test}$	experimental punching shear strength

**Greek characters****Lower Case**

$\beta$	tangent angle of the critical shear crack
$\beta_p$	secant angle of the failure surface calculated by applying the upper bound theorem of limit analysis
$\gamma_0$	angle between critical shear crack and vector of displacement due to shear deformation at $z = 0$
$\gamma_s$	angle between critical shear crack and vector of displacement due to shear deformation
$\delta_s$	sliding due to shear deformation
$\eta_\epsilon$	reduction factor accounting for the presence of transverse strains
$\eta_{fc}$	reduction factor accounting for the brittleness of concrete in compression
$\xi$	reduction factor accounting for the reduced stiffness of orthogonal reinforcement comparing to the stiffness of reinforcement axisymmetrically
$\rho$	flexural reinforcement ratio
$\tau_1$	shear stresses causing a flexural crack to become an inclined flexural crack governing the shape of the critical shear crack
$\tau_{1,\sigma}$	shear stresses causing a flexural crack to become an inclined flexural crack governing the shape of the critical shear crack accounting for an in-plane stress $\sigma$
$\tau_{1,\sigma,test}$	experimentally calculated shear stresses causing a flexural crack to become an inclined flexural crack governing the shape of the critical shear crack accounting for an in-plane stress $\sigma$
$\sigma_p$	in-plane stress
$\sigma_1$	principal tensile stress
$\chi_r$	radial curvature
$\chi_t$	tangential curvature
$\chi_{cr}$	curvature associated with cracking
$\chi_1$	curvature associated with stabilized cracking
$\chi_y$	curvature associated with yielding of the reinforcement
$\chi_{TS}$	reduction of curvature associated with tension-stiffening effect due to reinforcement bond
$\psi$	rotation of the slab
$\psi'$	corrected rotation accounting for the influence of in-plane stresses

---

$\psi_{csc}$	rotation of the slab at the critical shear crack
$\psi_R$	rotation of the slab at failure

**Upper Case**

$\Delta$	crack sliding
$\Delta\chi_N$	variation of curvature due to in-plane stresses

**Acronyms**

CSCT	Critical Shear Crack Theory
LVDT	Linear Variable Differential Transformer
CSC	Critical Shear Crack
CR	centre of rotation



# Chapter 7

## Conclusions and Outlook

### 7.1 Introduction

This thesis deals with punching shear failures of reinforced concrete members without transverse reinforcement subjected to a concentric and monotonic loading. In addition to Chapters 1 (Introduction) and 7 (Conclusions and Future Research), this document is composed of five chapters. The first four chapters correspond to four journal articles dealing with different issues related to the topic of the present document. The sixth chapter presents an additional work which was not included in none of the journal articles (previous chapters).

In an attempt to better understand the differences between the punching shear behaviour of slender and squat members, an experimental programme comprising a total of five compact full-scale reinforced concrete footings was carried out in the framework of this thesis. The experimental results of this series of tests were published in a journal article (Simões *et al.*, 2016a) together with three additional tests performed in IBETON/EPFL as part of a private project funded by Peikko. The investigated variables included the column size, the side length of the footing (both influencing the span-to-effective depth ratio), the influence of transverse reinforcement composed of double-headed studs and the potential influence of top horizontal reinforcement. Beyond the results of the experimental programme, the second chapter of this thesis presents also an interpretation of the kinematics of the tested footings based on measurements recorded in the shear-critical region. The experimental results show that shear deformations significantly influence the state of deformation of the shear-critical region of footings at failure. This result emphasizes the need to consider these deformations in a theory consistently describing the phenomenon involved in a punching failure.

The third chapter, corresponding to the second published journal article (Simões *et al.*, 2016b), presents a theoretical work consisting on the investigation of the strength of compact reinforced concrete footings without transverse reinforcement based on the application of the upper bound theorem of limit analysis. Although the application of such theory to brittle failures may be arguable (Bažant and Cao, 1987), its application for failures triggered by yielding of the flexural reinforcement or crushing of concrete has been shown to be suitable (Nielsen and Hoang, 2011). As the experimental evidences presented in the second chapter of this document suggest that punching shear failures of compact reinforced concrete footings may be governed by crushing of the diagonal concrete struts, limit analysis was used to investigate the different potentially governing failure mechanisms and associated regimes. Actually, regardless of some debatable assumptions associated to the application of limit analysis, the work presented in the third chapter of this document allows to explain some experimental observations from the theoretical point of view. A comparison of the theoretical results against experimental results from the literature indicates that strain- and size-effects have to be accounted in the definition of the plastic concrete compressive strength in order to correctly predict the punching strength of compact

footings. This result accentuates the need for a mechanical theory to consistently deal with punching failures of both compact and slender reinforced concrete members, as the punching strength appears to be a function of the same parameters in both cases (influenced by strain- and size-effects).

The fourth chapter, corresponding to the third published journal article (Muttoni *et al.*, 2017), presents a review and discussion of the theoretical principles of the Critical Shear Crack Theory (CSCT) for punching shear failures of members without transverse reinforcement. This chapter shows that the punching failures of slender and squat members are dealt in a consistent manner by the CSCT, mainly because the mentioned theory accounts for both flexural and shear deformations in the kinematics at failure. The application of the principles of this theory to perform a refined calculation of the failure criterion for punching shear failures is discussed and presented based on previous works on the topic (Guidotti, 2010; Simões *et al.*, 2016b), eventually justifying the use of a simplified and single failure criterion. In addition, an analytical derivation of closed-form expressions for punching shear design of members without transverse reinforcement is presented based on a newly proposed failure criterion (proposed by Muttoni and Fernández Ruiz (2017) and mechanically justified in this chapter) and a simplified non-linear load-rotation relationship (earlier developed by Muttoni (2008)). A comparison of the different possible approaches of CSCT against experimental results of both slender (slabs) and squat (footings) members without transverse reinforcement is also presented, showing good agreement.

The fifth chapter, corresponding to the fourth published journal article (Simões *et al.*, 2018), presents a complete validation of the analytical failure criteria of the CSCT for punching shear failures of slender slabs without transverse reinforcement. A refined mechanical model is developed on the basis of the theoretical principles of the CSCT (reviewed and discussed in fourth chapter) and supported on recent experimental findings available in the scientific literature (reviewed in the first part of the journal article). The refined mechanical model shows very good agreement with the experimental results by comparison with a database of experimental tests and selected series of tests. Eventually, the refined mechanical model allows a theoretical validation of the analytical failure criteria of the CSCT as well as of its main assumptions.

Finally, the sixth chapter discusses the extension of the refined mechanical model for punching shear failures of prestressed slabs and isolated reinforced concrete footings. It is shown that the extended mechanical model is able to explain theoretically the experimentally observed trends. Furthermore, the consistent agreement obtained in the preliminary comparisons of the theoretical and the experimental results shows that the theoretical principles of the CSCT (based on which the model was developed) are also valid to deal with the punching shear failures of these members. Further work remains nevertheless to be performed in the future to fully validate the proposals of extension of the mechanical model for these cases.

In summary, the work presented in this document includes both experimental and theoretical contributions for reinforced concrete isolated footings. While the experimental work consists of a series of tests, the theoretical work includes, not only the analysis of compact footings applying the kinematical theorem of limit analysis (third chapter), but also the discussion on how and why CSCT also applies for squat members (fourth and sixth chapters). With respect to slender members, the contributions are only theoretical. Firstly, a review of the principles of CSCT for punching shear failures is provided, clarifying from the mechanical point of view how it can be used to perform a refined calculation of the failure criterion (fourth chapter). Subsequently, a refined calculation of the failure criterion is presented based on the principles of CSCT and supported on experimental measurements available in the scientific literature (fifth chapter). Additional theoretical work also included the development and vali-

ation of closed-form expressions of the CSCT for punching shear design of slabs and footings without transverse reinforcement (fourth chapter).

The following two sections present a summary of the main conclusions of this thesis and a list of potentially interesting topics for future research.

## 7.2 Conclusions

Considering that the five main chapters deal with different issues within the topic of research of this thesis, this section is divided by chapters. The main conclusions of each chapter are separately synthesized in the following.

### Experimental programme on the punching behaviour and strength of footings

The results of an experimental campaign of full-scale reinforced concrete footings (0.550 m height) subjected to a uniform soil pressure were presented in the second chapter of this thesis (refer to Simões *et al.* (2016a)). The main conclusions are listed below:

- The punching strength of reinforced concrete footings without transverse reinforcement and under uniform soil pressure increases with the decrease of the span-to-effective depth ratio. Still with respect to the members without transverse reinforcement, also the inclination of the failure surface experimentally observed seems to become steeper with the decrease of the span-to-effective depth ratio. These experimental evidences are consistent with those previously presented by Hegger *et al.* (2009) and Siburg and Hegger (2014);
- Detailed measurements performed in the shear-critical region suggest that concrete crushing of the diagonal strut carrying shear is the phenomenon triggering the punching failure of compact reinforced concrete footings without transverse reinforcement. The experimental observations are in agreement with the numerical results obtained by Hallgren and Bjerke (2002), who have also suggested the crushing of the diagonal concrete strut as the phenomenon leading to the punching failure of compact footings (after redistribution of internal forces);
- The experimental measurements reveal that, although the flexural deformations seem to be important also in the case of compact footings, important shear deformations take place and influence the state of deformations of the shear-critical region;
- The comparison of the experimental results of two identical footings where only the top reinforcement was varied (refer to specimens PS13 -with top reinforcement- and PS14 -without top reinforcement) suggests that a very compact reinforced concrete footing under uniform soil pressure may have a higher punching shear resistance if top horizontal reinforcement is used. This result requires further experimental evidence to be confirmed, as only one typology of footing was tested for comparison. It is not clear whether the increase of 8% of the normalized punching shear resistance was due to the confinement given by this reinforcement to the diagonal compression strut carrying shear, due to dowel action of this reinforcement or if it is only a result of scatter intrinsically associated to punching shear tests;
- The experimental results suggest that a transverse reinforcement system composed of vertical double-headed studs is an effective system to increase the punching shear strength and deformation capacity of compact reinforced concrete footings. Nevertheless, its efficiency appears to be influenced by the span-to-effective depth of the member, with an efficiency decay observed with

the decrease of the span-to-effective depth ratio. These results are in agreement with the experimental observations previously reported by Hegger *et al.* (2009) and Siburg and Hegger (2014), who have observed a decrease of the efficiency of stirrups as transverse reinforcement system with decreasing shear slenderness;

- The experimentally measured load-rotation relationships of the specimens with transverse reinforcement showed a significant plateau before failure (increasing rotation without increase of shear forces). In addition, the plateau occurred at shear forces remarkably lower than those calculated assuming a pure flexural failure (applying yield-line theory (Johansen, 1962)). This consists on an experimental evidence that a flexural-shear regime seems to occur at high shear forces in the case of compact reinforced concrete footings. Similar observations were previously reported by, for example, Lips (2012) and Lips *et al.* (2012) for the case of slender slabs with large amounts of transverse reinforcement.

### **Application of the upper bound theorem of limit analysis to calculate the strength of reinforced concrete footings without transverse reinforcement**

The *Chapter 3* of this thesis presents a theoretical approach based on the application of the upper bound theorem of limit analysis to calculate the strength and the governing failure mechanisms of reinforced concrete footings without transverse reinforcement (refer to Simões *et al.* (2016b)). The principal conclusions presented in this chapter are listed in the following:

- Pure flexural failures of compact reinforced concrete footings occur only for low amounts of the bottom mechanical reinforcement ratio. On the other hand, pure punching shear failures take place for large amounts of this parameter. A continuous transition between pure flexural and punching shear failures occurs for intermediate values of the bottom mechanical reinforcement ratio, resulting into a pronounced flexural-shear regime. The significance of this regime was shown to increase with decreasing span-to-effective depth ratio;
- The lower strength obtained for the flexural-shear regime when compared to a pure flexural failure can be explained by the presence of an inclined concrete strut with a significant width in the edge of the column, which reduces the bending lever arm and, consequently, the moment capacity;
- The failure mechanism representing the punching shear failure corresponds either to a vertical translation of the outer portion of the slab (as originally assumed by Braestrup *et al.* (1976) for punching shear failures of slabs) or to a clockwise rotation (rotation opposite to the one expected for a flexural failure) with an instantaneous centre of rotation at the height of the bottom flexural reinforcement (thus not activating it). The latter failure mechanism is governing in the case of more compact footings without top reinforcement, while the former is governing all the remaining cases (footings with moderate slenderness or footings with sufficient amount of top reinforcement to avoid the latter mechanism);
- The difference between the two potentially governing failure mechanisms associated to punching shear failures explains the theoretical positive effect of introducing top reinforcement. In the cases where the governing failure mechanism includes a clockwise rotation, the introduction of top reinforcement theoretically increases the punching strength (as this reinforcement is also activated). In terms of failure mechanisms, the transition from a mechanism characterized by clockwise rotation to a mechanism described by vertical translation of the outer portion of the footing occurs with the increase of the amount of top reinforcement;

- The potential increase of the punching strength with the introduction of top reinforcement in the case of very compact footings may be explained from a physical perspective by the confinement given by top reinforcement to the diagonal concrete strut (Guidotti *et al.*, 2011). The experimental results presented in this thesis (refer to specimens PS13 and PS14 in Chapter 2) have shown an increase of the punching strength with the introduction of top reinforcement, which is in agreement with the theoretical results obtained in this chapter. The increase of punching strength was nevertheless very limited ( $\approx 8\%$  of the normalized resistance) and was only verified for a given case. Further experimental research is needed to confirm experimentally that top reinforcement may increase the punching strength in the case of very compact footings without transverse reinforcement;
- According to the theoretical results, the inclination of the failure surface of footings subjected to a uniform soil pressure (in the regime of punching failures) is mostly a function of the span-to-effective depth ratio. This theoretical result is consistent with the experimental observations made by Hegger *et al.* (2009) and Siburg and Hegger (2014) and with the experimental results reported in this thesis (refer to Chapter 2);
- Fair agreement was found between theoretical and experimental results of Hallgren *et al.* (1998) and Dieterle and Rostásy (1987) for reasonable values of the reduction factor accounting for the influence of the strain- and size-effect. Constant values have been adopted for this reduction factor to compare the theoretical and the experimental results. Nevertheless, the comparisons have shown that this reduction factor cannot be taken as a constant, as it is rather a function of different geometrical and mechanical properties. As a result, a rational approach to estimate this factor is required.

### **Review of the theoretical principles of the Critical Shear Crack Theory for punching shear failures of members without transverse reinforcement and development of closed-form design expressions**

The theoretical principles of the CSCT for punching shear failures are reviewed in the *Chapter 4* of this thesis. In addition, closed-form design expressions based on the CSCT are also analytically derived. The main conclusions of the work presented in this chapter (Muttoni *et al.*, 2017) are listed below:

- The mechanical model of the CSCT for punching shear failures considers that strains localize at a crack with a flexural origin (the so-called critical shear crack) at failure. The kinematics of the critical shear crack (CSC) includes a rotation (associated to flexural deformations) and a shear deformation. The internal stresses developing along the CSC may be calculated on the basis of the displacements resulting from the adopted kinematics. The distribution of internal stresses calculated using suitable fundamental material laws forms an inclined concrete strut;
- According to the mechanical model of the CSCT, the punching strength, obtained by integration of the internal stresses, is a function of the crack opening and crack roughness. A decrease of the punching strength occurs with an increase of the crack opening and a decrease of the crack roughness;
- The slenderness of the slabs not only influences the relative contribution to the crack opening at failure of the rotation and of the shear deformation, but also influences the shape of the CSC. Accounting for this, the mechanical model of the CSCT is applicable for both slender and squat members;

- A simplified failure criterion with a power-law function including an upper limit representing a maximum achievable punching strength (as recently proposed by Muttoni and Fernández Ruiz (2017)) seems to suitably address the different failure modes that can occur in slender and squat members;
- Closed-form design expressions can be analytically derived based on the mechanical model of the CSCT by combining the power-law failure criterion (Muttoni and Fernández Ruiz, 2017) and a simplified load-rotation relationship (Muttoni, 2008). The proposed expressions allow a clear identification of the role of the parameters governing the punching strength. In addition, the simplicity of the derived expressions may help improving the easiness of use of the CSCT in practice;
- The analytical derivation of closed-form design expressions based on a mechanical model allows the inclusion of additional effects influencing the punching strength with a rational basis. This has been shown for compressive membrane action, whose influence can be considered in the closed-form design expression by deriving it adopting a simplified load-rotation relationship properly (Einpaul *et al.*, 2015, 2016; Muttoni and Fernández Ruiz, 2017) accounting for this effect;
- The derived closed-form design expressions have shown fairly good agreement with the experimental results for both slender slabs and compact footings. The comparison with individual series of tests has also been shown that the derived expressions consistently capture the influence of the main geometrical and mechanical parameters.

### **Validation of the Critical Shear Crack Theory for punching failures of members without transverse reinforcement based on a refined mechanical model**

A refined mechanical model for punching shear failures of slender slabs without transverse reinforcement is presented in the *Chapter 5*. The model (which can be seen as an improvement of the mechanical models of Guidotti (2010) and Clément (2012)) is developed on the basis of the theoretical principles of the Critical Shear Crack Theory and is supported on recent experimental findings. The main conclusions of the work presented in this chapter include:

- The results of the mechanical modes show a very good accuracy with the experimental results. In addition, also the influence of all parameters significantly influencing the punching shear strength of slender slabs are consistently captured with the presented model;
- A decrease of the punching shear strength is observed with increasing rotation. This is justified by the decay of the contribution of the shear-transfer actions associated to larger crack openings: aggregate interlock stresses decrease, concrete softens and dowel action reduces due to concrete spalling or yielding of the bars;
- The results of the refined mechanical model concentrate in a narrow band if the normalized punching shear strength is depicted as a function of the normalized rotation of the slab. This indicates that a single analytical failure criterion can be used for design and assessment without lack of accuracy. In this sense, the analytical hyperbolic (Muttoni, 2008) and power-law (Muttoni and Fernández Ruiz, 2017; Muttoni *et al.*, 2017) failure criteria of the Critical Shear Crack Theory can be successfully used for those purposes;
- The results of the mechanical model show that the opening of the critical shear crack at failure (accounting for both rotation and shear deformation) are correlated to the product of the slab rotation and effective depth. In addition, a linear relationship between both parameters appears to

be a reasonable approximation, which mechanically justifies the simplified assumption originally considered by Muttoni (2008) of a crack opening proportional to the multiplication of the rotation by the effective depth ( $w \propto \psi \cdot d$ );

- A size-effect law with a slope of approximately  $-1/3$  in a double-logarithmic scale is predicted by the refined mechanical model, which is in agreement with the theoretical works of Fernández Ruiz and Muttoni (2017).

### **A discussion on the extension of the refined mechanical model for punching shear failures of prestressed slabs and footings without transverse reinforcement**

A discussion on the possible extension of the mechanical model of *Chapter 5* for prestressed slabs is presented in *Chapter 6*. The punching strength and associated deformation capacity is computed by intersecting the load-rotation relationship (calculated as proposed by Clément *et al.* (2014)) with the failure criterion. The refined calculation of the failure criterion is adapted from *Chapter 5* in order to include the influence of in-plane stresses in the definition of the shape of the CSC and on the displacement field occurring along it. The main conclusions are listed below:

- A satisfactory agreement is found in the preliminary comparison of the results of the extended model against the experimental results of Clément *et al.* (2014);
- According to the refined mechanical model, the increase of the punching strength for increasing in-plane compressive stresses is justified by the decrease of the crack opening along the CSC (leading to larger extents of the region with smearing cracking, as well as to higher internal stresses developing in both regions of localized and smeared cracking). This result is in agreement with the results of previous models developed consistently with the principles of the CSCT (Clément, 2012; Clément *et al.*, 2014);
- The extension of the model for prestressed slabs requires nevertheless further theoretical validation (at the level of the hypotheses) and an extensive experimental validation (comparison with databases of experimental results).

A possible extension of the model for the cases of isolated reinforced concrete footings is also discussed in *Chapter 6*. Again, deformations and load-carrying capacities at failure are calculated by intersecting the load-rotation relationship and the calculated failure criterion. For that purpose, the load-rotation relationship proposed by Muttoni (2008) for slender slabs is adapted for footings considering a suitable geometry of the failure surface (function of the slenderness as theoretically observed in *Chapter 3*) and sectional response of the member (accounting for the reduced moment capacity, in accordance to the theoretical results of *Chapter 3*). The refined calculation of the failure criterion as presented in *Chapter 5* is adapted by considering a variable location of the CSC at the level of the flexural reinforcement, whose value is determined by minimization of the total punching shear strength. The main results are presented in the following:

- A reasonable agreement is found from the comparison of the calculated and experimentally measured load-rotation relationships of the specimens presented in *Chapter 2*. Further experimental validation is nevertheless still required;
- The extended model shows a good accuracy in terms of coefficient of variation when compared to a database of experimental results and selected series of tests. The average of the measured-to-calculated punching strength is slightly lower than the unit, thus suggesting that the model may possibly overestimate the punching strength of footings. These results indicate that the model

is able to correctly predict the influence of the different geometrical and mechanical parameters governing the punching strength (justifying the rather low value of the coefficient of variation), but not exactly the measured strength (slight overestimation). Further work is thus required in order to improve the extension of the mechanical model presented in *Chapter 6* for footings;

- Even if some additional work of validation and improvement may still be required, the extended model seems to be able to explain from the theoretical point of view some of the experimental trends reported in the scientific literature (as the increasing influence of concrete compressive strength in the punching strength with the decrease of the slenderness of the member).

Considering the satisfactory agreement found in the preliminary comparisons of the theoretical and experimental results for the cases of prestressed slabs and footings, the theoretical principles of the CSCT (forming the basis of the mechanical model) are shown to be also valid to deal with punching failures of such members. Further theoretical and experimental validation of the extension of the mechanical model for those cases remains still to be performed in the future to confirm the results presented in *Chapter 6*.

### 7.3 Outlook

Some questions remain open with respect to the punching shear behaviour and strength of reinforced concrete members. Further experimental, numerical and theoretical work is still required to approach a consensus in this topic. Some possible ideas for future research are listed below:

- With respect to experimental works:
  - Additional experimental programmes with detailed measurements (by using newly available measuring techniques) of the shear-critical region are needed to better understand the state of deformations of this region (cracking development and associated kinematics, as for instance performed by Clément (2012), Einpaul (2016), and Einpaul *et al.* (2017)). These measurements could play an important role in the validation of the results of any mechanical or numerical model by means of other parameters than the punching and deformation capacities (e.g. cracking development, internal crack widths, kinematics of the cracks developing in the shear-critical region).
- With respect to numerical works based on non-linear finite element methods:
  - The use of non-linear finite element methods constitutes an opportunity to better understand the state of strains and stresses in the shear-critical region. Refined numerical modelling of this region can be performed using advanced finite elements combined with sophisticated concrete constitutive laws. Such models not only allow the calculation of the punching behaviour and strength, but also enable a better understanding of the phenomena involved in these failures. Furthermore, the numerical models may also be used to validate some hypotheses which may be required to develop simple mechanical models;
- With respect to the mechanical model presented in this thesis:
  - The fundamental material laws used for the regions along the critical shear crack with localized and smeared cracking need further experimental validation (fundamental material laws and potential transition between different regimes). Additional experimental and theoretical works on the fundamentals of the shear-transfer in concrete are of interest. Also additional experimental programmes including information with respect to the internal cracking development are of interest in order to refine the assumptions of the mechanical model (e.g. crack spacing, geometry and kinematics of the critical shear crack);

- 
- Analyze analogies and convergence with the mechanical models of Swedish School (Kinunen and Nylander, 1960; Broms, 1990; Hallgren, 1996; Broms, 2005, 2016);
  - The application of the mechanical model presented in this thesis to prestressed slabs requires further theoretical work and experimental validation;
  - The extension of the mechanical model for isolated reinforced concrete footings requires additional work. The proposed load-rotation relationship of Muttoni (2008) adapted for isolated footings discussed in this thesis requires further validation. Also at the level of the refined calculation of the failure criterion, it is necessary to understand whether the assumptions related to, for example, tangential crack spacing, radial extent of the region with tangential cracks and shape of the critical shear crack adopted for the case of footings are valid or need to be improved. A full validation of the extended mechanical model for footings is required;
  - The mechanical model can be further extended to deal with punching failures of reinforced concrete members with transverse reinforcement. This would allow to investigate on the governing failure modes (crushing of concrete struts, failure within or outside the shear-reinforced region) as a function of the different geometrical and mechanical properties. A mechanical model for members with transverse reinforcement would also allow to validate some of the assumptions of the simplified failure criterion of Critical Shear Crack Theory for punching failures of members with transverse reinforcement. The case of squat members with transverse reinforcement could be investigated as well, in order to better understand the activation of the transverse reinforcement in cases where flexural deformations are limited;
  - It may be of interest to extended the mechanical model presented in this document to investigate the influence of long-term effects or imposed deformations.
  - With respect to the Critical Shear Crack Theory for punching shear failures:
    - The consistency of the failure criteria of the CSCT for punching shear failures of footings without transverse reinforcement may be investigated based once the extended mechanical model for footings is fully validated;
    - An additional work after a complete validation of the extended mechanical model for prestressed slabs may be the derivation of an analytical failure criterion, which not only accounts for the influence of in-plane stresses, but also enables the derivation of closed-form expressions for the punching shear design of prestressed slabs (the correction of the hyperbolic failure criterion of the CSCT proposed by Clément *et al.* (2014) does not allow the derivation of closed-form solutions);
    - Discussion of the assumptions of the CSCT for punching shear design of members with transverse reinforcement and derivation of closed-form solutions for those cases.

## 7.4 References

- Bažant Z. P.; Cao Z. (1987):** „Size Effect in Punching shear Failure of Slabs“. *ACI Structural Journal*, Vol. 84, No. 1, pp. 44–53.
- Braestrup M. W.; Nielsen M. P.; Jensen B. C.; Bach F. (1976):** *Axisymmetric Punching of Plain and Reinforced Concrete*. Tech. rep. 75. Structural Research Laboratory, Technical University of Denmark, p. 33.
- Broms C. E. (1990):** „Punching of flat plates - a question of concrete properties in biaxial compression and size effect“. *ACI Structural Journal*, Vol. 87, No. 3, pp. 292–304.
- Broms C. E. (2005):** „Concrete flat slabs and footings: Design method for punching and detailing for ductility“. PhD thesis. Stockholm, Sweden: Department of Structural Engineering, Royal Institute of Technology, p. 114.
- Broms C. E. (2016):** „Tangential strain theory for punching failure of flat slabs“. *ACI Structural Journal*, Vol. 113, No. 1, pp. 95–104.
- Clément T. (2012):** „Influence de la précontrainte sur la résistance au poinçonnement de dalles en béton armé“. PhD thesis. Lausanne, Switzerland: EPFL, p. 224.
- Clément T.; Ramos A. P.; Fernández Ruiz M.; Muttoni A. (2014):** „Influence of prestressing on the punching strength of post-tensioned slabs“. *Engineering Structures*, Vol. 72, pp. 56–69.
- Dieterle H.; Rostásy F. (1987):** „Load-carrying behaviour of isolated reinforced concrete foundations of square columns (In German: Tragverhalten quadratischer Einzelfundamente aus Stahlbeton)“. *Deutscher Ausschuss für Stahlbeton*, Vol. 387, pp. 1–91.
- Einpaul J. (2016):** „Punching strength of continuous flat slabs“. PhD thesis. Lausanne, Switzerland: EPFL, p. 209.
- Einpaul J.; Fernández Ruiz M.; Muttoni A. (2015):** „Influence of moment redistribution and compressive membrane action on punching strength of flat slabs“. *Engineering Structures*, Vol. 86, pp. 43–57.
- Einpaul J.; Ospina C.; Fernández Ruiz M.; Muttoni A. (2016):** „Punching shear capacity of continuous slabs“. *ACI Structural Journal*, Vol. 113, No. 4, pp. 861–872.
- Einpaul J.; Fernández Ruiz M.; Muttoni A. (2017):** „Measurements of internal cracking in punching test slabs without shear reinforcement“. *Magazine of Concrete Research*. doi: 10.1680/jmacr.16.00099.
- Fernández Ruiz M.; Muttoni A. (2017):** „Size effect on punching shear strength: Differences and analogies with shear in one-way slabs“. In: *Bulletin 81 / ACI SP-315: Punching shear test of structural concrete slabs: Honoring Neil M. Hawkins*. Ed. by Ospina C. E.; Mitchell D.; Muttoni A. Lausanne, Switzerland: International Federation for Structural Concrete, pp. 59–72.
- Guidotti R. (2010):** „Punching shear of slabs with column load (In French: Poinçonnement des planchers-dalles avec colonnes superposées fortement sollicitées)“. PhD thesis. Lausanne, Switzerland: EPFL, p. 189.
- Guidotti R.; Fernández Ruiz M.; Muttoni A. (2011):** „Crushing and Flexural Strength of Slab-Column Joints“. *Engineering Structures*, Vol. 33, No. 3, pp. 855–867.
- Hallgren M. (1996):** „Punching Shear Capacity of Reinforced High Strength Concrete Slabs“. PhD thesis. Stockholm, Sweden: Department of Structural Engineering, Royal Institute of Technology, p. 206.
- Hallgren M.; Bjerke M. (2002):** „Non-linear finite element analyses of punching shear failure of column footings“. *Cement and Concrete Composites*, Vol. 24, No. 6, pp. 491–496.

- Hallgren M.; Kinnunen S.; Nylander B. (1998):** „Punching shear tests on column footings“. *Nordic Concrete Research*, Vol. 21, pp. 1–22.
- Hegger J.; Ricker M.; Sherif M. (2009):** „Punching Strength of Reinforced Concrete Footings“. *ACI Structural Journal*, Vol. 106, No. 5, pp. 706–716.
- Johansen K. W. (1962):** *Yield-line Theory*. Cement and Concrete Association.
- Kinnunen S.; Nylander H. (1960):** *Punching of Concrete Slabs Without Shear Reinforcement*. Tech. rep. 158. Stockholm, Sweden: Transactions of the Royal Institute of Technology, p. 112.
- Lips S. (2012):** „Punching of Flat Slabs with Large Amounts of Shear Reinforcement“. PhD thesis. EPFL, p. 217.
- Lips S.; Fernández Ruiz M.; Muttoni A. (2012):** „Experimental Investigation on Punching Strength and Deformation Capacity of Shear-Reinforced Slabs“. *ACI Structural Journal*, Vol. 109, No. 6, pp. 896–900.
- Muttoni A. (2008):** „Punching shear strength of reinforced concrete slabs without transverse reinforcement“. *ACI structural Journal*, Vol. 105, No. 4, pp. 440–450.
- Muttoni A.; Fernández Ruiz M. (2017):** „The Critical Shear Crack Theory for punching design: from a Mechanical Model to Closed-Form Design Expressions“. In: *Bulletin 81 / ACI SP-315: Punching shear test of structural concrete slabs: Honoring Neil M. Hawkins*. Ed. by Ospina C. E.; Mitchell D.; Muttoni A. Lausanne, Switzerland: International Federation for Structural Concrete, pp. 237–252.
- Muttoni A.; Fernández Ruiz M.; Simões J. T. (2017):** „The theoretical principles of the critical shear crack theory for punching shear failures and derivation of consistent closed-form design expressions“. *Structural Concrete*, pp. 1–17. doi: 10.1002/suco.201700088.
- Nielsen M. P.; Hoang L. C. (2011):** *Limit analysis and concrete plasticity*. 3<sup>rd</sup> edition Boca Raton. USA: CRC Press.
- Siburg C.; Hegger J. (2014):** „Experimental Investigations on Punching Behaviour of Reinforced Concrete Footings with structural dimensions“. *Structural Concrete*, Vol. 15, No. 3, pp. 331–339.
- Simões J. T.; Bujnak J.; Fernández Ruiz M.; Muttoni A. (2016a):** „Punching shear on compact footings with uniform soil pressure“. *Structural Concrete*, Vol. 17, No. 4, pp. 603–617.
- Simões J. T.; Faria D. V.; Fernández Ruiz M.; Muttoni A. (2016b):** „Strength of reinforced concrete footings without transverse reinforcement according to limit analysis“. *Engineering Structures*, Vol. 112, pp. 146–161.
- Simões J. T.; Fernández Ruiz M.; Muttoni A. (2018):** „Validation of the Critical Shear Crack Theory for punching of slabs without transverse reinforcement by means of a refined mechanical model“. *Structural Concrete*, pp. 1–26. doi: 10.1002/suco.201700280.



# Curriculum Vitae - João Tiago Simões

## Personal Information

João Tiago Ramos Bernardo de Santa Rita Simões

19 September 1989

Lagos, Portugal

Rue du Simplon 3B  
1006 Lausanne (VD), Switzerland

jtbsimoes@gmail.com



## Education

### PhD Degree

Structural Concrete Laboratory (IBETON), École Polytechnique Fédérale de Lausanne  
Lausanne, Switzerland

Apr. 2013 - Mar. 2018

### Master Degree in Civil Engineering

Integrated Master Program in Civil Engineering - Structures Profile  
Faculdade de Ciências e Tecnologias, Universidade Nova de Lisboa - Portugal

Sep. 2010 - Dec. 2012

### Bachelor Degree in Civil Engineering Sciences

Bachelor Program within the Integrated Master Program in Civil Engineering  
Faculdade de Ciências e Tecnologias, Universidade Nova de Lisboa - Portugal

Sep. 2007 - Jul. 2010

## Professional Experience

### PhD Research Assistant

Structural Concrete Laboratory (IBETON), École Polytechnique Fédérale de Lausanne  
Experimental and theoretical work focusing on the punching shear failures of structural concrete members.

Apr. 2013 - Mar. 2018

## Journal Publications

J. T. Simões, M. Fernández Ruiz, A. Muttoni, "Validation of the Critical Shear Crack Theory for punching of slabs without transverse reinforcement by means of a refined mechanical model", *Structural Concrete*, 2018, pp. 1-26, DOI: 10.1002/suco.201700280

A. Muttoni, M. Fernández Ruiz, J. T. Simões, "The theoretical principles of the Critical Shear Crack Theory for punching shear failures and derivation of consistent closed-form design expression", *Structural Concrete*, 2017, pp. 1-17, DOI: 10.1002/suco.201700088

J. T. Simões, D. M. V. Faria, M. Fernández Ruiz, A. Muttoni, "Strength of reinforced concrete footings without transverse reinforcement according to limit analysis", *Engineering Structures*, Volume 112, 2016, pp. 146-161

J. T. Simões, J. Bujnak, M. Fernández Ruiz, A. Muttoni, "Punching shear on compact footings with uniform soil pressure", *Structural Concrete*, Volume 17, No. 4, 2016, pp. 603-617

## Awards

### Best Lecture Award

Award received in the 11<sup>th</sup> fib International PhD Symposium in Civil Engineering in Tokyo in 2016

2016

### Award Professor António Mineiro

Student completing the Integrated Master Program in Civil Engineering of Faculdade de Ciências e Tecnologias of Universidade Nova de Lisboa with the highest grade in the academic year of 2011/2012

2012

## Languages

Portuguese: Mother tongue

English: Advanced level

French: Advanced level